AES 15 / 17 **The Shale Oil Potential of the Posidonia Formation in the Netherlands**

26-09-2014 **Wouter Willem Mezger**

Title	The Shale Oil Potential of the Posidonia Formation in the Netherlands
Author	W.W. Mezger
Date	September 2014
Professor	Prof. Dr. S. M. Luthi
Supervisors	Prof. Dr. S. M. Luthi Drs. M. Harings Dr. Ir. R. R. G. G. Godderij J. Lutgert Prof. Dr. Q. Fisher
Graduation Committee	Prof. Dr. S. M. Luthi Prof. Dr. P.L.J. Zitha Prof. Dr. Q. Fisher Drs. M. Harings
TA Report number	AES / TG / 14 – 17
Postal Address	Section for Applied Geology Department of Geoscience and Engineering Delft University of Technology P.O. Box 5028 The Netherlands
Telephone	(31) 15 2781328 (secretary)
Telefax	(31) 15 2781189

Acknowledgements

I would like to thank everybody who helped and supported me during my thesis work. Especially I would like to thank my direct supervisors Stefan Luthi (TU Delft) and Michiel Harings (EBN) for their guidance and support throughout my project. In addition I would like to thank Jan Lutgert and Raymond Godderij from EBN for the time they took to discuss my project and the suggestions they made on writing this report. I also would like to thank EBN for financing this project and all the colleagues for their hospitality.

From the School of Earth and Environment, Leeds University, I would like to thank Carlos Grattoni and Sam Holt for their help on setting up and performing all the experiments. Especially I would like to thank Quentin Fisher for his help on defining the objectives, the measurements and the interpretation of the results. Furthermore I would like to thank Ida Shafagh for her help on the TGA experiments.

Finally I would like thank my family and friends for their support during this project and my time in Delft. Especially I would like to thank my parents Chris and Annemarie Mezger and my brother Erik Mezger for their help and support throughout my graduation. At last I would like to thank my girlfriend Yverna Bosch for her help and support whenever needed.

Abstract

During the last decade shale formations have been successfully explored in the United States and both oil and gas is currently produced from them. This successful development led to a global interest in shale formations. To assess the worldwide shale oil and gas potential, the Energy International Agency (EIA) investigated the shale formations of 43 different countries outside the U.S.. In this, the Netherlands are evaluated to contain 2.7 billion barrels (Bbbl) of Technically Recoverable oil Resources (TRR) in the Epen, Geverik and Posidonia formations. Based upon previous research, Energie Beheer Nederland (EBN) has identified shale formations as possible oil and gas plays.

This study investigates the shale oil potential of the onshore Posidionia formation in the Netherlands and evaluates the assessment of the EIA report. Fourteen Posidonia samples from 7 wells were subjected to a number of measurements on both core plugs and chips. The samples experimental methods included TGA, NMR, SEM, GRI and steady-state flow to analyze the pore size and shape of the rock matrix, the Total Organic Carbon, the maturity, the porosity, the permeability, the pore content, the fluid storage and the flow mechanism of the samples. When combined these parameters can give a prediction of the shale oil potential of a rock. In addition, the samples were tested under three different sample conditions: drier, wetter or “as-received”. This was done because the in-situ conditions, dry, wet, of the samples may affect the measurement but are not known.

The Posidionia formation is known to have generated oil and on the Van Krevelen diagram, based on maturity and TOC, samples are located in the oil generating region of the plot. From the TGA and NMR experiments it was proven that oil is present in the shale samples, although this is identified as bound or trapped oil. Based on evaluations with NMR and GRI it was found that the sample material was dried out during storage and that the samples are likely to contain movable hydrocarbons. The SEM and NMR data suggested that some samples contain pore sizes large enough to allow oil to flow through the rocks. The sample condition is shown to be a crucial parameter for the determination of porosity and permeability. Different conditions resulted in porosity differences of up to a factor of three, for the measured sample porosity. The GRI experiment has proven the molecular sieving effect, meaning that permeability decreases if a gas is used with a larger molecule size.
The results were combined to assess the heterogeneity of the formation. based on the large spread of petrophysical properties of the samples it was found that the Posidonia shale is highly heterogeneous. Therefore it is concluded that a statement regarding the technically recoverable resources cannot be made at this stage. It is recommended to evaluate fresher sample material with the same methodology as used in this study.

Table of contents

Table of Figures

Table of Tables

Table of Equations

Nomenclature

A	Cross-sectional area to flow
A_{pore}	Pore surface area
ARI	Advanced Resources International
Bbbl	Billion barrels of petroleum liquids
B_0	Static magnetic Field
B_1	Oscillating magnetic field
BHN	Brinell Hardness Number
BSE	Back Scattered Electrons
CPMG	Carr, Purcell, Meiboom and Gill
D	Darcy
DTG	Differentiated Thermo Gravimetric
d	Diameter of chips
EBN	Energie Beheer Nederland
EIA	Energy Information Agency
FIB	Fixed Ion Beam
FID	Free Induction Decay
FV	Fluid volume in sample
GRI	Gas Research Institute
He	Helium gas
HI	Hydrogen Index
k	permeability
L	Length of sample
mD	milli Darcy
nD	nano Darcy
N	Nitrogen
NAM	Nederlands Aardolie Maatschappij
NE	Number of Echoes
NMR	Nuclear Magnetic Resonance
NS	Number of scans taken by NMR
OIP	Oil-In-Place
Pa	Pascal
P_{per}	Perimeter of pore
Φ	Porosity
Φ_{mic}	Porosity from 5 µm scale images
Φ_{mac}	Porosity from 100 µm scale images
Φ_{tot}	Total porosity from SEM Images
Q	Units of Volume per time
QEMSCAN	Quantitative Evaluation of Minerals by Scanning Electron Microscopy
R_0	Vitrinite Reflectivity Index
RD	Recycle Delay

RG	Receiver Gain
RVG	Roer Valley Graben
SHAPE	Shale Permeability Project
S	Measured Signal Amplitude size
SE	Secondary Electrons
SEM	Scanning Electron Microscope
SRV	Stimulated Reservoir Volume
TE	Inter Echo Spacing
TGA	Thermo Gravimetric Analysis
TRR	Technically Recoverable Resources
TOC	Total Organic Carbon
T_1	Longitudinal polarization time
T_2	Transverse Relaxation Time
TW	Polarization Time
USGS	United States Geological Survey
V_{rf}	Reference Volume
V_h	Sample holder Volume
WNB	West Netherlands Basin
γ	Value for roundness of pore
μ	Viscosity of fluid
ΔP	Pressure difference over length of sample

1 Introduction

In the last decades, fewer conventional oil and gas plays fields were found each year and production from existing fields became increasingly difficult. In the meantime unconventional resources including shale formations are becoming more and more important for oil and gas production. Energie Beheer Nederland (EBN), the state participant for hydrocarbon exploitation and exploration, identified shale plays as potential contributors for the Netherlands to increase reserves and maintain current production.

Within the United States of America the development of unconventional shale gas formations has changed the energy sector. Driven by the high price of liquid hydrocarbons and improved technology, currently shale oil plays are being explored. The successful exploration in the United States led to a global interest in shale formations. Currently, other countries are assessing the possibilities for unconventional shale development and in regard of this the Energy Information Agency (EIA) investigated the shale oil and gas opportunities for 43 different countries outside the United States, including the Netherlands.

Within the Netherlands three shale formations, Epen, Posidonia and Geverik formations were evaluated by the EIA, and they found them to contain a total of 2.9 billion barrels (Bbbl) of recoverable oil. The amount of recoverable oil for each formation is displayed in Figure 1. To put this into perspective: The quantity of recoverable oil equals 13 times the current estimated oil reserves of the Netherlands.

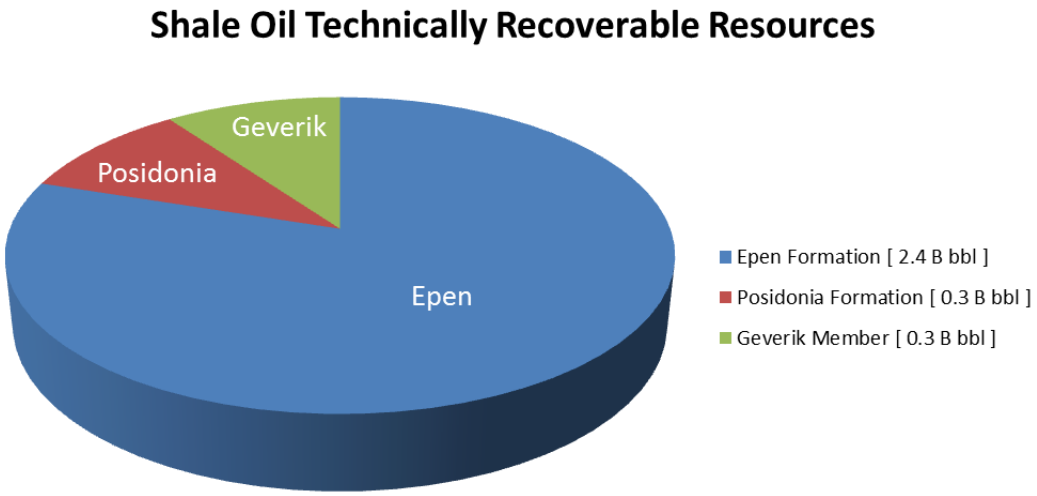

Figure 1: Shale oil resources in The Netherlands (U.S. Energy Information Administration, 2013)

Traditionally, the majority of hydrocarbons are extracted from so called conventional resources and production from unconventional gas & oil fields has often been economically difficult (Maugeri, 2013; Flores et al., 2011). Shale formations were known to be present in abundance in the subsurface but were considered as a cap rock (impermeable seal) or source rock for conventional formations. In addition shale formation are typically heterogeneous within a formation, making their evaluation difficult.

In order to assess the potential for shale formations containing hydrocarbons in The Netherlands, EBN has started three years ago researching these plays. They investigated the Lower Jurassic Aalburg-, Posidonia-, and Sleen Formation, and the Lower Carboniferous Geverik Member for their geomechanical and source rock properties (Noordoven, 2010; Kee, 2010; Bouw et al., 2012). The majority of these studies focused on topics such as the areal extents of the shale and the evaluation of the fraccability of the rock to create an artificial fracture network. Based on these investigation sweet spots were identified as well as the presence of potential liquid hydrocarbons. This has not been further evaluated for these formations in the Netherlands. The exploration of unconventional shale formations is still at a very early stage and little is known of potential production from them.

Because of the large shale oil resources indicated by the EIA and the ongoing advances in production technology, which are opening up new plays to exploration, the shale oil potential within the Netherlands needs to be better evaluated. The fundamental question for the Netherlands would be if any oil is present in the formations and if it has flow potential. For the testing of their rock properties, however, standard experiment can often not be used, and measurements often contain systematic errors. Multiple measurements on the same rock properties are therefore essential to define a suitable shale rock evaluation method.

The reservoir evaluation of shale plays, has to be related to rock properties such as permeability and porosity (Rylander et al., 2013; Aguilera, 2013; Chen, 2013). Laboratory measurements evaluating the permeability and porosity are often affected by systematic errors caused by the often exceedingly small values (Bohacs, 2013). In addition, conventional shale experiments are done using a gas, but hydrocarbon fluid parameters such as viscosity and density also largely influence the resource potential. Before the interest in shale formations, shale rock was often considered a reservoir seal or source rock for conventional oil formations. Shale formations were penetrated frequently, but were not extensively cored because of a lack of interest. In the Netherlands, some samples have been taken in the past but these samples are often over 40 years old and not well preserved. The effects of age on the samples and their hydrocarbon condition is not yet known, but quite possibly result in measurements which are not representative for the original in-situ condition.

1.1 Research Objectives

Within this project the Posidonia formation, one of the formations evaluated by the EIA, is studied for its shale oil potential. Fundamental shale oil parameters are investigated such as, the presence of free hydrocarbons, the porosity and the ability of the rock the accommodate flow. The main objective is to prove the presence of free movable liquid hydrocarbons to estimate the flow potential of the rocks, and to obtain a better understanding of the key factors influencing the flow through these shales. In addition to the previously mentioned properties, the larger scale heterogeneity of the formation and the effect of the sample condition on various measurements is evaluated. The results will be used to assess the possibility for shale oil plays in the onshore Netherlands and to assess the methodologies used by the EIA to calculate the TRR values.

1.2 Terminology

In order to be consistent throughout this study, the terminology used for the rocks is elucidated. Various types of reservoirs fit within the unconventional category, as shown in Figure 2. For this study, shale oil is of interest, an unconventional resource in which conventional oil is residing in low permeability (shale) rock. Contrary to tight oil formations, a shale oil formations is rich in clay and does not include other lithologies (Maugeri, 2013). Shale oil therefore represents a subset of unconventional tight oil formations (U.S. Energy Information Administration, 2013). The unconventional producing methods and other characteristics inevitably change over time and often differ among users of the term (U.S. Energy Information Administration_2, 2013). Therefore, unconventional oil is defined here as an umbrella term for oil production from reservoirs where the permeability, the fluid viscosity, the trapping mechanism, and other characteristics differ from conventional reservoirs. Furthermore producing this oil requires more elaborate production methods compared to the production of conventional oil.

Shale oil is often confused with tight oil and oil shale. Although these are not taken into account throughout this project, these definitions are briefly explained. Tight oil is a conventional formation with low permeability. The rock from which the oil is produced is not the source rock of the oil and, therefore, in the United States tight oil is often used instead of shale oil (U.S. Energy Information Administration, 2013).

Shale oil is a shale rock formations that contain conventional crude oil. The rock is both the source rock and reservoirs rock. Oil shale is defined as a fine-grained sedimentary rock that contains solid organic matter (kerogen) but no resident oil due to its immaturity (Dyni, 2006). In order to generate liquid, the kerogen-rich rock is artificially heated (Chaudhary et al., 2011).

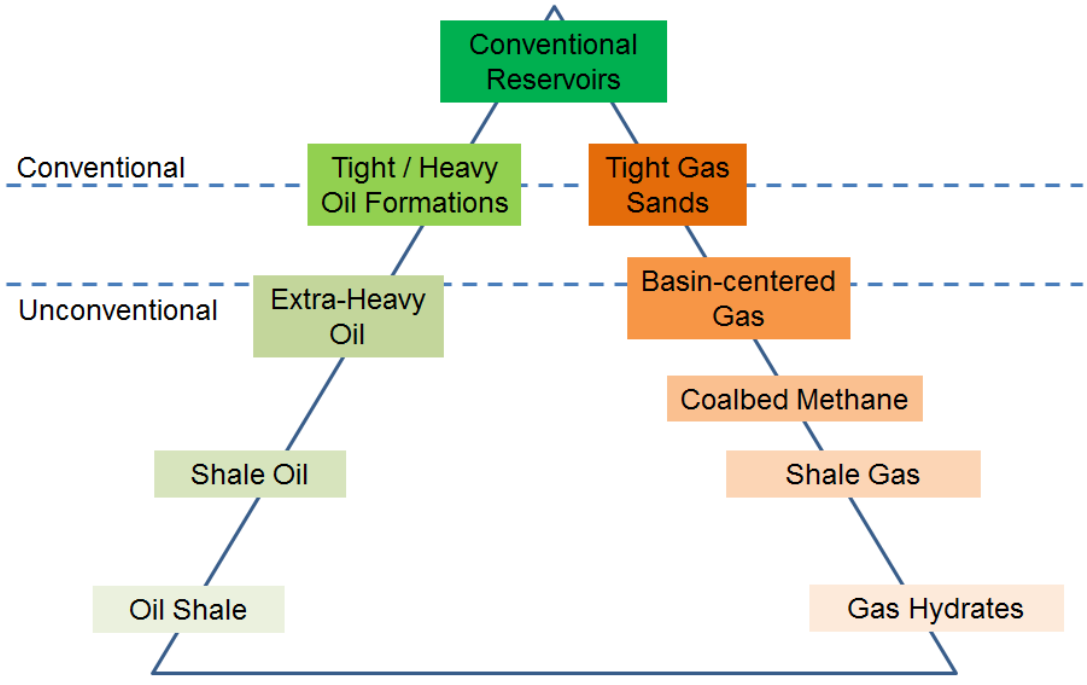

Figure 2: The petroleum- resource triangle from Chan et al. (2012). Modified by fitting the shale oil block in the triangle.

1.3 Research Outline

Following the general introduction, the additional chapters are used to describe and evaluate the shale oil potential of the Posidonia formation in the Netherlands. In chapter two an introduction is provided of the EIA shale oil resource assessment. The section focuses on three formations, and each is briefly described. In the third chapter the regional geology of the potential shale plays is introduced and explained. The fourth chapter begins with an introduction to shale oil production. Furthermore this section deals with the literature study used for the identification of properties which are important for shale formation evaluation. In the fifth chapter the experiments used for this project are described. The sixth chapter contains the results from these experiments. Chapter seven discusses the results and identifies correlations with the parameters introduced in the fourth section. The conclusion and future recommendations are given in chapter eight.

2 EIA Shale Oil Resource Assessment

This section describes and discusses the methodology used by the EIA to evaluate shale formations. Additionally the usefulness and uncertainty of various key properties are discussed. Some of these properties will be beyond the scope of this report and therefore only shortly mentioned.

2.1 EIA Resource Assessment Methodology

Based on a resource assessment methodology the EIA has indicated the Carboniferous Epen shale, the Carboniferous Geverik shale and the Jurassic Posidonia shale for possible shale oil exploration in The Netherlands. In Figure 3, the fundamental characteristics are summarized and each formation is discussed in the next section. The EIA uses English units, which is adopted in this report.

Carboniferous (Namurian) Epen Shale

The depth of the Epen Shale in the Dutch onshore ranges from 3,300 to 16,400 feet, averaging 8,500 feet in the wet gas/condensate area. The west-central portion has been excluded because the depth was below 16,500 feet. The thermal maturity varies from 1.0% to 1.3% in the center of the basin and 0.7% to 1.0% along the shallower and more southern parts. The gross organic-rich shale interval (explained in section 2.1.1) has a thickness of 1,500 ft and, based on a net-to-gross ratio of 30%, the net thickness becomes 450 feet. The TOC ranges from 1% to 15%, averaging 2.4%. The shale is over-pressured and because of its lacustrine deposition has a medium clay content.

Carboniferous (Namurian) Geverik Shale

A total of five wells have been drilled through the Geverik shale and none of these wells had the Geverik as a target. The depth of the Geverik shale ranges from 5,000 to 16,400 feet, with an average depth of 11,000 feet in the wet gas / condensate area. The deep west-central portion has been excluded because the depth was below 16,500 feet. Thermal maturity varies from 1.0% to 1.3% in the wet gas and condensate window. The gross organic-rich thickness is 225 feet and based on a net-to-gross ratio of 60% the net thickness is 135 feet. The TOC ranges between 2% and 7%, averaging 4%. The shale is slightly over-pressured and is assumed to contain a low to medium clay content due to its marine deposition.

Jurassic (Toarcian) Posidonia Shale

The Posidonia shale formation has been drilled many times, but unfortunately never as a target and it is not extensively sampled. The depth of the Posidonia shale ranges from 3,300 to 12,500 feet, averaging 6,500 feet in the oil-prospective area and 10,500 feet in the gas/condensate prospective area. The thermal maturity varies from 0.7% to 1.0% in the shallower portions (oil-window) and 1.0% to 1.3% in the wet gas/condensate window. The gross organic-rich thickness is 100 feet and based on a net-to-gross ratio of 90% the net thickness is 90 feet. The shale is evaluated to contain Type II marine kerogen with a total organic content ranging from < 1% to

16%, averaging 6%. The shale is slightly over-pressured with low to medium clay content according to the EIA.

The analysis of the shale oil potential is conducted in several steps and is based on the methodology used in the previous EIA report for the shale gas resources in 2011 (U.S. Energy Information Administration, 2011). The EIA had indicated three formations to be of potential interest for shale oil development in the Netherlands. From these three formations only the Posidonia is evaluated in this study but to be consistent with the EIA the Epen and Geverik are also mentioned in this section.

The systematic approach consists of five steps:

1) Conducting a preliminary geologic and reservoir characterization of the shale basins and formations
2) Establishing the areal extent of the major shale oil formations
3) Defining the prospective area for each shale oil formation
4) Estimating the risked shale oil-in-place
5) Calculating the technically recoverable shale oil resource

Offshore formations and conventional formations with low permeabilities are excluded from this evaluation.

Basic Data	Basin/Gross Area		West Netherlands ($2,750\ mi^2$)				
	Shale Formation		Epen		Geverik Member	Posidonia	
	Geologic Age		U. Carboniferous		U. Carboniferous	L. Jurassic	
	Depositional Environment		Lacustrine		Marine	Marine	
Physical Extent	Prospective Area (mi^2)		1,460	860	2,320	850	170
	Thickness (ft)	Organically Rich	1,500	1,500	225	100	100
		Net	450	450	135	90	90
	Depth (ft)	Interval	3,300 - 10,000	10,000 - 15,500	5,000 - 16,400	3,300 - 9,000	9,000 - 12,500
		Average	8,500	12,500	11,000	6,500	10,500
Reservoir Properties	Reservoir Pressure		Mod. Overpress.	Mod. Overpress.	Mod. Overpress.	Mod. Overpress.	Mod. Overpress.
	Average TOC (wt. %)		2.4%	2.4%	4.0%	6.0%	6.0%
	Thermal Maturity (% Ro)		0.85%	1.15%	1.15%	0.85%	1.15%
	Clay Content		Medium	Medium	Low/Medium	Low/Medium	Low/Medium
Resource	Oil Phase		Oil	Condensate	Condensate	Oil	Condensate
	OIP Concentration ($MMbbl/mi^2$)		60.4	19.0	6.1	13.2	4.1
	Risked OIP (B bbl)		39.7	7.4	6.3	5.0	0.3
	Risked Recoverable (B bbl)		1.98	0.37	0.32	0.25	0.02

Figure 3: EIA, shale oil reservoir properties for the Netherlands (U.S. Energy Information Administration, 2013)

2.1.1 Initial Assessment of Formations & Areal Extents

The resource assessment begins with the compilation of data, from public and confidential property related to the formations. Based on this information an initial indication was obtained for the location of potential shale oil plays worthy of further investigation. After the initial investigation, a sequel study on the available technical literature provided additional information on the following parameters:

- Depositional environment
- Depth
- Structure, including major faults
- Gross shale interval
- Organically rich gross and net shale thickness
- Total organic content
- Thermal maturity

Depositional environment: Provides a distinction between marine or non-marine shales. Clay content and brittle minerals, such as quartz, feldspar and carbonates vary among the different depositional environments. Non-marine shales tend to have a higher clay content and therefore are less favorable than marine shales. A ternary diagram shown in Figure 4 is used to display the shale mineralogy within various formations.

Depth: The prospective shale formation should not be less than 1,000 meters but not deeper than 5,000 meters. Areas shallower than 1,000 meters lack reservoir pressure and below 5,000 meters tend to have risks of reduced permeability and higher drilling and production costs.

Gross shale interval: Minimum thickness of seven meter gross shale interval is required

Total Organic Content (TOC): A minimum of two percent TOC is required for further evaluation.

Thermal maturity (R_0): Oil-prone prospective areas are required to have a thermal maturity within the range $0.7\% < R_o < 1.0\%$. The influence of the burial depth on the thermal maturity has not been investigated.

Geographical location: Is limited to onshore basins.

Each formation is assigned a risk factor based on the clay content and the geological complexity. When a prospective area has a high risk factor it is excluded from further evaluation. After evaluation with the above properties approximately half of the initially identified area is accepted as prospective shale play.

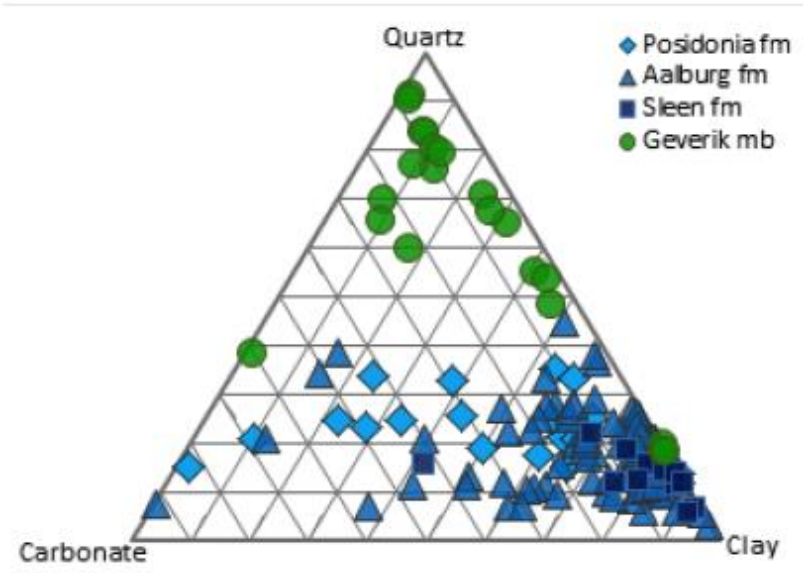

Figure 4: Ternary diagram showing the relative contents of quartz, carbonates and clay minerals of four prospective shale oil formations in the Netherlands (Bouw et al., 2012)

2.1.2 Shale Oil-in-Place Estimation

The next step of the evaluation method is to estimate the Shale Oil-in-Place. This process is governed, to a large extent, by two key parameters, the net organic-rich shale thickness and the oil-filled porosity. Besides these characteristics, pressure and temperature are important to determine the volume of gas in solution, defined by the formation volume factor.

Net organic-rich shale thickness: Is obtained from the net-to-gross ratio. The overall geologic interval including the organically-rich shale is derived from stratigraphic studies. The gross organically-rich shale thickness is obtained from log data and cross-sections. Barren rock within this gross thickness is accounted for by a net-to-gross ratio based on the organic richness of the shale. Furthermore a net-to-gross ratio is used to estimate the Net organic rich shale thickness.

Oil- and gas-filled porosity: Is determined by assembling porosity data from public literature. If this is not available, a comparison study based on mineralogy and maturity is carried out to compare the shale to U.S. shale plays. It is assumed that pores are filled with oil, including solution gas, free gas and residual water.

Pressure: Is mainly used to identify over pressured reservoirs, as these are able to produce a larger amount of the oil before bubble point is reached. When pressure data is not at hand a gradient of 0.433 psi/foot is assumed.

Temperature: Data related to the temperature of the reservoir is obtained from actual temperature data and when this is not at hand a 1.35 ºF per 100 ft and 60 ºF surface temperature is used.

All these parameters combined result in the following formula for oil-initially-in-place

$$OIP = \frac{7758\ (\ A * h) * \emptyset *\ S_0}{B_{oi}}$$

Equation 1: Formula to calculate oil-initially-in-place

OIP	oil-in-place (bbl)
A	area in acres (with the conversion factors of 7,758 barrels per acre foot)
h	net organically-rich shale thickness, in feet
$\emptyset$	porosity, dimensionless
S_0	fraction of the porosity filled by oil, dimensionless
B_{0i}	oil formation volume factor used to adjust oil volume in reservoirs to stock-tank barrels. Determined by standard reservoir engineering methods (Ramey, 1964; Vasquez et al., 1980) or estimated from correlations (McCain, 1990).

2.1.3 Risked Oil-in-Place Formulation

Prior to establishing the TRR, Success/Risk Factors for each formation are assigned, as these are used to estimate the risked oil-in-place.

Play Success Probability Factor: Captures the likelihood that a significant portion of the formation is able to develop an attractive oil/gas flow-rate. This factor is expressed in percent and is 75% for the shale oil formations in the Netherlands.

Prospective Area Success (Risk) Factor: This combines a series of concerns that could downgrade a portion of a prospective area of development. Concerns are mainly related to the subsurface such as low thermal maturity (R_0 < 0.8%) or high structural complexity (faults etc.). Furthermore this factor captures the uncertainty which is significant due to the sparse amount of geologic/reservoir data available. Increasing this factor can be realized by carrying out more rigorous exploration (EIA, 2013). For the Netherlands this factor is estimated to be 60%.

From the success and risk factor a single composite success factor is calculated by multiplying the play success probability factor (75%) by the prospective area success factor (60%). This composite success factor, 45% for the Netherlands, will be used for the calculation of the risked OIP.

2.1.4 Technically Recoverable Resources (TRR)

TRR is obtained by multiplying the risked OIP by a shale oil recovery factor. This recovery factor takes into account the geological inputs such as mineralogy of the shale for stimulation strategies, the presence of micro-scale natural fractures, etc. Shale formations can be roughly divided into two main classifications, shales with high percentage of quartz and carbonate, and shales with a high clay content. The latter tend to be more ductile and are likely to deform instead of shattering when pressure is increased with injection. This difference in behavior on pressure increase and the ability of the shale to fracture has a massive impact on the implemented stimulation methods. Furthermore, the rock formation incorporates the pressure regime such as over-pressure. In the EIA study three recovery factors have been assumed depending on the rock properties.

Favorable oil recovery: This is classified as a recovery efficiency factor of 6% of the risked oil-in-place and used for formations that have a low clay content, a low to moderate geologic complexity and favorable reservoir properties such as over-pressured shale and high oil-filled porosity.

Average oil recovery: Is classified as 5% recovery of the risked oil-in-place and applicable for reservoirs with medium clay content, moderate geologic complexity and average reservoir pressures.

Less favorable oil recovery: Is 3% recovery factor of the risked oil-in-place for formations with medium to high clay content, moderate to high geologic complexity and below average reservoir pressure.

In the literature the importance of the Stimulated Reservoir Volume (SRV) has been introduced in order to obtain a realistic recovery factor (Jin et al, 2013; Wan et al, 2013). Lowering the fracture spacing is one of many methods available to enlarge the SRV but finding the most efficient hydraulic well stimulation method is greatly dependable on the mineralogy and other reservoir properties of the shale formation. The desired stimulation method regarding shale gas development for Dutch formations has already been discussed in Noordoven (2012) and Kee (2010). With newly acquired data from the present study a better insight into the shale oil potential could be obtained. In order to summarize the aforementioned methodology it is displayed in the flowchart of Figure 5.

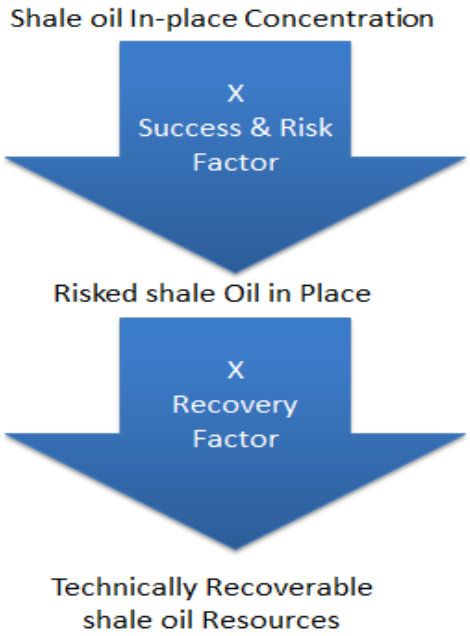

Figure 5: Flowchart of evaluation of potential shale oil formations by the EIA

2.2 Discussion of the Methodology

The scope of this study is to provide a more in-depth understanding of the shale formation properties that affects the producability. Therefore the EIA methodology will be analyzed in detail for the Dutch subsurface shale oil resources.

In the evaluation process the risked shale oil-in-place is multiplied by a play success probability factor of 75% and a prospective area success factor of 60%. Combined, this results into a composite success factor of 45%. These numbers could not be verified nor could any source could be found. It is assumed that these values are based on the knowledge of Advanced Research Institute (ARI), the authors of the EIA report. In Appendix A.1 all risk and success factors for various formations of the Netherlands are listed. Aside from the play area, the success factor and the success probability factor, the recovery factor largely influences the outcome of the TRR. Analogue values for recovery factor estimations are conducted from a database provided by ARI. The Advanced Resources proprietary data base consists of 28 tight oil plays in seven U.S. shale and tight sand/lime basins. In APPENDIX A.2 data regarding the properties influencing oil recovery such as the reservoir pressure, the thermal maturity and the formation volume factor of the 28 formations of the United States are listed. APPENDIX A.3 provides values of the oil recovery factor for each formation.

3 Shale Plays

The Netherlands contains several oil and gas plays and among these fields is one of Europe's largest onshore oil fields (Schoonebeek) and a giant gas field (Groningen). Several of the oil plays are located in the West Netherlands Basin (WNB), that extends into the Roer Valley Graben (RVG) in the Southeast. The geographical location of the WNB and other surrounding formations is displayed in Figure 6. In general it is accepted that the Posidonia shale formation acted as source rock and charged most of the oil fields in the Netherlands. Aside from the existing oil fields within the WNB, several sources (EIA, 2013; Bouw et al., 2012; Van Balen et al., 1999) report the WNB and the RVG to contain a series of oil-prospective shale formations. Understanding the general geological setting and structures of the various formations is essential to analyze the potential of these plays.

3.1 Geological History

The majority of the Dutch onshore oil fields are located within the WNB and the same basin appears to harbor shale oil prospects (Bouw et al., 2012). The WNB, part of a Late Jurassic/Early Cretaceous transtensional system is located in the central part of the Netherlands. It is bounded by the London-Brabant Massif in the South, and merges in the south-east with the Roer Valley Graben. the Zandvoort Ridge / IJmuiden High separates it from the Central Netherlands Basin and the Broad Fourteens Basin in the North (Van Adrichem Boogaert et al., 1997). In general the WNB is described as a single structural entity, however it actually contains a number of smaller elements, bounded by long, northwest-trending faults. The faulting inside the WNB and the surrounding structural elements are shown in Figure 6. The deposition and evolution of the basin during the Late Carboniferous to Tertiary can be divided into four sub-phases as indicated on the stratigraphy chart in Figure 7 (Van Balen et al., 2000).

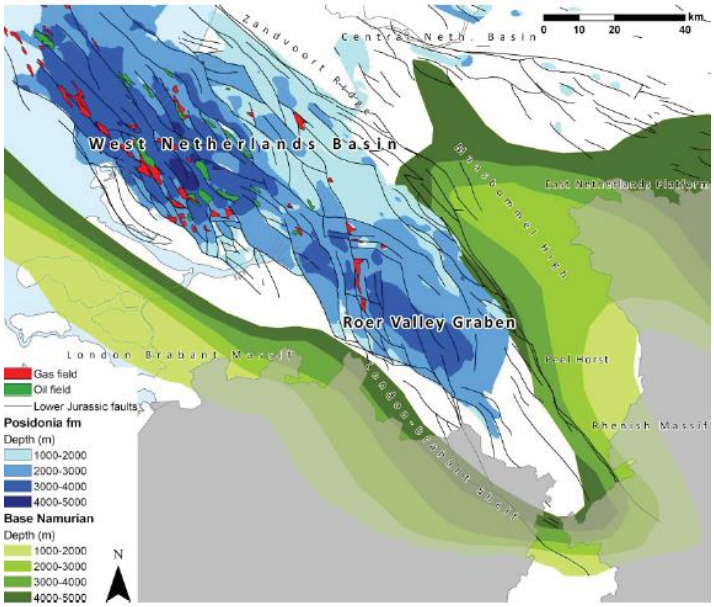

Figure 6: The West Netherlands Basin and surrounding structures (Bouw et al., 2012)

During the Carboniferous and Permian the supercontinent Pangaea was completed. As part of this process colliding continents formed mountain ridges leading to a decrease in continental crust and an increase in oceanic crusts. Consequently the potential ocean water storage volume increased, resulting in a sea level drop in this time period (Berendsen, 2004). In Northwestern Europe shallow-marine, continental basins followed by a swampy environment were mainly filled with fine-grained material from Variscan mountains. During Late Carboniferous-Early Permian, the Mesozoic WNB developed upon the Variscan origin Campine. This was followed by uplift, which occurred especially for the Zandvoort Ridge (De Jager et al., 2007). After the uplifting erosion took place during the Westphalian D to Early Permian. This resulted in a succession of a basal organic-rich shale and coal-bearing strata (Van Adrichem et al., 1997).
The continent Pangaea started to break up during the Mesozoic. The Early Triassic was characterized by regional thermal subsidence in which the WNB formed northwards-dipping basin. During the Middle and Late Triassic the WNB formed a large-scale half-graben bound in the North by a major fault zone.
Rifting ceased in the Netherlands from the Middle Triassic onwards, but continued in this time period between Greenland and Scandinavia resulting in the opening of the Central Atlantic Ocean. Following regional subsidence and a relatively quiet period during Late Triassic and Early Jurassic in which some faulting occurred in the Dutch Central Graben, a wide epicontinental sea developed (De Jager et al., 2007). Consequently, locally over 1,800 m of fine-grained clastics of the Altena Group were accumulated, including the Posidionia organic-rich shales during the Early Jurassic. During the Middle Jurassic a great part of the Dutch offshore was uplifted and sedimentation was restricted to specific areas (De Jager et al., 2007). Rifting occurred again in the Middle Jurassic along a North West – South East structural trend that divided the basin into different subunits, including the Broad Fourteens, West Netherlands, Central Netherlands, Vlieland Basins and RVG. This rifting process occurred in short discrete pulses, resulting in igneous activity that had a local impact on the maturity of the organic matter (Van Balen et al., 2000).

During the Late Cretaceous and Paleocene inversion-related uplifting of basins evolved from exerted stresses from the Alpine Orogenic system. The uplift created by these tectonic events led to the thinning or erosion of deposits in the Upper Cretaceous chalk and Lower Tertiary clastics (De Jager et al., 2007). The compressional stresses resulting in reverse faulting have formed many of the trap structures of the oil-bearing formations in the Netherlands (Van Balen et al., 2000). In the Maastrichtian-Danian period sediments accumulated on the WNB and the inversion movement stopped. Uplift occurred again during the Eocene-Oligocene, during which a large amount of the Paleogene sediments were removed (Van Balen et al., 2000).
Currently the majority of the North Sea area is still subsiding and the south-eastern area is uplifted by the Rhenish Massif (De Jager et al., 2007).

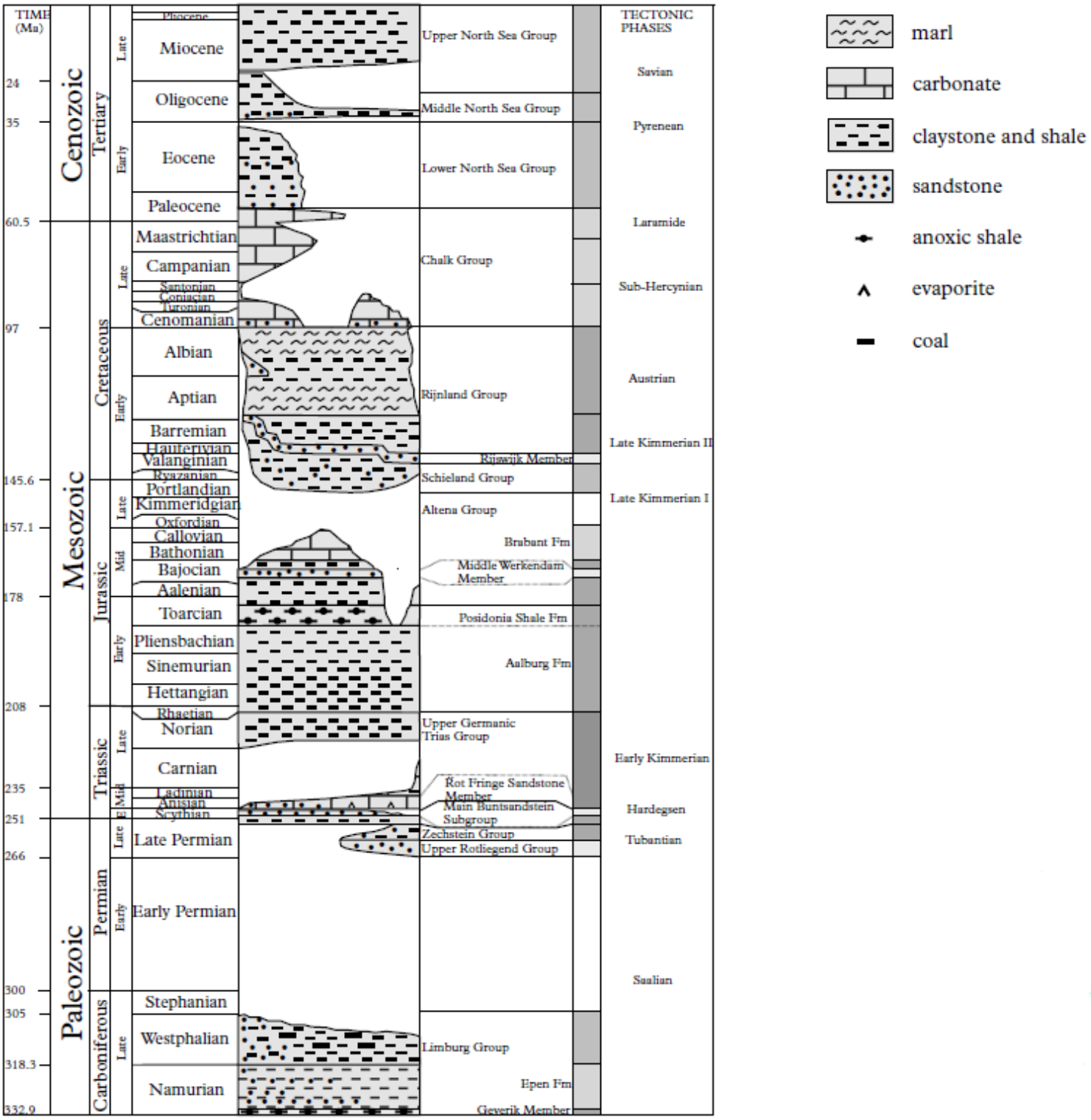

Figure 7: Stratigraphy of the West Netherlands Basin (Van Adrichem-Boogaert et al., 1997)

4 Key-Properties for Productive Shale Oil Plays

Within this section an introduction is given for the production from shale formations. In addition parameters will be introduced for the evaluation of shale formations.

4.1 Shale Oil Production

Within the last decade the technology for shale oil production has significantly developed, changing shale formations into viable plays. Before this leap forward in technology shale formations were not considered as reservoirs. Often shale was indicated as a cap rock for conventional plays because of its low matrix permeability. The combination of two production related elements made shale oil economically attractive and lead to an increase in the interest in shale oil formations (Chaudhary et al., 2011).

Firstly, the technology for horizontal drilling improved. This technology allows to create long horizontal well trajectories in those layers that are best suited for subsequent stimulation to increase production.

Secondly, new technology allowed to create multiple transverse hydraulic fractures from horizontal wells. This is essential for production, as typically the permeability of the rock matrix in shale formations is very low.

A combination of long horizontal wells and artificial fractures is fundamental for the production from shale oil formations. The purpose of both elements is to increase the connection between the reservoir rock and the wellbore. The total rock volume connected with the wellbore is called the Stimulated Reservoir Volume (SRV). It is the combination of the natural fracture network (if present), the wellbore exposure and the hydraulically induced fracture network. Both horizontal well placements and hydraulically induced fracturing result in an increase in SRV (Clarkson et al., 2010). Creating a complex fracture network is a function of the geomechanical properties of rock formations and the reservoir stresses. The artificial fractures are created by pumping a fluid under high pressure into the perforated horizontal well. The perforations allow communication between the fluid, loaded with proppants (ceramic balls or sand that are pumped into the fracture to prevent it from closing), and the reservoir rock. The pressure is increased by pumping fluid from the surface downhole and when sufficient pressure is applied from the wellbore to the shale formation can create fractures. Ideally the fracture remains open due to the proppant loading and therefore creates a highly permeable pathway.

The rock properties related to fraccing can be measured with the index of brittleness (Mullen et al., 2012). Brittleness of a formation influences the ability of a rock to propagate induced fractures and is measured as the Brinell Hardness. In previous work various rock mechanical properties of Dutch onshore formations were measured and compared with U.S. shale samples (Noordoven, 2012). Most of the Posidonia samples plot as soft shales by comparison with the U.S. shales, although some of the samples plot within the brittle area as shown in Figure 8. Only relative brittle rocks are considered suitable for fraccing.

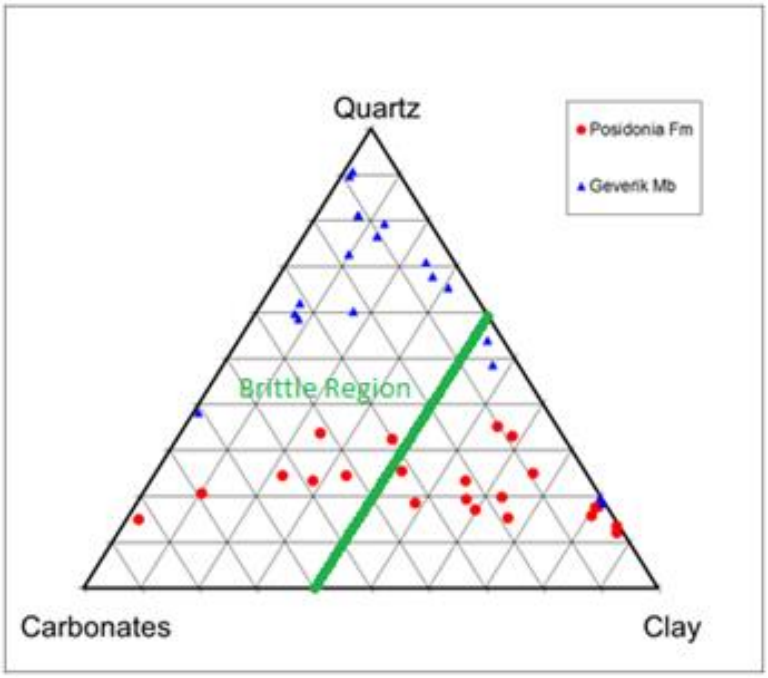

Figure 8: "Brittle Region" in a ternary mineralogical diagram after Rickman et al. (2008)

4.2 General Properties of Shale Oil Formations

Conventional methods for reservoir evaluation are not applicable for shales as they provide unreliable and faulty measurements. Therefore researchers worldwide are currently investigating petrophysical methods that are more appropriate for shale formations. Understanding the characteristics of a low-permeability reservoir systems is essential in identifying, characterizing and exploring shale oil plays (Blasingame, 2008; Clarkson, 2010).

Production of liquid hydrocarbon from organic shales depends on porosity, hydrocarbon saturation, pore pressure, matrix permeability and hydraulic fracture surface area as well as fracture conductivity (Rylander et al, 2013; Aguilera; 2013; Chen, 2013).

In order to analyze shale oil plays, sample material from the Netherlands is analyzed on total organic carbon, maturity, pore size and shape, porosity, permeability and fluid storage as well as flow mechanism. In the following sections the essence and applicability of these parameters will be explained.

4.2.1 Total Organic Carbon and Maturity

The viability of each play, conventional or unconventional, depends on the quality of the source rock. A source rock is defined as fine-grained organic-rich rock that is able to generate oil under the right pressure and temperature conditions (McCarthy et al., 2011). Besides the volume of the source rock, which is not taken into account here, the organic richness and thermal maturity determine the hydrocarbon-generating potential (Passey et al., 2010; Chen et al., 2012).

Organic richness is a parameter that refers to the amount and type of organic material present within a rock. The volumetric percentage of the organic material is defined as TOC, and a source rock's exposure to heat over time is referred to as thermal maturity.
Organic material is commonly analyzed with a Van Krevelen diagram, displayed in Figure 9. Within this illustration the organic matter is divided into four different kerogen types and three maturity ranges. A Van Krevelen diagram illustrates the maturing process of kerogen. This diagram allows to determine whether a certain analyzed rock sample has hydrocarbon generation potential (McCarthy et al., 2011). Within a shale oil formation organic content consist of bitumen and kerogen, which both have a different hydrocarbon generating potential. Bitumen is a soluble organic matter with high viscosity and a large molecule size. Kerogen is an insoluble material that consist of a mixture of organic chemical compounds that occur in source rocks. Kerogen has a relatively high molecular weight compared to bitumen and can be transformed into mobile hydrocarbons during the maturation process.
A four type Kerogene classification is often used to assess the quality of a source rock (SLB, 2013).

Type I kerogen is derived from algal plankton and is predominantly generated from lacustrine environments. Depending on its thermal evolution it can be oil-prone.

Type II kerogen is derived primarily from the remains of plankton that have been reworked by bacteria and is typically generated in reducing environments found in moderately deep marine settings. This type of kerogen is rich in hydrogen, low in carbon and therefore can generate liquid hydrocarbons and gas. This type is commonly found in the North Sea.

Type III kerogen is derived from terrigenous plant debris that is deposited in shallow-, to deep-marine or non-marine environments. It does not have a large liquid hydrocarbon generating potential and is mostly known to generate gas.

Type IV kerogen is generated from older sediments being reworked after erosion. The residual matter contains a high carbon content and is hydrogen-poor. This type has almost no potential in generating any oil or gas.

The generation of oil and gas dependents on the amount of hydrogen present within the kerogen because generation of oil ceases if the kerogen is depleted in hydrogen. Therefore, the hydrogen-rich kerogens (type I and II) are favorable for hydrocarbon generation. Determining the amount, type and thermal maturity of organic matter present in a rock is used to assess how much, when and what kind of petroleum might have been generated. Because carbon is an essential element of any organic compound, the organic richness of a rock can be assessed by measuring the organic carbon content (McCarthy et al., 2011). To conclude, the oil and gas potential of a formation is related to the carbon content and for this reason identified as a crucial property for the evaluation of a shale play. This property is evaluated with the Thermo Gravimetric Analysis (TGA) explained in section 5.6.

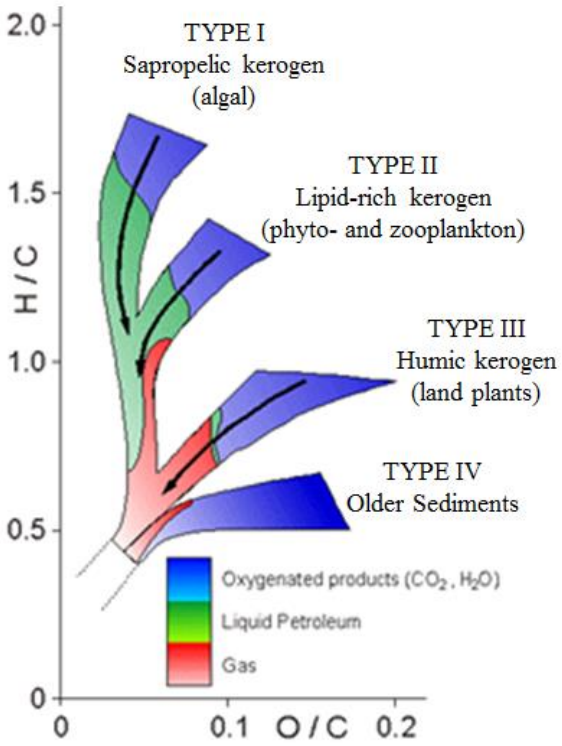

Figure 9: The Van Krevelen diagram with the pathways for hydrocarbon generation. The arrows indicate an increase in thermal maturity

4.2.2 Pore Size and Shape

The microstructure, and in particular the pore space size and geometry, influences the ability of a formation to store and produce liquid hydrocarbons (Curtis et al., 2013). Pore space is a void within a rock that can contain air, water, hydrocarbons or other fluids. Storage and transport of the oil is controlled by the microstructure of the rock (SLB, 2014). Pore size is defined as the average of the minor axis of an ellipse which is fitted to match the geometry and total surface of the pore. This is explained in detail in section 6.2.1.

Based on the pore throat apertures, defined as the smallest opening between two adjacent pores, the flow potential and storage capacity of porous media can be estimated (Aguilera, 2013; Chen et al., 2013; Ziarani et al, 2011; Blasingname, 2008). In addition, Aguilera (2013) has developed a method, mainly for conventional formations, to estimate the permeability of shale oil formations based on pore throat apertures and porosity. In Figure 10, the porosity and pore throat aperture is used to obtain permeability results. In shales pore throats are often too small to be identified and therefore the pore size had been used instead. Pores present in the rock matrix are divided in megapores (d > 10 microns), macropores (2.5 – 10 microns), mesopores (0.5 – 2.5 microns), micropores (0.1 – 0.5 microns) and nanopores (0.01 – 0.1 microns).

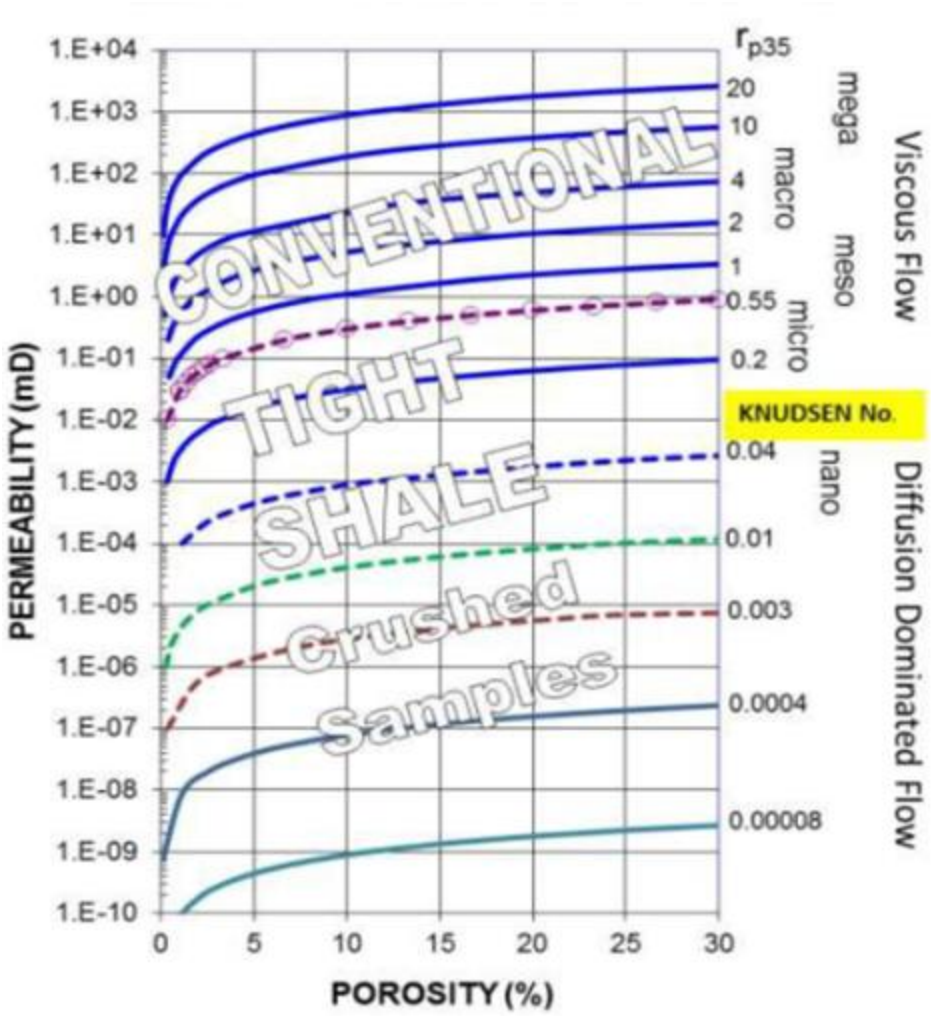

Figure 10: Flow types as a function of pore throat apertures, porosity and permeability. The right y-axis is in micrometer. Source: GFREE Research Team, U of Calgary, 2013

Oil and gas have different molecule sizes that can result in different relative permeability measurements. It is possible that the size of the oil molecules exceeds the size of the pore throats in an organic shale systems (Nelson, 2010). Figure 11 illustrates the different sizes of molecules, varying from methane (0.0004 microns), to heavy oil (0.010 microns). In general, pores larger than 1 – 2 microns are needed for oil molecules to flow through the rock matrix (Bohacs et al., 2013). To obtain an better understanding of the influence of molecule size on the pore throat aperture within shales, shale rock samples are evaluated with different gasses and fluids to account for the various molecules sizes. The Scanning Electron Microscope (SEM) is used to identify the different pore sizes, shown in section 5.2, with the results given in chapter 6.

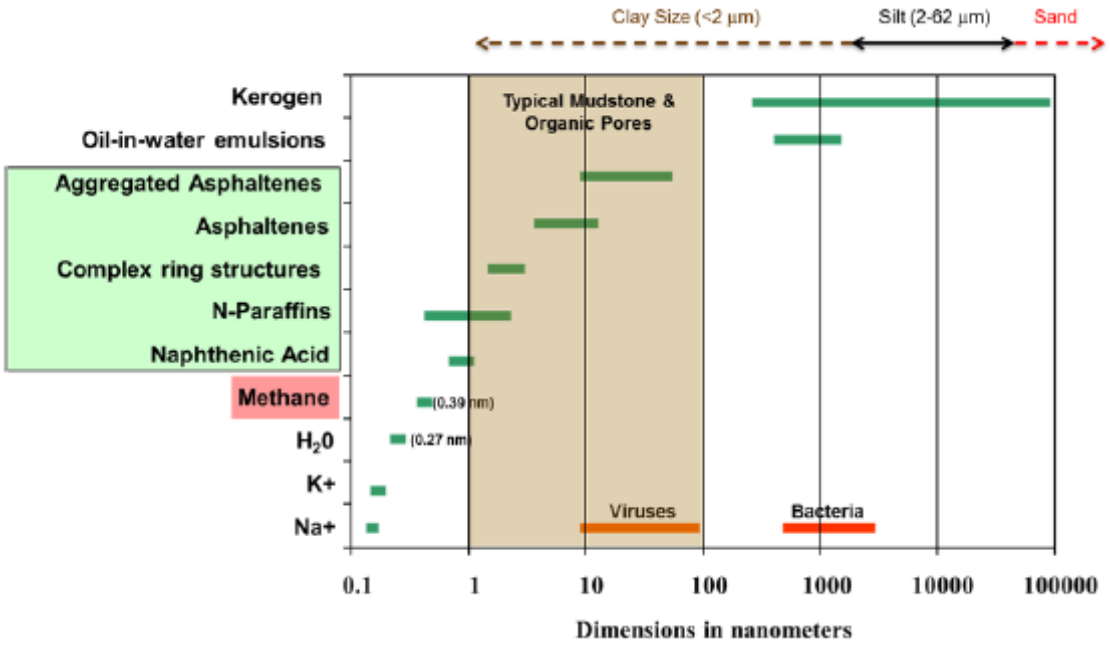

Figure 11: Comparison of the size of various molecules. Compounds of black oil are larger than methane and water molecules after Momper (1978)

4.2.3 Porosity

Porosity is a fundamental property for reservoir rock evaluation and provides a measurement for the rock to store hydrocarbons. Various types of porosities occur within a shale, and fluids can reside in combinations of inter-granular, intra-granular, inter-crystalline, intra-kerogen and intra-pyrobitumen / char pores or fractures (Bohacs et al., 2013). Development of different pore types is however to be a function of the thermal maturity of the rock and, especially, the development of secondary nano-porosity in the organic matter. Therefore this has an effect on shales, that are dominated by organic matter (Curtis et al., 2010). In Figure 12, a SEM image of a section of the Barnett Shale is used to illustrate the presence of porosity in organic matter, intra-organic porosity. So for shale oil analysis it appears to be sufficient to distinguish the total porosity from the effective porosity. Total porosity is defined as porosity of both isolated and connected pores. Effective porosity only includes the interconnected pores (Rylander et al., 2013).

Porosity is evaluated with both the SEM methodology explained in section 5.2 and the Gas Research Institute (GRI) experiment explained in section 5.4.

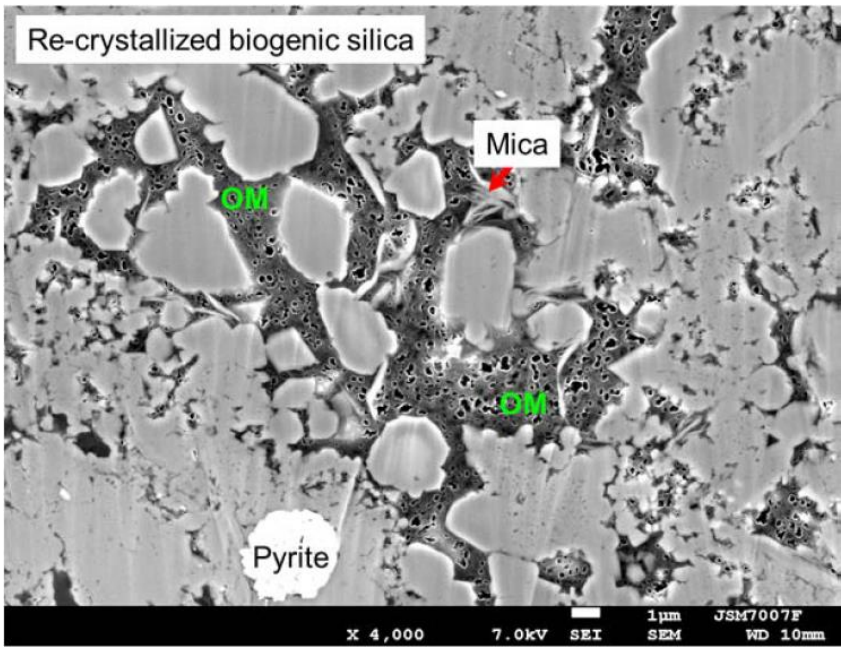

Figure 12: 1 µm scale SEM Image of a Barnett shale. The majority of porosity is located in organic material. The organic matter is the black area in this picture. The porosity are the slightly darker smaller areas located within the organic matter mostly surrounded by a grey/white perimeter line (Bohacs et al., 2013).

4.2.4 Permeability

Permeability is a measure of the flow potential of a rock. Although the initial production from shale formations usually originates from induced fractures, the matrix permeability is important to charge these fractures after initial production.

Measurements of the permeability are complicated due to the low values, in the order of micro-to-nano-Darcies in shale formation. For this reason little has been done to study oil flows in shales, and measurements can be affected by a systematic error (Wang et al., 2010). Overall reservoir permeability accounts for both the matrix and natural fracture characteristics. Matrix permeability and natural fracture characteristics are a function of the original depositional composition, the texture, the bedding, the stratal stacking and the burial history. Fracture characteristics also depends on the burial history (Bohacs et al., 2013).

Because shale permeability is an extrinsic property of a rock, significant differences can be observed between the in-situ permeability and laboratory permeability. An intrinsic property is a property of a material and is independent on the form of the sample. An extrinsic parameter however can vary depending on the methodology and the sample size used. In other words, the result of the permeability measurement can change when the laboratory set-up, for example the confining pressure on a sample, is changed (Rosen et al., 2014).

In this study, the permeability is measured with the GRI gas method explained in section 5.4 and the steady-state flow experiment explained in section 5.5.

4.2.5 Fluid Storage and Flow Mechanism

Essential for any type of reservoir is its ability to store and flow liquids in the rock matrix. Shale rocks are typically characterized by their low permeabilities and small pore radii that result in a poor connectivity within the formation (Oleas et al., 2010). The water or hydrocarbons present in the shales are stored in a variety of local micro-environments that include structures such as pores in the mineral matrix, clay surfaces, pores in kerogen, etc. (Handwerger et al., 2012). Understanding the different methods to contain and store liquids in a formation is essential for the evaluation of the production potential. With several experiments the total amount of liquids in samples can be determined and subdivided into different categories. These categories, clay water, tightly bound capillary liquids and free movable liquids are briefly explained following Rylander et al. (2013).

Clay bound water is a fraction of water that is bound in unconventional rocks with mostly a high argillaceous content. This liquid can be considered part of the rock matrix instead of a fluid within a pore network because it is completely immobile.

Capillary trapped fluids are trapped within minerals and solid organic matter. They are trapped by the small pore radii and interfacial tensions within the rock matrix and, therefore. not easily produced. In general the trapped fluids reside in various pores through the entire maturity range. The pore may be occluded with a second fluid or may contain a very viscous material, such as bitumen and heavy oil, which prevents the fluid from moving.

Free fluids reside in pores large enough to accommodate fluids not affected by capillary pressures and molecular forces. Most of these pores are intergranular or intragranular within the shale oil formations.

Both clay bound water and trapped fluids are considered as non-producible but in addition free fluids are not producible if they are trapped in a pores with pore throats smaller than the fluid molecules.

Understanding the flow behavior of shale is complex. Production analysis is complicated by formation- and fluid-related properties. Particularly viscosity is key to evaluating potential fluid flow. Little is known about the fluid composition within shale plays in the Netherlands and, therefore, the focus of this study will be on investigating the ability of rock samples to flow any fluids. Identifying flow regimes will at this stage not be crucial to evaluate the potential of formations. This property is analyzed with the nuclear magnetic research T_2 method explained in section 5.3.

5 Data Acquisition and Laboratory Methodology

In this section the data acquisition and the laboratory methodology are outlined. The core selection method is introduced and the experiments used to evaluate the various parameters are explained.

5.1 Core Material

The focus of oil companies operating in the Netherlands has predominantly been on conventional oil & gas plays and consequently shale formations were rarely cored. For the planned experiments both core plugs and chips are needed for proper evaluation, but the choice was therefore quite limited.

EBN had made a for the SHAle PErmeability (SHAPE) project. SHAPE is a joint industry project that aims to develop new methods to measure the permeability of shale rocks (SHAPE, 2014). As part of SHAPE a selection of 36 samples have been made from cores of 12 different boreholes. The cores were stored in core storage of TNO and the Nederlandse Aardolie Maatschappij (NAM). A list of the selected samples for the SHAPE project and the available type of sample material is shown in Appendix B.1.

Shale formations are known to be heterogeneous and therefore a sufficient number of samples needs to be tested to obtain a representative static of a shale formation. Within SHAPE both the Aalburg and the Posidonia shales are evaluated. Based on the results of previous studies, the source rock capacity, the amount of core material available per formation, the duration of the experiments and the amount of experimental data collected, only the Posidonia formation is selected to be evaluated in the present study.

In total, 14 samples from seven different boreholes of the initial 36 samples of the SHAPE project have been used for experiments. The location of the seven wells is indicated in Figure 13 and Figure 14, and the name of the wells with the associated numbers of the samples is listed in Table 1. The depths of the samples range between 1,051.5 meters and 3,062.5 meters.

Plugs are taken from larger cores provided by NAM and TNO, but not for every core it was possible to take a plug due to heavy laminations in the rock. For some cores, mainly of low permeability, the release of pore pressure during coring can result in enhancement of existing fractures or delamination along bedding planes. If possible, plugs were drilled perpendicularly to the core axis. The preferable plug size is 1.5 inch (3.81 cm) in diameter. The length is variable because of the broken laminations within the core. Because most of the plugs were heavily fractured while being drilled, additional square blocks of core where sanded down to a plug size. This method was used with success as it applied minimum shearing and tensile forces to the sample.

Core chips are made by crushing pieces of core rock. The crushed rock was sieved to the desired chips diameter size range of $500 < \mu m < 750$.

During the experiments the chips have been tested under three different conditions: "as-received", wet and dry. "As-received" is the condition of the chips before any pre-processing, i.e. an ambient condition. The wet condition involved a time-consuming process of wetting the material by placing the chips in a humidity chamber containing 92% NaCl fluid. Weight increase was continuously measured during the process of the chips absorbing water until an equilibrium was reached. On average the wetting process took about 3 – 5 days. The samples were tested immediately after the wetting was finished in a concealed space to ensure the preservation of the material conditions. A similar methodology was used to prepare for "dry" conditions, using a laboratory oven set to 100 ºC. The weight of the chips was measured during the drying process until no further weight loss occurred. The duration of the drying process was about 3 – 5 days. When samples were not involved in either the drying or wetting process, they were kept in a desiccator to minimize changes in sample conditions.

In addition to the selected samples from the SHAPE project, five different bags of Posidonia drill cuttings from an offshore well, obtained on March 2014, were tested. The cuttings were sampled in ten meter intervals between 3,020 and 3,070 meters depth. Furthermore additional core samples were taken from the HLM-1 well (EBN 20), as this was identified as a promising interval according to SHAPE results. Overall, this project has benefited greatly from measurements of the SHAPE project.

Lab Sample number	**Depth(MD)**	**Well**	**Year Drilled**	**Lab Sample Number**	**Depth(MD)**	**Well**	**Year Drilled**
EBN 19	1675.8 m	ZOM – 2	1957	EBN 26	2510.0 m	LOZ – 01	1952
EBN 20	1051.5 m	HLM – 1	1951	EBN 27	1429.0 m	VLM – 01	1994
EBN 21	1718.0 m	AND – 02	1953	EBN 28	1675.0 m	ZOM – 02	1957
EBN 22	3062.5 m	BRK – 02	1951	EBN 29	1677.5 m	ZOM – 02	1957
EBN 23	3062.5 m	BRK – 02	1951	EBN 30	1678.0 m	ZOM – 02	1957
EBN 24	3074.0 m	BRK – 02	1951	EBN 32	1233.0 m	ZWE – 01	1952
EBN 25	2509.5 m	LOZ – 01	1952	EBN 35	1242.5 m	ZWE – 01	1952

Table 1: Data of samples used in this study

Figure 13: Area of interest for sample material and location of well ZWE-01

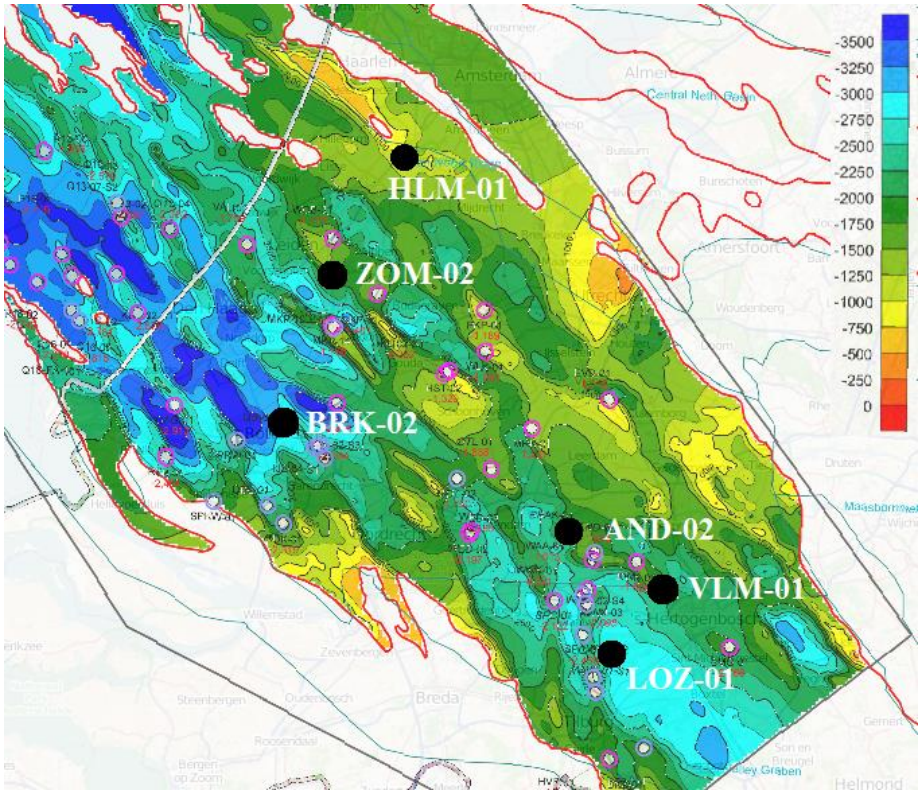

Figure 14: Well locations displayed on a depth contour map of the top Posidonia formation (NuTech, 1950). Note that well ZWE-01 is not displayed on the map due to its geographical location (see Figure 13)

5.2 Scanning Electron Microscope (SEM)

The SEM used to visualize the pores structure of the samples was a Hitachi SU-70 FEB SEM and all the specifications can be found in Appendix B.2. Commonly backscattered electron images (BSE) and secondary electron images (SE) are obtained from the SEM. BSE images shown in Figure 16, are used in this project for the identification of the non-mineralogic content (pores and organic carbon). SE images, shown in Figure 17, are used in this project for the identification of the open pore space.

The principle method of a SEM is based on firing electrons with a high kinetic energy towards a sample surface. To obtain this high kinetic energy electrons are accelerated from an electron gun using high voltage electromagnetic lenses and scan coils (Curtis et al., 2010). When the electrons hit solid material the decelerating process dissipates a variety of signals produced by electron-sample interaction. Among this variety of signals, secondary electrons (SE) and backscattered electrons (BSE) are most commonly used for imaging samples. SEM is utilized under vacuum conditions and because electrons are used to form the image, the sample is prepared and polished with a broad Fixed Ion Beam (FIB). A schematic drawing of the SEM method and set-up is shown in Figure 15.

Figure 15: Schematic drawing (Purdue University) of the working principle of a SEM and the used SEM setup at Durham University (www.dur.ac.uk).

For the subdivision of individual pores into pore classes, two image resolutions for the SEM have been used following a method by Anselmetti et al. (1998). The pore classes are divided in nanopores (0.01 – 0.1 micron), micropores (0.1 – 0.5 micron), mesopores (0.5 – 2.5 micron) and macropores (2.5 – 5 micron). SEM images of a resolution of 5 µm are used for the evaluation of nano- and micro-pores. For the identification of the meso- and macro-pores, SE and BSE images in the resolution of 5 µm and 100 µm are used. The utilized software is Fiji Is Just ImageJ, version 2014. This software is an open source Java image processing program, broadly used within the life sciences. Both SE and BSE SEM Images are analyzed with a thresholding process,

in which an image is evaluated on grayscales. An indication of the pore size diameter was obtained by fitting an ellipse over each pore and measuring its minor and major axis. The most important parameters of the images included the number of pores, the pore surface area, the perimeter and the minor axis. The images obtained with the SEM are used to measure the non-mineral content [%], the open pore space [%] and the pore sizes. The formulas for the calculation of the percentage parameters are suggested by Anselmetti et al. (1998) and shown in Equation 2.

$$\phi_{mic} = \frac{\sum Area_{mic}}{\sum Area_{tot\ image\ mic}}$$

$$\phi_{mac} = \frac{\sum Area_{mac}}{\sum Area_{tot\ image\ mac}}$$

$$\phi_{tot} = \phi_{mac} + \phi_{mic} * (1 - \phi_{mac})$$

Equation 2: Formulas used to calculate the porosity from SEM images

Φ_{mic}	Porosity from 5 µm scale images
Φ_{mac}	Porosity from 100 µm scale images
Φ_{tot}	Total porosity
$Area$	Identified pore area on a 5 µm or 100 µm scale image
$Area_{tot}$	Total Area of the SEM image

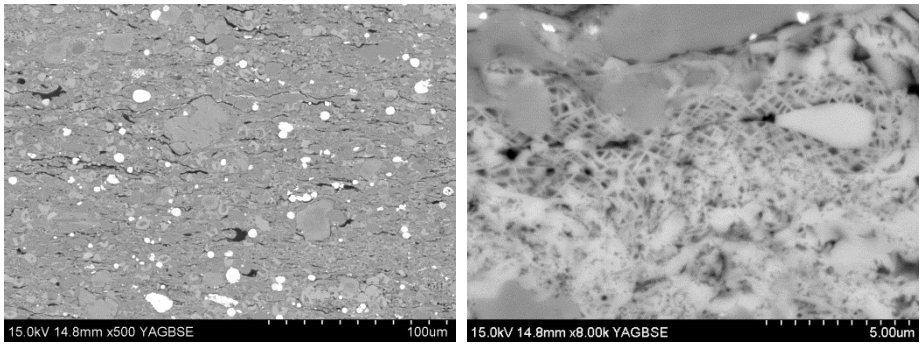

Figure 16: BSE images (EBN 23) on a 100 µm and 5 µm scale, in which TOC and open pore space can be obtained using a thresholding process.

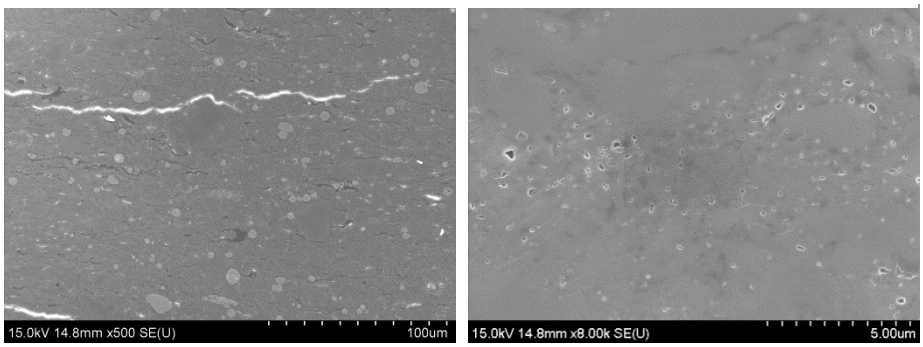

Figure 17: SE images (EBN 23) on a 100 µm and 5 µm scale. The open pore space is easier to identify on a larger magnification.

5.3 Nuclear Magnetic Resonance (NMR)

The NMR methodology can evaluate several reservoir related properties but within this project it is used for the indication of Free-Fluid Index & Bulk Volume, the pore size distribution and the properties of reservoir fluids.

NMR measurements are based on physical principles and for the correct interpretation the basic NMR concepts such as nuclear magnetism, polarization, T_1 relaxation time, pulse tipping, free induction decay, spin echoes, T_2 relaxation time and CPMG pulse sequences, are essential (Coates et al., 1999).

The measurements obtained by the NMR refers to the response of atomic nuclei (protons) to magnetic fields. The spinning proton creates a current loop with a magnetic field aligned with the spin axis. Therefore the hydrogen nucleus can be considered a bar magnet of which the magnetic axis is aligned with the spin axis of the nucleus. These hydrogen nuclei are in the absence of an external magnetic field randomly oriented as shown in Figure 18 (Coates et al., 1999).

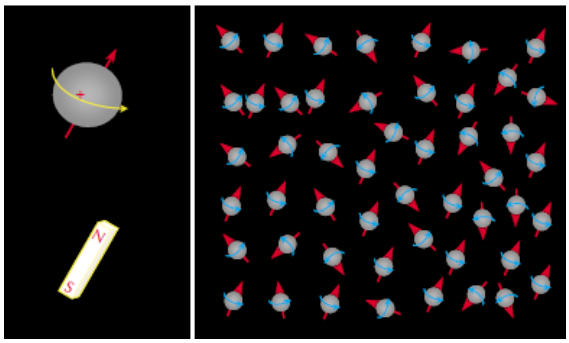

Figure 18: Hydrogen nuclei represented as a magnetic bar (left) and in absences of an external magnetic field, nuclear magnetic axis are randomly orientated(right) (Coates et al., 1999).

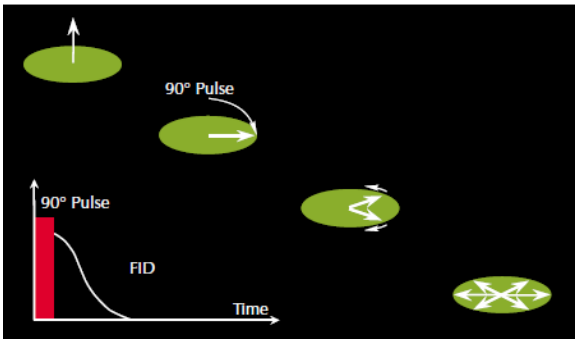

Figure 19: Application of a 90º B_1 pulse after which the proton start the diphase and a FID signal is measured (Coates et al., 1999).

The first step in making a NMR measurement is to align, or polarize, the spin axes of the protons in a particular direction. This is obtained by applying a static magnetic field (B_0) that exerts a torque on the nucleus to align the nuclear spin axis with the magnetic field.

After the axis are aligned, or polarization is completed, the second step is to tip these protons from their new equilibrium position. This is accomplished by applying an oscillating magnetic field (B_1) perpendicular to the initial magnetic field (B_0). The application of the magnetic field B_1 causes the protons to phase with each other and the change in energy state and in-phase precession caused by B_1 is called Nuclear Magnetic Resonance. As the B_1 field is subsequently removed, the protons tip back to the original direction in which the static magnetic field aligns them. This process is called dephasing and, as the process of losing phase coherency progresses, the net magnetization decreases. This usually exponential decay is measured and is called Free Induction Decay (FID). This process of dephasing is reversible when a 180º B_1 pulse is applied to the static magnetic field B_0 and the signal detected is called a spin echo (Coates et al., 1999). Spin echoes decay very rapidly but a 180º degree pulse rephases the magnetization components and therefore can create a series of spin echoes called a spin echo train. The process of creating and

measuring the echo is shown in Figure 19. The time between pulses is the inter-echo spacing (TE) and the pulse sequence of starting with a 90º pulse followed by a number of 180º pulses is called the CPMG sequence. The number of all the pulses in the pulse train is the number of echoes (NE). The amplitude of the spin echoes is recorded as a function of time and shows an exponential decay. This time constant of the transverse magnetization decay is called the transverse relaxation time, referred to as T_2. This property is used to indicated if the fluid is clay bound, capillary bound or free within larger pores. The observed echo train and its amplitude contains most of the petrophysical information and can be linked to the properties of the pore fluids in the samples.

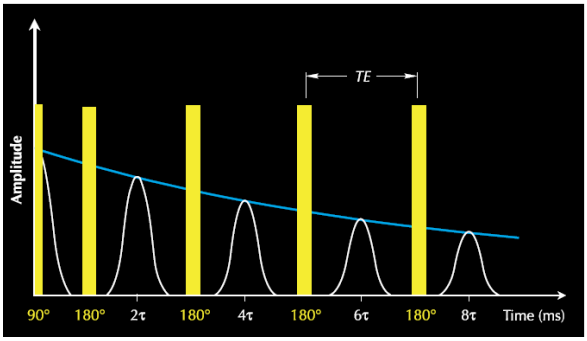

Figure 20: A spin-echo train created by multiple 180º B_1 pulses from the CPMG sequence. The blue line indicates the decaying amplitude of the exponential T_2 curve (Coates et al., 1999).

The longitudinal polarization time of the protons T_1, is an indication of the fluids present in a sample, because water, oil and gas have very different T_1 polarization times. This property indicates the degree of proton alignment as a function of the time that a proton is exposed to an external magnetic field.
In addition to the previous mentioned parameters the polarization time TW can be adjusted. TW is the time between measurements of two echo trains.

The NMR instrument used for measuring the samples is a MARAN Ultra Benchtop NMR Analyzer from Oxford Instruments. The raw data is obtained using the CPMG sequence for the measurement of T_2 and evaluated using the RINMR program. The resonance frequency, 2 MHz, number of scans (NS) is 1,000, the inter-echo spacing (TE) is 0.2 ms, the receiver gain (RG) is 100% and the Recycle Delay (RD) is 6 seconds. They are kept constant for both plugs and chips and obtained from the evaluation of shale in SHAPE. The data is analyzed using WinFit software packages with PETGAS constants for fitting of relaxation data into multiple or distributed exponentials.

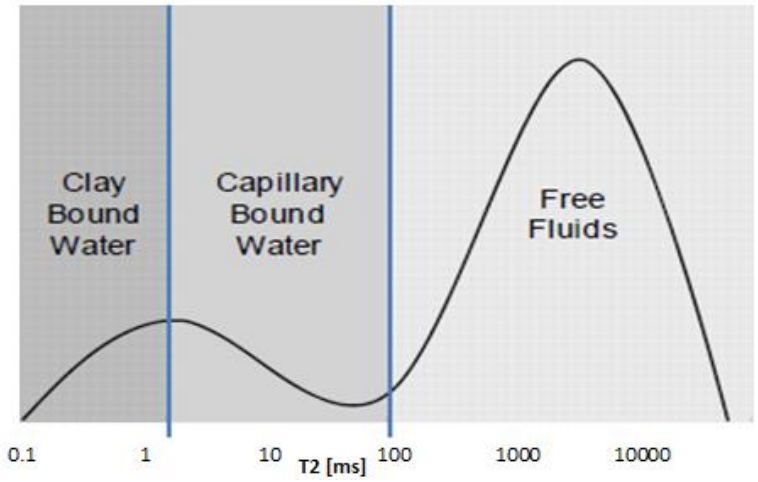

Figure 21: Typical NMR graph with lines indicating the differences in the fluid stages (Rylander et al., 2013).

This experiments were carried out under ambient conditions for selected chips and plugs. However, it was not possible to place the samples under any confining pressure. Sample preparation is necessary to ensure the same conditions throughout the experiment because during the measuring process the materials tend to heat up. Therefore, the plug is wrapped in plastic kitchen foil and the chips placed in a sealable glass jar, of approximately the same size as the plugs. Before and after the experiment the samples are weighted on a MENTOR electronic scale capable of measuring with an accuracy of 0.001 gram accurate. Excel calculations from the fitted data result in a graph of the normalized signal versus $T_{2,}$ from which the type of fluids in the sample can be analyzed, as shown in Figure 21.

Per sample the amount of fluid [cc] is calculated from a correlation based on the measured amplitude size, the number of scans, the weight of the sample and the hydrogen index as shown in Equation 3. This correlation was found as part of SHAPE by Carlos Grattoni from School of Earth and Environment, Leeds University. The formula was obtained after 24 calibration runs and used throughout SHAPE and therefore adapted for fluid volume calculation in this research.

$$FV = \frac{\frac{S}{NS} - 21.274}{194.82} * HI$$

Equation 3: Calculation of fluid in sample after the work of Grattoni, C.

FV	Fluid volume in sample	[cc]
S	Measured Signal Amplitude size	[-]
NS	Number of scans taken by NMR	[-]
HI	Hydrogen Index	[-]

5.4 GRI Method

This method was developed by the Gas Research Institute (GRI) to provide a quick experiment that can evaluate rock properties, such as the permeability and the porosity on various types of rock material including drill cuttings (Luffel et al., 1993). GRI measurements can be used on both plugs and crushed rock material and is based on Boyle's Law. This law describes the inversely proportional relationship between the absolute pressure and the volume of a gas, assuming the temperature in a closed system is kept constant.

To evaluate the matrix permeability, shale core samples are crushed and sieved to a grain size of 500 < µm < 750 as suggested by Core Laboratories. The shale is likely to part along microfractures and bedding planes and therefore any fractures or cracks in the plugs are eliminated. This method does thus not take into account the geological structure or fractures in the samples. Any connected micropores, which may be aligned with laminations, are destroyed during the crushing process and unaccounted for during the measurement (Rosen et al., 2014). Therefore, 1.5 inch plugs of the same core if available, are evaluated in addition to the crushed material. With the apparatus used for this project it was, however, not possible to place material under any stress condition in order to close any non-natural fractures.

The GRI experiments are carried out on several experimental set-ups varying, in upstream volumes, called respectively G2, G3 and S1. The G2 and G3 set-ups were designed and built at Leeds University, School of Earth and Environment Laboratory, and the S1 set-up was purchased. In Figure 22 a schematic illustration of the GRI apparatus is shown. The set-up consists of a reference volume cell (V_{rf}), a sample holder cell (V_h), a pressure transducer (P) and three high pressure valves. The main difference between the G2 / G3 and the S1 set-up is the pressure that can be used. The pressure transducer range of the G2 and G3 is limited to 250 psi while the S1set-up can go up to 1000 psi. All apparatus are placed in a temperature controlled room kept constant at 23º C.

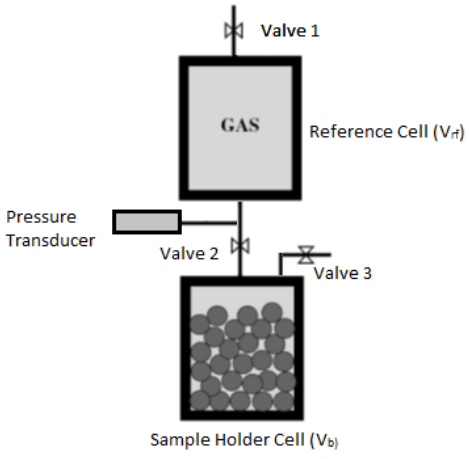

Figure 22: Schematic illustration of the GRI set-up

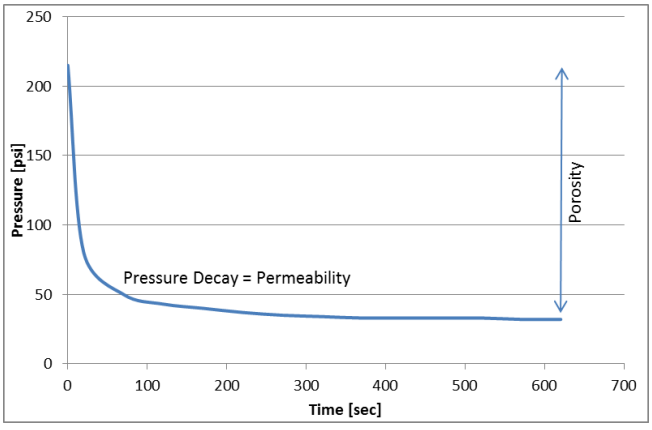

Figure 23: GRI curve the porosity can be calculated from the initial and the end pressure. Permeability is obtained from the pressure decay

During the measurement, helium or nitrogen is expanded from the reference cell, with a known volume and pressure, into the sample holder cell. The pressure of the gas drops rapidly as it fills up the empty volume in the sample holder cell and decreases slowly as the gas moves into the pore of the samples, illustrated in Figure 23. When the pressure remains stable all pores are filled. After this initial measurement the valve separating the reference volume cell and sample holder cell is closed, the reference cell is refilled with gas at high pressure and expanded into the sample holder cell. By using this process three different measurements on different pressures are obtained. The formulas used for this are listed in Appendix B.3.

Essential for accurate measurements is to know the exact volumes of the various cells and, therefore, all three set-ups were calibrated with a reference plug of 7% porosity. Leak tests were executed throughout the measurement to ensure the validity of the experiments. All three set-ups are used to measure rock material with helium, and G2 has in addition been used for nitrogen gas. Before each experiment the chips and plugs are weighed before loading them into the sample holder cell.

5.5 Steady-State Flow

Little has been done to measure fluid flow through shale sample plugs because permeability is known to be very low within shale samples. Therefore measurements can be dominated by error margins of the transducers used (Wang et al., 2010). In order to accurately measure the water permeability on the shale samples, a straightforward method is developed to measure the fluid's permeability in the nano-darcy to micro-darcy range. The method uses a constant high pressure gradient across the samples to force the fluid into the sample. In Figure 24 an illustration of this system is provided. For this method a WILLE GEOTECHNIK Automatic Double Pressure Controller pump with built in pressure- and flow-rate transducer was used.

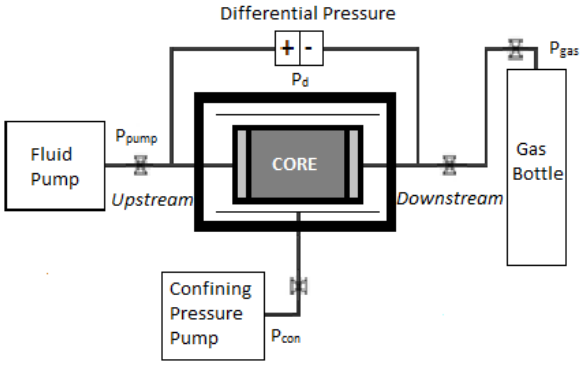

Figure 24: Illustration of steady-state flow experiment set-up

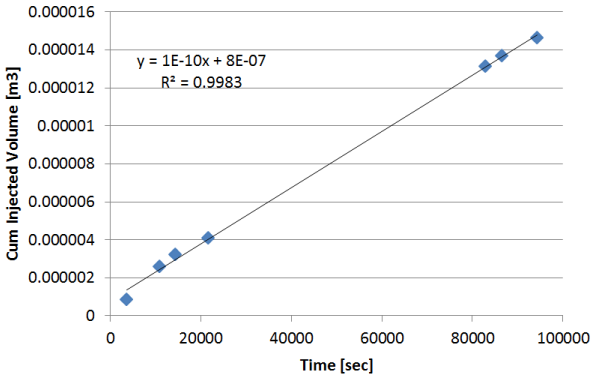

Figure 25: Results from steady-state experiment

During measurements the sample was placed in an isotactic stress cell with a confining pressure of 1000 psi. This was applied by the core holder to create a representative in-situ reservoir condition by closing any induced fractures during the coring process (Rosen et al., 2014). The fluid flow is generated by a pressure differential over the sample and therefore it is essential to ensure equal pressure conditions on both the upstream and downstream side in the core holder. This is realized by forcing nitrogen with 300 psi, from the downstream side through the sample with the upstream valve closed. Time is allowed during the process to enable the nitrogen gas to equilibrate over the sample until the pressure differential is negligible. When the pressure in and across the core is stabilized, the pressure within the pump is set to the same value before opening the upstream valve to prevent any gas or water flow. Water flow is obtained by forcing deionized water into the sample with a constant upstream pressure of 2,100 kPa. This creates a large differential pressure to initiate flow towards the sample. The cumulative decrease in volume of the pumps cylinder is equal to the cumulative flow into the sample, which can be converted to an average flow-rate. Flow-rates are measured during regular time intervals until water droplets are spotted in the transparent hoses in the downstream volume. Figure 25 displays a result of a steady-state flow test versus time. The permeability for flow through a 1.5 inch diameter shale plug is obtained by Darcy's Law, displayed in Equation 4 and assuming a linear flow (Wang et al., 2010).
The duration of the experiment varied between one to two weeks and because of this time frame only few samples could be measured. Additionally, the set-up was only applicable for 1.5 inch in diameter plugs.

$$Q = \frac{-k * A}{\mu} \frac{\Delta P}{L}$$

Equation 4: Darcy's law used for permeability calculations

Q	Units of Volume per time	m^3/s
k	Intrinsic permeability of sample	m^2
A	Cross-sectional area to flow	m^2
μ	Viscosity of fluid	Pa·s
ΔP	Pressure differential over sample ($P_{downstream}$ - $P_{upstream}$)	Pa
L	Length of sample	m

5.6 Thermo Gravimetric Analysis (TGA)

Because of the complex storage and flow mechanisms in shales, the quality of the sample material is important to evaluate the system (Handwerger et al., 2012). To study the fluid content of a sample, the TGA method was used.

TGA measures the mass loss as a function of temperature and the rate of loss. However, such an analysis only provides general information about the overall reactions of shale. Shale is composed of a wide range of minerals, fluids and kerogen, which will react in parallel and in series once heated to high temperatures, resulting in a large number of reactions.

TGA was performed on cleaned and dried samples using a Mettler Toledo TGA/DSC1 balance with nitrogen as the purge gas with a flow-rate of 50 ml/min. All thermal experiments were conducted at atmospheric pressure and a heating rate of 10 ºCmin-1 was applied over the temperature range of 30 – 1000 ºC. All samples were crushed and ground to a fine powder (d < 100µm). The mass and temperature measurements of the instrument were calibrated beforehand using calcium oxalate as standard.

The general TGA pattern for the majority of the shale samples is a slight weight loss at temperatures below 200 ºC and a main weight loss at temperatures above 350 ºC. Three distinct temperature zones can be identified during the heating process: 1. Low temperature region: 30 – 200 ºC, 2. Middle temperature region: 200 – 600 ºC and 3. High temperature region: 600 – 1000 ºC. However; the samples may not represent same trend in all of these regions. The various temperature regions and a TGA graph is illustrated in Figure 26.

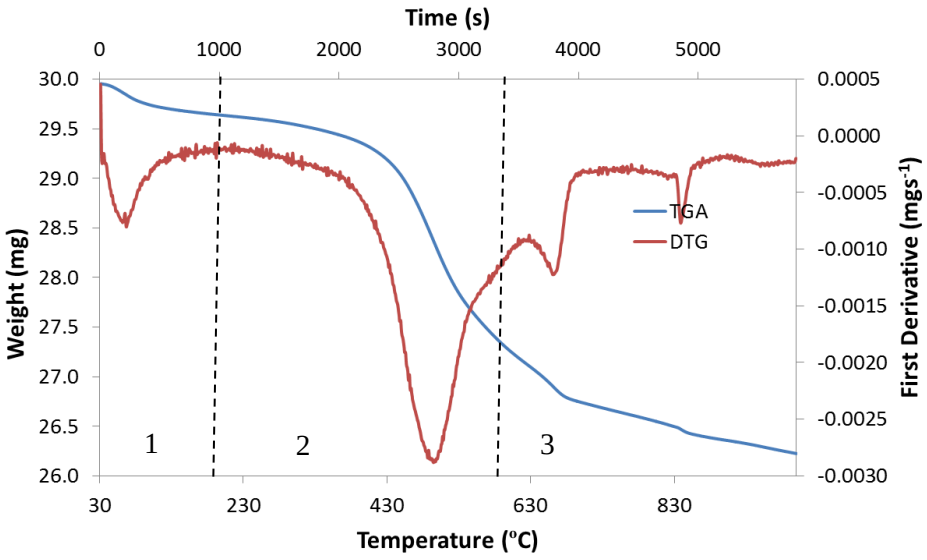

Figure 26: TGA analysis of a shale sample with the blue line showing weight of the sample. The red line is the derivative of the mass curve (Handwerger et al., 2012).

Following suggestion by Handwerger et al. (2012) a distinction between possible free and clay bound fluid is made based upon the evaporating temperatures. The low temperature region corresponds to free fluids, the middle region to capillary bound fluids and the high region to structural formation water.

6 Results

Shale samples have been measured with different experimental methods. The results are shown in this section and organized according to the analyzed parameters and the experiment.

6.1 Hydrocarbon Identification & Characterization

Essential for any reservoir is the presence of hydrocarbons in the rock. However, due to the age of the samples (over 30 years old), and therefore the presumable low liquid hydrocarbon content, measuring the hydrocarbon content is difficult. For this project, the NMR and TGA retort method have been used to measure the hydrocarbon properties.

6.1.1 TGA Hydrocarbon Identification & Characterization

The TGA retort experiment is used to identify and characterize any potential hydrocarbon fluids present in shale samples. The TGA analysis was carried out as part of the SHAPE project. The results were allowed to be used in this study. In addition to the SHAPE samples drill cuttings obtained in February 2014 were tested.

Figure 27 illustrates a general TGA result of the cuttings for three different temperature regions, which are divided by the dotted lines and identified by the numbers in the graph. The main weight loss starts at about 350ºC, where the weight decreases rapidly with the increase in temperature caused by the expulsion of volatile hydrocarbons. This weight is attributed to the decomposition of kerogen into pyrolitic bitumen and later to the decomposition of bitumen into gas and liquid products (depending on the type of the shale). In the third region, above 600ºC, decomposition of carbonate minerals including calcite, dolomite and anchorite takes place.

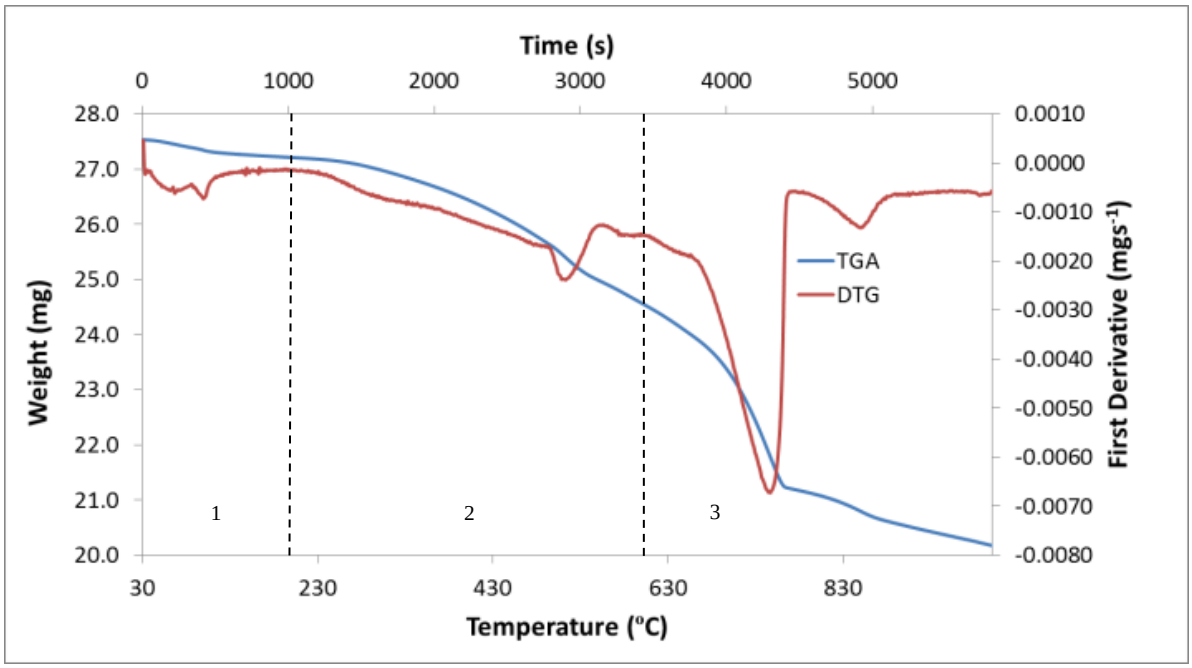

Figure 27: TGA on newly obtained drill cuttings, weight change for each cutting bag (left), characteristic TGA, DTG graph (right).

For each of the samples the percentage weight loss for the different regions is displayed in Figure 28. It is observed that the 14 samples vary widely in the percentage of weight loss indicating the heterogeneous nature of the Posidonia shale.
Handwerger et al. (2012), suggest that the lower and middle temperature regions are of particular interest because of the ability to contain producible hydrocarbons.

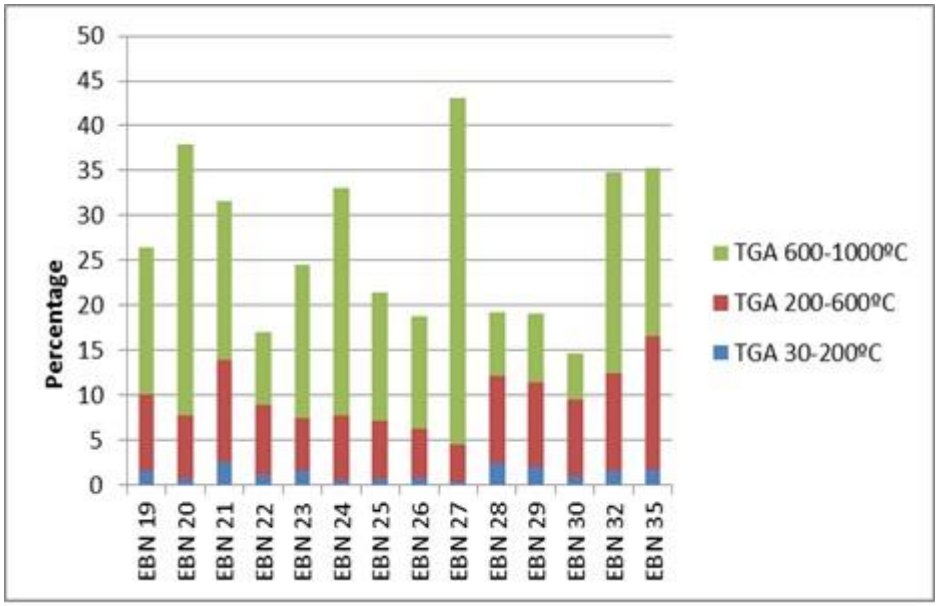

Figure 28: Percentage of weight change as a function of total weight loss from SHAPE: TGA 30 - 200 ºC (blue), TGA 200-600 ºC (red) and TGA 600 – 1000 ºC (green).

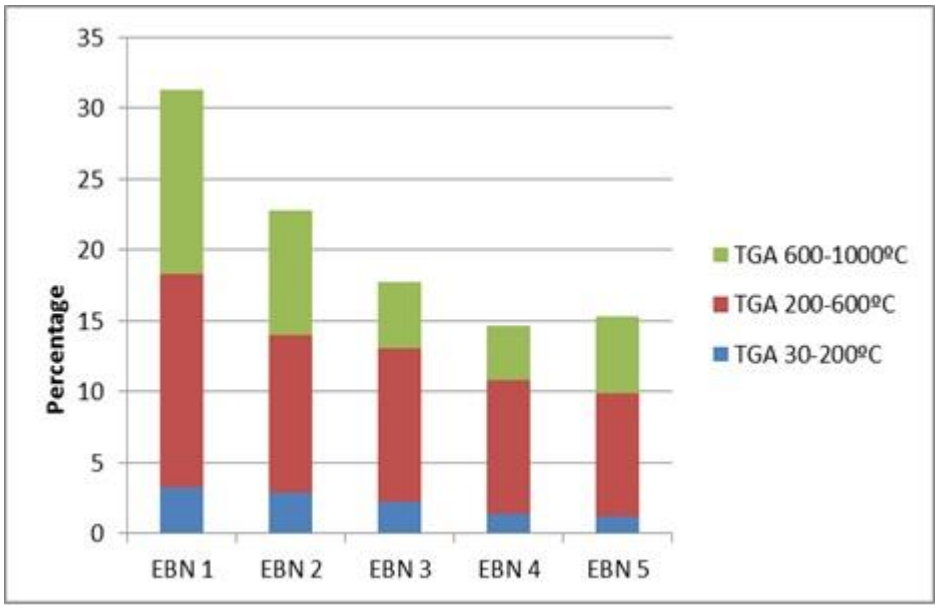

Figure 29: Percentage of weight change as function of total weight loss from TAQA drill cuttings: TGA 30 - 200 ºC (blue), TGA 200-600 ºC (red) and TGA 600 – 1000 ºC (green).

The possibility that lighter components may have evaporated from of the sample, leaving only the immobile hydrocarbons. This possibility can be evaluated by comparing the results of new samples of the same formation with older sample material. Therefore drill cuttings obtained

from TAQA in February, 2014 are evaluated with TGA, and the result of the normalized weight loss in the lower and middle temperature region is plotted in Figure 30. The normalized weight loss is calculated by dividing the absolute weight loss for the specific temperature region divided by the total absolute weight loss. The fresh cuttings plot in the highest region, suggesting a possible correlation between age of a sample and mobile hydrocarbons. The small amount of weight change in the first temperature region, and to a greater extent the weight change in the second region indicates small amounts of movable fluids.

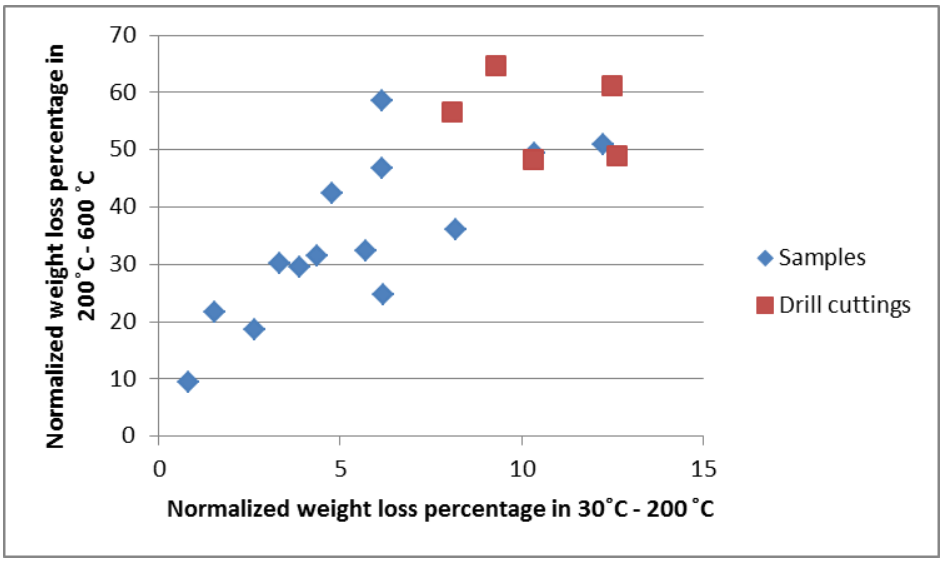

Figure 30: Lower and middle temperature region TGA results plotted for SHAPE samples and cuttings.

6.1.2 NMR Hydrocarbon Identification and Characterization

The NMR method has often been used to determine the fluid saturations in samples. In the majority of the measurements, the NMR T_2 relaxation time is displayed as semi-log distribution versus the normalized signal (Tinne et al., 2014). In this project the amount of fluid contained within a sample is calculated with Equation 3, and the correlation shown in Figure 31. This correlation uses the measured signal per scan from the NMR experiment to calculate the fluid [cm^3] present in the sample. This correlation was suggested by Grattoni, C. and validated by several calibrations. The results of these calibrations and the final correlation is shown in Figure 31. The samples are not similar in weight and therefore the calculated fluid volume is normalized by dividing it with the total weight of the sample. The calculated fluid volume percentages are displayed with the histogram in Figure 32.

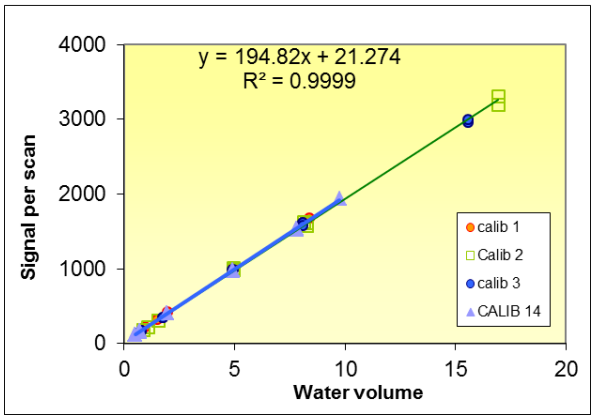

Figure 31: Correlation of water volume and signal per scan obtained after several calibrations on the same NMR instrument as used in this project (calibration results obtained by C. Grattoni, 2014)

The average fluid volume within the 14 measured samples is 0.003 [cc/gram], indicated by the green line in Figure 32. The samples EBN 21, EBN 23, EBN 25, EBN 28, EBN 29 and EBN 30 are above the mean, and EBN 25 and EBN 29 show the highest fluid volumes per gram. As for this project no data was available from other shales, the evaluation of the material is limited to the samples within the EBN selection.

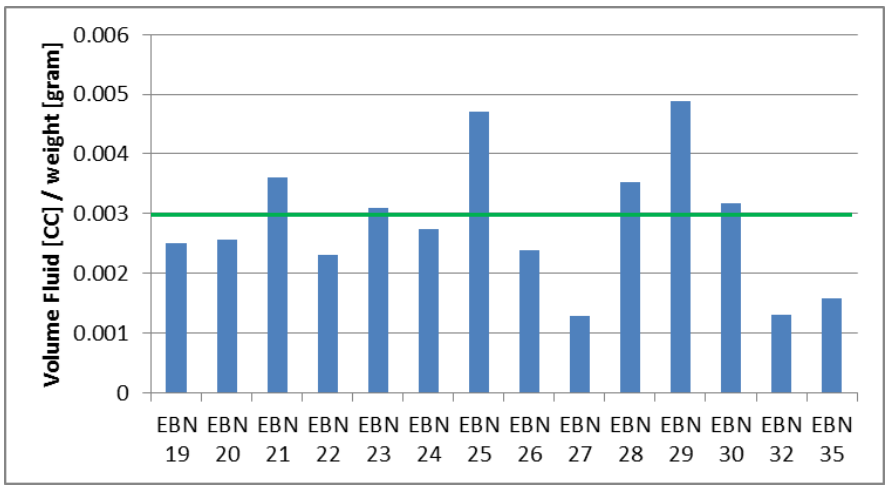

Figure 32: Histogram of the volume of fluid of the samples in the condition "as-received"

In addition to the measurement of the amount of fluid in a sample, a correlation suggested by Rylander et al., (2013) based on the T_1 and T_2, is used to estimate the core pore fluid using a T_1/T_2 ratio. The ratio implies that if T_1 / T_2 is larger than seven, the fluid is considered to be oil or bitumen and anything lower is indicated as water. In Figure 33 the blue line (T_2 = 3 ms) distinguishes clay bound water (T_2 < 3 ms) and water in the intergranualar pore space (T_2 > 3 ms). Oil is divided by the yellow line (T_2 = 10 ms) in oil located in small pores and therefore bound (T_2 < 10 ms), while large pores (T_2 > 10 ms) contain free oil.
Due to the length of the T_1 measurement only five chip samples are selected for T_1 in the "as-received" condition. The selection has not randomly been made but evolves from a selection process, based on several parameters described in section 7.1. From Figure 33 it is observed that all of the samples fall into the bound region. However, EBN 20, EBN 20B and EBN 25 are identified as possibly oil-bearing.

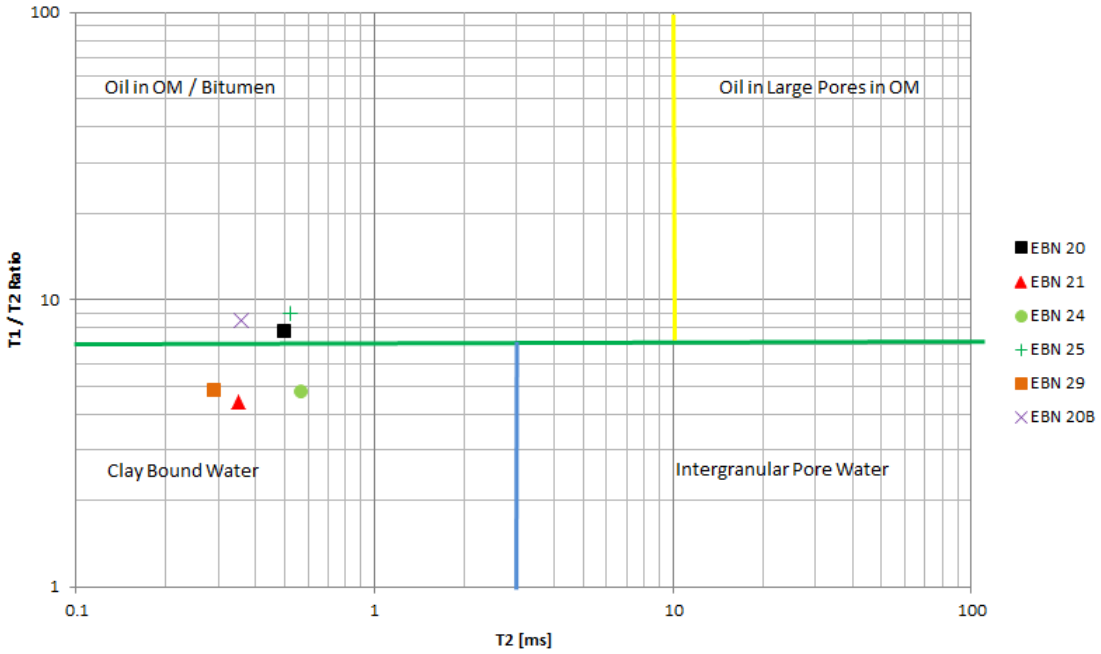

Figure 33: T1/T2 ratio vs. T2 plot NMR measurement of 5 core samples at ambient conditions after Rylander et al. (2013)

Because most fluids are indicated as bound in Figure 33, additional experiments to evaluate the capability of a sample to absorb fluids have been carried out. Figure 34 displays the increase in the amount of fluid [cc] per gram of a sample. When the sample is wetted or dried it is observed that the majority of the shale samples can absorb significantly more fluid when placed within a humid area compared to the amount of fluid a sample loses when dried. Based on this observation it is suggested that the majority of the fluids have migrated out of the sample.

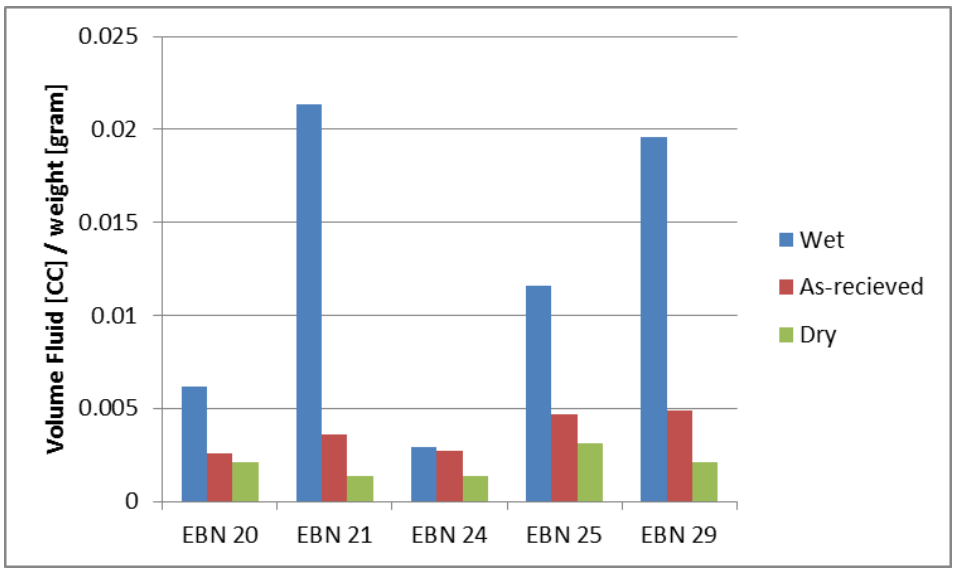

Figure 34: Histogram illustrating a significant increase in the water content of a sample when wetted, and a small decrease in water content when dried.

6.2 Pore Classification

Pore size has been measured with both the SEM and NMR. Identified pores from the SEM images are based on the pore size and subdivided into four different groups, nanopores (0.01 – 0.1 micron), micropores (0.1 – 0.5 micron), mesopores (0.5 – 2.5 micron) and macropores (2.5 – 5 micron) following suggestions by Aguilera (2013). Note that the pore group interval increases with an increase of the pore size, illustrated in Figure 35. Within the nanopore group the interval in which the pores are measured is 0.09 micron. The interval of the macropore group is 2.5 micron, almost 28 times larger.

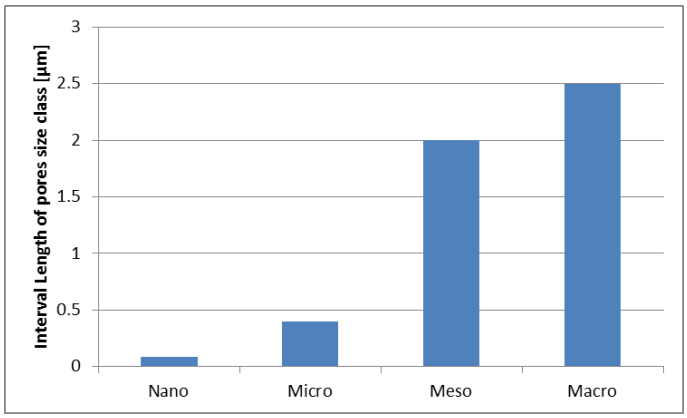

Figure 35: Illustration of the increase of interval of each pores aperture class

6.2.1 SEM Pore Classification

Pore size was measured with the FIJI software. The process used the fitting of an ellipse to obtain the size of the pore. For each identified pore an ellipse with equal surface area as the pore was fitted taking into account the pore geometry as shown, in Figure 36. This resulted in a minor axis and a major axis for the pores. Because the pores are identified on a 2D SEM image, the minor axis of the ellipse is taken as the pore size. Investigation of the pore sizes in literature (Anselmetti et al., 1998) used the square root of the pore area.

Because the identification used a thresholding process on the image it occurred that fractures, which are drilling-induced, were identified as pores. Including these fractures in the pore space would result in additional open pore space. To account for any cracks that may have occurred during the coring process and that need to be excluded from evaluation,

Equation 5 is used. Fractures have a specific geometry as these are often very long and narrow open spaces. To evaluate this γ, the value of roundness of the pore, is introduced and based on this property fractures were excluded. For a spherical pore γ = 1.0 and cracks may have a value of γ > 5.0, hence all pores containing a value for γ > 5 are excluded from the pore size measurement.

$$\gamma = \frac{P_{per}}{2\sqrt{\pi A_{pore}}}$$

Equation 5: A spherical pore has a value of 1 and cracks value of >5, an ideal interparticle pore has a value of 1.9 (Anselmetti et al., 1998)

γ	Value for roundness of pore	-
P_{per}	Perimeter of pore	m
A_{pore}	Pore surface area	m^2

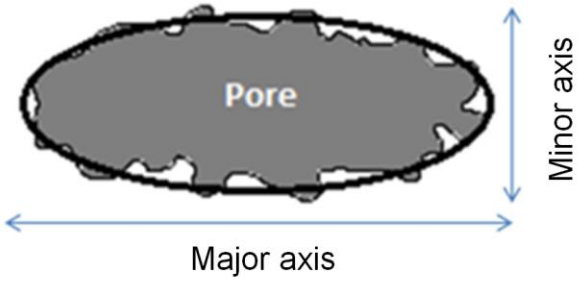

Figure 36: Pore size classification on minor and major length

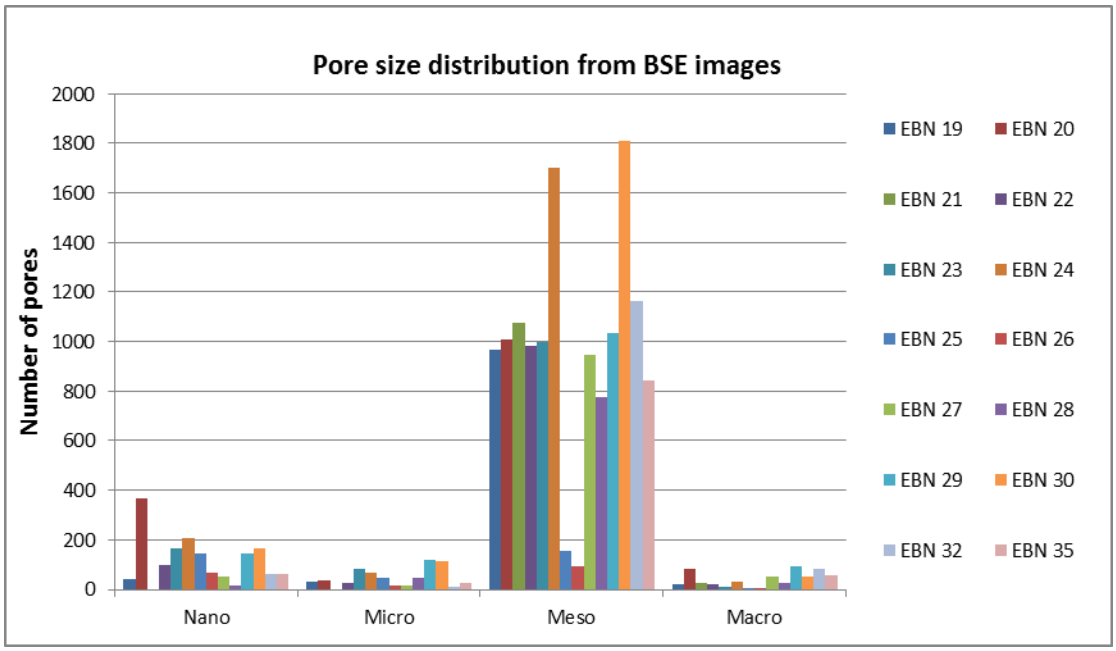

Figure 37: Pore size distribution of SEM from on backscattered electron images

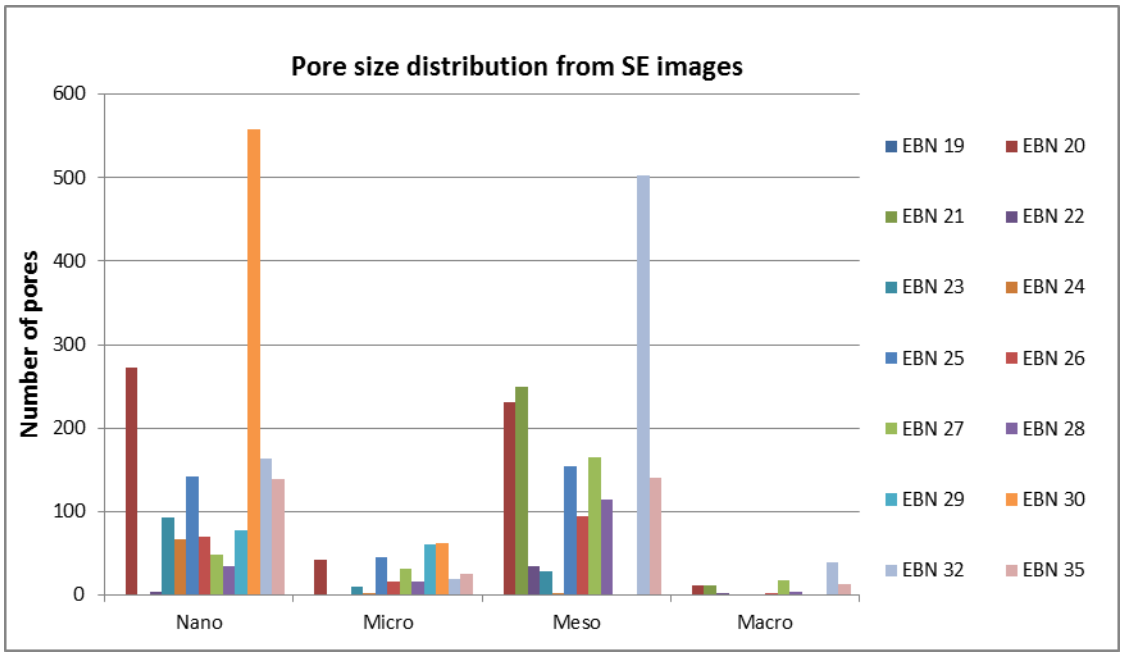

Figure 38: Pore size distribution of SEM from secondary electron images

The data obtained from the SEM is filtered on the γ parameter and grouped, on the minor axis value, in the pore size classes. For all the samples the number of pores in each pore size classes are shown in the histogram of Figure 37. The SEM images used for identification of the pores are listed in APPENDIX D. The data regarding the pore size is used to determine the ability of oil to flow through the shale as from literature it is found that oil flows mainly through the meso- and macropores. In the graph in Figure 37 it is seen that the majority of the samples have an increase in pore numbers in the meso-size class.
The mesopore size class on BSE has an average over the samples of 968 pores per sample. The second largest group in pore number, the nanopore size class has an average of 118 pores per sample, which is about 8 times less than the mesopore size class. For the SE images both the nano- and mesopore size class are equal with an average of 126 pores per sample.

In the BSE histogram of Figure 37 an increase in number of pores is observed in the mesopores classification. The same phenomenon occurs less prominently in the SE image histogram in Figure 38. The differences between the histograms of BSE and SE images is related to their properties. BSE images are used to measure TOC and open pore space, while SE images identifies open pore space. Backscattered images are analyzed with a thresholding process, applicable for both resolutions. By contrast, in the SE images, the open pore space can be better identified on larger magnifications, as shown in Figure 17. Another explanation is in the increase of the range of the pore-class, the mesopores range is more than six times as large compared to the micropores, shown in Figure 35.

For the shale to flow oil on a production time frame it is likely that pores larger than 1 – 2 micrometer are required (Bohacs et al., 2013). Assuming thus that pores larger than 1.5 µm are able to flow oil, the percentage of the absolute number of pores in the range of 1.5 – 5 µm has been calculated and displayed in Table 2 and 3. For sample EBN 21 no BSE 100 µm image and 5 µm SE image was available. EBN 19 didn't have a 5 µm nor a 100 µm SE image and EBN 29 and 30 had no 100 µm SE images. Hence, for these samples not every pore size class could be obtained.

BSE Images			
Sample Number	Percentage of total number of pores with pores size diameter > 1.5 µm	Sample Number	Percentage of total number of pores with pores size diameter > 1.5 µm
EBN 19	13.17	EBN 26	3.28
EBN 20	15.82	EBN 27	17.60
EBN 21	11.01	EBN 28	11.46
EBN 22	9.66	EBN 29	21.56
EBN 23	4.47	EBN 30	10.05
EBN 24	8.23	EBN 32	19.70
EBN 25	1.89	EBN 35	18.16

Table 2: Total percentage of number of pores from BSE Images larger than a pore size of 1.5 µm

SE Images			
Sample Number	Percentage of total number of pores with pores size diameter > 1.5 µm	Sample Number	Percentage of total number of pores with pores size diameter > 1.5 µm
EBN 19	ND	EBN 26	1.37
EBN 20	7.54	EBN 27	18.06
EBN 21	20.38	EBN 28	11.9
EBN 22	9.76	EBN 29	ND
EBN 23	7.56	EBN 30	ND
EBN 24	1.39	EBN 32	16.53
EBN 25	26.59	EBN 35	10.88

Table 3:Total percentage of number of pores from SE images larger than a pore size of 1.5 µm

In addition to the absolute number of pores, Figure 39 illustrates the contribution of each pore size to the open pore space plus TOC percentage. The dotted green line is the pore size larger than 1.5 µm. However it would be favorable to have a sample with a large open pore space and TOC percentage with the largest increase in the size above 1.5 µm, as for example in EBN 20.

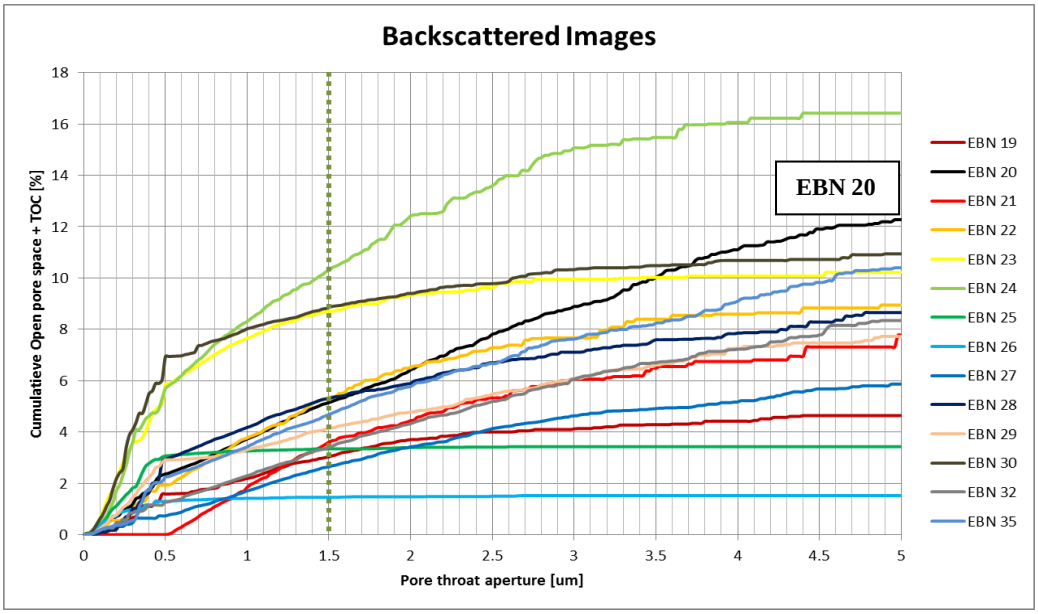

Figure 39: The cumulative open pore space +TOC versus the pore size aperture. The green dotted line indicates the 1.5 um pore throat aperture required for potential flow.

Pore geometry affects the physical properties of rocks, as cracks and elongated pores have different effects than round pores (Anselmettti et al., 1998). Figure 40 shows the variety of pore types and their associated pore shape parameter γ measured from a single sample. Anselmetti et al. (1998) showed that an increase in pore size often results in an increase of the mean value of γ, indicating a more complex branching geometry this then leads to better pore connectivity and higher permeabilities. From Figure 40 this correlation can be confirmed for a shale sample.

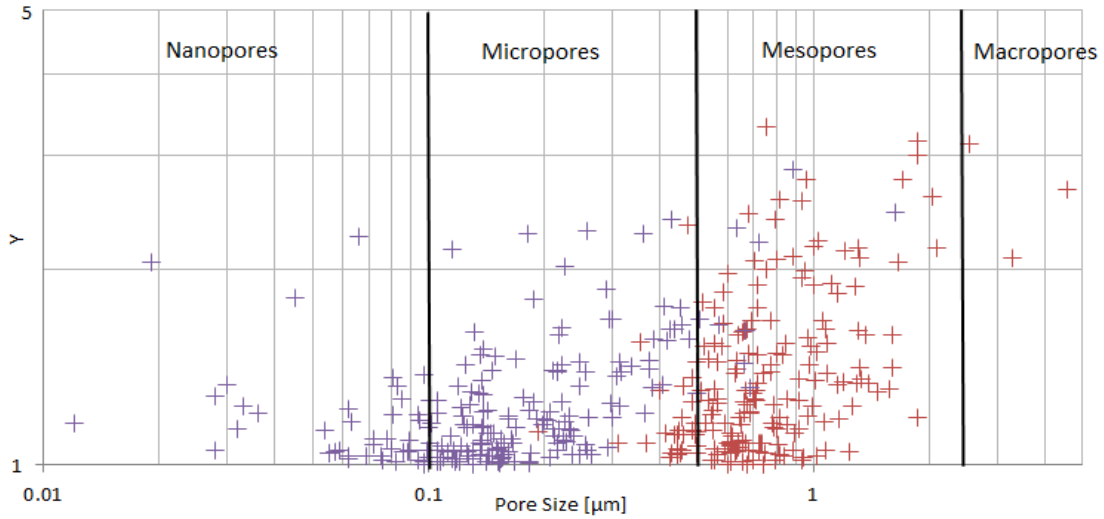

Figure 40: Plot of the pore shape parameter γ vs. the pore size of individual pores from sample EBN 23. The plot is based on both backscattered and secondary images and two different resolutions (100 µm, 5 µm). For better visibility a random subselection of pores in each pore group is made and plotted after Anselmetti et al.(1998).

6.2.2 NMR Pore Classification

The NMR method is used to determine several properties of shale samples of which one can be related to the pore size. Samples have been evaluated in "as-received", dry and wet condition as previously described. The T_2 distribution is used to describe a system containing multiple pore sizes and fluids (Rylander et al., 2013; Tinni et al., 2014). An individual pore can be characterized by the T_2 relaxation time, obtained with Equation 6.

$$\frac{1}{T_2} = \frac{1}{T_{2bulk}} + \frac{1}{T_{2surface}} + \frac{1}{T_{2diffusion}}$$

Equation 6: Formula used to determine the T2 value of an NMR measurements

T_2	Transversal relaxation time
$T_{2\,bulk}$	Bulk relaxation, function of the viscosity of the fluid
$T_{2surface}$	Interaction between the rock and the wetting fluid, a function of pore size
$T_{2diffusion}$	Diffusivity of the fluid a function of the applied magnetic field gradient

The result of a NMR T_2 measurement is displayed in Figure 41 and Figure 42. Figure 41 displays various peaks on different locations along the T_2 axis, showing the percentage of total fluid in different pore size classes. Figure 42 shows the cumulative increase of the signal versus the T_2 measurement. According to Rylander et al. (2014) an increase in T_2 correlates with an increase of pore size and T_2 values above 10 ms are needed to allow hydrocarbon flow in shales. A signal of 100 ms is sufficient for interparticle flow.

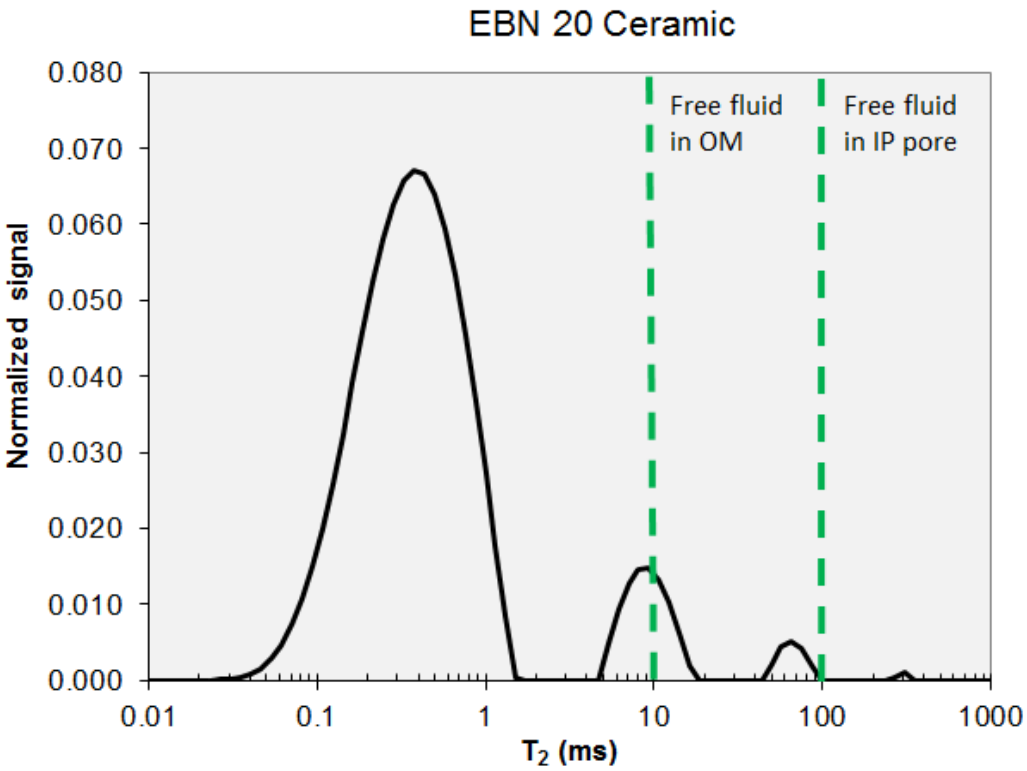

Figure 41: The normalized T_2 distribution from the NMR measurement on chips of the EBN 20 sample.

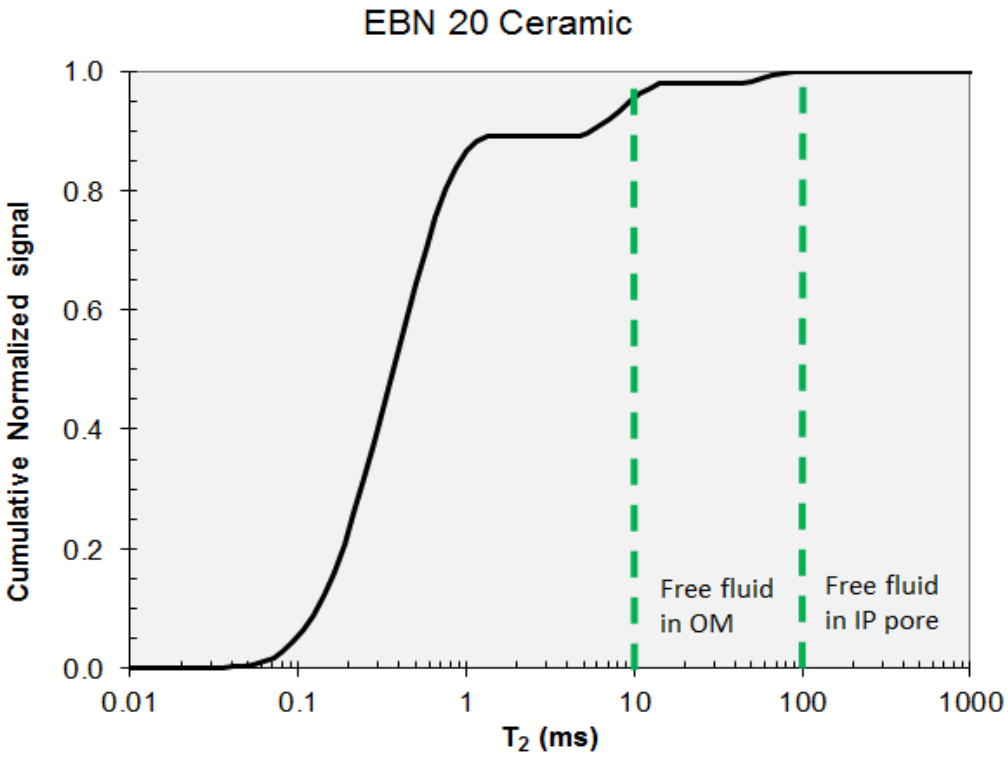

Figure 42: The cumulative normalized T_2 distribution of the NMR measurement on chips of the EBN 20 sample

It is observed in Figure 41 that the measured pore sizes are large enough to allow flow in sample EBN 20. Similar graphs for all EBN samples are displayed in APPENDIX E.1. However for this particular sample ~ 95% of the pores present in the sample is smaller than the minimally required 10 ms and ~ 0.002% is larger than 100 ms. The normalized T_2 distribution of EBN 20 shown in Figure 41 is obtained after post-processing the raw data for time and signal amplitude. A NMR measurement contains multiple measurements for time (T_2) and signal amplitude, as outlined in section 5.3. In order to obtain a graph as Figure 41 the signal is normalized according to Equation 7.
The cumulative normalized graph is a representation of the increase in percentage of the total signal with T_2.

$$Normalized\ Signal = \frac{Indvidual\ Signal}{\sum Individual\ time\ signals}$$

Equation 7: Calculation of the Normalized T_2 signal

Figure 43 illustrates the T_2 distribution for each of the analyzed samples and shows that the majority of the samples have comparable distributions. Figure 44 displays the cumulative graph for all evaluated samples. In addition, the mean value per sample for T_2 time is listed in Table 4 and the corresponding average of all samples is found to be 0.459 ms. The samples of EBN 20, EBN 24, EBN 32 and EBN 35 show a mean T_2 higher than the average and therefore have favorable pore size distributions.

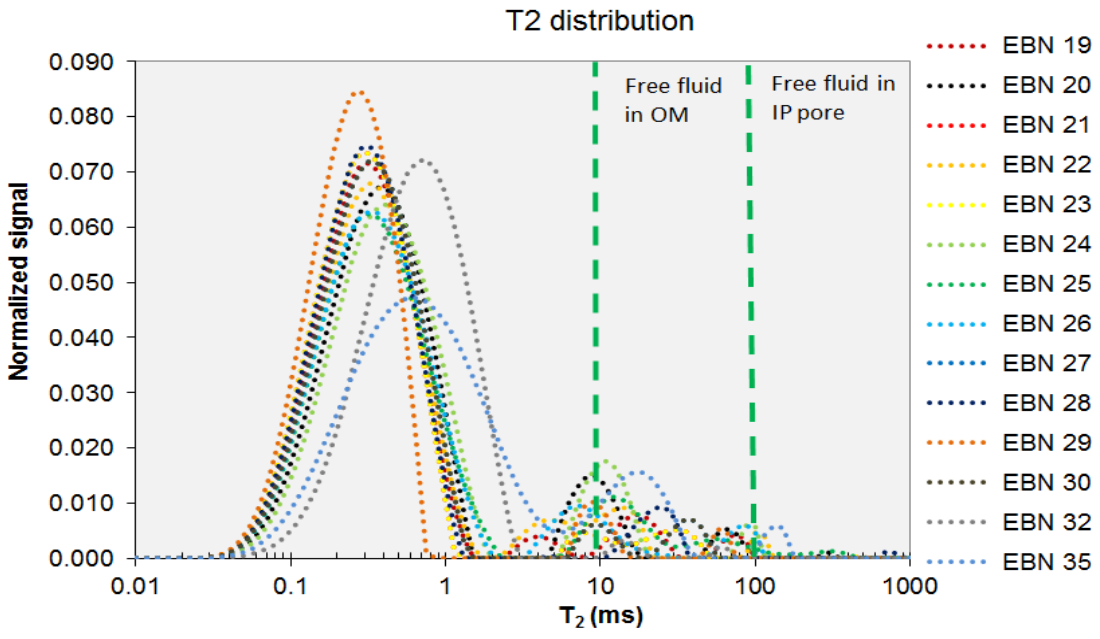

Figure 43: T2 distribution on chips sample material in condition "as-received". Only sample EBN 32 is measured in the 'wet' condition. The abbreviation in the figures are, OM= Organic Matter and IP= Inter Particle

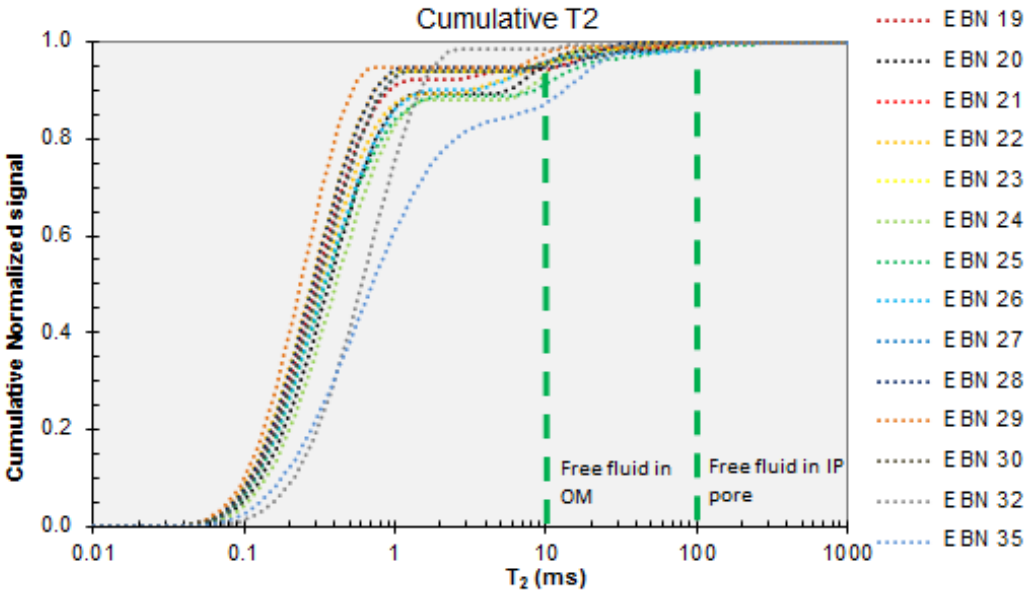

Figure 44: Cumulative normalized T_2 distribution. Note that sample EBN 32 is measured in the 'wet' condition.

NMR T_2			
Sample Number	**Mean T_2 [ms]**	**Sample Number**	**Mean T_2 [ms]**
EBN 19	0.40	EBN 26	0.47
EBN 20	0.50	EBN 27	0.39
EBN 21	0.35	EBN 28	0.356
EBN 22	0.44	EBN 29	0.291
EBN 23	0.35	EBN 30	0.390
EBN 24	0.57	EBN 32	0.639
EBN 25	0.52	EBN 35	0.752

Table 4: Mean T_2 values for all shale samples

The most promising samples, selected with the methodology later introduced in section 7.1, are in addition measured under three different chips conditions, to investigate the effect of wetting on the pore sizes. From Figure 45 it is observed that the pore size increases when the sample is dried and this phenomenon is explained in section 7.6. The range in porosity is on average over the five samples 61.56%.

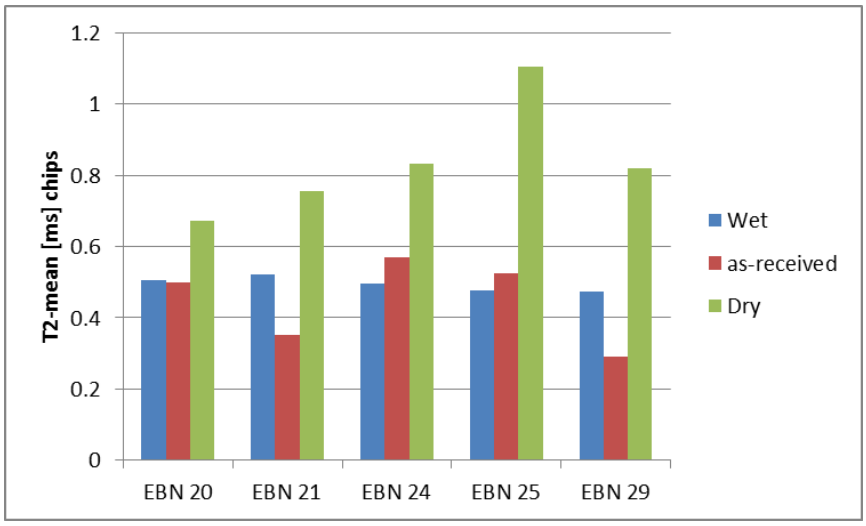

Figure 45: NMR T_2 measurements on chips under different conditions

6.3 Fundamental Reservoir Properties

Porosity and permeability are both fundamental reservoir properties and important for shale oil production. The GRI method is used to determine both porosity and permeability, and a steady-state fluid flow experiment is used to obtain fluid permeability measurements.

6.3.1 GRI Porosity Method

The porosity was calculated using Boyle's law method according to the procedure described in Appendix B.. For every sample, crushed into chips, a total of three pressure transient measurements was performed. During this process the pressure increased each time in the sample holder and therefore the porosity dependency on pressure and gas compressibility was observed. All EBN samples are measured with helium and the most promising samples are additionally tested with nitrogen.

From the GRI method the apparent porosity is obtained. This indicates that the porosity is dependent on the mean pressure and gas compressibility. A correlation between the increase in mean pressure and porosity is evident in Figure 46 for nitrogen gas porosity, but the porosity measured with helium is to a lesser extent correlated with pressure. This is due to amount of gas that is absorbed by the absorbent and is dependent on the type of gas and material used.

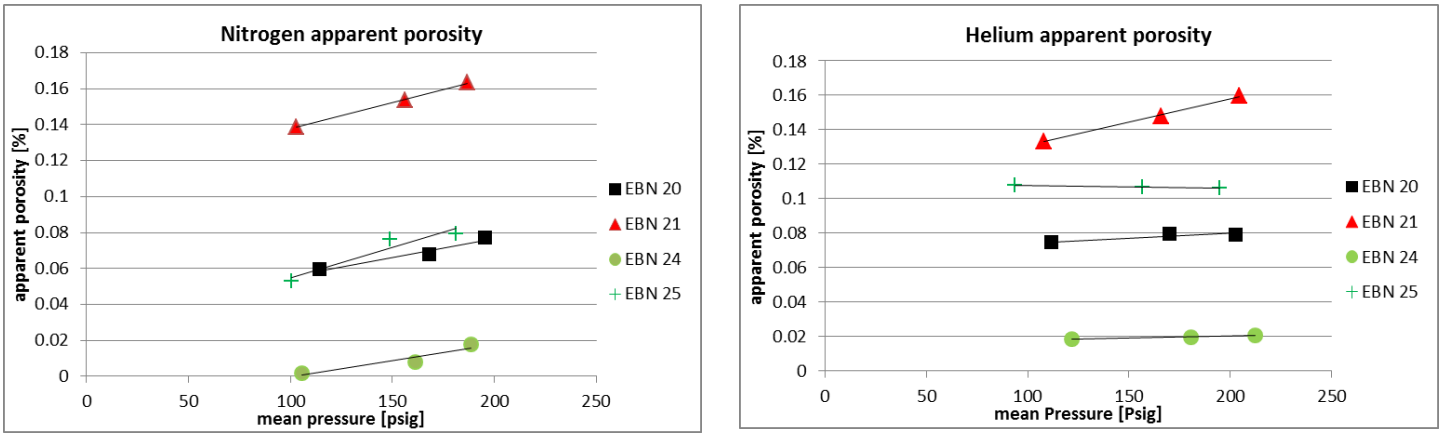

Figure 46:Apparent porosity versus mean pressure for nitrogen (left) and helium (right), illustrating an increase in porosity with an increasing mean pressure

Gas used in the GRI experiments is observed to be influenced by temperature. Therefore, all the experiments are executed in a temperature-controlled room, in which the temperature only varies by less than 0.5 ˚C. For the GRI method sensors able to measure the pressure with an accuracy of 0.001 psi are used. Temperature effects such as the activation of the air-conditioning is indicated in the pressure measurement. A pressure change was noted when the air-conditioning was active and the change in pressure was seen in the measurement. This is shown with the blue line in Figure 47.

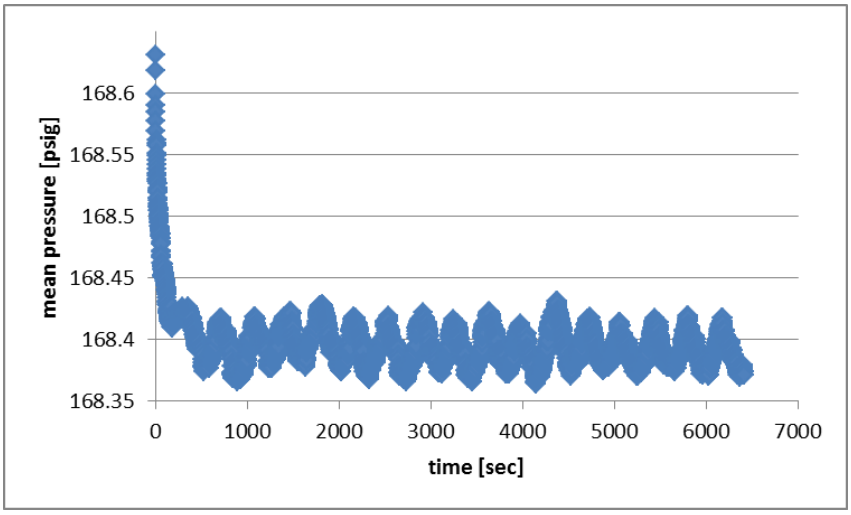

Figure 47: GRI measurement on EBN-27 under "as-received"condition chips, illustrating the temperature effect

For the pressure transient data apparent porosities are calculated. The averages of the three measurements are listed in Table 5. All GRI measurements are listed in APPENDIX E. Additional measurements for core porosity were performed if a core plug was available. From the tested samples it is observed that the core porosity is larger than the chips porosity. A possible explanation for this is the effect of fractures being present in the core plugs. These are not taken into account when the volume of the plug is obtained, calculated as a cylinder by measuring its outside dimensions. Fractures residing inside the plug, imposed by either its natural appearance or induced during the coring process add significant "volume" to the plug, not taken into account by this methodology. The total volume of the material is calculated by dividing the weight of the sample by the bulk density, obtained from the data from the SHAPE project.

GRI Helium					
Sample Number	**Porosity Chips [%]**	**Porosity Plug [%]**	**Sample Number**	**Porosity Chips [%]**	**Porosity Plug [%]**
EBN 19	15.93		EBN 26	8.92	
EBN 20	7.76	8.47	EBN 27	4.72	6.93
EBN 21	14.69	19.85	EBN 28	6.84	11.91
EBN 22	3.58		EBN 29	14.40	19.73
EBN 23	3.47		EBN 30	6.45	
EBN 24	1.87		EBN 32	19.96	16.76
EBN 25	10.69	8.88	EBN 35	11.45	21.48

Table 5: GRI Helium gas porosity results

The condition and in particular the age of the sample has been observed in other cases to impact the result of an experiment. In order to estimate the possible influence of the sample condition, the porosity was measured under dry, wet and "as-received" sample condition. Due to the limited time only the most promising samples are evaluated like this. Furthermore, these samples have also been analyzed with nitrogen to evaluate the effect of gas with a larger molecule size, and the results are shown in Table 6.

GRI chips porosity			
	Helium		**Nitrogen**
Condition	**Wet**	**Dried**	**"As-received"**
EBN 20	6.93	8.99	7.47
EBN 21	14.48	18.06	15.19
EBN 24	5.05	5.7	0.92
EBN 25	9.45	14.8	6.76
EBN 29	15.8	21.74	15.51
EBN 35	9.64	12.95	Not Measured

Table 6: GRI measurements on selected chips for different conditions with helium and nitrogen gas to investigate for different molecule sizes

Figure 48 illustrates the effect of porosity measurements on different conditions. All samples except for the "as-received" condition of EBN 24 show an increasing porosity when moving from wet to dry. The observed differences are likely caused by the reduction of pore space, due to the swelling of the rock when water is absorbed by the rock matrix. The effect of the sample condition on the porosity measurement is large, because the measured porosity varies with 41.92% on average between the conditions.

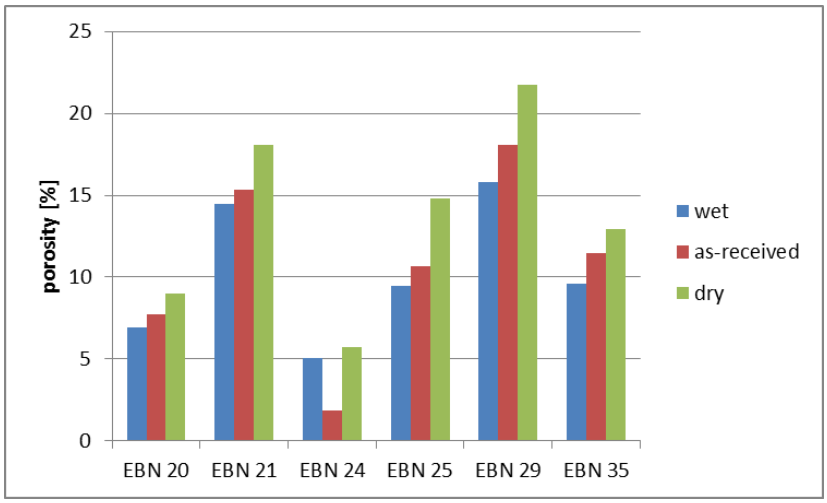

Figure 48: Porosity measurement with helium for three different conditions

Figure 49 combines the porosity measurements of helium and nitrogen, showing a decrease of apparent porosity when nitrogen is used. The porosity is not adjusted for the compressibility of the nitrogen gas, which was shown in Figure 46 but even so the nitrogen is lower for every sample when compared with helium gas. This is explained by the larger molecule size of the nitrogen (Guarnieri, 2012). A suggestion is made by Guarnieri (2012) that the molecule size of a gas can impact porosity measurements. Based on the experimental result it can be assumed that this correlation is confirmed for the EBN samples. Consequently, it is likely that the effective shale porosity for liquids is even lower due to the fact the molecule size for oil increases by a factor 3 – 4 compared to helium gas.

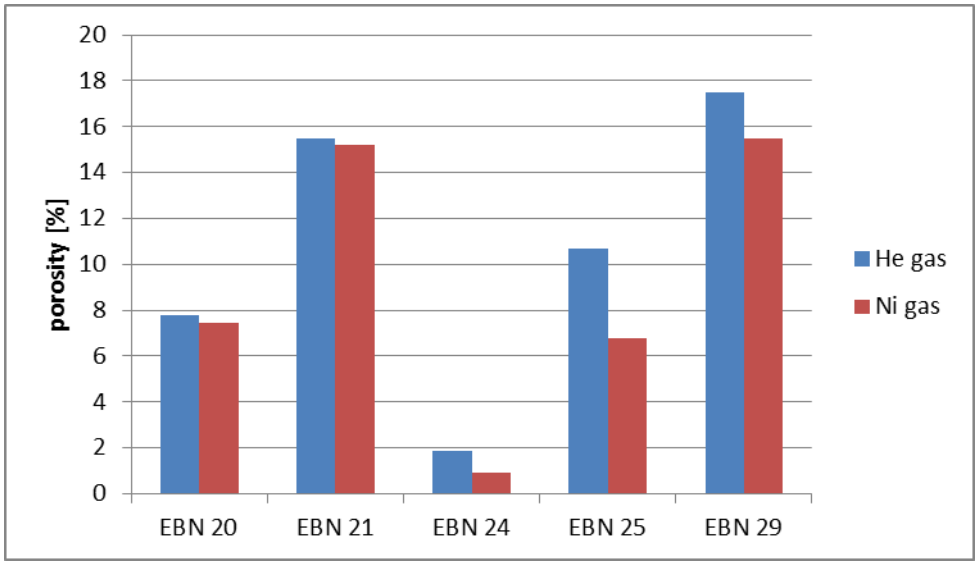

Figure 49: Chips in "as-received" condition measured with helium and nitrogen gas

6.3.2 GRI Permeability Method

Permeability from the GRI method is obtained by history matching a numerical model to the measured pressure versus time data. The model made in Eclipse, [trademark of Schlumberger], consists of an upstream, downstream and a rectangular shaped sample within the downstream model. The total amount of cells is 10x10x22 divided into different permeability and porosity scales to represent the volumes surrounding the samples and the sample itself. The sample is modelled with a single porosity system (phi) and permeability (k_m). The upper and lower volumes are each given a different porosity (phiup, phidown) to account for volume changes of different samples. These four parameters are used for an input model in Tempest (Enable), which executes the model in Eclipse to create a data set for the parameters used. This method creates a model that is not limited to one sample, but instead a correlation applicable to multiple samples is obtained. The graph displays the correlation of the chips divided by the square root of permeability on the y-axis and halfway time (in hours) it takes to reach half of the decline from initial to end pressure / porosity (calculated by GRI per individual sample) on the x-axis. The correlation from the Eclipse model is shown in Figure 50.

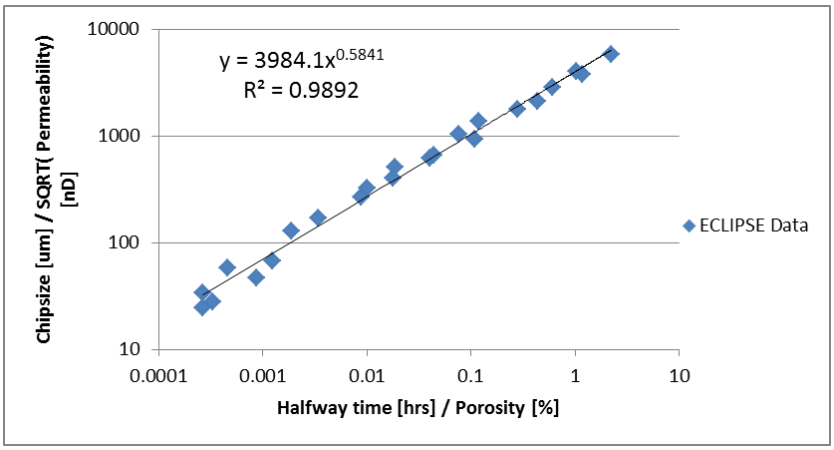

Figure 50: Eclipse model correlation from which permeability can be obtained

The correlation in Figure 50 consists of four parameters, the chip size, the halfway time, the porosity and the square root of the permeability. The chip size is known and the porosity results from the GRI data. Halfway time however is more difficult and is obtained after post-processing the GRI pressure versus time data.
The total pressure drop is calculated as the difference between the initial and end pressure of the experiment. However, the end pressure is straightforward, while the initial pressure is not. The initial pressure is not taken as the pressure within the upstream volume, instead it is taken as the pressure after the gas has expanded from the upstream into the downstream volume without any gas entering the sample material yet. Because of the temperature effect of expanding gas the first seconds of the measurement are not useful. In order to achieve an initial pressure, the initial pressure is calculated by fitting a trend line to the data points, starting from the first point where the pressure starts to decline again, shown in Figure 51. The initial pressure is taken where the trend line intersects the Y-axis. Using this method, the temperature effects on the measurement are eliminated. With the halftime [hrs], GRI porosity value [%] and an average chip size of 625 µm, the permeability can be calculated.

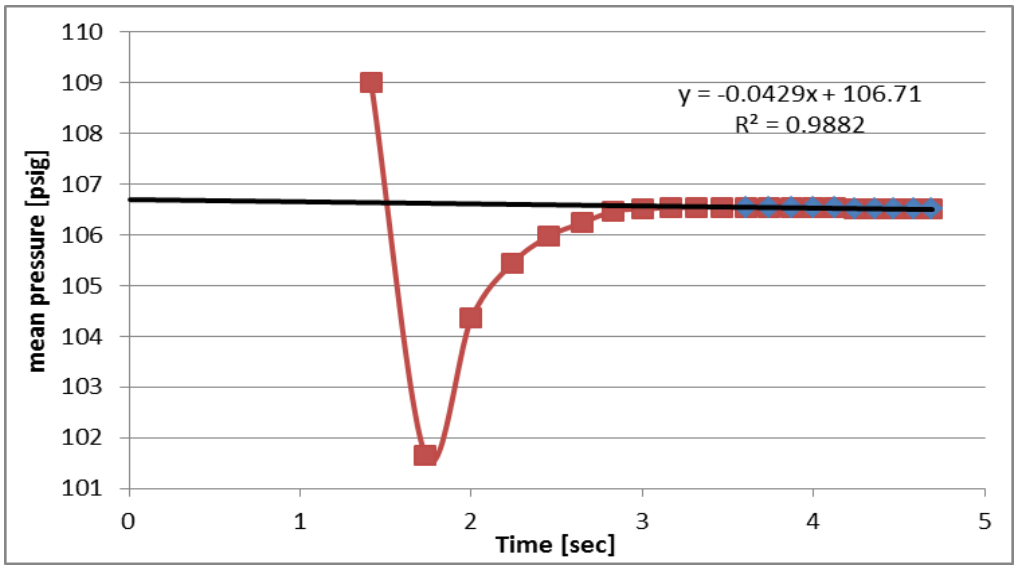

Figure 51: Methodology to determine the initial pressure

During the writing of this report no industry standard methodology for permeability measurements was available. This is a result of the extremely low values obtained during the measurement process and the differences between different laboratories. Therefore in this project it was decided to select the most promising samples, as later described in section 7.1, and evaluate the influence of using different gasses and fluids on the permeability. In addition to GRI with helium, the nitrogen permeability is determined using the same methodology as described for GRI helium and explained in APPENDIX E: GRI Data. From the results, shown in the histogram of Figure 52, it is observed that the chips permeabilities with nitrogen are the lowest. For the other three conditions no clear correlation can be found. The range of permeabilities is observed to lie within the nano-darcy range for helium and nano- to pico-darcy for nitrogen.

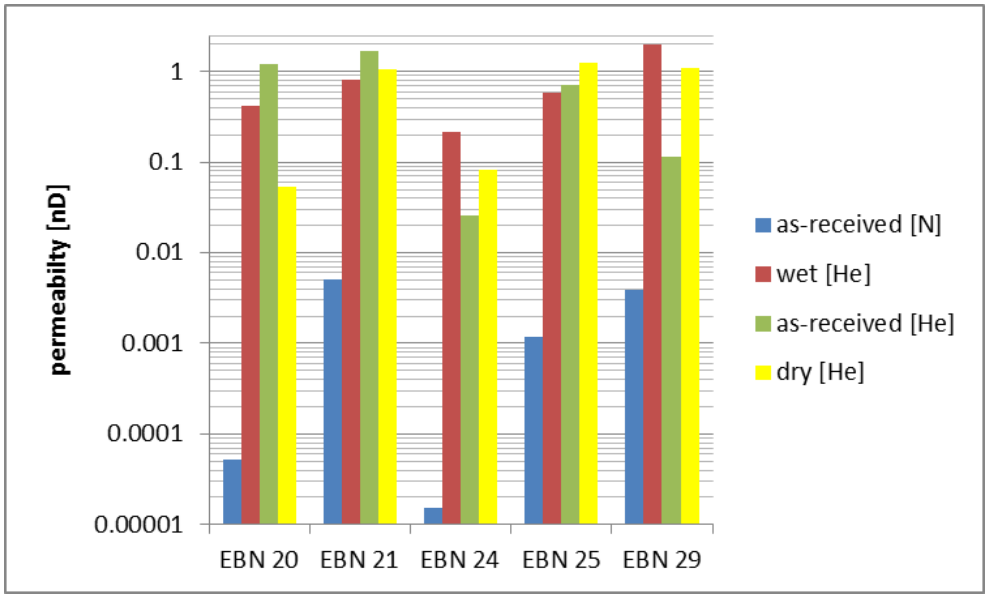

Figure 52: Permeability calculations for the most promising samples obtained from ECLIPSE using data from the GRI experiments

6.3.3 Steady-State Flow Permeability

Full core permeability was measured with the apparatus described in section 5.5. These experiments are time-consuming and can only be performed on good quality core plugs, i.e. plugs without any obvious fractures. Hence, from the most promising samples only four plugs were available. In Table 7 the calculated permeability assuming Darcy flow are listed. It is observed that sample EBN 29 has a high permeability value, but unfortunately this measurement was affected by damage on the core during the measurement. In total two of the plugs parted because of the applied confining pressure This could be distinguished before analyzing the core itself by rapid gas equilibration and high flow-rates. The results are elaborated upon in the discussion.

Steady-State Flow Core Permeability with Water	
Sample Number	**Permeability [nD]**
EBN 20	0.023
EBN 21	0.121
EBN 25	0.067
EBN 29 (Broken during measurement)	*1.775*

Table 7: Permeability results for steady-state flow water measurements. Note EBN 29 was broken during the measurement process

7 Evaluations

7.1 Selection of the Most Promising Samples

A selection from the available samples is made to obtain additional data from more elaborate experiments. The selection was made because these additional experiments, i.e. steady-state flow, nitrogen porosity, NMR T_1, GRI porosity and permeability and plug NMR T_2 are very time-consuming in both sample preparation and in the duration of the experiment. The initial 14 samples were evaluated and subsequently the most promising samples were selected. This was based on the evaluation of the parameters listed in Table 8. The methodology ranks each of the samples for every parameter. For example the sample with the highest porosity is ranked as one and the sample with the lowest porosities ranked 14. This process is repeated for all eight parameters. All parameters are equally weighted and the five samples with the highest total rank were used for the additional measurements. Appendix G.1 contains the ranking sheet. This selection process resulted in the selection of the samples EBN 20, EBN 21, EBN 24, EBN 25 and EBN 29.

Parameter		
Porosity	NMR fluid content	NMR T2 means
SEM open pore space	Non-mineral content	TOC
S1/TOC	Production Index (SHAPE)	

Table 8: Evaluation parameters for the selection process

7.2 Validation of Experimental Results

The experiments introduced for this project are working on the limit of the operating envelope. Therefore the NMR, GRI and steady-state flow set-ups are often calibrated to ensure the quality of the measurements. The GRI set-ups are calibrated with the use of a reference plug of 8.27% porosity. In addition, every two weeks a leak test was executed for the duration of the experiment. The NMR was calibrated daily with a sample of base oil and the steady-state flow experiment is calibrated with the same reference plug as used for the GRI experiment. For the interpretation of the SEM data no systematic method for evaluating the values obtained with the SEM analyses is known in the literature. Interpretation of the open pore space and the non-mineral content can therefore be influenced by the interpreter, as some of it is picked by hand. It was expected that open pore space would become decreasingly smaller due to the pressure increase with depths. In Figure 53 the open pore space versus depth is plotted and it is seen that open pore space decreases with increasing depth. Therefore this correlation supports the validity of the methodology used to analyze SEM images.

None of the experiments of this project provided results that could be interpreted without post-processing. During the process of post-processing, additional parameters were used, of which some were obtained from SHAPE. Because the methodology works at the limit of the operating envelope of the equipment, it is likely that these parameters do have an error margin. The error margins of the parameters of SHAPE are not taken into account for this project.

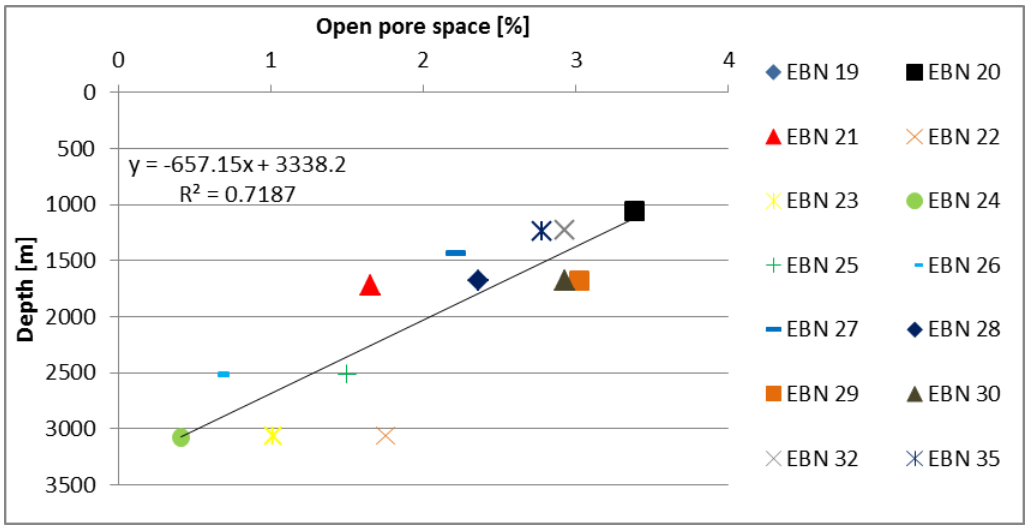

Figure 53: Cross plot open pore space versus the depth from SEM evaluation

7.3 Hydrocarbons

A prerequisite for any reservoir, unconventional or conventional, is the presence of hydrocarbons within the rock. Results from our experiments are compared with those from producing shales from the U.S.. In particular the Eagle Ford shale, has been identified as a potential analog for the Posidonia formation (Noordoven, 2011; Kee, 2010; Bouw, 2012). As part of the SHAPE project, TGA and Rock Eval experiments have been performed to evaluate the presence of oil. The results from these experiments are analyzed to support the discussion on the presence of hydrocarbons.

The hydrocarbon potential of a rock can be evaluated with the Van Krevelen diagram. In Figure 54, EBN samples are plotted in the diagram, indicating that the majority of the samples is immature except for EBN 20, EBN 24 and EBN 25. The EBN 26 sample is not displayed because the O-C ratio of 0.6 which lies outside of the plotted area. Most of the samples plot in the immature region of the Type II kerogen, the most suitable one for oil generation. Although the maturity is generally fairly low some samples (EBN 22, 23, 24, 25) plot within the mature region. EBN 22, 23 and 24 are from 3,000 meters or deeper and EBN 25 from 2,509.5 meters. These are the four deepest samples of the set and therefore a correlation between depth and maturity is confirmed. Both TOC and maturity suggest therefore that oil was generated.

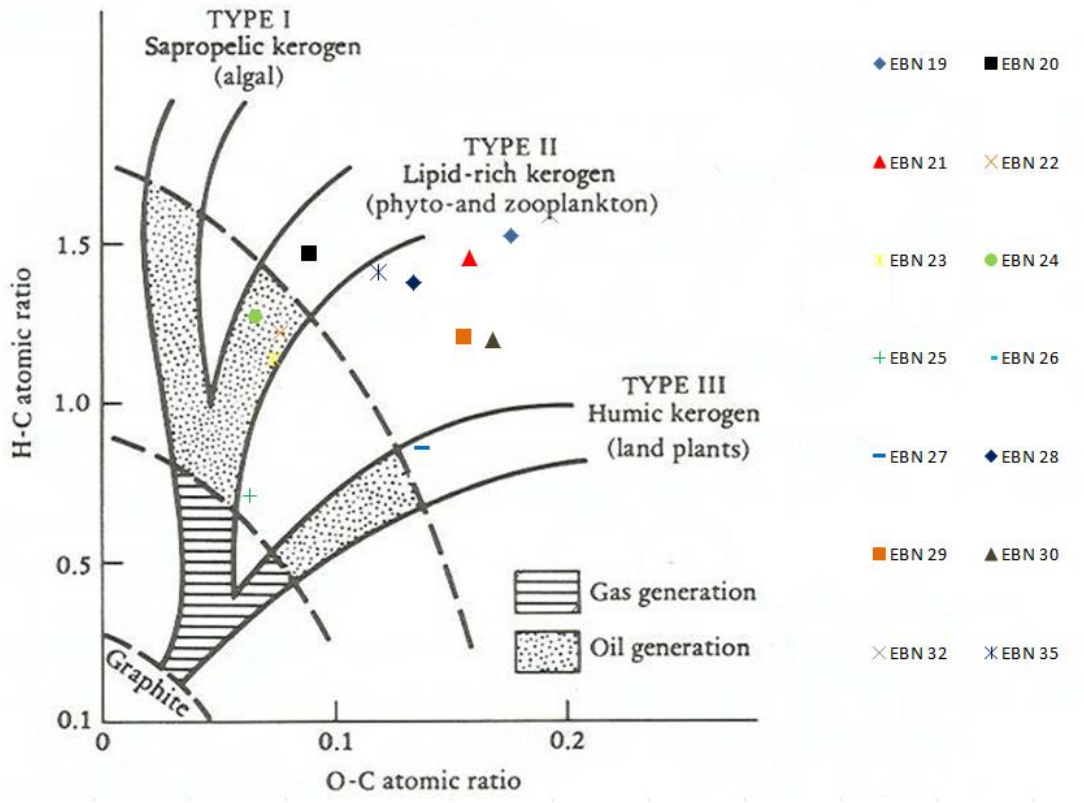

Figure 54: The Van Krevelen diagram data are from the SHAPE project.

Rylander (2013) has evaluated several samples from the Eagle Ford Shale on their fluid properties and using the T_1 and T_2 NMR measurements, they divided their crossplot into four areas as shown in Figure 55. The results of the Posidonia samples and the Eagle Ford shales

are displayed. Productive shales should contain oil located in organic matter with larger pores, indicated by the yellow circles. None of the evaluated, most promising, samples for the Posidionia plot in this region. However the EBN 20, EBN 20B and EBN 25 samples are located in the "bitumen" or "oil in small pores" region, indicating the presence of oil although it is likely to be non-movable.

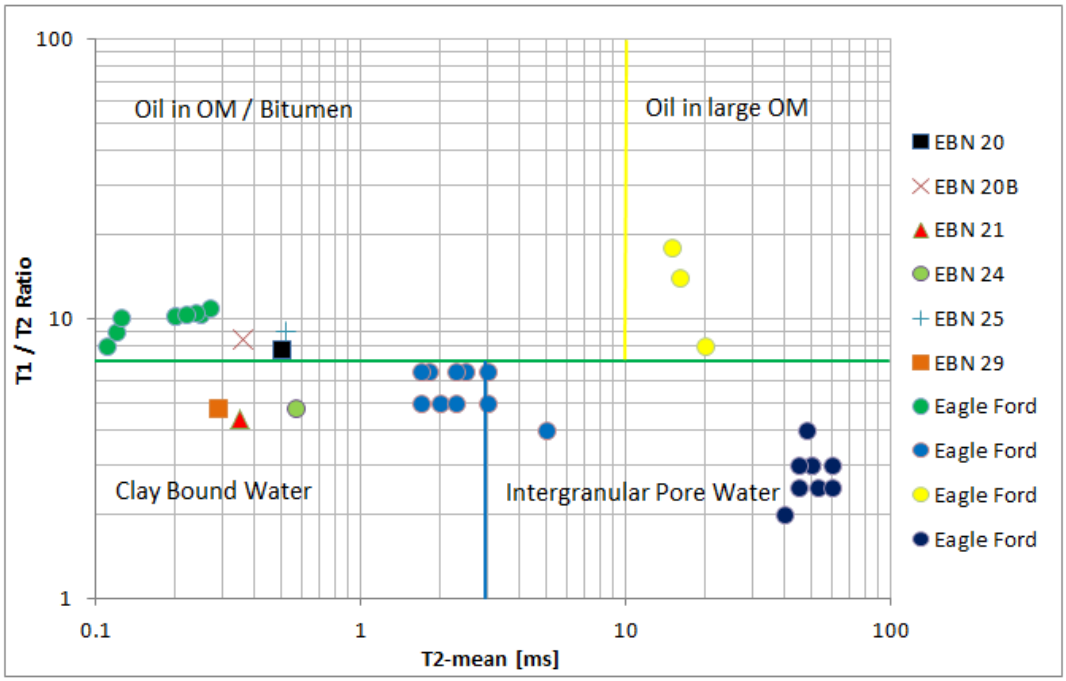

Figure 55: Eagle Ford shale samples compared with the Posidonia samples (Rylander et al., 2013)

Figure 56 displays a graph used by Jarvie (2012) to evaluate shale oil plays from the U.S.. Data from the Eagle Ford shale is plotted together with the EBN samples and it is seen that the EBN samples plot in the "low oil content region". This is in line with the results obtained from the NMR results and indicates the presence of non-producible. All potentially producible oil samples are located in the green area of the graph.

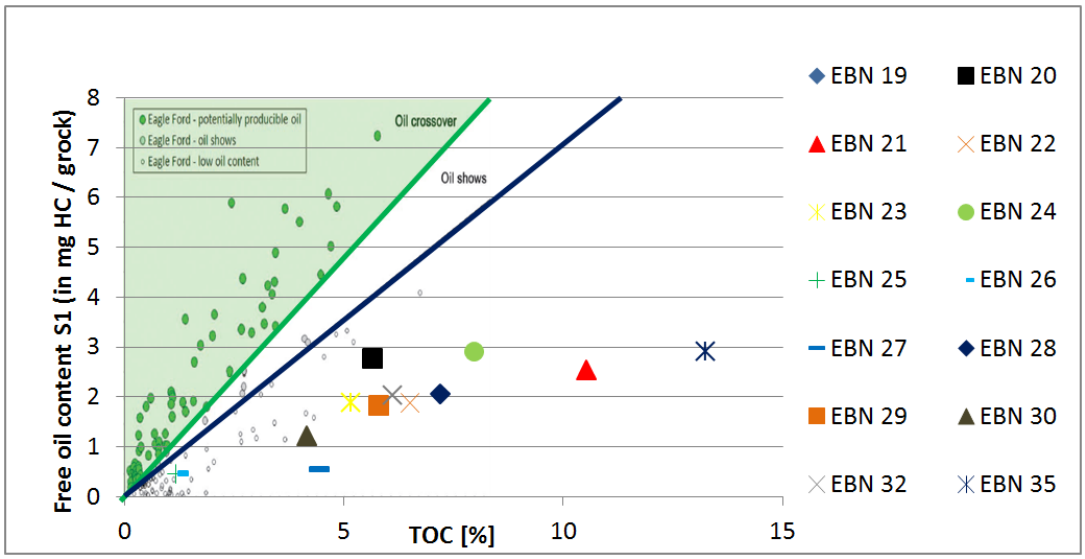

Figure 56: Plot of S1 vs TOC to evaluate the presence of oil (Jarvie, 2012). Data obtained from SHAPE project.

From the combination of the three different plots (Figure 54, Figure 55 and Figure 56), it is concluded that none of the samples contains movable oil. However, some samples indicate the ability to have generated hydrocarbons. From Figure 54 sample EBN 23, 24, and 25 are oil mature. Figure 55 shows that the highly mature EBN 25 plots within the bound oil region. Although EBN 25 has a low TOC content, it plots relatively close to the oil show line in Figure 56. Due to the low amount of TOC within this sample its oil generating potential is limited. In addition to EBN 25, EBN 20 is seen to be immature on the van Krevelen diagram, but oil shows are indicated on the NMR plot. Figure 56 confirms the potential of EBN 20, because it plots relatively close to the oil show line compared with the other samples. Based on these observation it is difficult to predict the oil potential of the samples because it is unclear whether the samples are dry due to age or due to a lack of oil present in the rock. In addition the dataset is limited with only five samples measured with for the NMR.

7.4 Porosity

Porosity is used to evaluate conventional and unconventional reservoirs. Among the techniques to measure this property are the GRI method and SEM images, which are used in this project.

Figure 57 shows the results of the SEM analysis and the GRI porosity measurement illustrating a large difference between these two porosity measurements. An important note to make is that this result does not implicate that one or both of the measurements are incorrect. The differences obtained can be explained by the methodologies used. The GRI method (section 5.4) uses helium and chips to measure the porosity. The SEM methodology (section 5.2) uses images of 5 and 100 µm magnification to do this.
It is observed that all measurements of the SEM porosity are lower than the GRI obtained values.
The SEM produces an image of a small area that was magnified resulting in an image with a scale of 5 µm. This image consist of pixels with a side length of 16.3 nm (10^{-9} m). Consequently only pores can be identified on the SEM images, that are larger than the pixel size. In practice, the limit of the open pores that could be identified on the SEM images is 0.02 µm. The helium used for the GRI experiment has a molecule diameter of 62 pm (10^{-12} m). This molecule size is almost three orders of magnitude lower than the pixel size of the SEM image. Therefore, the molecules of the gas can move into pores, that cannot be identified on the SEM images. This takes not into account that molecular forces can prevent a molecule from entering a pore.

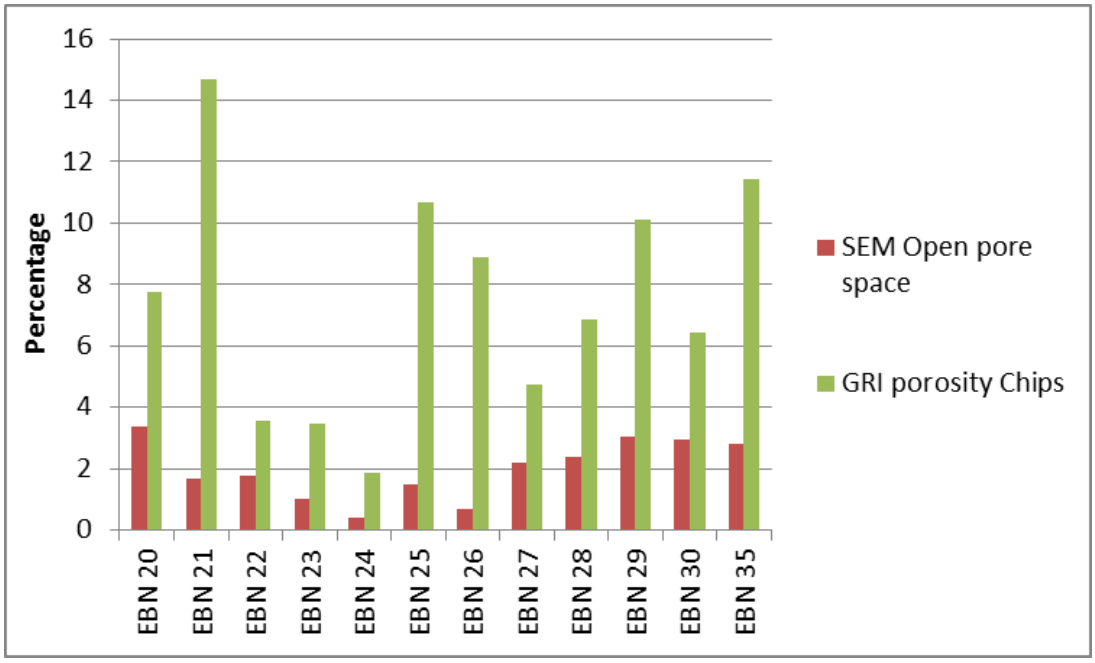

Figure 57: Open pore space (Secondary images, 5 and 100µm resolution) and GRI helium chips porosity. Note EBN 19 is not measured for Open pore space

Figures 58 and 59 show the total number of pores per square micron for the four pore size classes. Both the SE as well as the BSE results show a great increase of the number of pores towards the left., i.e. towards smaller pore sizes. Since the lower limit of this method is 20 nm it is very likely that the number of even smaller pores is very large.

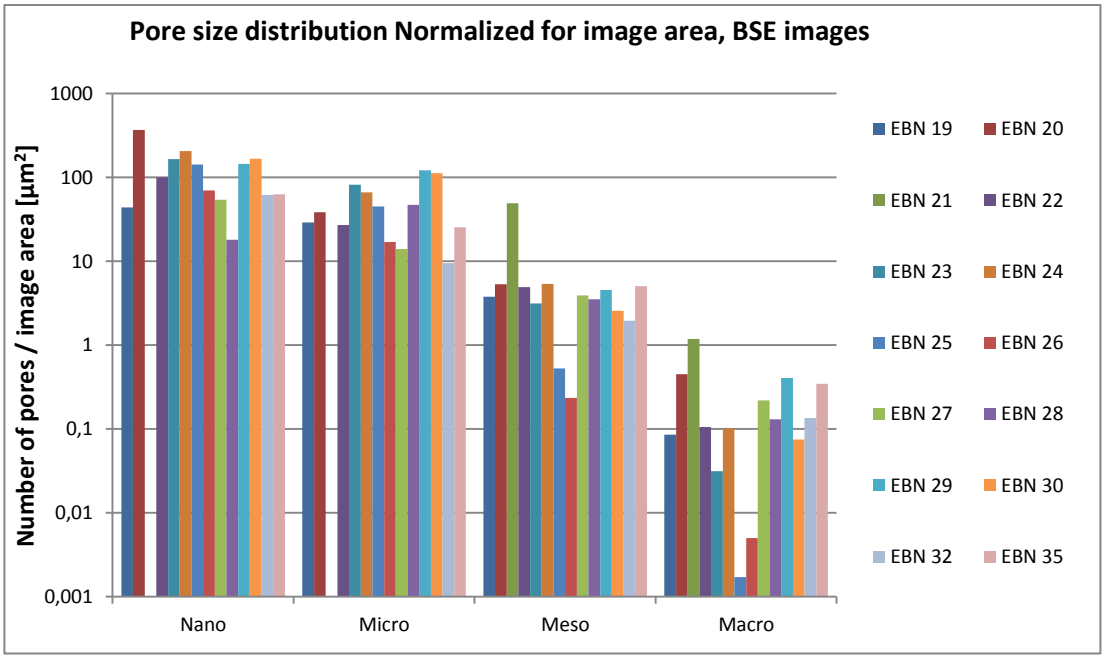

Figure 58: Pore size classes versus the number of pores when normalized with image area for BSE images

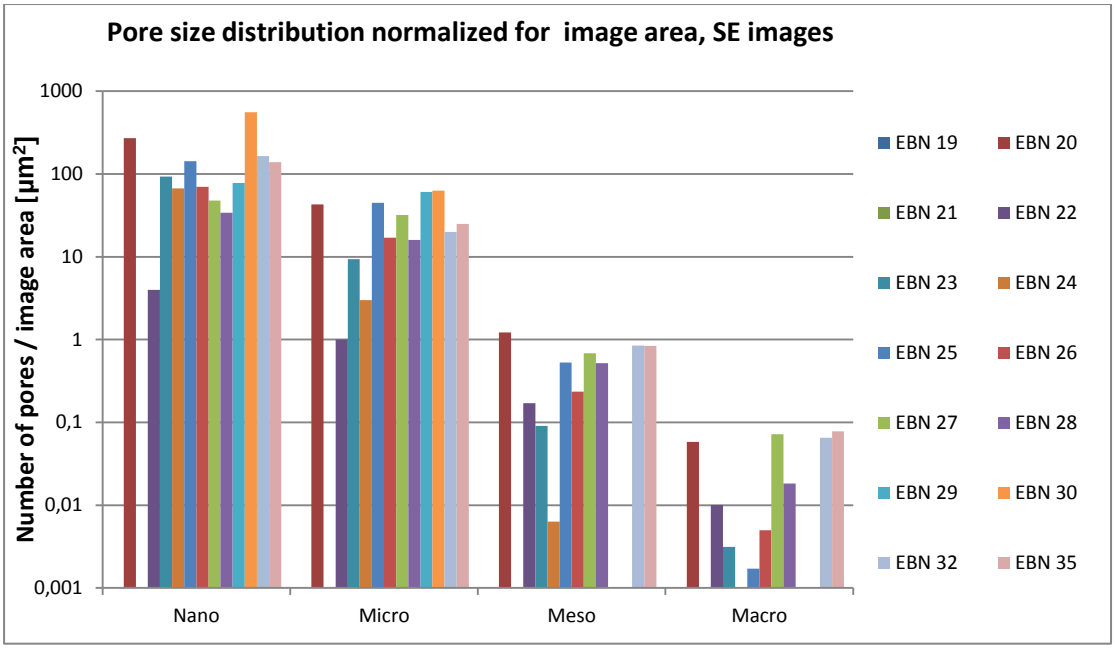

Figure 59: Pore size classes versus the number of pores when normalized with image area for SE images

The BSE and SE images are used to distinguish between open pore space on the SE images and non-mineral content on the BSE images with the methodology explained is section 5.2. Although a correlation was expected between the TOC values, non-mineral content and open pore space this was not found. Figure 60 displays the measured values of the BSE and SE images divided by the corresponding sample TOC value and normalized accordingly. In addition, all three parameters are normalized to the highest measured value. This is done to illustrate a possible correlation between TOC, BSE, and open pores and non-mineral content. It is expected that a high TOC value would correspond to a high non-mineral content measurement and low open pore space measurement. However, no correlation can be observed in Figure 60. EBN 25 displays the highest value for non-mineral content and open pore space but the lowest TOC measurement. By contrast, EBN 35 has the highest TOC measurement but the lowest combined value of non-mineral content and open pores. These observations can result of very fine-grained TOC that cannot be resolved by the SEM.

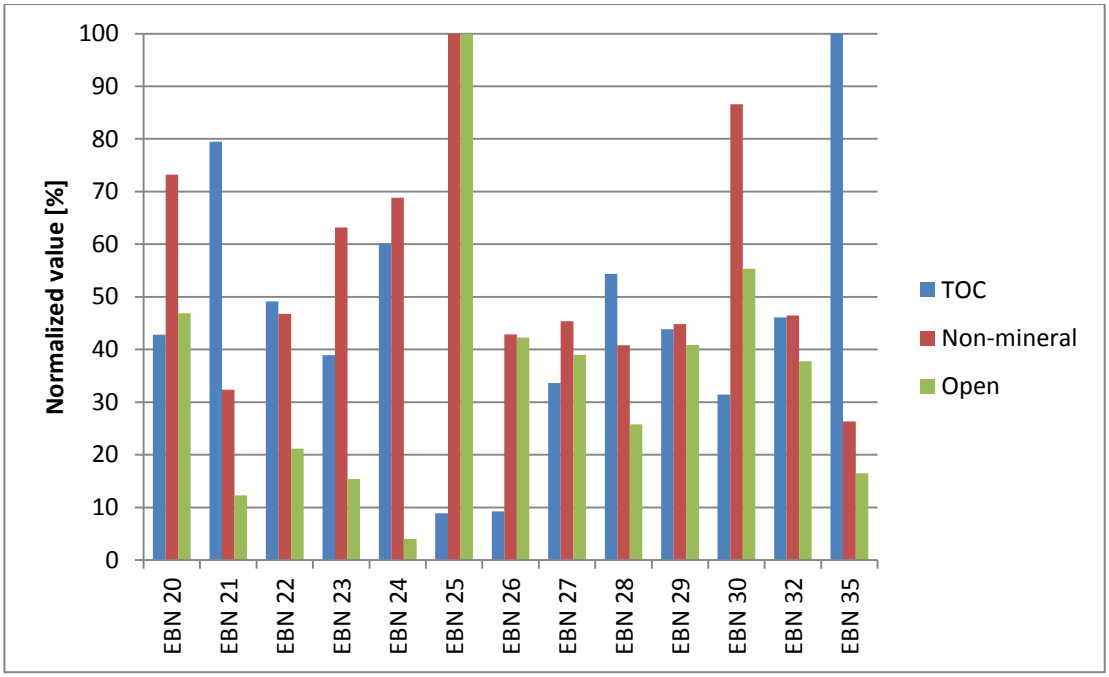

Figure 60: Histogram with TOC, non-mineral content and open-pore space. Note EBN 19 is not measured for open pore space

In Figure 57 a distinct difference is observed between GRI and SEM Open pore space. Based on these observation and the increase in number of pores with a decrease in pore size displayed in Figure 58 and Figure 59 the following can be concluded. A significant part of the porosity within a shale sample is located in pores smaller than 0.02 microns. Consequently, it is questionable if the helium porosity is representative for potential (liquid) hydrocarbon-bearing shale formations. Based on the GRI and SEM measurements, the average difference for a porosity measurement per sample is around a factor of four. This would directly imply a lower porosity for liquid hydrocarbons of at least this factor.

7.5 Predicting Flow

Experiments have been carried out to analyze the potential flow or predict the flow with the pore sizes measured on the samples. From Aguilera (2013) a three-axis graph combining the permeability, porosity and pores size is used to evaluate this. The R_{p35} pore size, which is the pore throat radius at 35% cumulative pore volume, is obtained from the SEM images. The porosity is obtained from the GRI helium experiment from which the permeability is modelled using the Tempest Enable software. To evaluate the correlation by Aguilera (2013) between pore size and flow-rate two different clusters are seen in Figure 61. The dark blue ellipse is plotted from the permeability (left-y-axis) and porosity (x-axis). The green ellipse is in addition plotted for the samples with the pore size (right-y-axis) and the porosity (x-axis).
Aguilera suggested that with porosity and pore size the permeability could be estimated. However, it is shown in Figure 61 that the blue and green ellipse are not overlapping and show different results for permeability and pore size. Aguilera (2013) used a R_{p35} pore throat aperture for the y-axis. This could not be measured with the SEM images used in this project and therefore the minor pore size axis, explained in section 6.2 is used instead. When plotted the correlation between gas permeability experiments and SEM analyses suggested by

Aguilera (2013) the pore sizes plot in a different region than the actual measurement. From this it can be concluded that the identified pores on the SEM images is the pore size and not the pore throat aperture.

The Eagle Ford shale is shown by the blue triangle and plots right in between the green and dark blue ellipse. It seems that the microstructure of the Posidonia formation contains larger pores but lower permeabilities than the Eagle Ford shale.

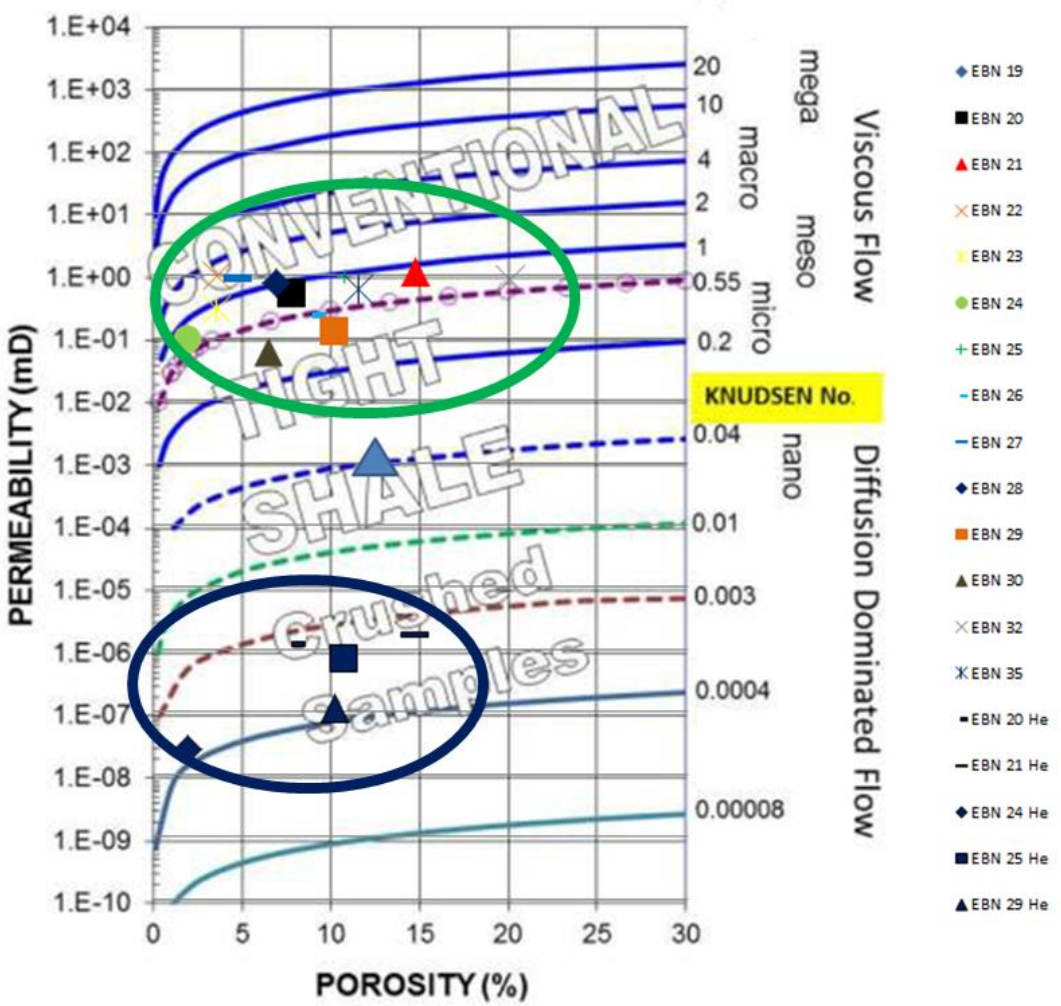

Figure 61: Analyzing shale samples on flow potential in comparison with Eagle Ford after Aguilera (2013). On the right axis the pore sizes are in micronmeter

If the porosity and the permeability of each sample are crossplotted on a logarithmic scale, illustrated in Figure 62 and Figure 63, a correlation is observed. An increase in permeability is observed for both chips and full core helium permeabilities. If this correlation can be confirmed with additional experiments it could be a method to significantly reduce the experiment time to estimate the flow potential of a sample.

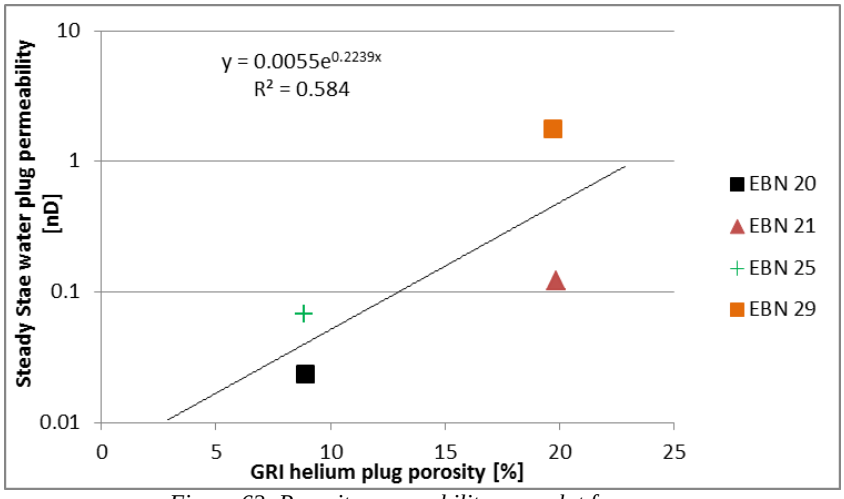

Figure 62: Porosity-permeability crossplot for cores

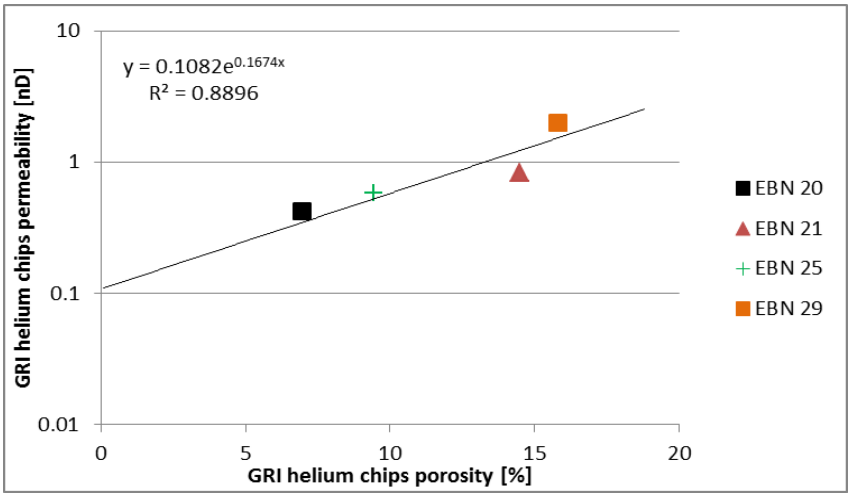

Figure 63: Porosity-permeability crossplot for chip samples measured with helium

In Table 9 the SE images are used to analyze the contribution of pores larger than 1.5 µm which are essential for oil flow through a shale rock matrix. It can be seen in that for each sample the contribution of porosity from larger pores to the total measured porosity (normalized porosity larger than 1.5 µm) varies between 0.0% to 84.6%. If the porosity consists of larger pores it is expected that the permeability increases. Permeability is calculated for the most promising samples and a correlation between the measured helium gas porosity and the normalized porosity of pores larger than 1.5 µm is observed. No correlation is found between total porosity and permeability, indicating that measurement of the porosity of pores larger than 1.5 µm is a more appropriate method for the effective porosity for shales.

Number	Total Porosity[%]	Absolute porosity larger than 1.5 µm [%]	Normalized porosity larger than 1.5 µm [%]	Helium Gas Permeability on Chips [nD]
EBN 20	3.38	0.93	27.52	1.21
EBN 21	1.58	1.03	65.52	1.66
EBN 22	1.29	1.09	84.60	-
EBN 23	1.01	0.42	41.70	-
EBN 24	0.40	0.01	2.18	0.03
EBN 25	1.49	0.95	63.85	-
EBN 26	0.65	0.03	4.84	-
EBN 27	2.20	0.79	35.94	0.72
EBN 28	2.31	0.50	21.80	-
EBN 29	3.01	0.00	0.00	0.11
EBN 30	2.93	0.00	0.00	-
EBN 32	4.28	2.02	47.03	-
EBN 35	2.82	0.80	28.54	-

Table 9: Table with the porosity related to oil flow capacity for SE images

The spread among the different permeability measurements is significant and therefore it is hard to conclude if flow through the rock matrix is possible. The permeabilities calculated from the pore sizes (Figure 61) seem to be high. However, the very low effective permeabilities measured on the shales with the flow experiments suggest that it is hard to produce from the shales' matrix permeability. This suggests that it is crucial to have high-permeability streaks throughout the reservoir in order to produce at economic oil flow-rates. None of the samples seems to have such high permeabilities, however, a larger number of samples and fresher material are likely to yield better insight into the permeability ranges in the Posidonia formation.

7.6 The Effect of Different Sample Conditions on NMR T_2

The most promising samples are tested under three different conditions, "as-received", dried and wetted. This is necessary because the in-situ condition for shale samples is not known and with this method the influence of conditions on the measurement is analyzed. In section 6.3.1 the effect is displayed for the porosities values but the physical change of the samples is discussed in the following section.

Two distinct graphs are obtained from the NMR measurements, a normalized signal versus T_2 and a cumulative signal versus T_2 as shown in Figure 41. The normalized signal graphs for sample EBN 21 are shown in Figure 64 for three different conditions. The numbers in the graphs 1, 2 and 3 indicate, 1) clay bound fluid, 2) capillary bound fluid and 3) free fluid. Both graphs of Figure 64 and Figure 65 display a distinctive difference in the peak distribution with changing chips conditions. In APPENDIX E.1 it is shown that these changes systematically occur for all samples. The changes are analyzed for three different regions: clay-bound fluid (1), capillary-bound fluid (2) and free fluid (3).

The first region, clay bound fluid, is the water that is absorbed to the clay in the rock matrix and that cannot be produced. From the cumulative graph shown in Figure 65 it is observed that clay bound water accounts for the majority of the fluid volume present in the sample. The normalized signal was obtained by dividing the signal associated with a specific time by the cumulative signal. When the sample is wetted, an increase is observed in the cumulative signal for the first region. From this it is concluded when the sample is wetted the clays absorb water This results in a higher peak for the first region.

The second region, capillary-bound water, illustrates a decrease in the peak in Figure 64 when the sample is wetted. This indicates that during the wetting process the percentage of fluid that is capillary-bound decreases during the wetting process. This observation is confirmed by the cumulative graph in Figure 65, in which the capillary-bound water decreases from 15% (dry condition) to 2% (wet condition) of the total water present in the sample.

For the third region, accounting for the free fluid in the rock, a decrease is observed in Figure 64. This illustrates that when a sample is wetted no increase of the percentage of free fluids occurs.

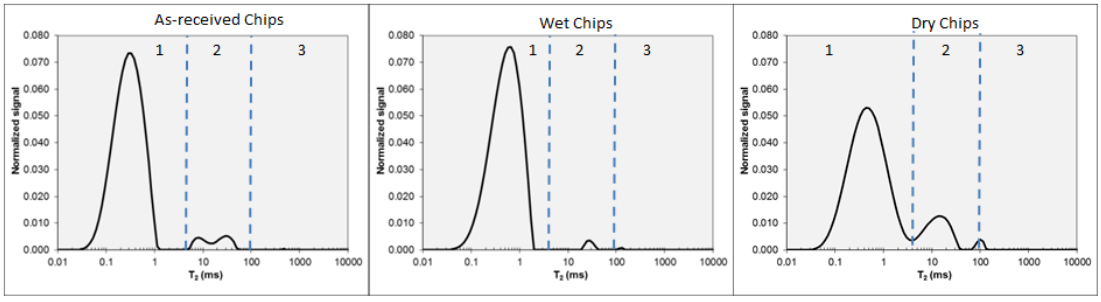

Figure 64: NMR signal for different chips conditions

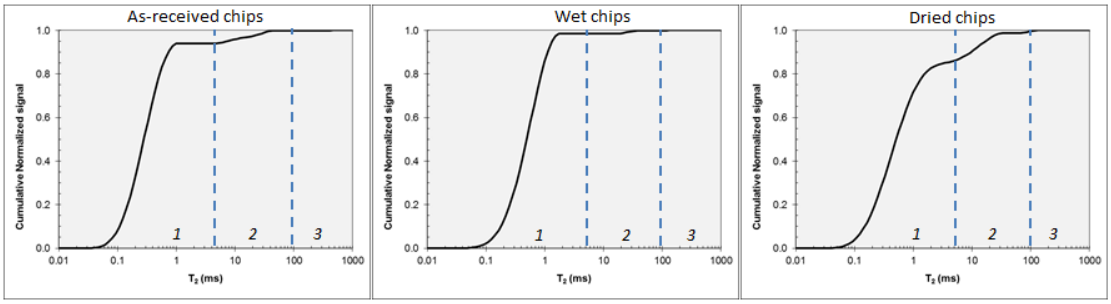

Figure 65: NMR Cumulative signal for different chip conditions

Interpretation based on only the elementary NMR graphs shown in Figure 64 and Figure 65 suggests that wetting leads to an increase in region one and a decrease in region two and three. However, it has to be taken into account that this is based on a normalized signal that doesn't provide information on the fluid volume present in a sample. Figure 66 provides the calculated absolute values of fluids [cm^3] present in each of the three regions. An increase of the total water content of each region is observed when the sample is wetted. It is, however, obvious that the increase in water content in the bound region is much larger compared to the increase in capillary-bound and free fluid water. This explains the behavior of the curves in Figure 64 and Figure 65 as the normalized signal for the first groups increases more rapidly than the other two groups.

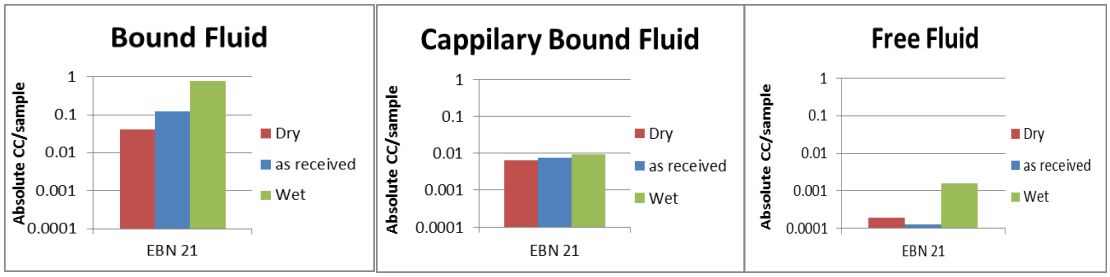

Figure 66: Water contents for different conditions and fluid regions for sample EBN 21

It was expected that when the samples are dried that the free movable fluids and capillary bound fluids would evaporate first, due to their mobility, leaving only bound water behind. In Figure 65 this is not shown for the dried chips, instead an increase in the percentage of the total fluid is observed for the 2nd and 3rd region. This is explained by the fact that only a small amount of water was originally present in the sample. The majority of the water is present within the clay-bound region and therefore more water evaporates from that region compared to the other two. Because of the decrease in the total water content an increase occurs in the percentage of the second and third region, resulting in the graphs displayed in Figure 64 and Figure 65. On the other hand a significant increase in the free fluid content was expected when a sample was wetted, filling up, open pore space with fluid. Instead the graphs illustrate a percentage decrease in the wetting process for the free fluid region and an increase of the clay bound water region. In Figure 67 and 68 the same graphs as shown previously for the chips are shown for the plugs. The plugs are analyzed before and after a steady-state flow experiment in which water was forced into the plugs. In these graphs an increase in the percentage of bound fluid is observed and the percentage of total fluid decreases in region 2 and 3. Figure 69 illustrates the increase of fluid content for each different region compared to

the “as-received” condition. The amount of fluid contained within the sample is obviously much higher compared to the wetted chips condition. This is a result of the water being forced into the sample instead of absorption. The changes also correlate with those observed between the “as-received” and wetted chips, although these are much larger.

The methodology used to wet chips is by placing a cup filled with chips in a humidity chamber so the water can be absorbed by the chips. During absorption the weight is continuously measured and if the weight of the chips doesn’t increase anymore over time the chips are considered wet. The process, however, does not force any fluids into the sample, which was done for the steady-state experiment. Instead, water is only absorbed by the chips. Interesting is that both of the experiments show the same behavior on the NMR graphs.

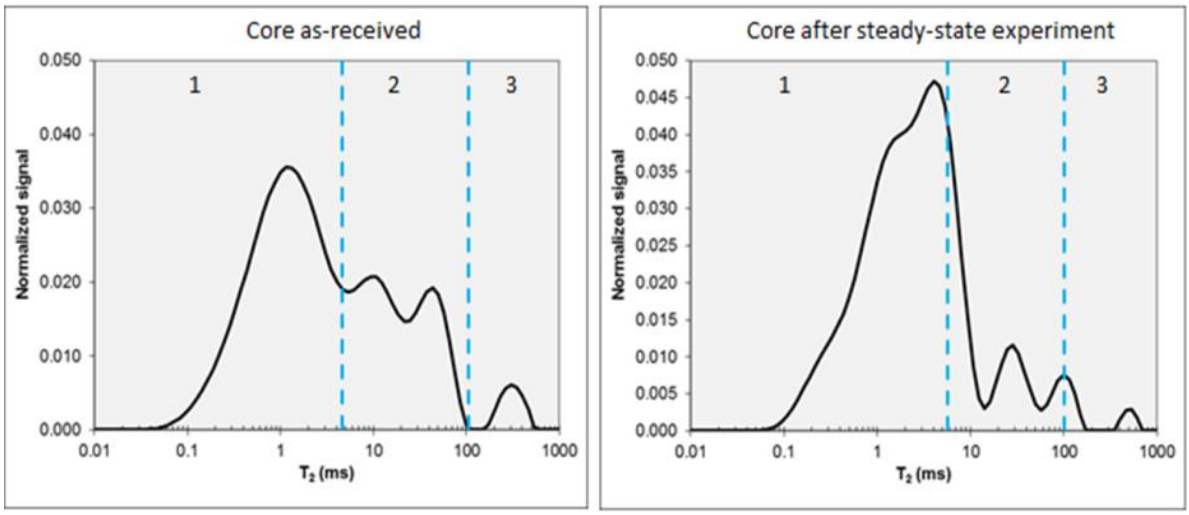

Figure 67: Normalized NMR T_2 signal of sample EBN 21

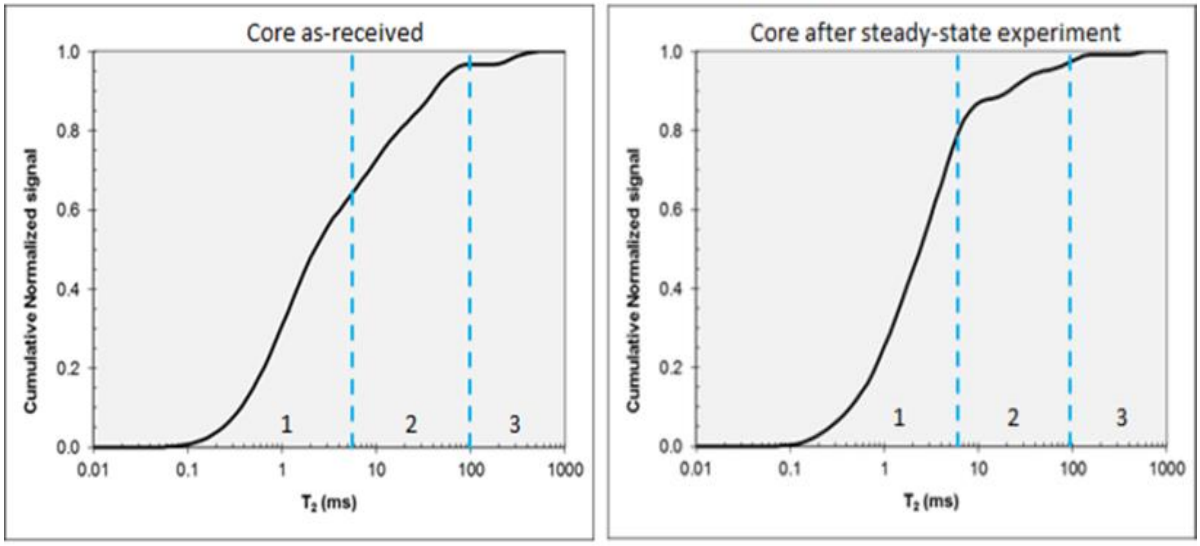

Figure 68: Cumulative NMR T_2 signal for plugs before and after imbibition of sample EBN 21

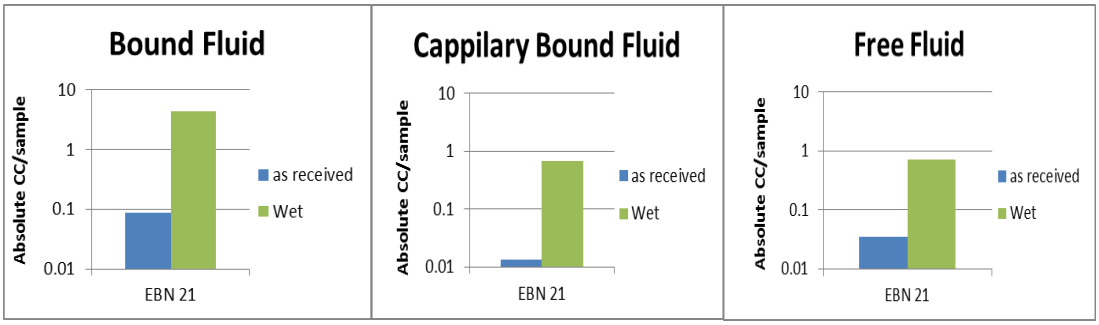

Figure 69: CC per sample for the wet and dry conditions indicating the increase of fluid per region

It was previously explained that the chips were analyzed on different conditions to provide a in the fresh state conditions condition. Both methods used to wet the sample illustrate that a majority of the fluid is absorbed by the clays. The fluid, that remains in the free fluid region is almost an order of magnitude lower for the steady-state experiment compared to the bound region. Since the fluid is mainly absorbed by the rock matrix is concluded, that the samples have continuously dried during storage. From the NMR results it cannot be concluded if the wet samples represent the in-situ condition because it cannot be checked if all pores are saturated with water after the imbibition.

7.7 The Effect of Using Helium, Nitrogen and Water on Permeability Measurements

The in-situ fluid conditions in the shale samples are not known and permeability is an extrinsic rock property. For this reason, the effect of using gas and fluid has been evaluated on the permeability results. Figure 70 illustrates that the use of different gases, i.e. nitrogen and helium, results in different permeabilities.

Flow through a rock matrix is restricted by the pore throats connecting larger pore spaces. The medium, either different gases or fluids, need to be able to flow through these pore throats. The pore throats in our shale samples were found to be very small. Bigger molecules will therefore be more restricted in their flow compared to smaller molecules. In general it is accepted that a larger molecule size will result in a smaller permeability.

Permeability has been tested with, water and nitrogen and helium. Based on the molecule size, water was expected to have the lowest permeability and helium the highest.

However, in Figure 70 it is shown that the permeability for a plug water permeability measurement scales within the helium and nitrogen chips permeability range. It is important to note that the fluid permeability is performed on a core within a different experimental set-up.

Firstly, the differences between the helium and nitrogen gas permeability is discussed. The helium has a molecule diameter of 62 pm (10^{-12} m) and nitrogen a molecule size of about three times that size. With the GRI experiment the gas is forced into the sample material. It is probable that a large part of the porosity of the samples is situated in very small pores, with pore throats smaller than 0.1 µm. Therefore gas with a larger molecule size cannot move through the smaller pores resulting in a smaller permeability. This process where some molecules cannot move through certain pore throat apertures is called molecular sieving.

Secondly, helium and nitrogen gas are different gases by their absorption capacities onto the grains of the sample. Helium is inert and does not get absorbed and therefore flows through the pores. Nitrogen on the other hand, can be absorbed onto the rock matrix. The absorption of nitrogen results into a volume increase of the rock which results into the swelling of grains. Consequently, by the increase of pore size the open pore space within a rock matrix gets reduced, resulting in the reducing of the pore throats (Guarnieri, 2012).

Water has a larger molecule size than nitrogen and is absorbed by the sample material. However, water has a higher permeability compared to nitrogen and this effect is remarkable. The helium and nitrogen measurements are performed on chips, but the water permeability is measured on plugs. The chips are prepared by crushing of sample material and therefore the original sample structure, including fractures and high permeability streaks, are, if present, not taken into account. The plugs used for water permeability remains within the original rock structure with the possibility to have permeability enhancing structures. Based on the result shown in Figure 70, it is concluded that the core samples are likely to contain higher permeability streaks.

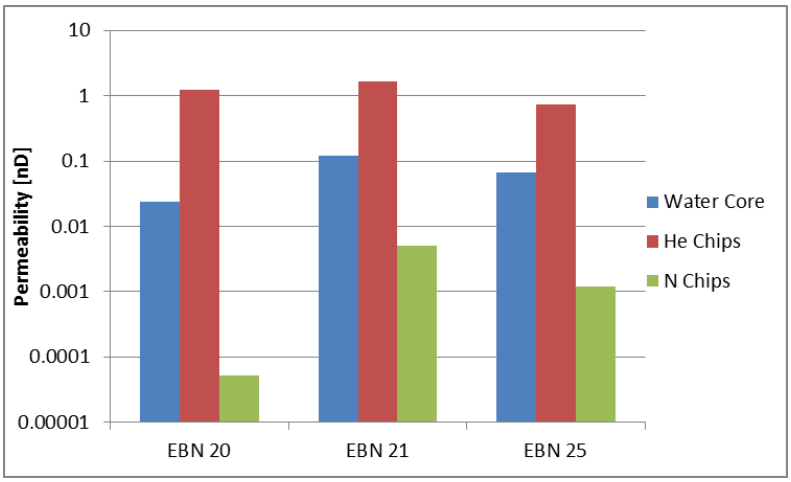

Figure 70: Permeability for water and different gases on "as-received" condition sample material

High permeability streaks within shales known in the Eagle Ford shale, where they account for a large percentage of the production (Maugeri, 2013). Although it is premature to conclude from these measurements if the observation can be explained solely by this effect. High permeability streaks can increase the production potential of a shale formation. They are found to occur often in highly heterogeneous formations. The heterogeneity is evaluated in the next section.

7.8 Heterogeneity

Experimental results from Posidonia samples have been obtained for several parameters, allowing to assess the shale oil potential. These sample measurements are used to provide an indication of the Posidonia formation and, therefore, the results are up-scaled to formation level. Upscaling is the process of extrapolating the local data within a formation to assess the complete formation as illustrated in Figure 71. The success of upscaling depends on two parameters, the amount of data points within the formation and the heterogeneity of the formation – i.e. if a formation is homogeneous, fewer data points are necessary to obtain a representative result. Therefore, the variations of the measured properties are used to assess the degree of heterogeneity of the Posidonia formation.

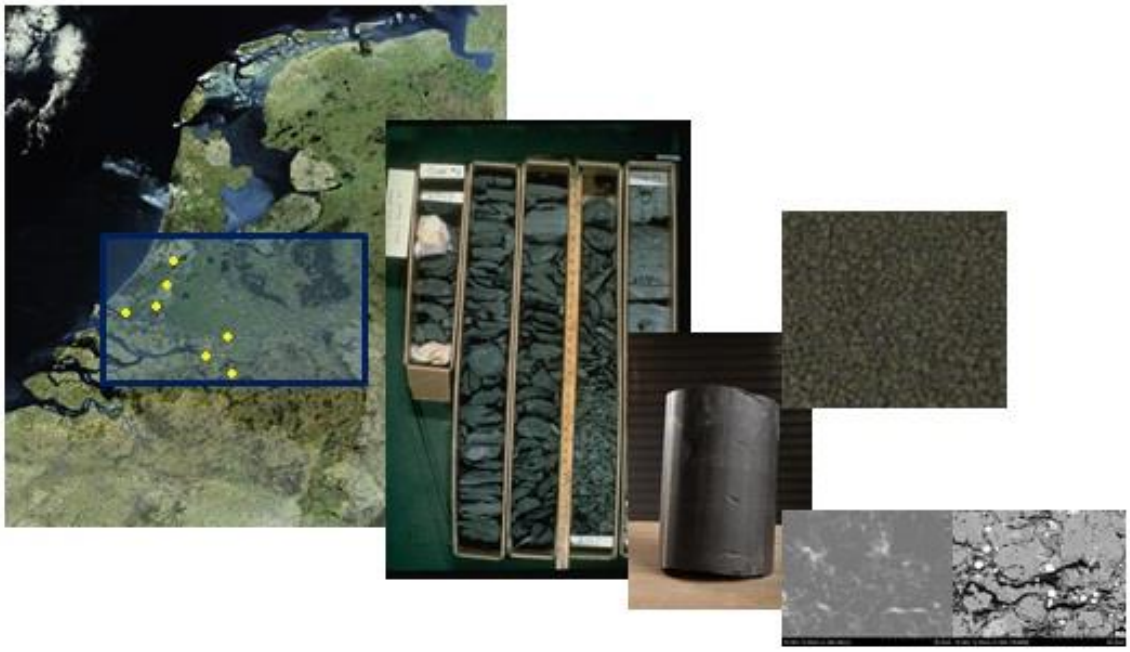

Figure 71: Illustrating the process from SEM Images and core material to reservoir level

Although the amount of samples used within this project is small and hardly represent the complete formation, the heterogeneity is evaluated on several parameters in a 3D plot.
BSE SEM data are displayed in Figure 72, with the meso-, micro- and nano-pore groups on three axis. It is observed that the samples do not cluster but are widely spaced apart. This is an indication that the Posidonia formation is quite heterogeneous.

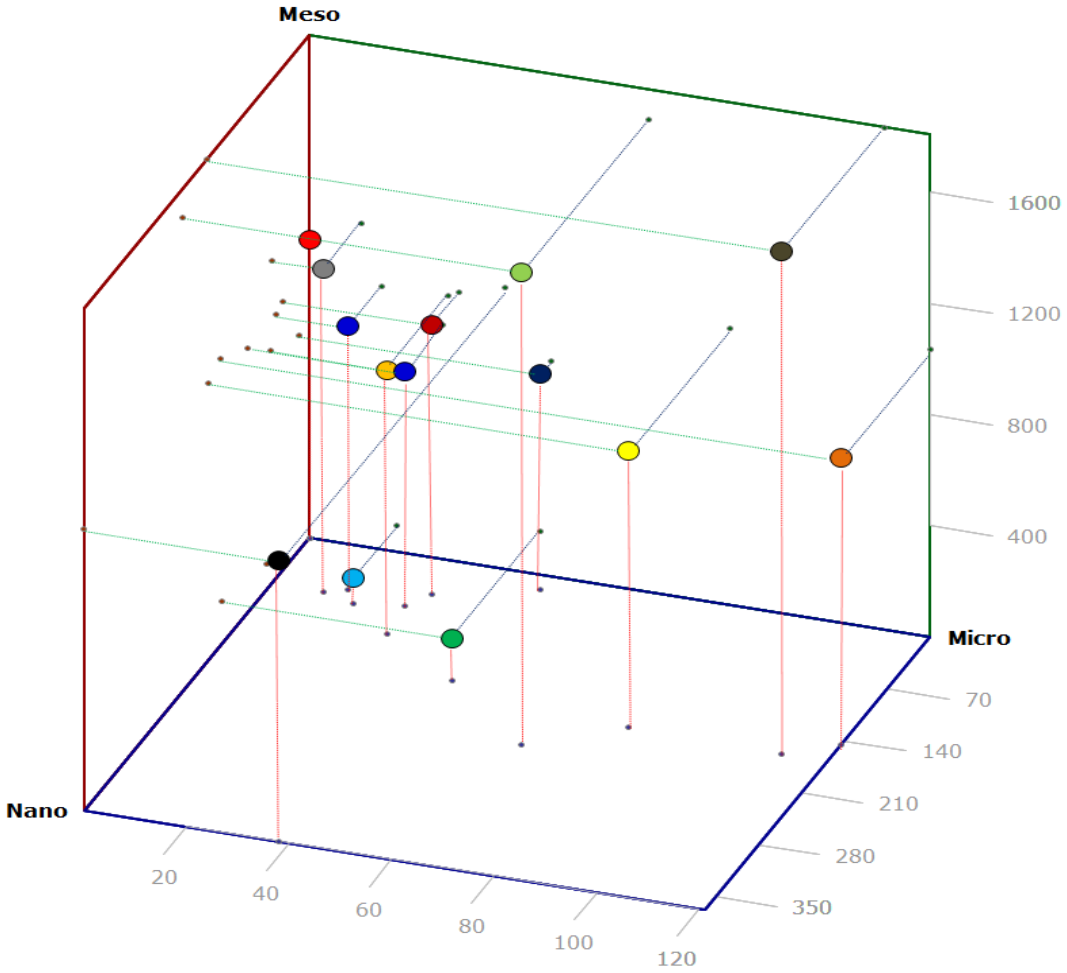

Figure 72:BSE SEM Image data plotted in a 3D-cube

In addition to the SEM data, key parameters such as porosity, T_2 time, TOC and permeability are plotted in a 3D plot, shown in Figure 74. The figure illustrates a large spread among the sample. It should be noted that heterogeneity is not only observed between different wells but also in samples from the same core. This suggests that the heterogeneity occurs within small layers in a single well and not just over large distances. Unfortunately, no data was publicly available to compare these plots with samples from producing shale oil plays.

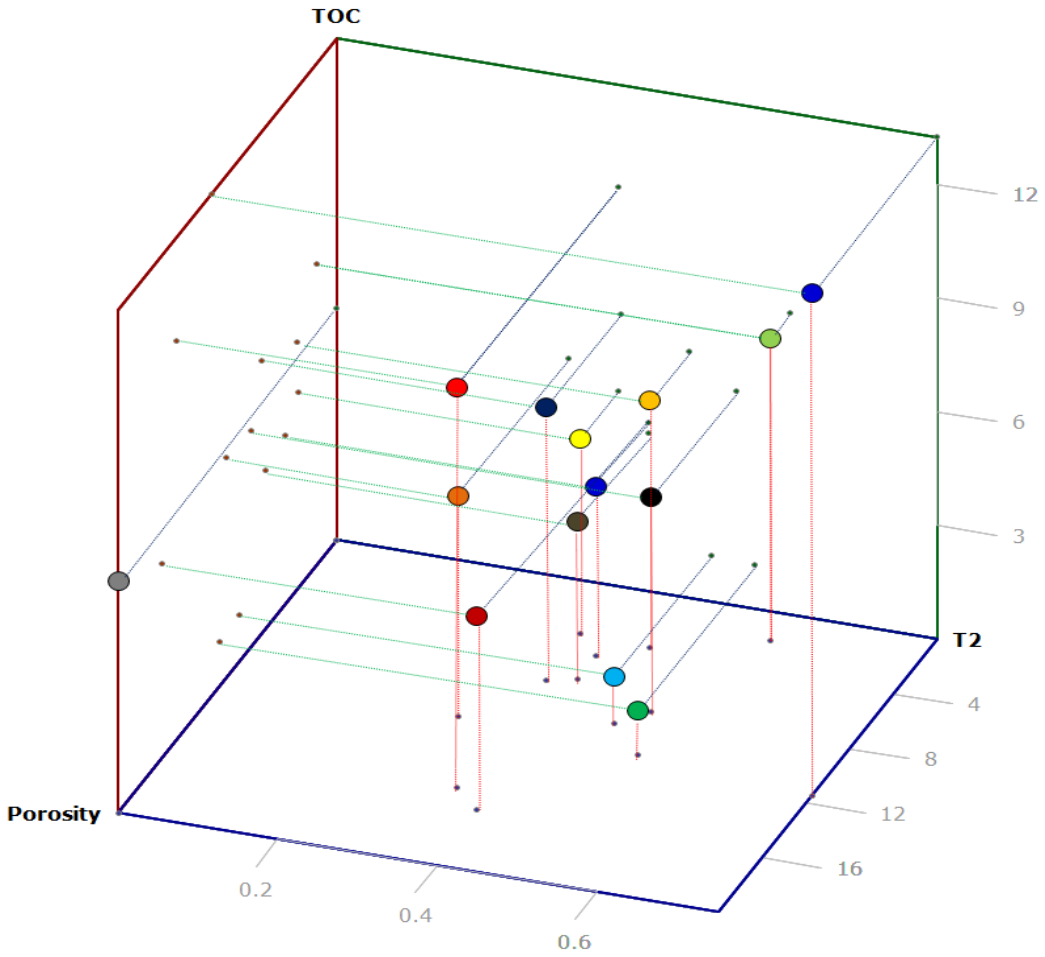

Figure 73: 3D plot for all samples on porosity(GRI), NMR T_2 and TOC(TGA)

Figure 74 shows the average TOC values plotted on a map of the top of the Posidonia formation in the West Netherlands Basin. No trend can be observed, and the highest TOC measurement lies next to the lowest TOC value. Other maps with different parameters yielded similar results and are listed in the Appendix G.2.

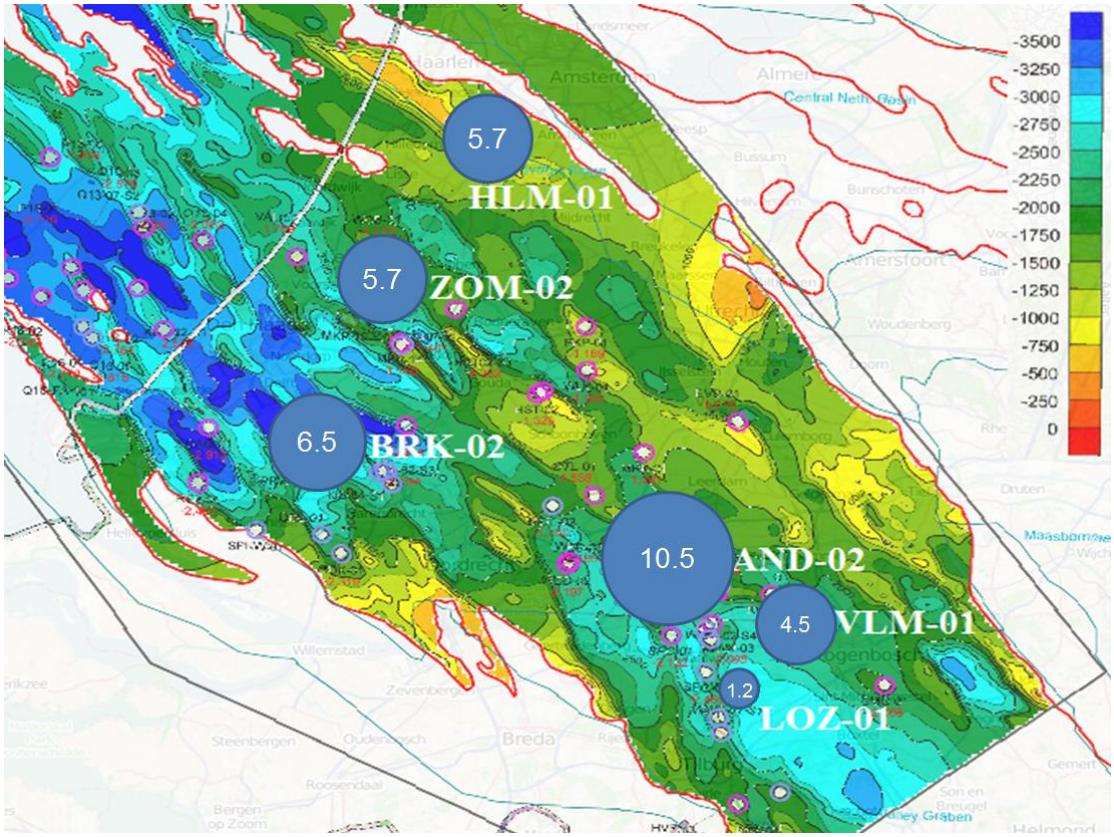

Figure 74: TOC percentage indicated by the number and the size of the circle plotted on a depth chart of the top Posidonia

The various measurements and results illustrate that the analyzed parameters are not evenly distributed over the area. The presence of heterogeneities within a formation generally has a negative influence on the success of upscaling reservoir data. Therefore, upscaling from this limited data set implies that numerous assumptions need to be made, decreasing the reliability of the model.

7.9 Validation of the EIA Report

In the second chapter of this report the methodology for shale oil potential by the EIA is described. This methodology was used to determine the TRR of three formations within the Netherlands. This project has evaluated some of the critical parameters such as, the presence of liquid hydrocarbons, the porosity and the permeability for the Posidonia formation. In this section the results obtained and interpreted during this project will be used to validate the EIA data of the Posidonia shale. A significant part of the EIA study has been on defining the areal extent of the plays in the subsurface. Although this is essential for reservoir evaluation, and misinterpretation can result in large changes of the result, this analysis is not taken into account here. The focus of this report is solely on providing information based on the methodology once the areal extent has been determined.

The EIA study mentioned that the methodology is based upon a conventional approach evaluating shale properties. However, the fundamental question, if there is any oil present and whether it can be produced, is not investigated into detail. Parameters used to evaluate a shale

formation are the initial depositional environment, the depth, the TOC content, the maturity and the geographical location. It is however doubtfull that the identified parameters are correct for an assessment. The fundamental properties of a shale play if it is hydrocarbon-bearing and whether it can be produced through the rock matrix are not evaluated.

The EIA report evaluates three formations, covering an area of 2.750 mi^2 with a limited amount of data points. In order to provide a thorough basis for the potential of the shale plays only the Posidonia Formation was analyzed in this project because this was the only formation with core material. This lack of data is an illustration of the shortcomings of the EIA report. Based on the information provided by the EIA and the additional experiments carried out during this project, the following is concluded on the EIA report: There is not enough information available to make a sound estimation of the potential TRR of the three formations.

Within the EIA report it is assumed that the organic material present within the Posidonia shale formation is of the type II lipid-rich kerogen. The TOC percentage is estimated to range from less than 1% to 16% , with an average of 6%. Both the TOC and the type of kerogen has been analyzed in the SHAPE project and included in this project. Regarding the TOC content for the evaluated samples of the Posidonia the EIA study is correct. However, the type II kerogen is analyzed for five samples, EBN 20, 22, 23, 24 and 25 out of 14 samples. In addition to the type II kerogen, type III humic kerogen is found in sample EBN 27, but the majority is found to fall in between the type II and type III kerogen.
Thermal maturity is not measured during this project but according to the van Krevelen diagram in Figure 54 the majority of the samples are immature for oil generation. This is in contradiction with the EIA report which assumes an average thermal maturity of 1.15% which would fall in to the gas maturity range (McCarthy et al., 2011). In addition to TOC content and the thermal maturity this research investigates the presence of liquid hydrocarbons within sample material with other methods, such as TGA and NMR T_2. From the results of these experiments, several conclusions regarding liquid hydrocarbons can be made. The most important one, however, is that the presence of movable liquid hydrocarbons still has to be proven. Although explanations have been given on the absence of free hydrocarbon fluids, it is premature to assume the presence of these liquids. On the other hand, the potential of oil is evident in some of the evaluated samples. Furthermore, it was proven with a steady-state flow experiment that potentially flow through the matrix is possible. However, all the hydrocarbons found were analyzed to be immobile.

In order to calculate the oil-initially-in-place (formula is listed in Equation 1), the oil saturation is used. However, the presence of the oil is not proven, an estimate for this factor is obtained by comparing the shale with other shale plays in the U.S.. It is observed throughout this project that the Posidonia formation is highly heterogeneous. This heterogeneity, based on 14 different samples from seven well locations, makes it extremely difficult to compare the data from the Posidionia with other formations from the U.S..

Heterogeneity throughout the reservoir restricts the possibility to upscale the limited amount of data correctly to the areal extent of the Posidonia formation. There is a very limited amount of data to make an oil-in-place prediction, even if the reservoir was homogenous. For this

reason no statement regarding the potential TRR of the Posidonia can be made. The heterogeneity of the reservoir influences the elementary reservoir evaluation parameters such as, porosity, permeability and the presence of hydrocarbons. Because the EIA has also based its assessment on a limited data set it is likely that the estimation for the TRR within their Posidonia shale formation has a very large error bar.

8 Discussion and Conclusions

Several samples of the Posidonia formation contain hydrocarbon shows that indicate the presence of bound oil or bitumen. In addition, some of the samples were water bearing. All of the fluids, hydrocarbon or water, are indicated as bound and therefore no movable oil is proven. Due to the age of the samples (over 40 years) this does not imply that oil is not present in the shale. It is expected that the light hydrocarbons have moved out from the samples, as the formation is known to have an oil-generating potential, because it acted as the source rock of several reservoirs. On the other hand, samples can also be immature and therefore possibly have not generated any oil. The use of recently obtained drill cuttings has confirmed that it is likely that the lighter hydrocarbons have evaporated from the sample over time.

The pore structure with accompanying pore sizes is found to be sufficient to accommodate oil flow through the matrix with a common pore size in the meso scale. Fractures observed were excluded from the measurement because the nature, drilling-induced or tectonic, could not be determined.
To a large extent the condition of the sample, wet, dry or "as-received" is of influence on the measured porosities and pore sizes of the samples. The pore sizes decreased when a sample is wetted and vice versa increased in a dry condition. If the in-situ condition is unknown before an experiment, the differences with the in-situ porosity are significant. The pore structure has the ability to absorb and accommodate water when it was exposed to humid air. This is an indication of open pores spaces as well as connectivity of the pores. In addition, it was found that oils with a larger molecule sizes than gas can be stored in these pores.

A large difference in permeability is found between several permeability-related experiments. Based on the pore size, permeability of the shale is estimated within the range of 0.01 – 1.00 mD for gases. However the GRI method with helium gas measured a permeability in the range of 10^{-5} – 10^{-2} mD. The use of a gas with a larger molecule size results in smaller permeabilities in the range of 10^{-8} – 10^{-5} mD. By contrast, the water permeability on plugs scales between helium and nitrogen in a range of 10^{-5} – 10^{-3} mD. From this it is concluded that the permeability decreases with increasing molecule sizes for the analyzed chips. An increase in water permeability is due to the full core analyses and the apparent fractures in the core. This illustrates the importance of fractures for the flow potential in shale reservoirs.

The Posidonia shale formation is found to be highly heterogeneous based on various parameters. The most consistent trend found in the formation is a decrease in porosity with depth. Because of the heterogeneity found in the parameters it difficult to upscale the data points to formation level with limited data without making large assumptions and increased errors. A statement regarding the TRR of the Posidonia formation, which has been made in the EIA report, is therefore not possible here because of a lack of sufficient information.

Additional findings are:

- Pore size measured with the SEM should be interpreted with care because the greyscale is not sufficient to provide a threshold image. In addition, open pores are best observed on SEM secondary images with a 5 µm scale.
- The estimated pore size distributions show that pores in the mesopore class are dominant. The shales are characterized by a complex system of pore sizes and pore shapes. Several micro-fractures were observed on different shale samples which will influence the flow capacity of the shale formation. Cumulative open pore space and organic matter in percentage identified on the SEM BSE images is observed to increase linearly with the pore size.
- The open pore space identified on the BSE SEM images decreases with depth.
  A biased view of the pore structure is given in 2D images and this does not correlate with permeability measurements. This indicates that SEM BSE images do not directly provide insights into the connectivity or permeability
- The majority of the hydrocarbon found in the Posidionia shale, as analyzed with the NMR experiment, is bound oil and probably not possible to produce. Furthermore, some of the samples plot in the clay bound water region, indicating no hydrocarbons are present.
- The shale samples absorb significantly more water when placed in a humid area compared to the amount of fluid, which is lost when dried. This is an indication that the open pore space is large enough to have contained free movable hydrocarbons. In addition this is an indication that the sample material has been dried during storage.
- The TGA analysis illustrated the possible effect of age on the samples, as all the evaluated recently obtained samples show a higher amount of fluid loss in the 30˚C – 200˚C. This indicates that it is reasonable to assume that the lighter hydrocarbons have evaporated from the old core material during the aging process.
- Measurements on permeability and porosity is challenging because of the small pores in the rock matrix. This results in extremely low measurements, which are on the boundary of the experimental working envelope. The GRI method is sensitive to temperature differences and this can result in a pressure difference of ~ 0.1 psig even in a temperature-controlled room.
- Due to the low matrix permeability, fractures are important for the total permeability. From flow-related experiments it was found that cores, which include fractures, provided higher permeability measurements.
- Samples are found to be highly heterogeneous, therefore no valid prediction can be made on the potential TRR in the Posidonia formation.

9 Recommendations

In order to improve the evaluation of shale oil plays in the Netherlands, new sample material should be acquired.

It is strongly recommended to obtain new cores in a new well. These cores should be brought to surface in a method that the in-situ condition is preserved. In addition the core should be retrieved and stored in a canister to preserve the original composition of hydrocarbons. The core should be evaluated with the methodology used in this project, focusing on the NMR T_1 & T_2 and TGA measurements.

Additional research is recommend to investigate the T_1 values for all of the samples to extend the plot shown in Figure 33(T_1/T_2 ratio vs. T_2 plot NMR).

Steady-state permeability measurements performed with multiple fluids are recommended to be executed for all samples. In addition, the same experiment should be repeated with an oil with similar characteristics as the potential hydrocarbon fluid present in-situ.

Measuring the fluid permeability with a different set-up is beneficial to evaluate and to verify the results. Therefore, it is recommended to evaluate all of the samples with a different fluid in the permeability experiments.

Additional analysis of SEM images, both BSE and SE, are recommended to obtain a better understanding of the apparent pore sizes. This data can be used to re-evaluate and improve the correlation between pore sizes and permeability.

Samples from producing shale oil formations should be tested with the same experiments as suggested here. This enables a direct comparison of the results for the Posidonia shale samples with those from producing fields. No industry-standard permeability measurement is available and the results differ between laboratories. Therefore, it is recommended to perform permeability-related experiments on samples from producing shale oil fields in the same laboratory as used in this project.

Micro-fractures influence the permeability and porosity of both chips and core plugs. To reduce this effect, a set-up in which the GRI core holder can be placed under a predefined pressure would reduce the influence of these micro-fractures and provide a more reliable value of permeability and porosity.

In order to understand shale formations and to estimate the potential of a shale oil play, the accumulation of data is essential. Heterogeneity of the structure makes it difficult to compare formations in general with producing plays. Therefore, additional in-depth research for the fundamental parameters on an extensive set of core material of the Posidonia formation is recommended. This is likely to provide new insights into the shale oil potential of the Posidonia formation.

The EIA has made an initial assessment of three shale formations within The Netherlands. Although it is certain that the provided amount of TRR for the Posidonia is not correct, it has indicated the possibility for shale oil development within The Netherlands. From this research it is advised for any follow-up research of the EIA to focus on confirming the presence and classification of the hydrocarbons in shale formations.

References

Van Adrichem Boogaert, H.A., Kouwe, W.F.P., 1997, Stratigraphic nomenclature of the Netherlands, revision and update by RGD and NOGEPA. Mededelingen Rijks Geologische Dienst (Haarlem) 50.

Aguilera, R.; 2013; Flow Units: From conventional to tight gas to shale gas to tight oil to shale oil reservoirs; SPE 165360

Arshad, A.; Al-Majed,A.A.; Maneaouar,H.; Muhammadain,A.; Mtawaa, B.; 2009; Carbon Dioxide (CO2) Misccible Flooding in Tight Oil reservoirs: A case study; SPE 127616

Van Balen, R.T.; Bergen, F.; Leeuw de, C.; Pagnier, H.; Simmelink, H.; Wees van, J.D.; Verweij, J.M.; 2000; Modelling the hydrocarbon generation and migration in the West Netherland Basin, the Neterlands; Geologie en Mijnbouw / Netherlands Journal of Geosciences 79 (1): 29-44

Berendsen, H.J.A.; 2004; De vorming van het land, Inleiding in de geologie en de geomorfologie

Blasingame, T.A.; 2008; The characteristic flow behavior of low-permeability reservoir systems; SPE114168

Bohacs, K.M.; Passey, Q.R.; Rudnicki, M.; Esch, W.L.; Lazar, O.R.; 2013; The spectrum of fine grained reservoirs from 'Shale Gas' to 'Shale Oil'/Tight liquids: Essential attributes, Key controls, Practical characterization; IPTC 16676

Bouw, S.; Lutgert, J.; 2012; Shale plays in The Netherlands; SPE 152644

Chaudhary, A.S.; Ehlig-Economides, C.; Watterbarger, R.; 2011; Shale oil production performance from a stimulated reservoir volume; SPE 147596

Chan, P.; Etherington, J.R.; Aguilera, R.; 2010; A process to evaluate unconventional resources; SPE 134602

Chen, C.; Balhoff, M.; Mohanty, K.K.; 2013; Effect of reservoir heterogeneity on improved shale oil recovery by CO2 Huff-n-puff; SPE 164553

Chen, J; Li, B.; Georgi, D.; 2012; Petrographic features of kerogen in unconventional shale and their effect on Hydrocarbon Petrophysics; SPE 162612

Clarkson, C.R.; Pedersen, P.K.; 2010; Tight oil production analysis: Adaption of existing rate-transient analysis techniques; CSUG/SPE 137352

Coates, G.R.; Xiao, L.; Prammer, M.G.; 1999; NMR Logging Principles & Applications; Halliburtion Energy Services Publication H02308

Curtis, M.E.; Ambrose, R.J.; Sondergeld, C.S.; 2010; Structural Characterization of Gas Shale on the Micro- and Nano-Scales; CUSG/SPE 137693

Curtis, M.E.; Sondergeld C.H.; Rai, C.S.; 2013 Investigation of the Microstructures of Shales in the Oil Window; SPE168815/URTeC 1581844

Driskill, B.; Walls, J.; Sinclair, S.W.; DeVito, J.: 2013; Micro-scale characterization of the Eagle For Formation using SEM methods and digital rock modeling; SPE 168848

Dyni, J.R.; 2006; Geology and resources of some world oil-shale deposits; USGS scientific Investigations report 2005-5294, http://geology.com/usgs/oil-shale/

EIA; 2012; Oil and Gas Security, Emergency Response of IEA Countries, The Netherlands; http://www.iea.org/publications/freepublications/publication/Oil&GasSecurityNL2012.pdf

Flores, C.P.; Holditch, S.A.; Ayers, W.B.; 2011; Economics and technology drive development of unconventional oil and gas reservoirs: Lesson learned in the United States; SPE 146765

Guarnieri, R.V.; 2012; Measurements of gas permeability on crushed gas shale; MSc. Research project (Utrecht University)

Handwerger, D.A.; Wilberg, D.; Pagels M.; Rowland B.; Keller J.F.; 2012; Reconciling Retort versus Dean Stark Measurements on Tight Shales; SPE 159976

Handwerger, D.A.; Suarez-Rivera, R.; Vaughn, K.I.; Keller, J.F.; 2011; Improved Petrophysical Core Measurements on Tight Shale Reservoirs Using Retort and Crushed Samples; SPE 147456

Houben, M.E.; Barnhoorn, A.; Drury, M.R.; Peach, C.J.; Spiers, C.J.; 2014; Microstructural Investigation of the Whitby Mudstone (UK) As an Analog for Posidonia Shale; We E103 09; Eage Conference Amsterdam

Hughes, J.D.; 2013; A reality check on the shale revolution; Nature, Volume 494, p307 – 308

De Jager, J.; Wong, T.; Batjes, D.A.J; Geology of the Netherlands; 2007; Royal Netherlands Academy Arts and Sciences

Jarvie, D.M.; 2012; Shale Resource Systems for Oil and Gas: Part 2 – Shale Oil Resource Systems; AAPG Memoir 97, p. 89 – 119

Jin, C.J.; Siera, L.; Mayerhofen, M.; Halliburton; 2013; A production optimization approach to completion and fracture spacing optimization for unconventional shale oil exploitation; SPE 168813

Kee, L.J.F.; 2010; Onshore shale gas potential of the lower Jurassic Altena group in the West Netherlands Basin and Roer Valley Graben; Master Thesis of Utrech University

Luffel, D.L.; Hopkins, C.W.; Holditch, S.A.; Schettler, P.D.; 1993; Matrix Permeability Measurements of Gas Productive Shales; SPE 26633

Maugeri, L.; 2013; The shale oil boom a U.S. phenomenon; HARVARD Kennedy School, Belfer Center for science and international affairs

McCarthy, K.; Rojas, K.; Niemann, M.; Palmowski, D.; Peters, K.; Stankiewicz, A.; 2011; Basic petroleum geochemistry for source rock evaluation; Oilfield review summer: 23, no. 2, Schlumberger

Mullen, M.; 2012; Fracability Index – More Than Just Calculating Rock Properties; SPE 159755
Martin, A.J.; Solomon, S.T.; Hartmann, D.J.; 1997; Characterization of Petrophysical flow units in carbonate reservoirs; AAPG Bulletin, v. 81, No.5, P. 734 – 759

Mills et al.; 2008; The myth of the oil crisis: overcoming the challenges of depletion, geopolitics, and global warming; Greenwood Publishing Group. pp. 158–159. ISBN 978-0-313-36498-3

Noordoven, Q.A.L.V.; 2011; Characterization of production potential in Jurassic and carboniferous shale plays of the Netherlands; Master thesis of Delft University of Technology

Oleas, A.M.; Osuji, C.E.; Chenevert, M.E.; Sharma, M.M.; 2010; Entrance pressure of oil-based mud into shale: Effect of shale water acitivity, and mud properties; SPE 116364

Pang, J.; Zuo, J.; Zhang, D.; Schlumberger; Liangui Du; Hess Corporation; 2013; Effect of Porous Media on Saturation Pressures of Shale Gas and Shale Oil; IPTC 16419

PwC; 2013; Shale Oil: The next energy revolution; http://www.pwc.com/gx/en/oil-gas-energy/index.jhtml

Ramey, H.J.; 1964; Rapid methods of estimating reservoir compressibilities; Journal of Petroleum Technology, p 968 – 970

Rosen, R.; Mickelson, W.; Sharf-Aldin, M.; Kosanke, T.; PaiAngle, M.; Patterson, R.; Mir, F.; Narasimhan, S.; Amini, A.; 2014; Impact of Experimental Studies on Unconventional Reservoir Mechanisms; SPE 168965

Rylander, E.; Singer, P.M.; Jiang, T.; Lewis, R.; McLin, R.; 2013; NMR T2 distrubutions in the Eagle Ford shale: Reflections on Pore Size; SPE164554

SHAPE Project; 2014; http://shape.leeds.ac.uk/

Tinni, A.; Odusina, E.; Sulucarnain, I.; Sondergeld, C.; Rai, C.; 2014; NMR Response of Brine, Oil, and Methane in Organic Rich Shales; SPE 168971

U.S. Department of Energy; 2000; Helium and Nitrogen Sizes; http://www.newton.dep.anl.gov/askasci/chem00/chem00243.htm

U.S. Energy Information Administration, 2013; Technically Recoverable Shale Oil and Shale Gas Resources: An Assessment of 137 Shale Formations in 41 Countries Outside the United States; http://www.eia.gov/analysis/studies/worldshalegas/

U.S. Energy Information Administration, 2011; World Shale Gas Resources: An Initial Assessment of 14 Regions Outside the United States; http://www.eia.gov/analysis/studies/worldshalegas/

U.S. Energy Information Administration_1; 2013; Drilling productivity report, For key tight oil and gas regions; http://www.eia.gov/petroleum/drilling/pdf/dpr-full.pdf

U.S. Energy Information Administration_2; 2013; Glossary; http://www.eia.gov/tools/glossary/

Vasquez, M.; Beggs, H.D.; 1980; Correlations for fluid physical property predictions; Journal of Petroleum Technology, pp. 968 – 970

Walls, J.D.; Sinclair, S.W.; 2011; Eagle ford shale reservoir properties form digital rock physics; First Break, Volume 29 – issue 6 – June 2011, p 97 – 101

Wan, T.; Sheng, J.J.; Soliman, M.Y.; 2013; Evaluate EOR potential in fracture shale oil reservoirs by cyclic gas injection; URTeC 1611383
Wang, D.; Butler, R.; Liu, H.; Ahmed, S.; 2010; Flow-rate Behavior and Imbibition in Shale; SPE 138521

Wei, C.; 2013; Microstructure characterization for a shale gas reservoir by combining visualization technique and physical measurement; SPE 167610

Wile, R.; 2013; Why America's Shale Boomn Will Last for Years; Business Insider

Ziarani, A.S.; Aguilera, R.; 2010; Knudsen's permeability correction for tight porous media; Transp Porous Med (2012) 91:239 – 260

APPENDIX A: Input Parameters of the EIA Report

Appendix A.1

The used play success factor, prospective areas success factor and composite success factor

Continent	Region	Basin	Formation	Play Success Factor	Prospective Area Success Factor	Composite Success Factor
South America	Colombia	Middle Magdalena Valley	La Luna/Tablazo	80%	70%	56%
		Llanos	Gacheta	55%	45%	25%
	Colombia/Venezuela	Maracaibo Basin	La Luna/Capacho	70%	50%	35%
	Argentina	Neuquen	Los Molles	100%	50%	50%
			Vaca Muerta	100%	60%	60%
		San Jorge Basin	Aguada Bandera	50%	40%	20%
			Pozo D-129	60%	40%	24%
		Austral-Magallanes Basin	L. Inoceramus-Magnas Verdes	75%	60%	45%
		Parana Basin	Ponta Grossa	40%	30%	12%
	Brazil	Parana Basin	Ponta Grossa	40%	30%	12%
		Solimoes Basin	Jandiatuba	50%	30%	15%
		Amazonas Basin	Barreirinha	50%	30%	15%
	Paraguay	Parana Basin	Ponta Grossa	40%	30%	12%
	Uruguay		Cordobes	40%	40%	16%
	Paraguay/Bolivia	Chaco Basin	Los Monos	50%	30%	15%
	Chile	Austral-Magallanes Basin	Estratos con Favrella	75%	60%	45%
Eastern Europe	Poland	Baltic Basin/Warsaw Trough	Llandovery	100%	40%	40%
		Lublin	Llandovery	60%	35%	21%
		Podlasie	Llandovery	60%	40%	24%
		Fore Sudetic	Carboniferous	50%	35%	18%
	Lithuania/Kaliningrad	Baltic Basin	Llandovery	80%	40%	32%
	Russia	West Siberian Central	Bazhenov Central	100%	45%	45%
		West Siberian North	Bazhenov North	75%	35%	26%
	Ukraine	Carpathian Foreland Basin	L. Silurian	50%	40%	20%
		Dniepr-Donets	L. Carboniferous	50%	40%	20%
	Ukraine/Romania	Moesian Platform	L. Silurian	55%	40%	22%
	Romania/Bulgaria		Etropole	50%	35%	18%
Western Europe	UK	N. UK Carboniferous Shale Region	Carboniferous Shale	60%	35%	21%
		S. UK Jurassic Shale Region	Lias Shale	80%	40%	32%
	Spain	Cantabrian	Jurassic	80%	50%	40%
	France	Paris Basin	Lias Shale	100%	50%	50%
			Permian-Carboniferous	80%	40%	32%
		Southeast Basin	Lias Shale	60%	30%	18%
	Germany	Lower Saxony	Posidonia	100%	60%	60%
			Wealden	75%	60%	45%
	Netherlands	West Netherlands Basin	Epen	75%	60%	45%
			Geverik Member	75%	60%	45%
			Posidonia	75%	60%	45%
	Sweden	Scandinavia Region	Alum Shale - Sweden	60%	50%	30%
	Denmark		Alum Shale - Denmark	60%	40%	24%

APPENDIX A.2

Oil Recovery Efficiency for 28 U.S. Tight Oil Plays

Basin	Formation/Play	Age	Oil In-Place (MBbls/Mi^2)	Oil Recovery (MBbls/Mi^2)	Oil Recovery Efficiency (%)
Williston	Bakken ND Core	Mississippian-Devonian	12,245	1,025	8.4%
	Bakken ND Ext.	Mississippian-Devonian	9,599	736	7.7%
	Bakken MT	Mississippian-Devonian	10,958	422	3.9%
	Three Forks ND	Devonian	9,859	810	8.2%
	Three Forks MT	Devonian	10,415	376	3.6%
Maverick	Eagle Ford Play #3A	Late Cretaceous	22,455	1,827	8.1%
	Eagle Ford Play #3B	Late Cretaceous	25,738	2,328	9.0%
	Eagle Ford Play #4A	Late Cretaceous	45,350	1,895	4.2%
	Eagle Ford Play #4B	Late Cretaceous	34,505	2,007	5.8%
Ft. Worth	Barnett Combo - Core	Mississippian	25,262	377	1.5%
	Barnett Combo - Ext.	Mississippian	13,750	251	1.8%
Permian	Del. Avalon/BS (NM)	Permian	34,976	648	1.9%
	Del. Avalon/BS (TX)	Permian	27,354	580	2.1%
	Del. Wolfcamp (TX Core)	Permian-Pennsylvanian	35,390	1,193	3.4%
	Del. Wolfcamp (TX Ext.)	Permian-Pennsylvanian	27,683	372	1.3%
	Del. Wolfcamp (NM Ext.)	Permian-Pennsylvanian	21,485	506	2.4%
	Midl. Wolfcamp Core	Permian-Pennsylvanian	53,304	1,012	1.9%
	Midl. Wolfcamp Ext.	Permian-Pennsylvanian	46,767	756	1.6%
	Midl. Cline Shale	Pennsylvanian	32,148	892	2.8%
Anadarko	Cana Woodford - Oil	Upper Devonian	11,413	964	8.4%
	Miss. Lime - Central OK Core	Mississippian	28,364	885	3.1%
	Miss. Lime - Eastern OK Ext.	Mississippian	30,441	189	0.6%
	Miss. Lime - KS Ext.	Mississippian	21,881	294	1.3%
Appalachian	Utica Shale - Oil	Ordovician	42,408	906	2.1%
D-J	D-J Niobrara Core	Late Cretaceous	33,061	703	2.1%
	D-J Niobrara East Ext.	Late Cretaceous	30,676	363	1.2%
	D-J Niobrara North Ext. #1	Late Cretaceous	28,722	1,326	4.6%
	D-J Niobrara North Ext. #2	Late Cretaceous	16,469	143	0.9%

APPENDIX A.3

Tight Oil Data Base Used for Establishing Oil Recovery Efficiency Factors

Basin	Formation/Play	Age	Reservoir Pressure	Thermal Maturity (% R_o)	Formation Volume Factor (B_{oi})
Williston	Bakken ND Core	Mississippian-Devonian	Overpressured	0.80%	1.35
	Bakken ND Ext.	Mississippian-Devonian	Overpressured	0.80%	1.58
	Bakken MT	Mississippian-Devonian	Overpressured	0.75%	1.26
	Three Forks ND	Devonian	Overpressured	0.85%	1.47
	Three Forks MT	Devonian	Overpressured	0.85%	1.27
Maverick	Eagle Ford Play #3A	Late Cretaceous	Overpressured	0.90%	1.75
	Eagle Ford Play #3B	Late Cretaceous	Overpressured	0.85%	2.01
	Eagle Ford Play #4A	Late Cretaceous	Overpressured	0.75%	1.57
	Eagle Ford Play #4B	Late Cretaceous	Overpressured	0.70%	1.33
Ft. Worth	Barnett Combo - Core	Mississippian	Slightly Overpressured	0.90%	1.53
	Barnett Combo - Ext.	Mississippian	Slightly Overpressured	0.80%	1.41
Permian	Del. Avalon/BS (NM)	Permian	Slightly Overpressured	0.90%	1.70
	Del. Avalon/BS (TX)	Permian	Slightly Overpressured	0.90%	1.74
	Del. Wolfcamp (TX Core)	Permian-Pennsylvanian	Slightly Overpressured	0.92%	1.96
	Del. Wolfcamp (TX Ext.)	Permian-Pennsylvanian	Slightly Overpressured	0.92%	1.79
	Del. Wolfcamp (NM Ext.)	Permian-Pennsylvanian	Slightly Overpressured	0.92%	1.85
	Midl. Wolfcamp Core	Permian-Pennsylvanian	Overpressured	0.90%	1.67
	Midl. Wolfcamp Ext.	Permian-Pennsylvanian	Overpressured	0.90%	1.66
	Midl. Cline Shale	Pennsylvanian	Overpressured	0.90%	1.82
Anadarko	Cana Woodford - Oil	Upper Devonian	Overpressured	0.80%	1.76
	Miss. Lime - Central OK Core	Mississippian	Normal	0.90%	1.29
	Miss. Lime - Eastern OK Ext.	Mississippian	Normal	0.90%	1.20
	Miss. Lime - KS Ext.	Mississippian	Normal	0.90%	1.29
Appalachian	Utica Shale - Oil	Ordovician	Slightly Overpressured	0.80%	1.46
D-J	D-J Niobrara Core	Late Cretaceous	Normal	1.00%	1.57
	D-J Niobrara East Ext.	Late Cretaceous	Normal	0.70%	1.26
	D-J Niobrara North Ext. #1	Late Cretaceous	Normal	0.70%	1.37
	D-J Niobrara North Ext. #2	Late Cretaceous	Normal	0.65%	1.28

Appendix A.4

EIA gas calculations

In addition to the free oil In-Place a amount of free gas In-Place is provided. This calculation is, to a large extent, based on four characteristics namely; Pressure, Temperature, Gas-Filled Porosity and Net Organically-Rich Shale Thickness. Combining this data with established PVT reservoir engineering equations and conversion factors results into the following GIP equation.

Equation 8: Formula to calculate the Gas Intitial In Place (GIP)

$$GIP = \frac{43{,}560 * A * h * \emptyset * (S_g)}{B_g}$$

$$B_g = \frac{0{,}02829\ z\ T}{P}$$

A area in acres (with the conversion factors of 43,560 square feet per acre and 640 acres per square mile)

h is net organically-rich shale thickness, in feet

$\emptyset$ porosity, dimensionless

S_g fraction of the porosity filled by gas, dimensionless

B_g gas volume factor, in cubic feet per standard cubic feet and includes the gas deviation factor (z)

P Pressure, psi

T Temperature, degrees Rankin

Besides holding oil and gas, shales can include significant quantities of absorbed gas onto the surface of the organics and clays within a shale formation.

Within shale formation the surface of organics and clays can hold significant quantities of gas. These are called absorbed gas and are an addition to oil and gas within a shale formation and are calculated with the Langmuir isotherm.

The Langmuir isotherm provides a relation between the absorption of molecules of the absorbate on a solid surface of the absorbent to gas pressure and concentration at a fixed temperature. Estimates of the Langmuir value and pressure or obtained from published literature or internal data developed by Advanced Resources. Equation used for determining the Gas Content is listed below.

Equation 9: Formula to calculate the Gas Content

$$G_c = \frac{V_l\ * P}{P_l * P}$$

G_c Gas Content, measured as cubic feet of gas per ton of net shale

V_l Langmuir Volume function of organic richness and thermal maturity of shle

P_l Langmuir pressure, function of how readily the absorbed gas on organics in the shale matrix is released as a function of a ginite decrease in pressure.

Although many researches in the past have been focused towards shale gas potential, this research is targeting shale oil and therefore shale gas is beyond the scope of this research.

APPENDIX B: Data Acquisition and Laboratory Equipment

Appendix B.1

Methodology List of samples selected for the SHAPE project

					Core Plug	Chips	Extra bits
ebn1	EBN	EBN1	Carboniferous	691.8	✘	✓	✘
ebn2	EBN	EBN1	Carboniferous	691.8	✘	✘	✓
ebn3	EBN	EBN1	Carboniferous	934.5	✘	✘	✘
ebn4	EBN	EBN1	Carboniferous	934.5	✓	✓	✘
ebn5	EBN	EBN1	Carboniferous	945	✘	✘	✓
ebn6	EBN	EBN1	Carboniferous	945	✘	✘	✘
ebn7	EBN	EBN1	Carboniferous	970.2	✘	✓	✓
ebn8	EBN	EBN1	Carboniferous	978.6	✘	✓	✘
ebn9	EBN	EBN1	Carboniferous	984	✘	✘	✘
ebn10	EBN	EBN1	Carboniferous	984	✘	✘	✘
ebn11	EBN	EBN2	Jurassic	4237.5	✘	✘	✘
ebn12	EBN	EBN3	Carboniferous	978.8	✘	✘	✘
ebn13	EBN	EBN4	Jurassic	3063.2	✘	✓	✓
ebn14	EBN	EBN4	Jurassic	3063.3	✘	✓	✓
ebn15	EBN	EBN4	Jurassic	3074	✘	✘	✘
ebn16	EBN	EBN5	Jurassic	1672.5	✘	✓	✓
ebn17	EBN	EBN5	Jurassic	1672.9	✘	✘	✘
ebn18	EBN	EBN5	Jurassic	1674.8	✘	✓	✓
ebn19	EBN	EBN5	Jurassic	1675.8	✘	✓	✘
ebn20	EBN	EBN6	Jurassic	1051.5	✓	✓	✓
ebn21	EBN	EBN7	Jurassic	1718	✓	✓	✘
ebn22	EBN	EBN4	Jurassic	3062.5	✓	✓	✓
ebn23	EBN	EBN4	Jurassic	3062.5	✘	✓	✓
ebn24	EBN	EBN4	Jurassic	3074	✓	✓	✘
ebn25	EBN	EBN8	Jurassic	2509.5	✓	✓	✘
ebn26	EBN	EBN8	Jurassic	2510	✓	✓	✘
ebn27	EBN	EBN9	Jurassic	1429	✓	✓	✘
ebn28	EBN	EBN10	Jurassic	1675	✓	✓	✘
ebn29	EBN	EBN10	Jurassic	1677.5	✓	✓	✘
ebn30	EBN	EBN10	Jurassic	1678	✓	✓	✘
ebn31	EBN	EBN11	Jurassic	1232	✓	✓	✘
ebn32	EBN	EBN11	Jurassic	1233	✓	✓	✓
ebn33	EBN	EBN11	Jurassic	1236	✓	✓	✘
ebn34	EBN	EBN11	Jurassic	1237	✓	✓	✘
ebn35	EBN	EBN11	Jurassic	1242.5	✘	✓	✓
ebn36	EBN	EBN12	Jurassic	1260.5	✓	✓	✘

Appendix B.2
SEM Specification

Hitachi SU-70 Scanning Electron Microscope

- Schottky field emitter operating at 0.5 to 30 kV
- Hight current (>150 nA) for analytical applications

Imaging
- Secodary electron (SE) imaging:
  • Lower SE detector: SE+BSE electrons collected in the chamber provide images with enhanced topographic effects and good depth of field. High efficiency at long working distances.
  • Upper SE detector: secondary electrons are efficiently collected through-the-lens to provide images with extremely high spatial resolution. Ideal for short working distances (1.5-4.0 mm) and high resolution work. Imroved contrast using **E**x**B** filter.
-Backscattered electron (BSE) imaging:
  • YAG BSE detector: ideal for BSE imaging at analytical working distances (7.5-15.0 mm)
  • Low angle BSE detector: ideal for compositional information at long working distances
  • High angle BSE detector: **E**x**B** filter used to block high energy SE signal in preference for BSE. Ideal for BSE imaging at short working distances (1.5-7.0 mm)
- Flexible imaging options:
  • Field-free mode for imaging magnetic samples
  • Three main modes of operation untilising the Super **E**x**B** filer:
    (i) Pure SE(I)/(II) or
    (ii) SE + low angle BSE (variable ratio) or
    (iii) High angle BSE

Chemical analysis
- Analytical capabilities:
  • Oxford Instruments EDX system (INCA x-act LN_2-free analytical Silicon Drift Detector)
  • Oxford Instruments WDX system (INCAWave 700 spectrometer)
  • Oxford Instruments INCA software with the ability to perform qualitative and quantitative analysis, EDX elemental mapping, EDX Quant mapping, feature and phase analysis. Combined EDX+WDX analysis is also available.

Specialised techniques
- Gatan Mono-CL cathodoluminescence:
  • Room temperature PMT detector for panchromatic/monochromatic imaging and serial-CL
  • Pixis CCD camera for parallel-CL
  • Digiscan 2 software for spectrum imaging
- Hitachi and Metelect EBIC system

Appendix B.3

GRI Method

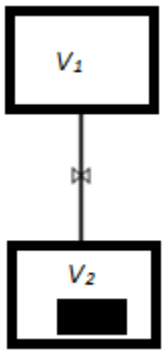

Porosity calculations

V_{rf}	Reference Volume
V_h	Sample holder Volume
P_1	Initial Pressure
P_2	Pressure in core holder surround the sample
P_3	Equilibration pressure after expansion
Φ	Porosity

Setup	S1	G2	G3
V_1 [cm^3]	44.6025	41.2665	34.7727
V_2 [cm^3]	89.5408	66.0852	63.6921
V_{cup} [cm^3]	-	8.08954	8.69167

Volume of the grains [cm^3]

$$V_{grains} = \frac{Weight\ grains}{bulk\ density}$$

Volume of core [cm^3]

$$V_{core} = \frac{0.25 * \pi * D^2 * L}{1000}$$

Formula used for GRI

$$P_1V_1 + P_2V_2 = P_3(V_1 + (V_2 - V_{grains}))$$

Volume of grains [cm^3] from GRI for the first run with $P_2 = 0$

$$V_{grainsgrirun\ 1} = \frac{-P_1V_1 + P_3V_1 + P_3V_2}{P_3}$$

Volume of grains [cm^3] from GRI for the second and third run with $P_2 \neq 0$

$$V_{grainsgri\ run\ 2} = \frac{-P_1V_1 - P_2V_2 + P_3V_1 + P_3V_2 + P_2V_{grainsgri\ run\ 1}}{P_3}$$

Porosity is obtained from

$$\Phi = \frac{Vgrains - Vgrainsgrirun\#}{V_{grains}} * 100$$

Within the formulas for porosity calculation the grains volumes can be replaced with cores.

APPENDIX C:Experimental Results Used for Sample Selection

				Sample	Porosity GRI				NMR (CC/Gram)*10^3			T2			SEM		TOC	S1	S1/TOC	PI
					Core	Chips						Mean			Non-minera	Open pore				S1/(S1+S2)
						Wet	*Normal*	*Dry*	*Wet*	*Normal*	*Dry*	*Wet*	*Medium*	*Dry*	*Material*	*Space*				
ZM-2	EBN5	Jurassic	1675.8	EBN 19			15.93			2.51			0.395		6.01		5.12	1.35	0.26	0.037
HLM-1	EBN6	Jurassic	1051.5	EBN 20	-		7.76	8.99		2.56	2.11		0.500	0.6705933	12.06	3.38	5.67	2.77	0.49	0.071
HLM-1	EBN6	Jurassic	1051.5	EBN 20B	8.47															
AND-02	EBN7	Jurassic	1718	EBN 21	19.85	14.48	15.36		21.376	3.61		0.520	0.352		9.9	1.65	10.53	2.54	0.24	0.037
BRK-02	EBN4	Jurassic	3062.5	EBN 22			3.58			2.32			0.442		8.85	1.75	6.51	1.88	0.29	0.058
BRK-02	EBN4	Jurassic	3062.5	EBN 23			3.47	16.37		3.09			0.352		9.47	1.01	5.15	1.90	0.37	0.083
BRK-02	EBN4	Jurassic	3074	EBN 24		5.05	1.87	6.06		2.74	1.38		0.568	0.8308424	15.94	0.41	7.96	2.91	0.37	0.068
LOZ-01	EBN8	Jurassic	2509.5	EBN 25	8.88	9.45	10.69	14.8		4.71	3.11		0.524	1.105	3.43	1.5	1.18	0.45	0.38	0.269
LOZ-01	EBN8	Jurassic	2510	EBN 26			8.9			2.38			0.470		1.53	0.66	1.23	0.45	0.37	0.254
VLM-01	EBN9	Jurassic	1429	EBN 27	6.93		4.72			1.28			0.390		5.88	2.21	4.46	0.54	0.12	0.055
ZOM-02	EBN10	Jurassic	1675	EBN 28	11.91		6.84			3.52			0.356		8.553	2.36	7.20	2.04	0.28	0.047
ZOM-02	EBN10	Jurassic	1677.5	EBN 29	19.73	15.8	10.12		19.622	4.88	2.11	0.474	0.291	0.8186201	7.57	3.02	5.81	1.81	0.31	0.064
ZOM-02	EBN10	Jurassic	1678	EBN 30	-	5.92	6.45		8.617	3.17		0.3028678	0.390		10.49	2.93	4.17	1.22	0.29	0.061
ZWE-01	EBN11	Jurassic	1232	EBN 31				12.32			0.79			1.2357405			9.13	2.08	0.23	0.037
ZWE-01	EBN11	Jurassic	1233	EBN 32	16.76	19.96			24.713			0.639	0.639		8.24	2.93	6.10	2.02	0.33	0.044
ZWE-01	EBN11	Jurassic	1236	EBN 33	13.32		14.59			1.14			0.920				9.23	2.67	0.29	0.042
ZWE-01	EBN11	Jurassic	1237	EBN 34	17.58		14.28	14.28		1.77			0.449				11.07	3.14	0.28	0.041
ZWE-01	EBN11	Jurassic	1242.5	EBN 35	21.48	9.6	11.45	12.9		1.59	1.33		0.752	1.0328051	10.14	2.78	13.24	2.9	0.22	0.035
ZWE-02	EBN12	Jurassic	1260.5	EBN 36			13.19			1.60			0.394				4.66	1.27	0.27	0.040

				Sample	Porosity GRI [He] Core	GRI Porosity [He] Chips			GRI Porosity [Nitrogen] Chips	NMR Chips (CC/Gram)*10^3			SEM	
Well	SHAPE #	Formation	Depth [MD]	Number		*Wet*	*ambient*	*Dry*	*Ambient*	*Wet*	*Normal*	*Dry*	Non-mineral *Material %*	Open pore *Space %*
HLM-1	EBN6	Jurassic	1051.5	EBN 20	8.89	6.93	7.76	8.99	7.47	6.147	2.56	2.11	12.06	3.38
AND-02	EBN7	Jurassic	1718	EBN 21	19.85	14.48	15.36	18.06	15.19	21.38	3.61	1.39	9.9	1.65
BRK-02	EBN4	Jurassic	3074	EBN 24		5.05	1.87	5.7	0.92	2.954	2.74	1.38	15.94	0.41
LOZ-01	EBN8	Jurassic	2509.5	EBN 25	8.88	9.45	10.69	14.8	6.76	11.6	4.71	3.11	3.43	1.5
ZOM-02	EBN10	Jurassic	1677.5	EBN 29	19.73	15.8	14.4	21.74	15.51	19.62	4.88	2.11	7.57	3.02
ZWE-01	*EBN11*	*Jurassic*	*1242.5*	*EBN 35*	*21.48*	*9.6*	*11.45*	*12.9*		*11.99*	*1.59*	*1.33*	*10.14*	*2.78*
HLM-1	EBN6	Jurassic	1051.5	EBN 20B	8.47						3.31			

				Sample	T2-mean [ms] Chips		T1-mean [ms] Chips	T1/T2 ratio chips	TOC	S1	S1/TOC	PI S1/(S1+S2)
Well	SHAPE #	Formation	Depth [MD]	Number	*Wet*	*as-received*	*Dry*	*as-received*	as-received	%	mg/gram		
HLM-1	EBN6	Jurassic	1051.5	EBN 20	0.505829497	0.500	0.670593341	3.881	7.765605236	5.67	2.77	0.49	0.071
AND-02	EBN7	Jurassic	1718	EBN 21	0.520	0.352	0.75625	1.547	4.394937528	10.53	2.54	0.24	0.037
BRK-02	EBN4	Jurassic	3074	EBN 24	0.496949066	0.568	0.830842429	2.717	4.7790232	7.96	2.91	0.37	0.068
LOZ-01	EBN8	Jurassic	2509.5	EBN 25	0.477	0.524	1.105	4.712	8.992084669	1.18	0.45	0.38	0.269
ZOM-02	EBN10	Jurassic	1677.5	EBN 29	0.474	0.291	0.818620097	1.395	4.800685443	5.81	1.81	0.31	0.064
ZWE-01	*EBN11*	*Jurassic*	*1242.5*	*EBN 35*	*0.352081569*	*0.752*	*1.032805063*			*13.24*	*2.9*	*0.22*	*0.035*
HLM-1	EBN6	Jurassic	1051.5	EBN 20B		0.359		3.032	8.450037436				

Sample	Helium Core permeability[nD]	Imbibition Water Core permeability[nD]	Imbibition Water 1 Core permeability {nD]	Imbibition Water 1 Water porosity [%]	Imbibition Water 1 Water Saturation [%]	Permeability Average [nD] Chips Helium			Permeability Average [nD] Chips Nitrogen
	Normal	*Normal*	*Normal*	*Normal*	*Normal*	*Wet*	*Ambient*	*Dry*	*Ambient*
EBN 20	?	0.023380803	?	7.03	86.15	0.4	1.2	0.1	0.0001
EBN 21	?	0.120818206	?	20.54	0.96	0.8	1.7	1.1	0.0051
EBN 24	-		-	-	-	0.2	0.0	0.1	0.000015
EBN 25	?	0.0673909	?	6.81	76.64	0.6	0.7	1.3	0.001196
EBN 29	43.289	1.775470668	broken	broken	broken	2.0	0.1	1.1	0.0038

	Sample	NMR Core T2-mean [ms]	NMR Core (CC/Gram)*10^3	NMR Core T2-mean [ms]	NMR Core (CC/Gram)*10^3
		Before imbi	*Before Imbi*	*After Imbi*	*After Imbi*
1051.5	EBN 20	0.226	1.09	1.451	13.88
1718	EBN 21	3.37	1.83	2.79	67.26
3074	EBN 24	-	-	-	-
2509.5	EBN 25	3.366	1.508	0.961582545	23.29
1677.5	EBN 29	Broken	Broken	2.08	59.65
1051.5	EBN 20B				

	Sample TAQA	TOC Washed in multipar
Depth [m]		%
3010-3020	EBN 1*	6.65
3020-3020	EBN 2*	3.47
3030-3040	EBN 3*	1.86
3040-3050	EBN 4*	1.23
3050-3060	EBN 5*	0.96
3010-3020	EBN 1*	6.65
3020-3020	EBN 2*	3.47
3030-3040	EBN 3*	1.86
3040-3050	EBN 4*	1.23
3050-3060	EBN 5*	0.96

APPENDIX D: SEM Images

Scanning Electron Microscope Images used for pore size evaluation

Name	**EBN 19**
Well name	**ZOM – 2**
Depth	**1675.8 m**
Formation	**Jurassic**

Backscattered	SEM Image	Threshold Image
5 um	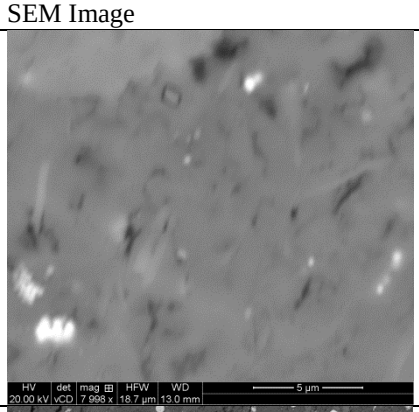	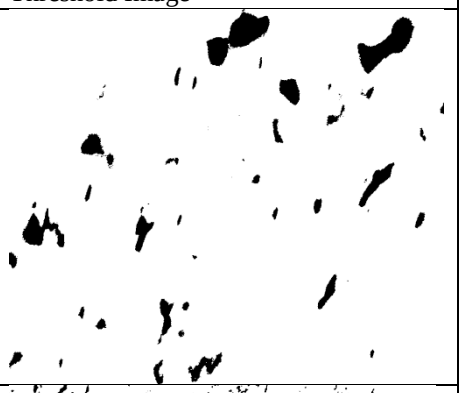
100 um	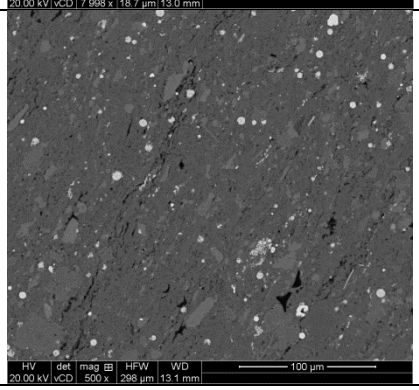	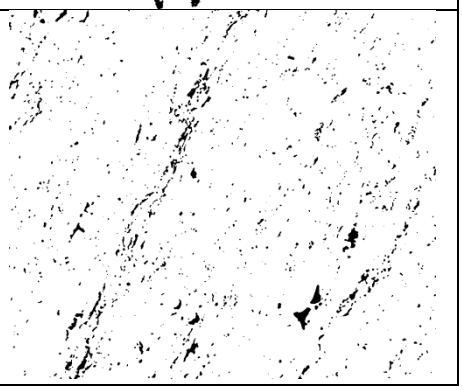

Name	**EBN 20**
Well name	**HLM – 1**
Depth	**1051.5 m**
Formation	**Jurassic**

Backscattered	SEM Image	Threshold Image
5 um	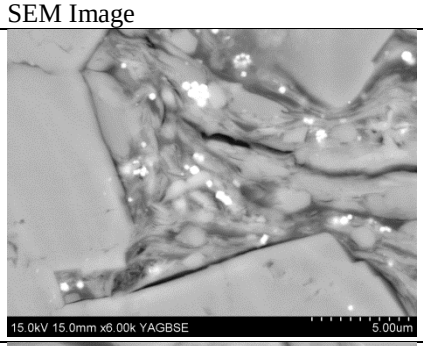	
5 um	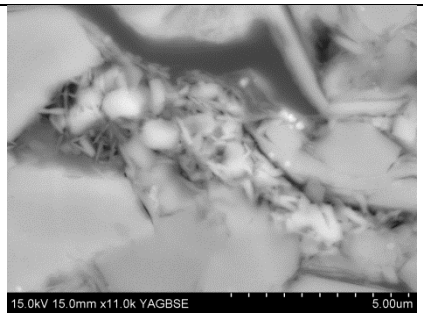	
5 um	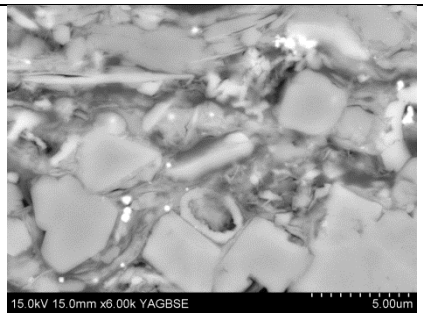	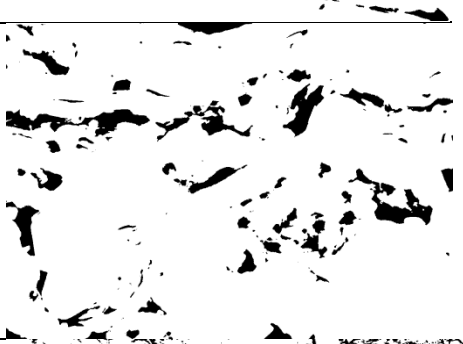
100 um	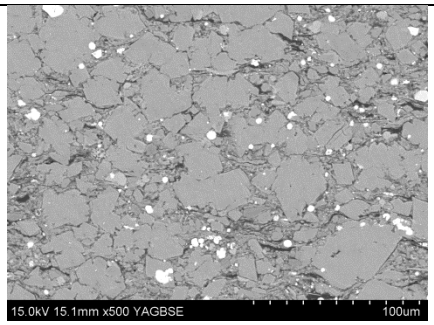	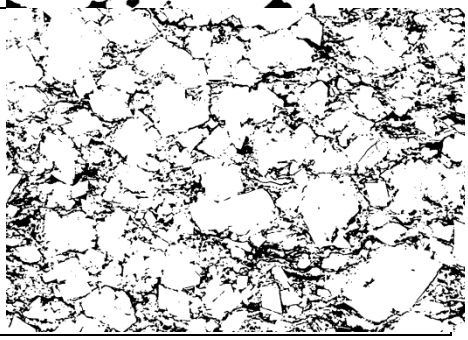

100 um	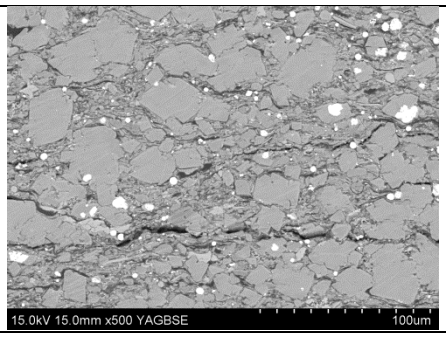	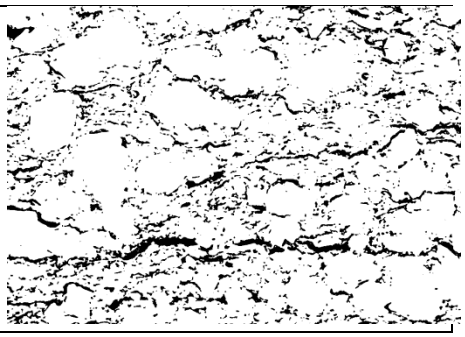

Secondary	SEM Image	Threshold Image
5 um	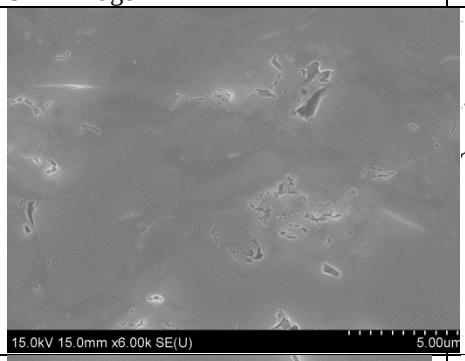	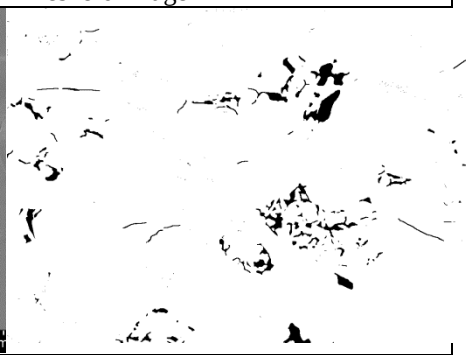
5 um	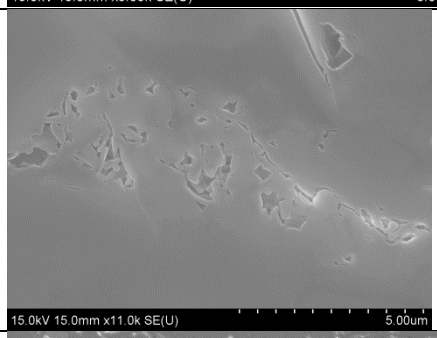	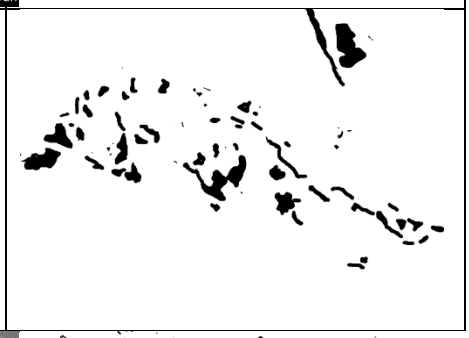
100 um	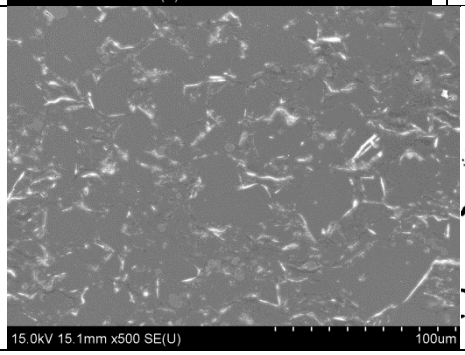	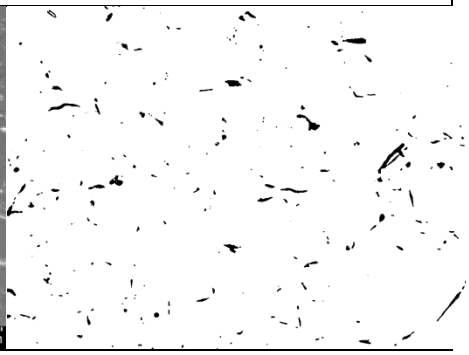

100 um	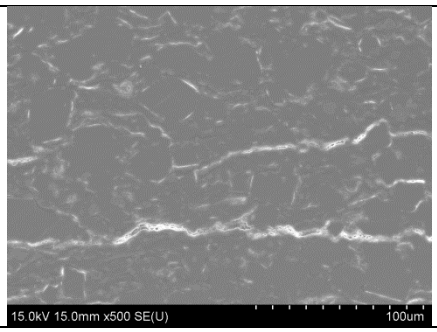	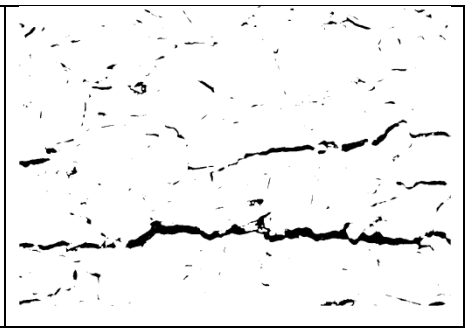

Name	**EBN 21**
Well name	**AND – 2**
Depth	**1718.0 m**
Formation	**Jurassic**

Backscattered	SEM Image	Threshold Image
5 um		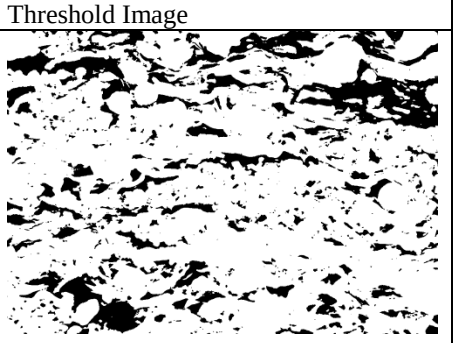
5 um	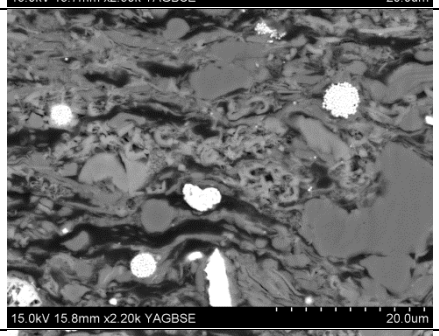	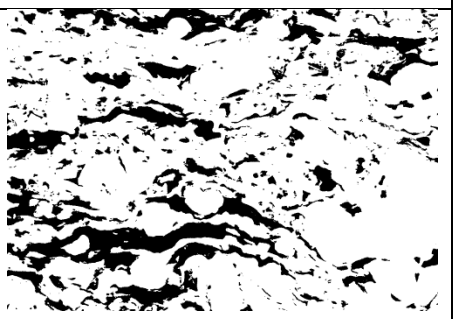
5 um	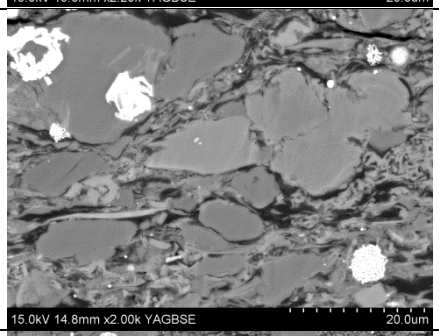	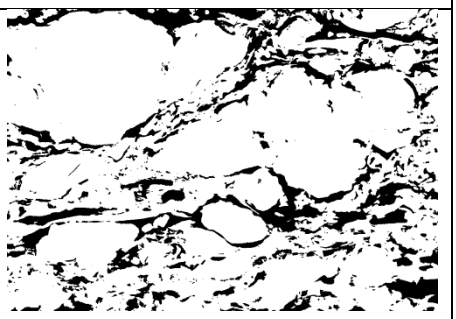
100 um	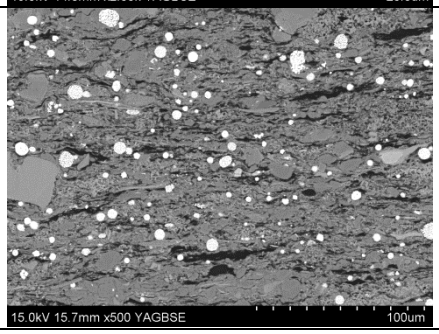	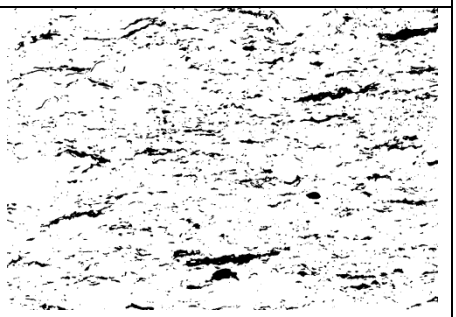

Secondary	SEM Image	Threshold Image
5 um	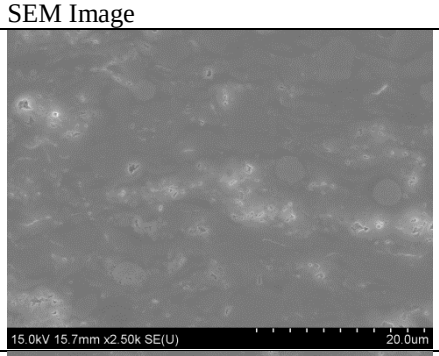	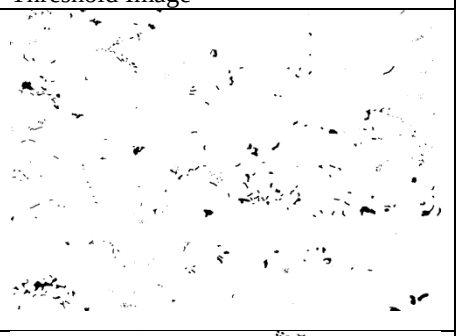
5 um	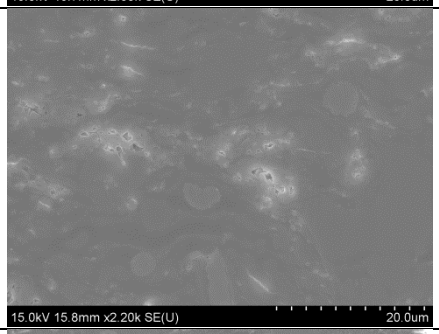	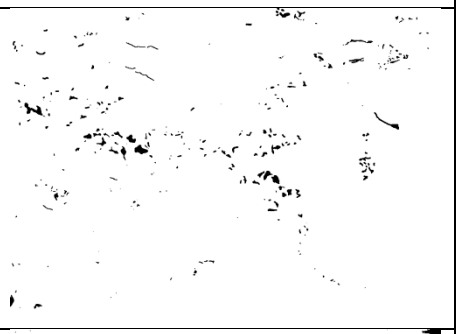
100 um	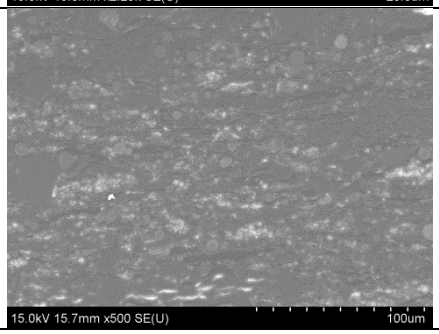	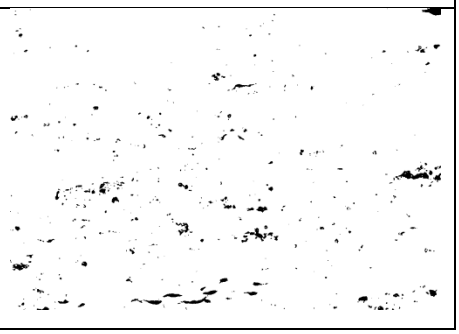

Name	**EBN 22**
Well name	**BRK – 2**
Depth	**3062.5 m**
Formation	**Jurassic**

Backscattered	SEM Image	Threshold Image
5 um	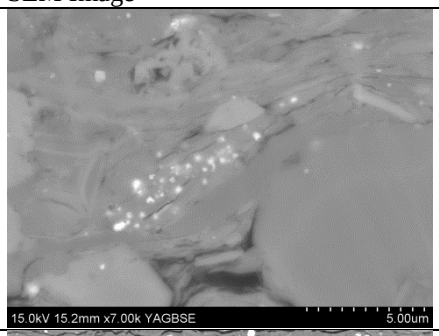	
100 um	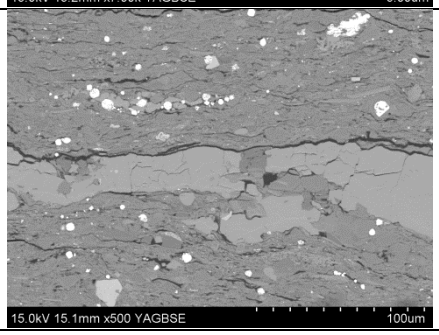	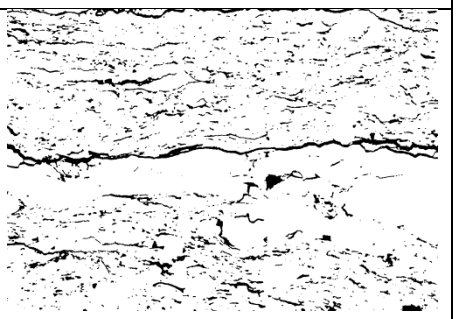

Secondary	SEM Image	Threshold Image
5 um		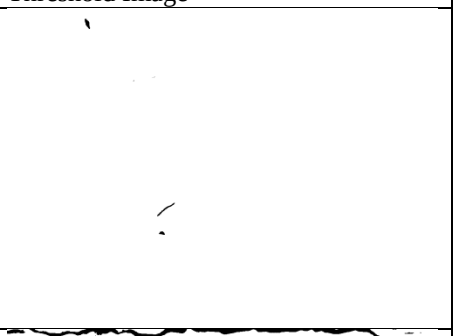
100 um	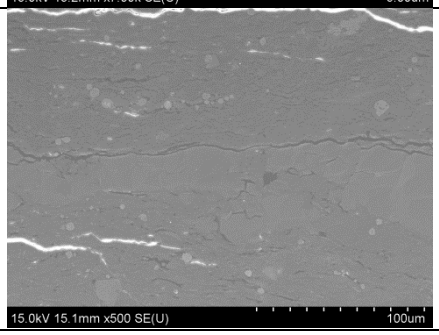	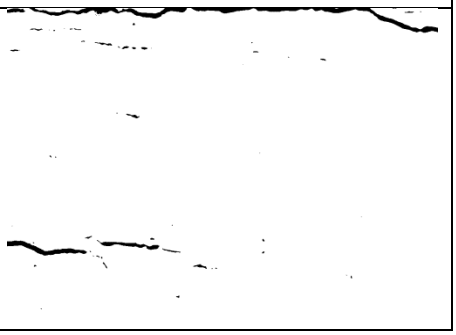

Name	**EBN 23**
Well name	**BRK – 02**
Depth	**3062.5 m**
Formation	**Jurassic**

Backscattered	SEM Image	Threshold Image
5 um	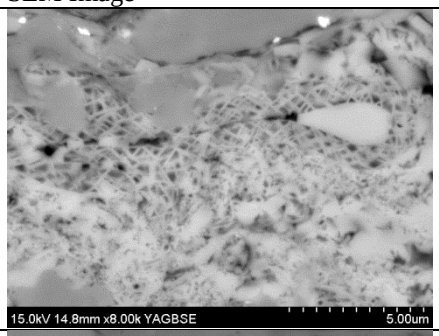	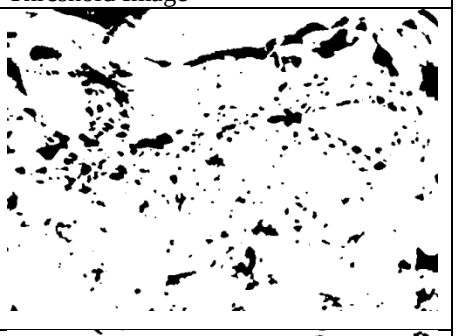
5um		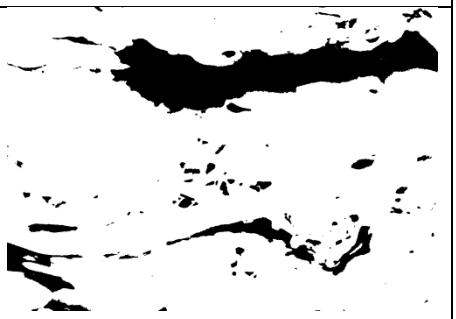
5 um	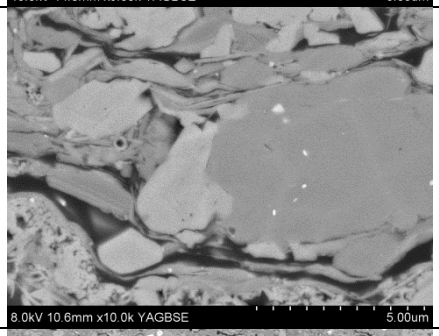	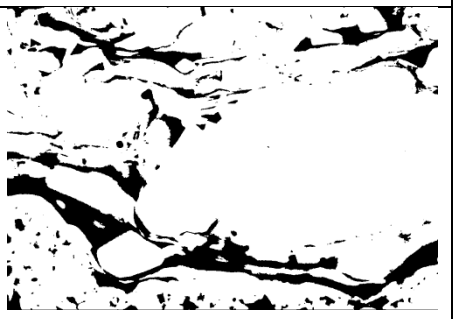
100 um	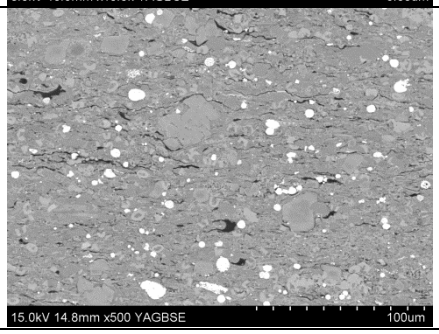	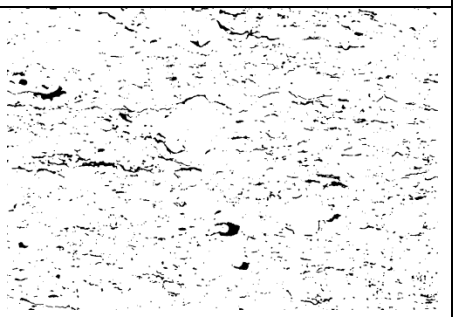

Secondary	SEM Image	Threshold Image
5 um	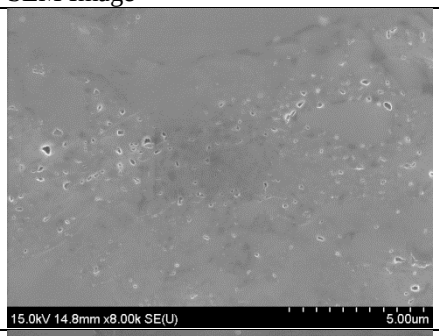	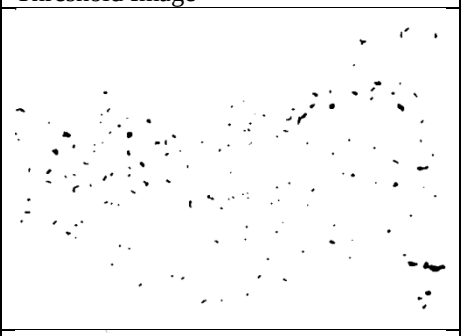
5 um	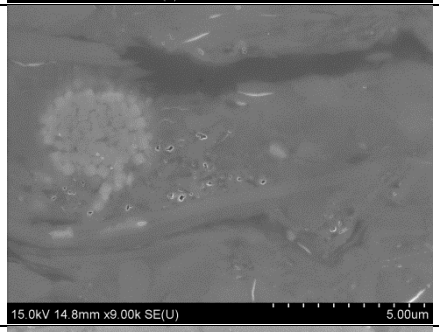	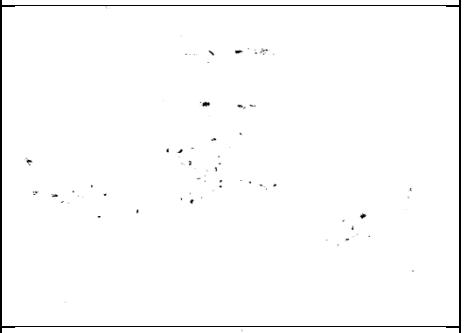
5 um	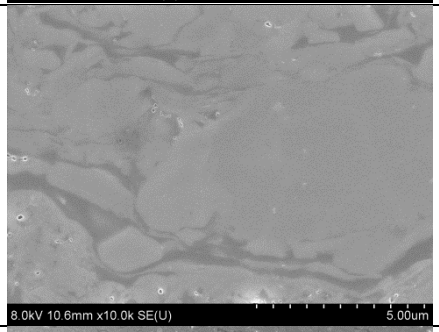	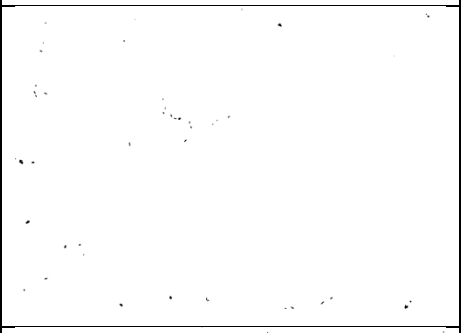
100 um	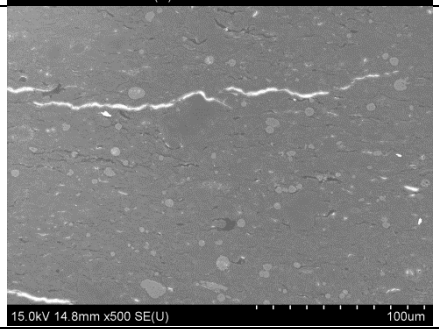	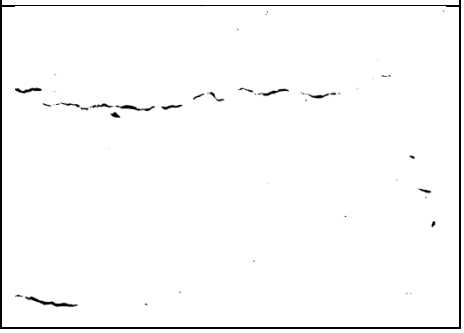

Name	**EBN 24**
Well name	**BRK – 02**
Depth	**3074.0 m**
Formation	**Jurassic**

Backscattered	SEM Image	Threshold Image
5 um	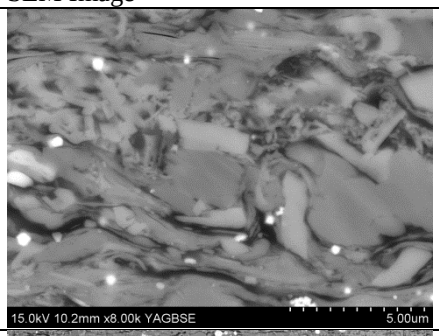	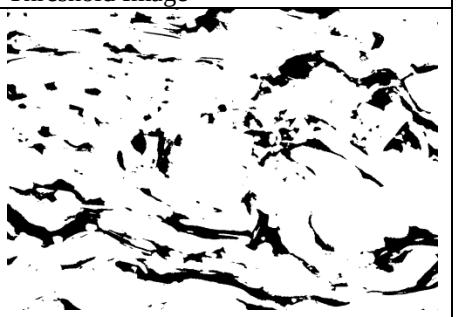
100 um	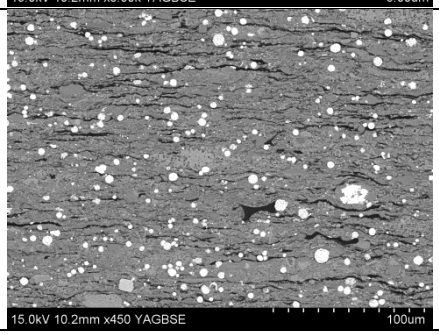	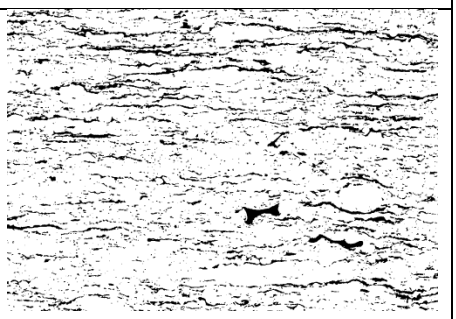

Secondary	SEM Image	Threshold Image
5 um	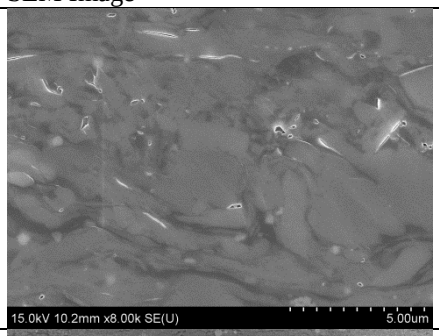	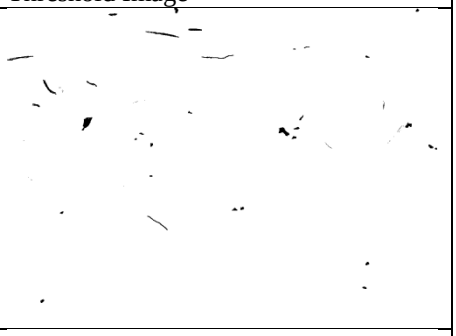
100 um	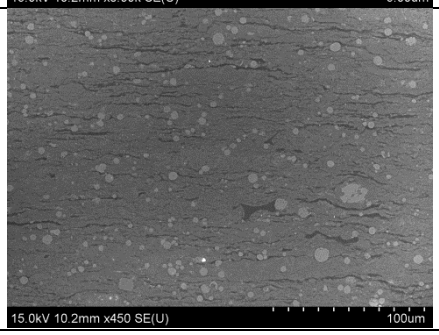	

Name	**EBN 25**
Well name	**LOZ – 1**
Depth	**2509.5 m**
Formation	**Jurassic**

Backscattered	SEM Image	Threshold Image
5 um	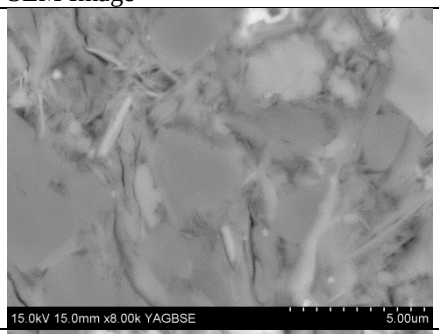	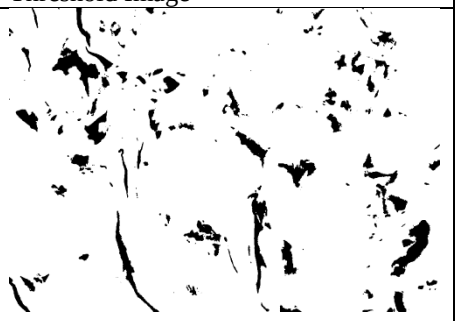
5 um	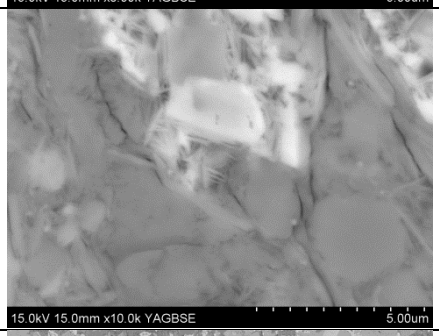	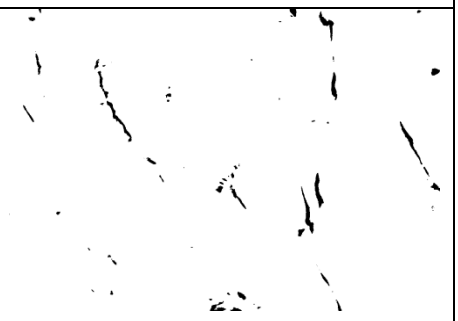
100 um	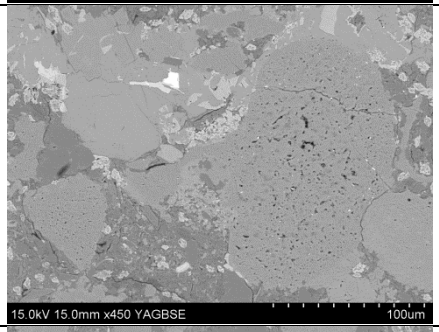	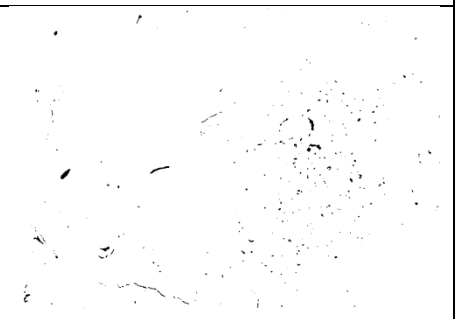
100 um	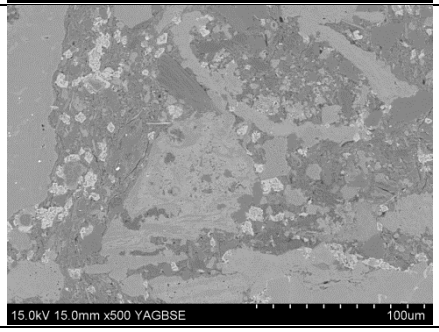	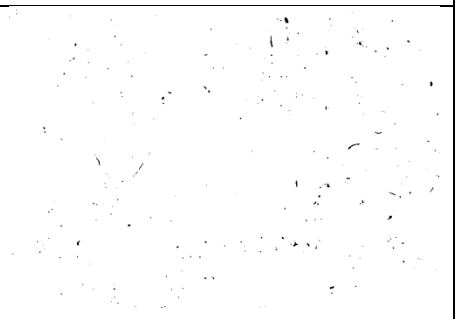

Secondary	SEM Image	Threshold Image
5 um	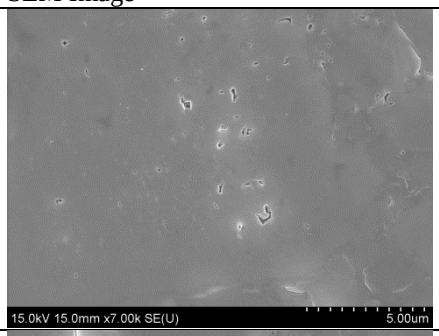	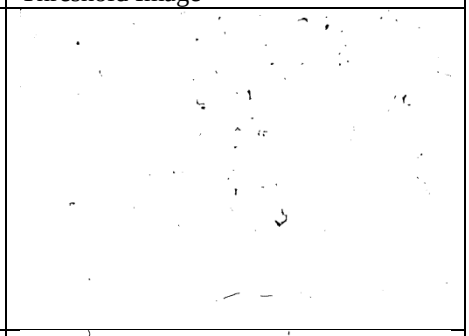
5 um	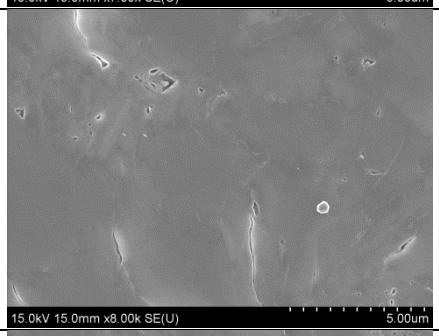	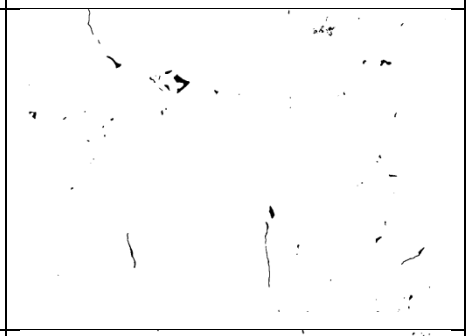
5 um		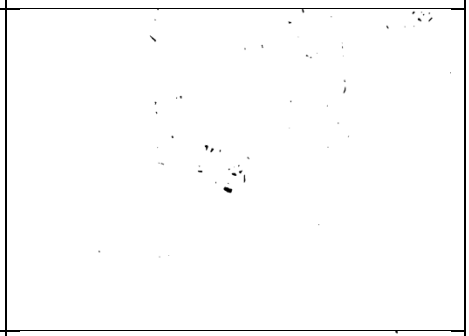
100 um	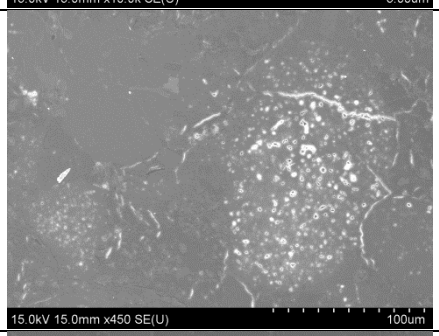	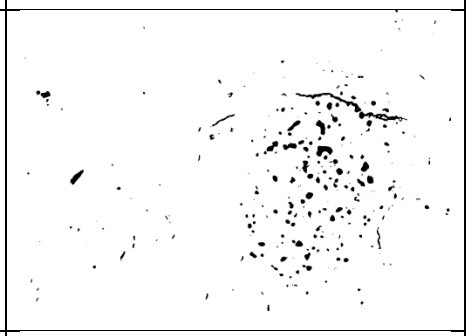
100 um	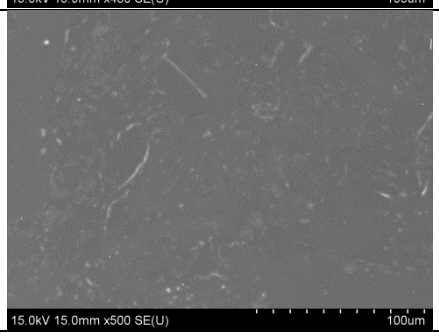	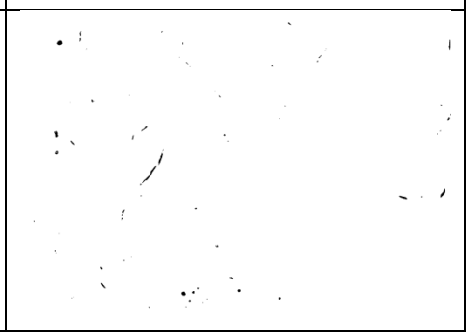

Name	**EBN 26**
Well name	**LOZ – 01**
Depth	**2510.0 m**
Formation	**Jurassic**

Backscattered	SEM Image	Threshold Image
5 um	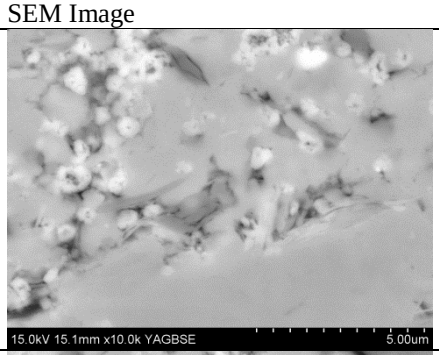	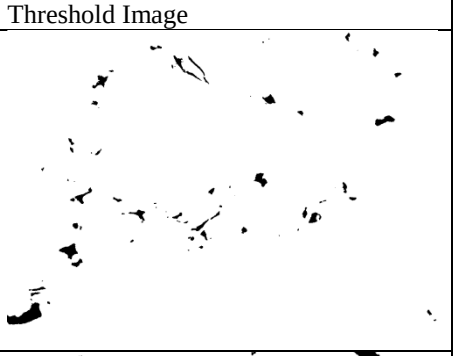
5 um	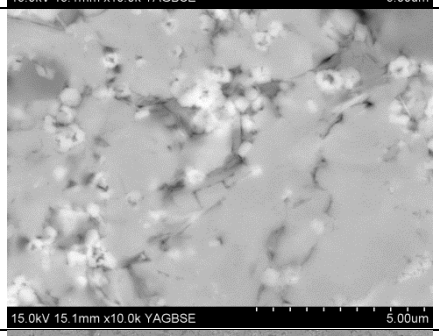	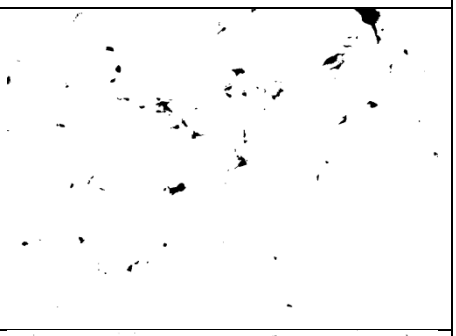
100 um	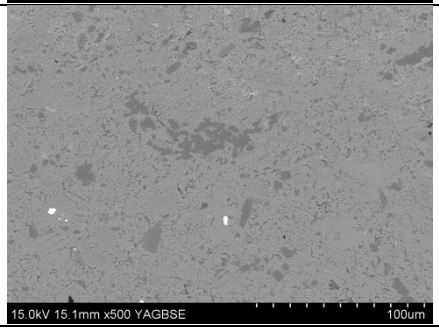	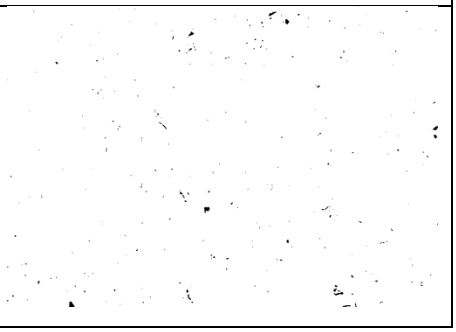

Secondary	SEM Image	Threshold Image
5 um	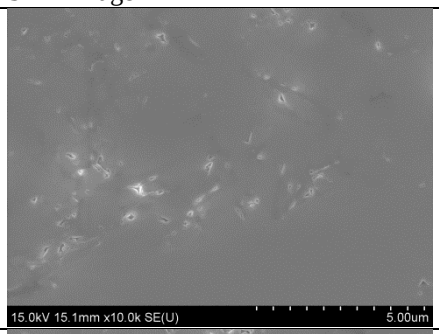	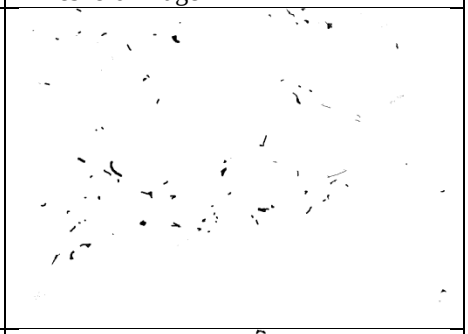
5 um	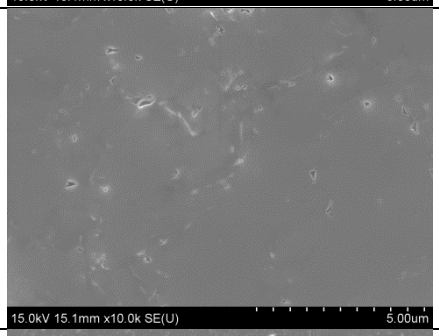	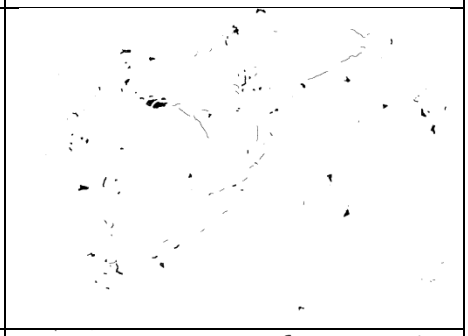
100 um	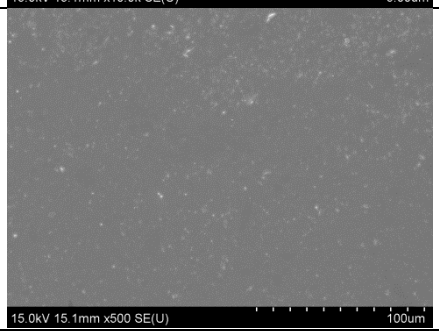	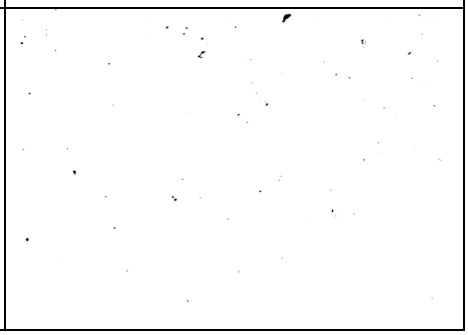

Name	**EBN 27**
Well name	**VLM – 1**
Depth	**1429.0 m**
Formation	**Jurassic**

Backscattered	SEM Image	Threshold Image
5 um	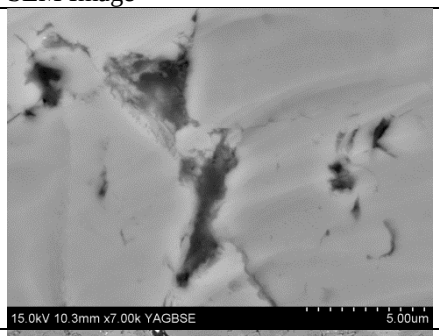	
100 um	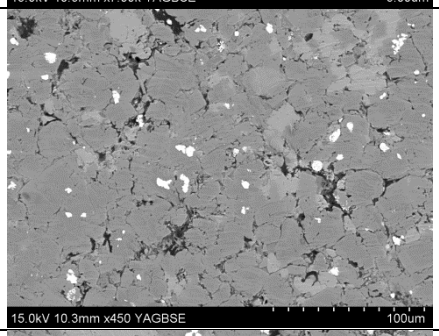	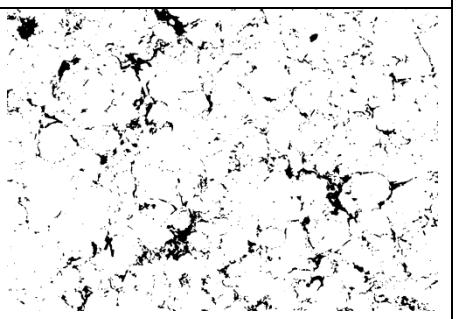
100 um	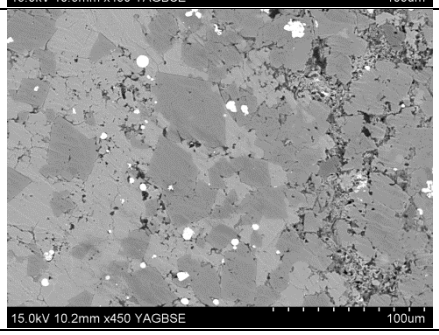	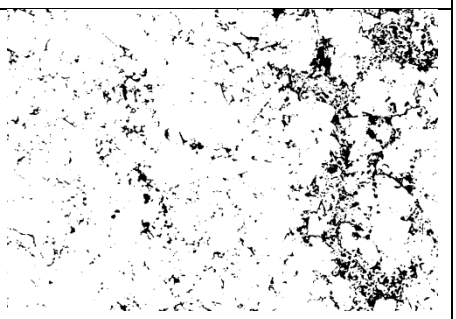

Secondary	SEM Image	Threshold Image
5 um	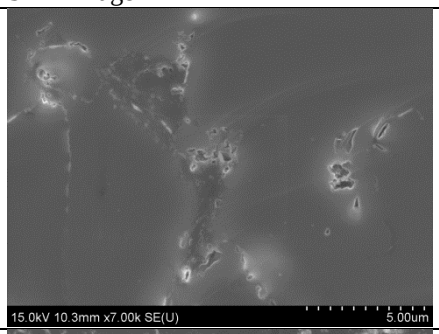	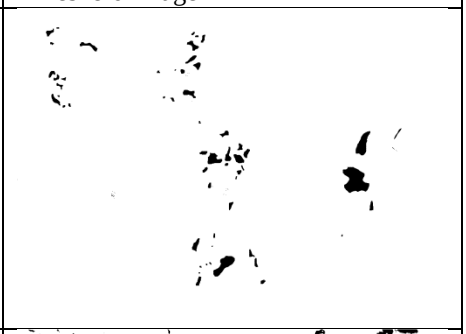
100 um	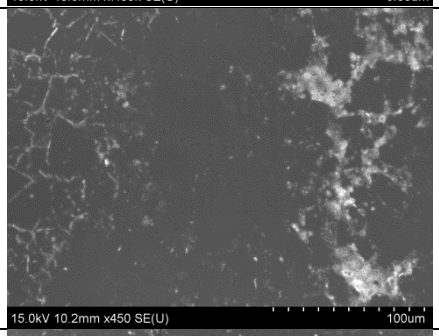	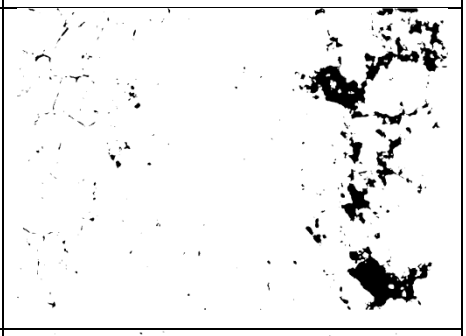
100 um	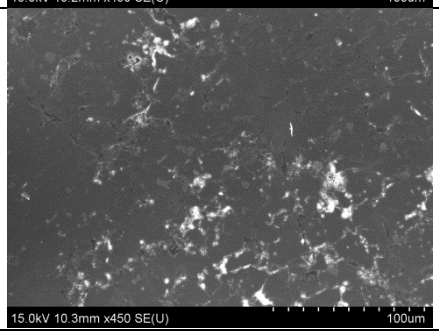	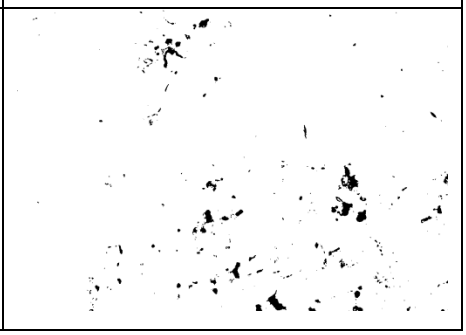

Name	**EBN 28**
Well name	**ZOM – 2**
Depth	**1675.0 m**
Formation	**Jurassic**

Backscattered	SEM Image	Threshold Image
5 um	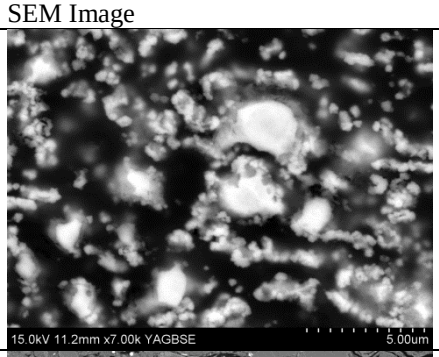	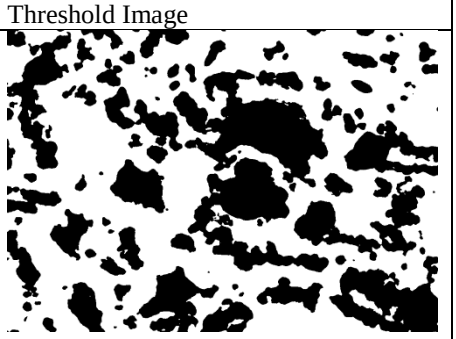
100 um	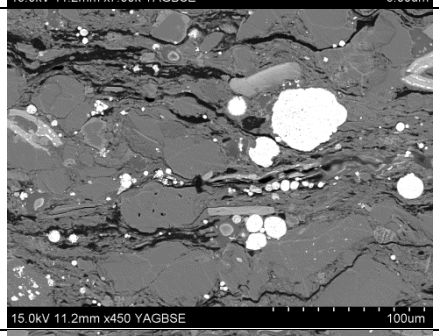	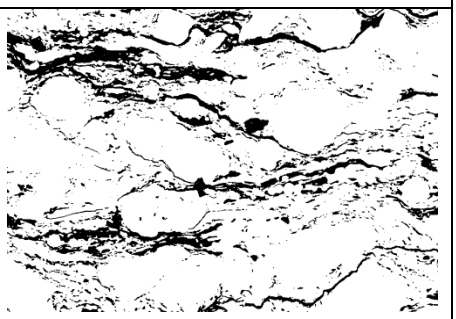
100 um	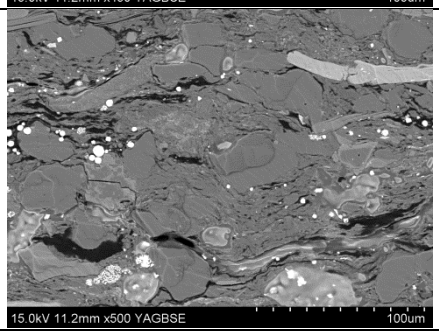	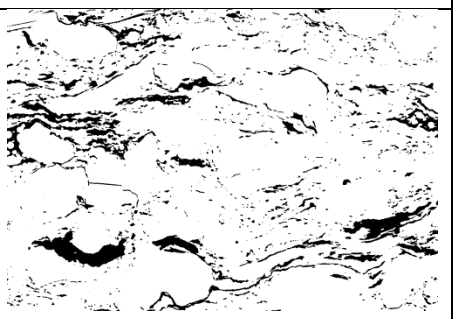

Secondary	SEM Image	Threshold Image
5 um	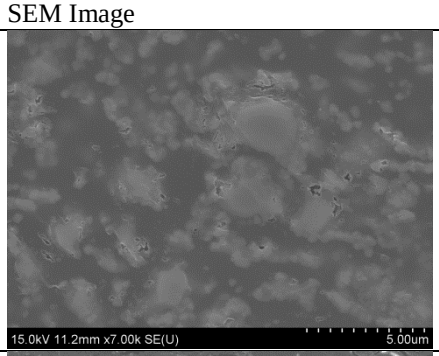	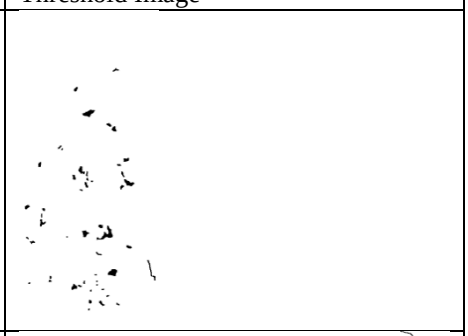
100 um	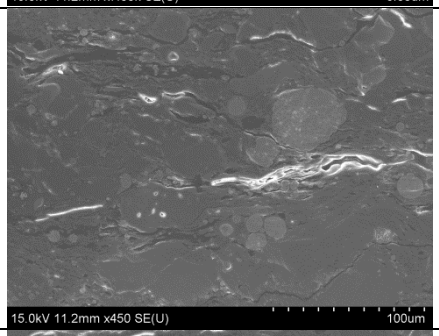	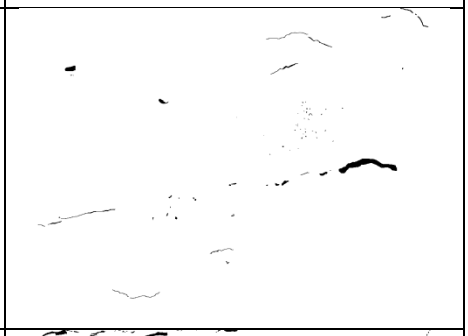
100 um	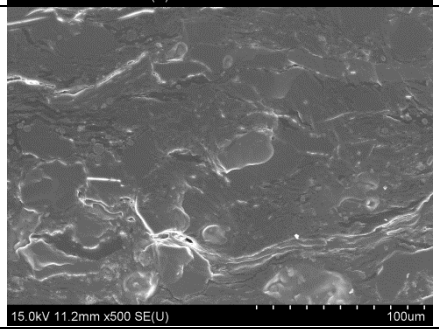	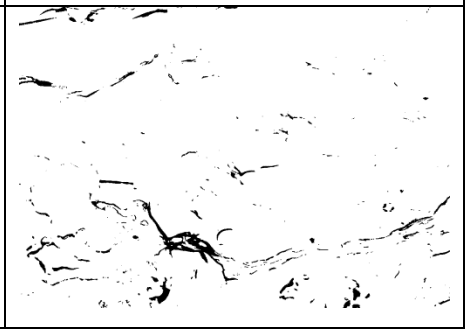

Name	**EBN 29**
Well name	**ZOM – 2**
Depth	**1678.0 m**
Formation	**Jurassic**

Backscattered	SEM Image	Threshold Image
5 um	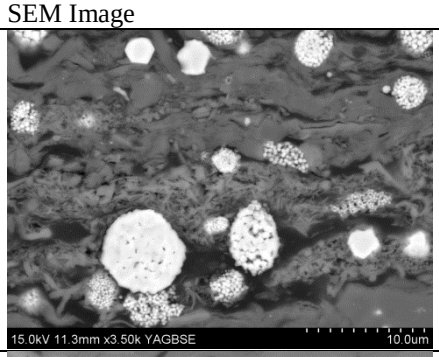	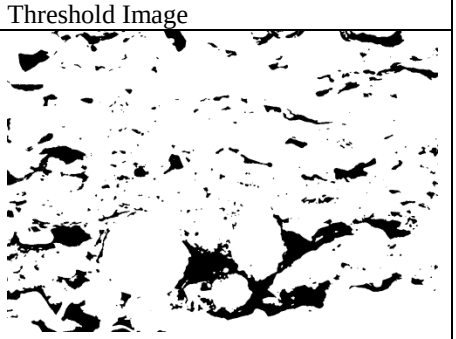
5 um	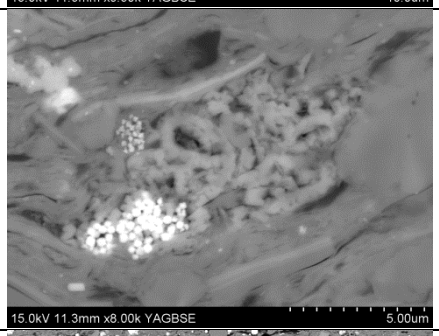	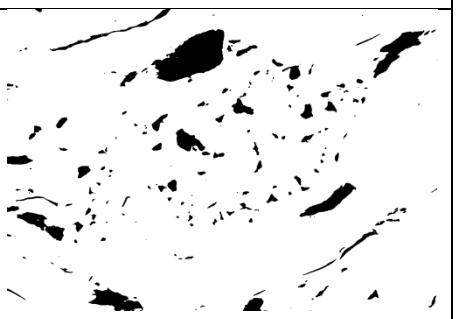
100 um	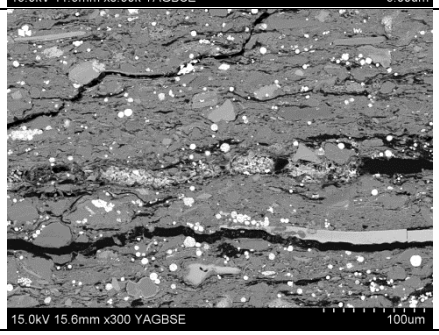	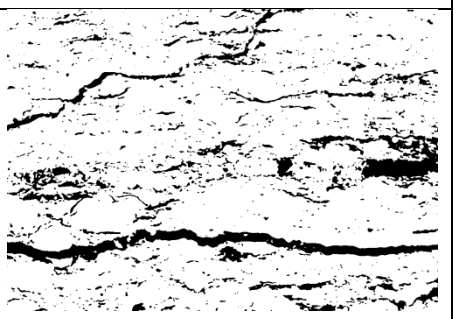

Secondary	SEM Image	Threshold Image
5 um	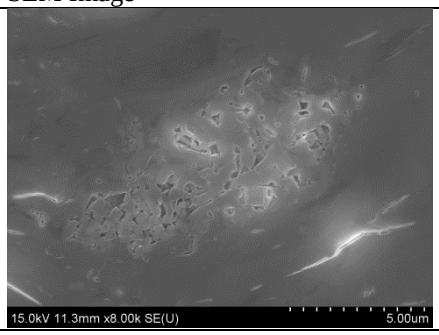	

Name	**EBN 30**
Well name	**ZOM – 02**
Depth	**1678.0 m**
Formation	**Jurassic**

Backscattered	SEM Image	Threshold Image
5 um	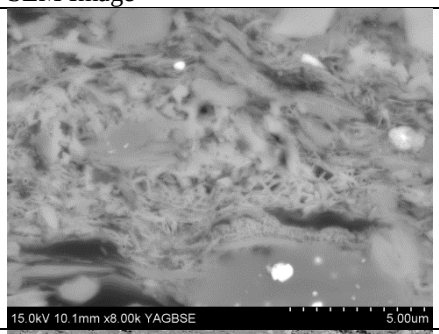	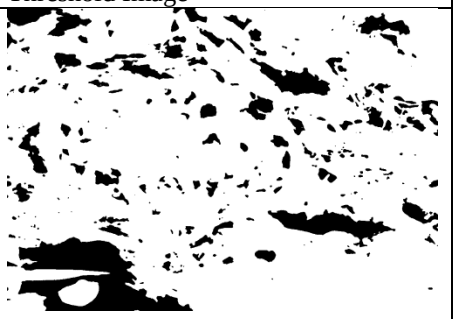
100 um	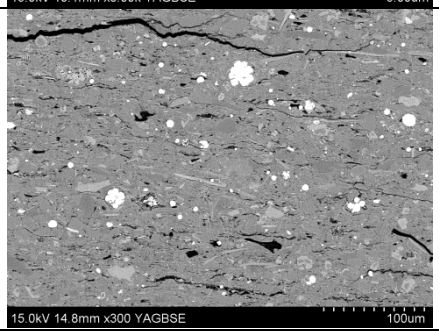	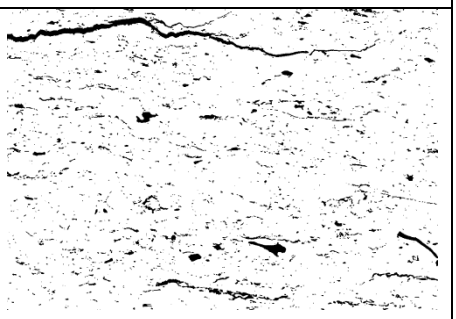

Secondary	SEM Image	Threshold Image
5 um	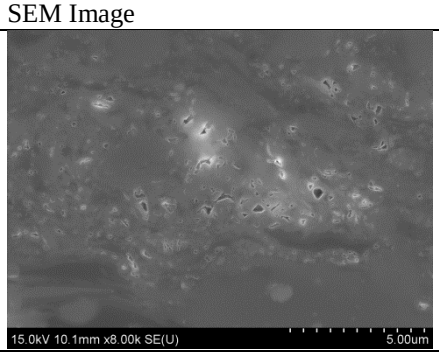	

Name	**EBN 32**
Well name	**ZWE – 1**
Depth	**1233.0 m**
Formation	**Jurassic**

Backscattered	SEM Image	Threshold Image
5 um	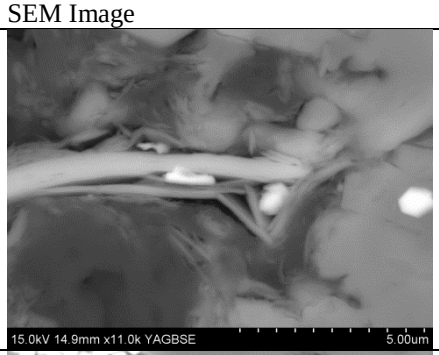	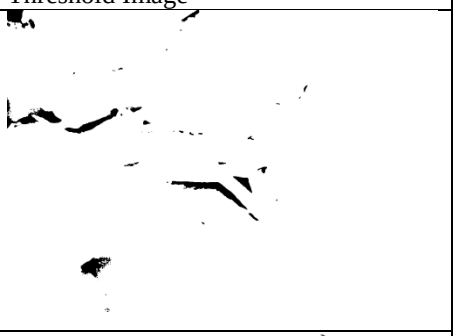
5 um	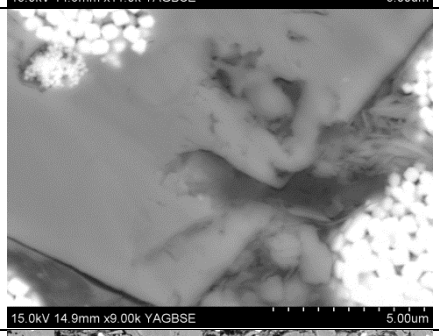	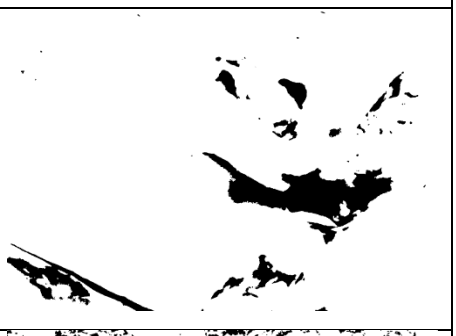
100 um	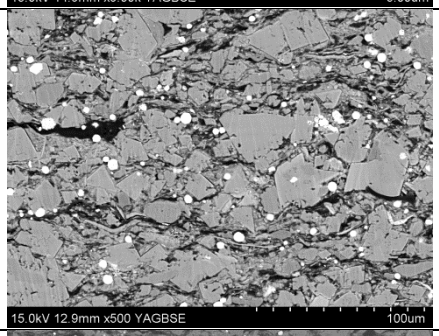	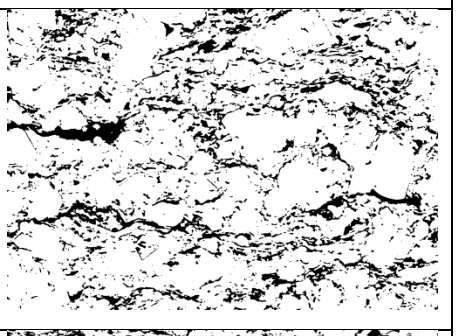
100 um	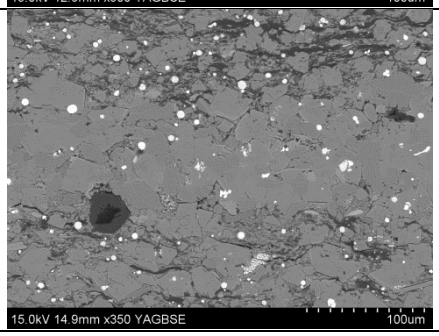	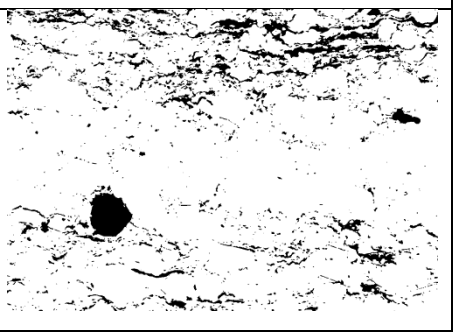

Secondary	SEM Image	Threshold Image
5 um	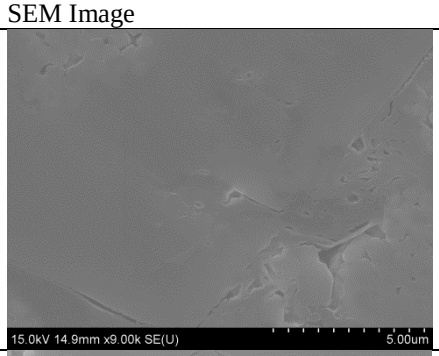	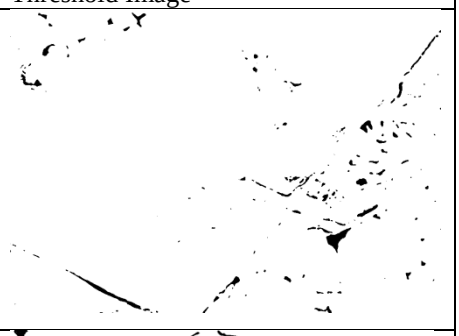
5 um	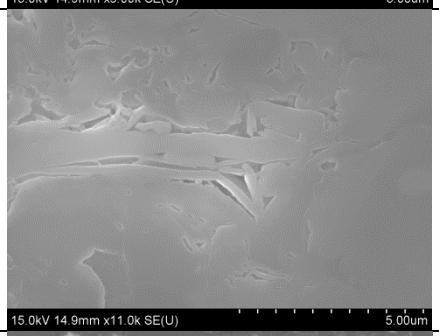	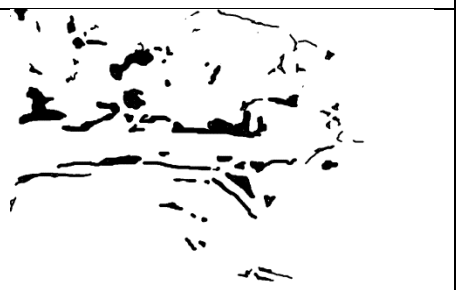
100 um	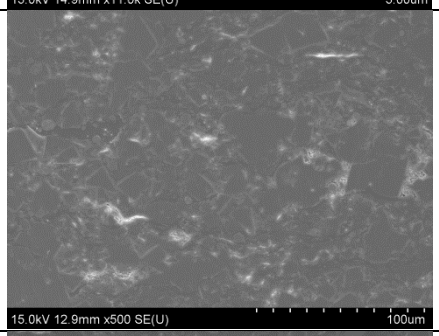	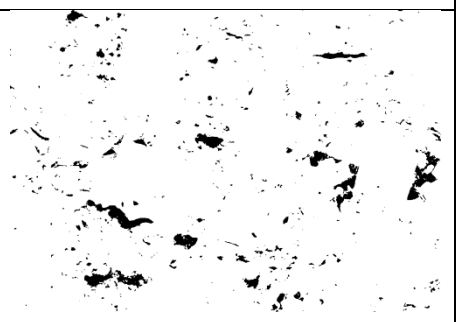
100 um	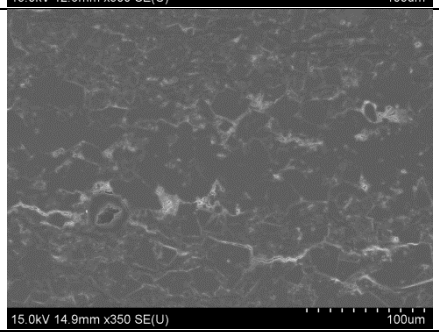	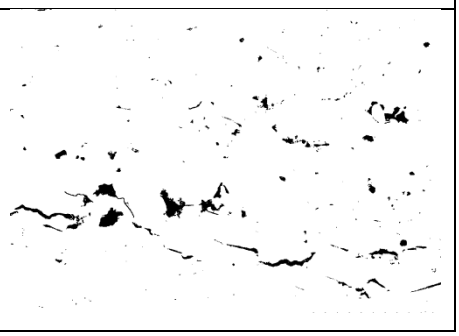

Name	**EBN 35**
Well name	**ZWE – 1**
Depth	**1242.5**
Formation	**Jurassic**

Backscattered	SEM Image	Threshold Image
5 um	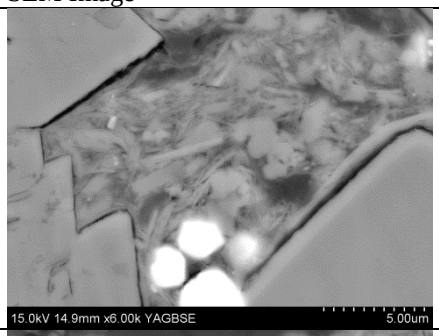	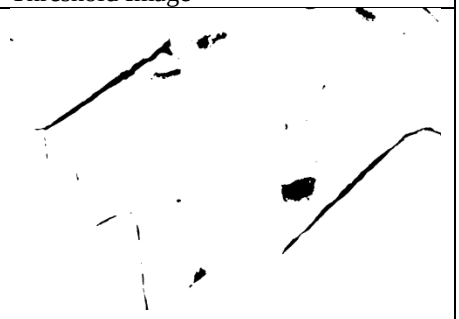
5 um	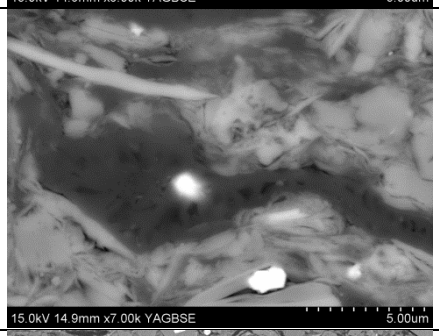	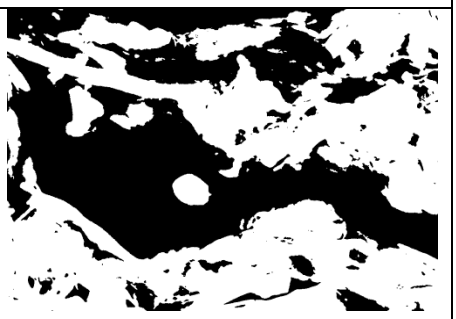
100 um	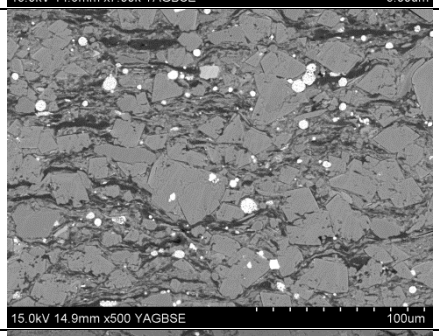	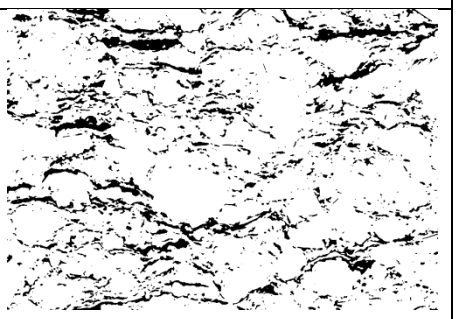
100 um	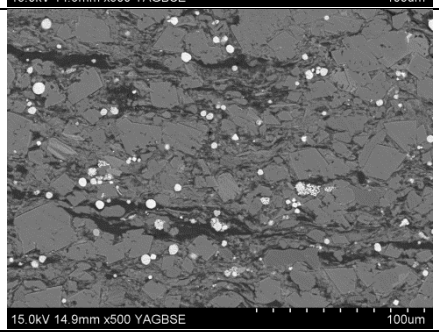	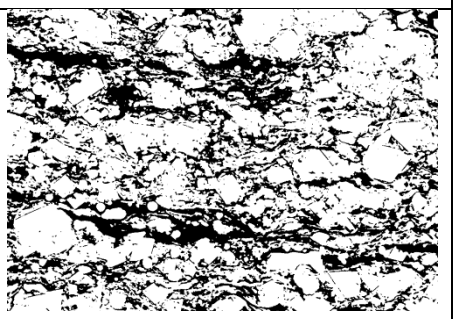

Secondary	SEM Image	Threshold Image
5 um	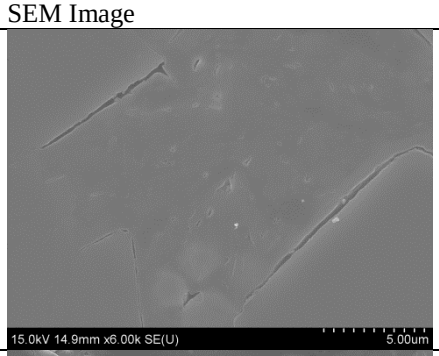	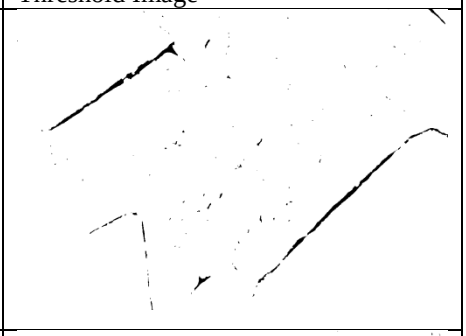
5 um	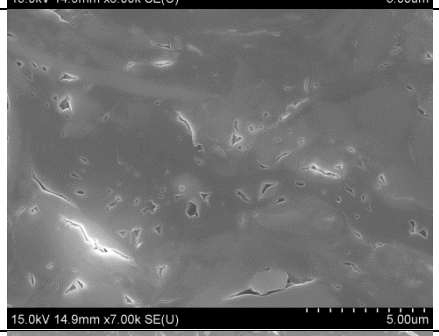	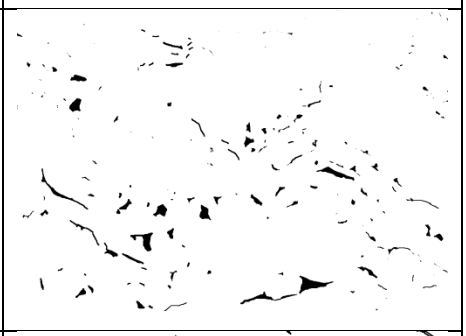
100 um	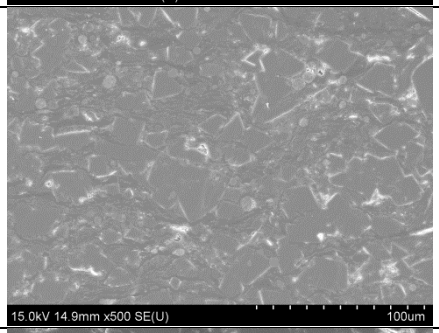	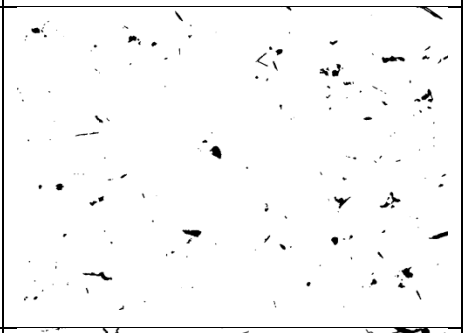
100 um	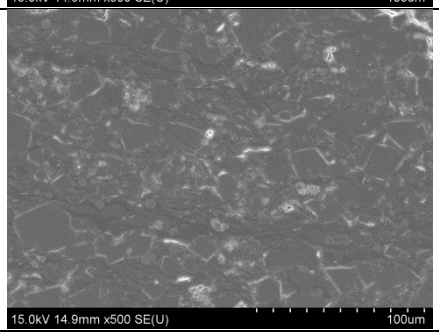	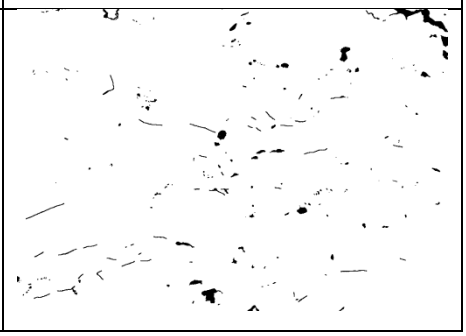

APPENDIX E: GRI Data

APPENDIX E.1

GRI pressure results

EBN 19

Condition	Chips GRI He Normal
Chips Size [um]	500<d<850
Weight [g]	51.04
Set-up	G2
Bulk density	2.14
Volume of grain [cm^3]	23.85
Volume of plug [cm^3]	-
Porosity [%]	15.93
Permeability[nD]	

Chips GRI He Normal	**P1 [psig]**	**P2[psig]**	**P3[psig]**	**Vcal [cm3]**	**Porosity [%]**
Measurement 1	246.049	0.000	116.400	20.122	0.156
Measurement 2	249.306	116.400	179.062	20.018	0.161
Measurement 3	242.890	179.020	209.190	20.014	0.161

EBN 20

Condition	Chips GRI He Normal	Chips GRI He Dry	Chips GRI He Wet	Full plug GRI He	Chips GRI N "as-received"
Chips Size [um]	500<d<850	500<d<850	500<d<850		500<d<850
Weight [g]	60.029	57.322	63.476	78.55	56.549
Set-up	G3	G2	G2	G3	G2
Bulk density	2.45	2.45	2.45	-	2.45
Volume of grain [cm^3]	24.50163	23.39673	25.90857	-	23.08122
Volume of plug [cm^3]	-	-	-	33.170807	-
Porosity [%]	7.762389	8.939305	6.930817	8.8898174	6.817155
Permeability[nD]					

Chips GRI He Normal	P1 [psig]	P2[psig]	P3[psig]	Vcal [cm3]	Porosity [%]
Measurement 1	243.79	0.00	111.86	22.68	0.07
Measurement 2	239.33	111.86	170.07	22.56	0.08
Measurement 3	240.97	169.83	202.44	22.56	0.08

Chips GRI He Dry	P1 [psig]	P2[psig]	P3[psig]	Vcal [cm3]	Porosity [%]
Measurement 1	238.83	0.00	114.58	21.33	0.09
Measurement 2	243.68	114.58	176.58	21.37	0.09
Measurement 3	247.61	176.58	210.30	21.22	0.09

Chips GRI He Wet	P1 [psig]	P2[psig]	P3[psig]	Vcal [cm3]	Porosity [%]
Measurement 1	229.33	0.00	113.78	24.18	0.07
Measurement 2	247.52	113.78	179.91	24.07	0.07
Measurement 3	220.59	179.91	200.11	24.09	0.07

Full plug GRI He	P1 [psig]	P2[psig]	P3[psig]	Vcal [cm3]	Porosity [%]
Measurement 1	244.69	0.00	110.94	30.46	8.89

Chips GRI N as-received	P1 [psig]	P2[psig]	P3[psig]	Vcal [cm3]	Porosity [%]
Measurement 1	236.88	0.00	114.14	21.71	0.06
Measurement 2	227.44	113.88	168.22	21.51	0.07
Measurement 3	225.73	168.22	195.38	21.30	0.08

EBN 21

Condition	Chips GRI He Normal	Chips GRI HeDry	Chips GRI He Wet	Full plug GRI He	Chips GRI Nitrogen Normal
Chips Size [um]	500<d<850	500<d<850	500<d<850	-	500<d<850
Weight [g]	35.66	34.92	36.55	-	35.29
Set-up	G2	G2	G3	G3	G2
Bulk density	1.95	1.95	1.95	-	1.95
Volume of grain [cm^3]	18.28	17.91	18.74	-	18.10
Volume of plug [cm^3]	-	-	-	41.89888	-
Porosity [%]	0.15	18.06	14.49	19.85116	15.19
Permeability[nD]					

Chips GRI He Normal	P1 [psig]	P2[psig]	P3[psig]	Vcal [cm3]	Porosity [%]
Measurement 1	239.035	0.000	107.800	15.848	0.133
Measurement 2	238.067	107.800	166.070	15.584	0.148
Measurement 3	251.880	166.070	204.173	15.367	0.160

Chips GRI He Dry	P1 [psig]	P2[psig]	P3[psig]	Vcal [cm3]	Porosity [%]
Measurement 1	243.800	0.000	108.600	14.711	0.179
Measurement 2	247.190	108.600	170.240	14.660	0.181
Measurement 3	243.332	170.240	202.760	14.650	0.182

Chips GRI He Wet	P1 [psig]	P2[psig]	P3[psig]	Vcal [cm3]	Porosity [%]
Measurement 1	247.330	0.000	104.327	16.029	0.145
Measurement 2	248.897	104.327	165.320	16.034	0.145
Measurement 3	225.133	165.320	190.517	16.019	0.145

Full plug GRI He	P1 [psig]	P2[psig]	P3[psig]	Vcal [cm3]	Porosity [%]
Measurement 1	228.67	0.00	108.07	33.58	19.85

Chips GRI N as-received	P1 [psig]	P2[psig]	P3[psig]	Vcal [cm3]	Porosity [%]
Measurement 1	228.199	0.000	102.620	15.586	0.139
Measurement 2	222.355	102.620	156.012	15.320	0.154
Measurement 3	225.545	156.012	186.833	15.144	0.163

EBN 22

Condition	Chips GRI He
Chips Size [um]	500<d<850
Weight [g]	55.85
Set-up	G2
Bulk density	2.42
Volume of grain [cm^3]	23.08
Volume of plug [cm^3]	-
Porosity [%]	3.58
Permeability[nD]	

Chips GRI He Normal	**P1 [psig]**	**P2[psig]**	**P3[psig]**	**Vcal [cm3]**	**Porosity [%]**
Measurement 1	220.380	0.000	107.040	22.390	0.030
Measurement 2	222.820	107.040	163.054	22.275	0.035
Measurement 3	250.190	163.054	204.867	22.087	0.043

EBN 23

Condition	Chips GRI He Normal	Chips GRI He dry	Chips GRI He Wet	Full plug GRI He	Chips GRI Nitrogen Normal
Chips Size [um]	500<d<850	500<d<850	500<d<850	-	500<d<850
Weight [g]	71.21	71.38	36.55	-	35.29
Set-up	G3	G2	G3	G3	G2
Bulk density	2.51	2.51	1.95	-	1.95
Volume of grain [cm^3]	28.37	28.44	18.74	-	18.10
Volume of plug [cm^3]	-	-	-	41.89888	-
Porosity [%]	3.47	16.37	14.49	19.85116	15.19
Permeability[nD]					

Chips GRI He Normal	**P1 [psig]**	**P2[psig]**	**P3[psig]**	**Vcal [cm3]**	**Porosity [%]**
Measurement 1	242.090	0.000	118.637	27.508	0.030
Measurement 2	210.910	118.637	163.790	27.479	0.031
Measurement 3	248.300	163.790	204.274	27.162	0.043

Chips GRI He Dry	**P1 [psig]**	**P2[psig]**	**P3[psig]**	**Vcal [cm3]**	**Porosity [%]**
Measurement 1	221.840	0.000	109.520	23.764	0.164
Measurement 2	222.720	109.520	165.423	23.772	0.164
Measurement 3	247.386	165.423	205.970	23.804	0.163

EBN 24

Condition	Chips GRI He Normal	Chips GRI He Dry	Chips GRI He Wet	Full plug GRI He	Chips GRI Ni Normal
Chips Size [um]	500<d<850	500<d<850	500<d<850	-	500<d<850
Weight [g]	63.21	58.54	46.48	-	46.39
Set-up	G2	G3	G3	-	G2
Bulk density	2.37	2.37	2.37	-	2.37
Volume of grain [cm^3]	26.67	24.70	19.61	-	19.58
Volume of plug [cm^3]	-	-	-	-	-
Porosity [%]	1.94	5.70	5.05	-	0.92
Permeability[nD]					

Chips GRI He Normal	**P1 [psig]**	**P2[psig]**	**P3[psig]**	**Vcal [cm3]**	**Porosity [%]**
Measurement 1	239.770	0.000	121.900	26.183	0.018
Measurement 2	237.220	121.938	180.479	26.152	0.019
Measurement 3	243.200	180.479	212.280	26.124	0.021

Chips GRI He Dry	**P1 [psig]**	**P2[psig]**	**P3[psig]**	**Vcal [cm3]**	**Porosity [%]**
Measurement 1	245.165	0.000	113.304	23.224	0.060
Measurement 2	241.860	113.304	172.990	23.343	0.055
Measurement 3	247.770	172.990	207.500	23.305	0.056

Chips GRI He Wet	**P1 [psig]**	**P2[psig]**	**P3[psig]**	**Vcal [cm3]**	**Porosity [%]**
Measurement 1	232.342	0.000	101.340	18.742	0.044
Measurement 2	228.495	101.340	156.340	18.507	0.056
Measurement 3	234.440	156.340	190.557	18.612	0.051

Chips GRI N as-received	**P1 [psig]**	**P2[psig]**	**P3[psig]**	**Vcal [cm3]**	**Porosity [%]**
Measurement 1	224.924	0.000	105.700	19.539	0.002
Measurement 2	224.660	105.700	161.387	19.421	0.008
Measurement 3	219.838	161.387	188.403	19.227	0.018

EBN 25

Condition	Chips GRI He Normal	Chips GRI He Dry	Chips GRI He Wet	Full plug GRI He	Chips GRI Nitrogen Normal
Chips Size [um]	500<d<850	500<d<850	500<d<850	-	500<d<850
Weight [g]	43.93	43.49	44.35	-	43.80
Set-up	G3	G3	S1	G2	G2
Bulk density	2.58	2.58	2.58	-	2.58
Volume of grain [cm^3]	17.03	16.86	17.19	-	16.98
Volume of plug [cm^3]	-	-	-	25.35341	-
Porosity [%]	10.69	14.81	9.45	8.888417	6.94
Permeability[nD]					

Chips GRI He Normal	**P1 [psig]**	**P2[psig]**	**P3[psig]**	**Vcal [cm3]**	**Porosity [%]**
Measurement 1	225.080	0.000	93.985	15.189	0.108
Measurement 2	244.011	93.985	156.670	15.211	0.107
Measurement 3	247.640	156.670	194.685	15.219	0.106

Chips GRI He Dry	**P1 [psig]**	**P2[psig]**	**P3[psig]**	**Vcal [cm3]**	**Porosity [%]**
Measurement 1	218.960	0.000	90.510	14.343	0.149
Measurement 2	225.150	90.510	146.090	14.300	0.152
Measurement 3	248.526	146.030	188.690	14.440	0.143

Chips GRI He Wet	**P1 [psig]**	**P2[psig]**	**P3[psig]**	**Vcal [cm3]**	**Porosity [%]**
Measurement 1	262.960	0.000	96.950	16.222	
Measurement 2	235.970	96.950	147.440	15.595	0.093
Measurement 3	337.570	147.440	217.070	15.535	0.096

Full plug GRI He	**P1 [psig]**	**P2[psig]**	**P3[psig]**	**Vcal [cm3]**	**Porosity [%]**
Measurement 1	228.48	0.00	102.106	23.10	0.088

Chips GRI N as-received	**P1 [psig]**	**P2[psig]**	**P3[psig]**	**Vcal [cm3]**	**Porosity [%]**
Measurement 1	222.078	0.000	100.404	16.077	0.053
Measurement 2	209.537	100.404	149.096	15.680	0.076
Measurement 3	220.464	149.096	181.130	15.633	0.079

EBN 26

Condition	Chips GRI He
Chips Size [um]	500<d<850
Weight [g]	38.44
Set-up	S1
Bulk density	2.62
Volume of grain [cm^3]	14.67
Volume of plug [cm^3]	-
Porosity [%]	8.90
Permeability[nD]	

Chips GRI He Normal	**P1 [psig]**	**P2[psig]**	**P3[psig]**	**Vcal [cm3]**	**Porosity [%]**
Measurement 1	441.250	0.000	159.070	13.474	0.082
Measurement 2	307.980	159.070	212.380	13.258	0.096

EBN 27

Condition	Chips GRI He	Full plug GRI He
Chips Size [um]	500<d<850	-
Weight [g]	51.67	-
Set-up	G2	G3
Bulk density	2.61	-
Volume of grain [cm^3]	19.80	-
Volume of plug [cm^3]	-	48.27386
Porosity [%]	16.95	6.93307
Permeability[nD]		

Chips GRI He Normal	P1 [psig]	P2[psig]	P3[psig]	Vcal [cm3]	Porosity [%]
Measurement 1	249.530	0.000	116.470	18.941	0.043
Measurement 2	228.170	116.470	168.489	18.879	0.046
Measurement 3	231.090	168.489	197.440	18.768	0.052

Full plug GRI He	P1 [psig]	P2[psig]	P3[psig]	Vcal [cm3]	Porosity [%]
Measurement 1	239.02	0.00	133.56	44.927	0.0693

EBN 28

Condition	Chips GRI He	Full plug GRI He
Chips Size [um]	500<d<850	-
Weight [g]	57.56	-
Set-up	G3	G2
Bulk density	2.30	-
Volume of grain [cm^3]	25.03	-
Volume of plug [cm^3]	-	45.44768
Porosity [%]	6.84	11.91
Permeability[nD]		

Chips GRI He Normal	P1 [psig]	P2[psig]	P3[psig]	Vcal [cm3]	Porosity [%]
Measurement 1	246.330	0.000	113.901	23.263	0.070
Measurement 2	236.660	113.901	170.900	23.367	0.066
Measurement 3	240.012	170.900	202.756	23.313	0.068

Full plug GRI He	P1 [psig]	P2[psig]	P3[psig]	Vcal [cm3]	Porosity [%]
Measurement 1	234.42	0.00	128.287	40.034	0.1191

EBN 29

Condition	Chips GRI He	Chips GRI He Dry	Chips GRI He Wet	Chips GRI Nitrogen Normal
Chips Size [um]	500<d<850	500<d<850	500<d<850	500<d<850
Weight [g]	39.41	38.39	40.20	38.82
Set-up	S1	G3	S1	G2
Bulk density	2.09	2.09	2.09	2.09
Volume of grain [cm^3]	18.85	18.37	19.23	18.58
Volume of plug [cm^3]	-	-	-	-
Porosity [%]	10.12	21.31	15.80	15.51
Permeability[nD]				

Chips GRI He Normal	**P1 [psig]**	**P2[psig]**	**P3[psig]**	**Vcal [cm3]**	**Porosity [%]**
Measurement 1	220.810	0.000	81.900	16.946	0.101

Chips GRI He Dry	**P1 [psig]**	**P2[psig]**	**P3[psig]**	**Vcal [cm3]**	**Porosity [%]**
Measurement 1	246.400	0.000	101.820	14.316	0.221
Measurement 2	250.839	101.820	163.815	14.530	0.209
Measurement 3	232.487	163.815	192.236	14.517	0.210

Chips GRI He Wet	**P1 [psig]**	**P2[psig]**	**P3[psig]**	**Vcal [cm3]**	**Porosity [%]**
Measurement 1	380.420	0.000	140.870	16.749	0.129
Measurement 2	484.150	140.870	266.520	16.086	0.164
Measurement 3	489.720	266.520	347.750	15.749	0.181

Chips GRI N "as-received"	**P1 [psig]**	**P2[psig]**	**P3[psig]**	**Vcal [cm3]**	**Porosity [%]**
Measurement 1	215.015	0.000	97.077	15.951	0.141
Measurement 2	215.179	97.077	149.850	15.616	0.159
Measurement 3	212.922	149.850	178.031	15.517	0.165

EBN 30

Condition	Chips GRI He	Chips GRI He Wet
Chips Size [um]	500<d<850	500<d<850
Weight [g]	63.42	56.94
Set-up	G2	G2
Bulk density	2.40	2.40
Volume of grain [cm^3]	26.43	23.73
Volume of plug [cm^3]	-	-
Porosity [%]	6.45	5.92
Permeability[nD]		

Chips GRI He Normal	P1 [psig]	P2[psig]	P3[psig]	Vcal [cm3]	Porosity [%]
Measurement 1	228.300	0.000	114.206	24.859	0.059
Measurement 2	236.050	114.206	174.660	24.624	0.068
Measurement 3	245.990	174.660	210.390	24.683	0.066

Chips GRI He Wet	P1 [psig]	P2[psig]	P3[psig]	Vcal [cm3]	Porosity [%]
Measurement 1	244.675	0.000	118.836	22.387	0.056
Measurement 2	221.301	118.836	168.460	22.315	0.059
Measurement 3	241.408	168.460	203.727	22.260	0.062

EBN 32

Condition	Chips GRI He	Full plug GRI He
Chips Size [um]	500<d<850	-
Weight [g]	50.55	-
Set-up	G3	G3
Bulk density	2.00	-
Volume of grain [cm^3]	25.27	-
Volume of plug [cm^3]	-	49.0363
Porosity [%]	19.96	16.76
Permeability[nD]		

Chips GRI He Normal	P1 [psig]	P2[psig]	P3[psig]	Vcal [cm3]	Porosity [%]
Measurement 1	230.700	0.000	102.270	20.025	0.208
Measurement 2	229.968	102.270	159.970	20.560	0.187
Measurement 3	235.577	159.970	192.400	20.027	0.208

Full plug GRI He	P1 [psig]	P2[psig]	P3[psig]	Vcal [cm3]	Porosity [%]
Measurement 1	234.25	0.00	122.785	40.816	0.1676

EBN 35

Condition	Chips GRI He Normal	Chips GRI He Dry	Chips GRI He Wet	Full plug GRI He
Chips Size [um]	500<d<850	500<d<850	500<d<850	-
Weight [g]	47.33	50.55	63.47	-
Set-up	G2	G3	S1	G3
Bulk density	1.96	1.96	1.96	-
Volume of grain [cm^3]	24.15	25.79	32.38	-
Volume of plug [cm^3]	-	-	-	13.31127
Porosity [%]	11.46	12.90	9.60	24.284
Permeability[nD]				

Chips GRI He Normal	**P1 [psig]**	**P2[psig]**	**P3[psig]**	**Vcal [cm3]**	**Porosity [%]**
Measurement 1	236.640	0.000	113.780	21.525	0.109
Measurement 2	234.764	113.780	171.510	21.305	0.118
Measurement 3	253.099	171.510	210.668	21.317	0.117

Chips GRI He Dry	**P1 [psig]**	**P2[psig]**	**P3[psig]**	**Vcal [cm3]**	**Porosity [%]**
Measurement 1	233.350	0.000	106.830	22.510	0.127
Measurement 2	225.470	106.830	161.260	22.565	0.125
Measurement 3	233.500	161.260	193.720	22.316	0.135

Chips GRI He Wet	**P1 [psig]**	**P2[psig]**	**P3[psig]**	**Vcal [cm3]**	**Porosity [%]**
Measurement 1	224.980	0.000	93.910	16.222	0.091
Measurement 2	441.060	93.920	236.660	15.595	0.093
Measurement 3	321.920	236.660	271.440	15.535	0.096

Full plug GRI He	**P1 [psig]**	**P2[psig]**	**P3[psig]**	**Vcal [cm3]**	**Porosity [%]**
Measurement 1	237.056	0.00	141.034	10.823	24.284

Appendix E.2

GRI Permeability calculation

Sample	GRI Porosity [He] Chips [%]			Halway time pressure [hr] Chips			Halway time pressure [hr] Chips			Halway time pressure [hr] Chips		
Number	*Wet*	*ambient*	*Dry*		*Wet*			*Ambient*			*Dry*	
				Run 1	*Run 2*	*Run 3*	*Run 1*	*Run 2*	*Run 3*	*Run 1*	*Run 2*	*Run 3*
EBN 20	0.0693	0.0776	0.0899	0.003055556	1.895555556	0.007777778	0.00277778	0.002916667	0.002638889	0.0425	0.028611111	0.331388889
EBN 21	0.1448	0.1469	0.1806	0.007222222	0.008611111	0.006111111	0.0025	0.003333333	0.070277778	0.03	0.004166667	0.0075
EBN 24	0.0505	0.0187	0.0606	0.007777778	2.118055556	0.004444444	0.02916667	0.014166667	0.016666667	0.03472222	0.010277778	0.541944444
EBN 25	0.0945	0.1069	0.148	0.010277778	0.056944444	0.003055556	0.00444444	0.006944444	0.0075	0.02583333	0.003888889	0.003611111
EBN 29	0.158	0.1012	0.2174	0.0025	0.002777778	0.038611111	0.02722222			0.03527778	0.004166667	0.014166667

Sample	GRI Porosity [Nitrogen] Chips [%]	Halway time pressure [hr] Chips Nitrogen			time [hrs]/phi[%] Chips Nitrogen			Permeability Chips Nitrogen		
Number	*ambient*		*Ambient*			*Ambient*			*Ambient*	
	Chips [%]	*Run 1*	*Run 2*	*Run 3*	*Run 1*	*Run 2*	*Run 3*	*Run 1*	*Run 2*	*Run 3*
EBN 20	*0.068171555*	*0.140555556*	*0.15972*	*1.911111111*	2.061791839	2.342945272	28.0338495	8.21909E-05	7.1007E-05	4.149E-06
EBN 21	0.151852992	0.004444444	0.009722	0.138888889	0.029268073	0.06402391	0.91462728	0.010693866	0.004366829	0.00020832
EBN 24	*0.009174473*	*0.2325*	*0.0375*	*0.319444444*	25.34205511	4.087428244	34.8188332	4.65701E-06	3.75631E-05	3.2377E-06
EBN 25	*0.069443228*	*0.013333333*	*0.02667*	*0.009722222*	0.192003363	0.384006727	0.14000245	0.001242856	0.000562319	0.00178392
EBN 29	0.15506	0.005833333	0.014167	0.055555556	0.037619846	0.091362483	0.35828425	0.008023997	0.002907182	0.00060875

Sample	time [hrs]/phi[%] Chips			time [hrs]/phi[%] Chips			time [hrs]/phi[%] Chips		
Number		*Wet*			*Ambient*			*Dry*	
	Run 1	*Run 2*	*Run 3*	*Run 1*	*Run 2*	*Run 3*	*Run 1*	*Run 2*	*Run 3*
EBN 20	0.044091711	27.35289402	0.112233	0.035796105	0.037585911	0.0340063	0.4727475	0.318254851	3.686194537
EBN 21	0.049877225	0.059468999	0.042204	0.01701838	0.022691173	0.478405567	0.16611296	0.023071244	0.041528239
EBN 24	0.154015402	41.94169417	0.088009	1.559714795	0.757575758	0.891265597	0.57297396	0.169600293	8.942977631
EBN 25	0.108759553	0.602586714	0.032334	0.04157572	0.064962062	0.070159027	0.17454955	0.026276276	0.024399399
EBN 29	0.015822785	0.017580872	0.244374	0.268994291	-	-	0.16227129	0.0191659	0.06516406

Permeability Chips			Permeability Chips			Permeability Chips		
	Wet			*Ambient*			*Dry*	
Run 1	*Run 2*	*Run 3*	*Run 1*	*Run 2*	*Run 3*	*Run 1*	*Run 2*	*Run 3*
0.9435432	0.000515694	0.316771942	1.203673	1.136986422	1.278003084	0.059046981	0.09374709	0.005360717
0.8169776	0.665232193	0.993033302	2.869068	2.050158722	0.058231989	0.200366077	2.01075898	1.011930478
0.2188704	0.000312986	0.420827565	0.014641	0.034037217	0.02815148	0.047167884	0.19556153	0.001903611
0.3286233	0.044471393	1.355553488	1.010581	0.599998814	0.548409237	0.189099382	1.72728945	1.883489774
3.123901	2.762125224	0.127636085	0.114097			0.205918441	2.49717478	0.597826648

Sample	Permeability Average [nD] Chips		
Number	*Wet*	*Ambient*	*Dry*
EBN 20	0.420276942	1.206220927	0.052718
EBN 21	0.825081016	1.65915307	1.074352
EBN 24	0.213337	0.02561005	0.081544
EBN 25	0.576216057	0.719662875	1.266626
EBN 29	2.004554108	0.114096869	1.100307

Sample	Permeability Average [nD] Chips Nitrogen
Number	*Ambient*
EBN 20	5.2449E-05
EBN 21	0.005089671
EBN 24	1.51526E-05
EBN 25	0.001196364
EBN 29	0.003846642

APPENDIX F: NMR Data

APPENDIX E.1

NMR graphs

Name	**EBN 19**
Well name	**ZOM – 2**
Depth	**1675.8 m**
Formation	**Jurassic**

Condition	Normalized Signal	Cumulative Normalized Signal
Chips "as-received"	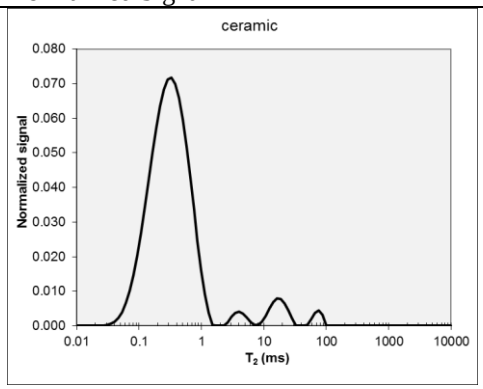	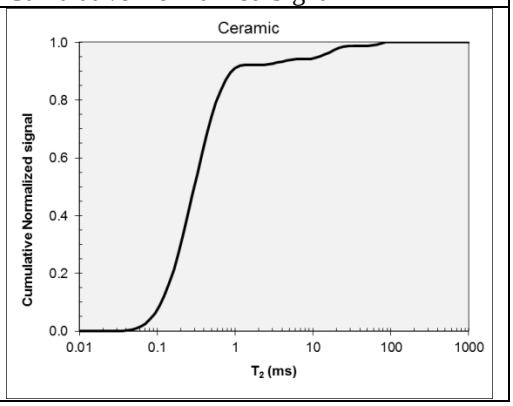

Name	**EBN 20**
Well name	**HLM – 1**
Depth	**1051.5 m**
Formation	**Jurassic**

Condition	Normalized Signal	Cumulative Normalized Signal
Chips "as-received"	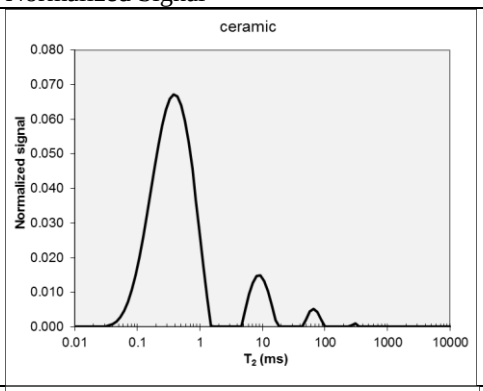	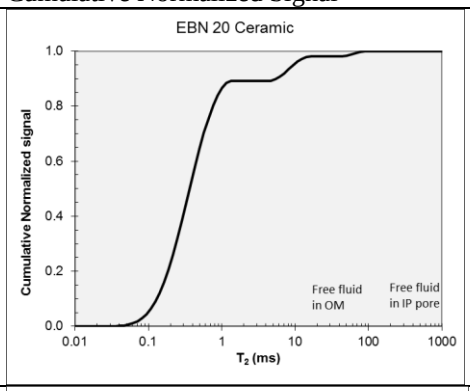
Chips Wet	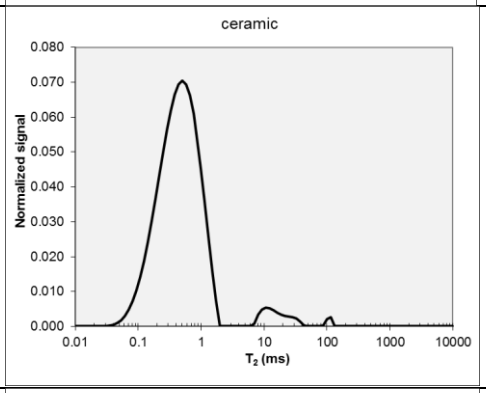	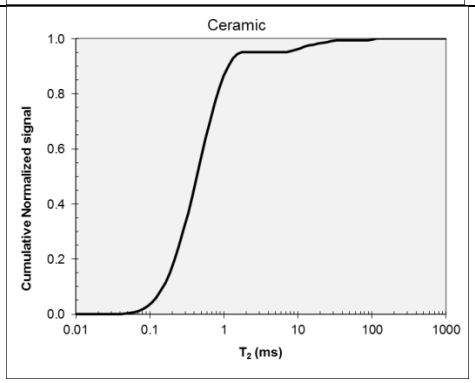
Chips Dry	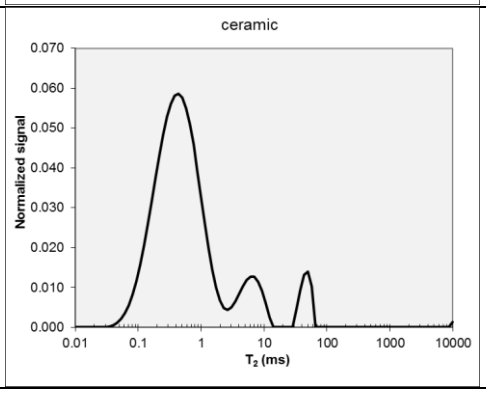	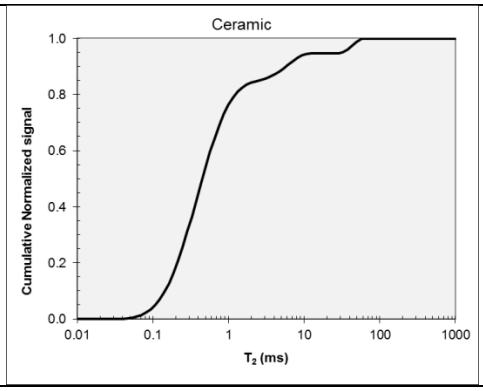

Plug ambient	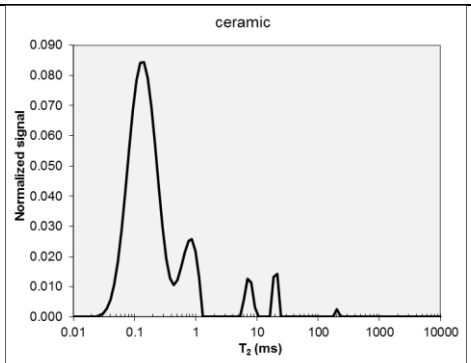	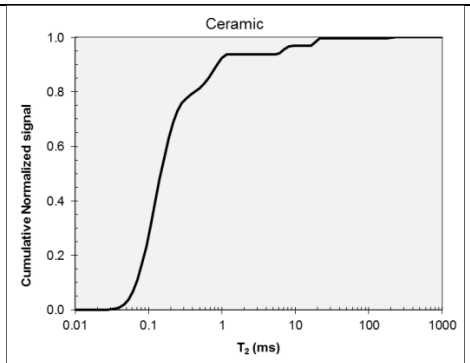
Plug After steady-state experiment	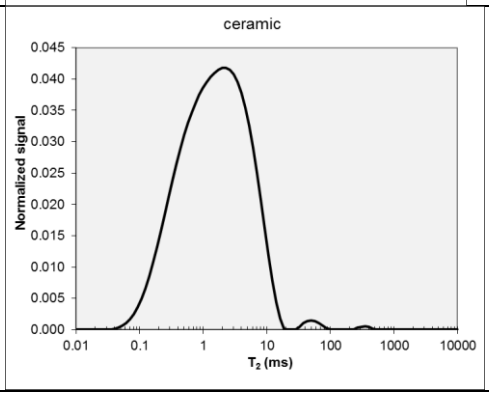	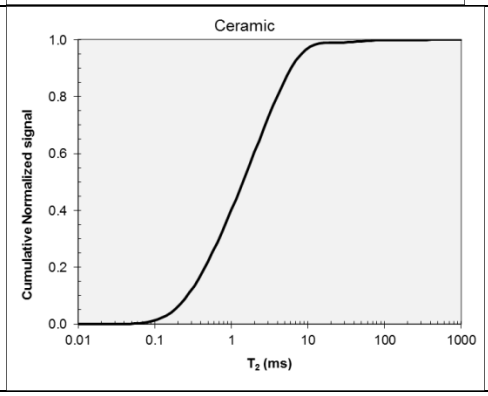

Name	**EBN 21**
Well name	**AND – 2**
Depth	**1718.0 m**
Formation	**Jurassic**

Condition	Normalized Signal	Cumulative Normalized Signal
Chips "as-received"	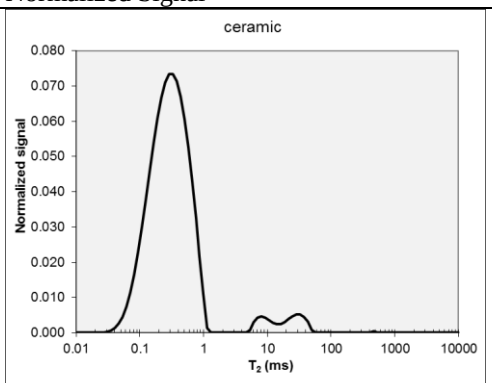	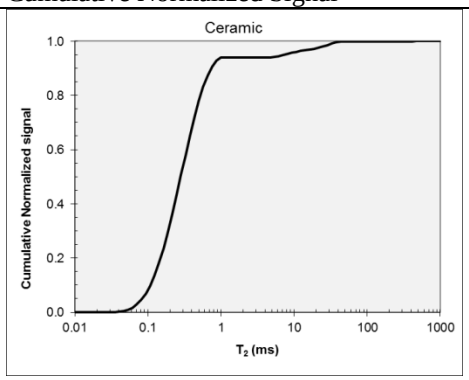
Chips Wet	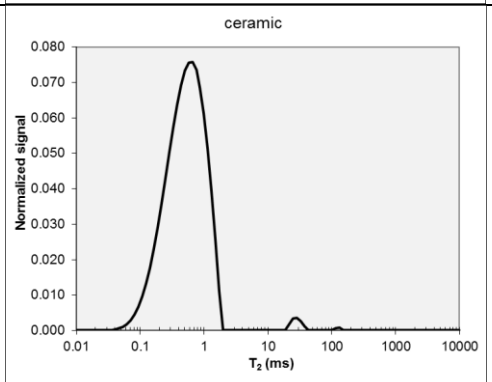	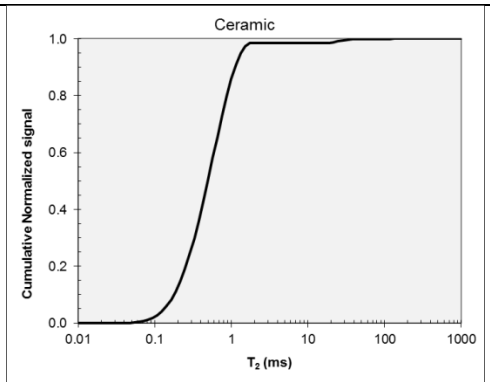
Chips Dry	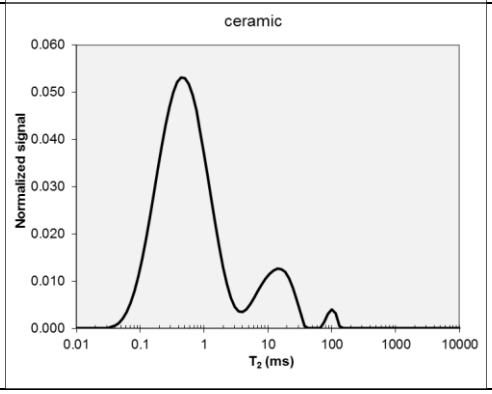	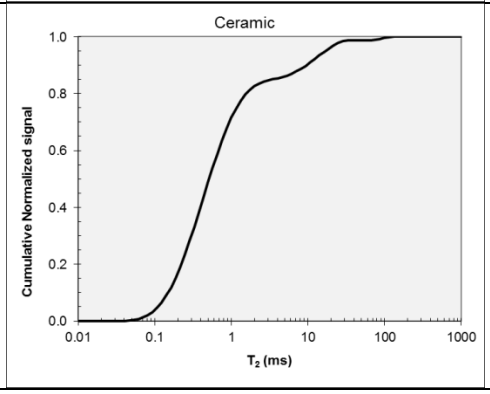

Plug ambient	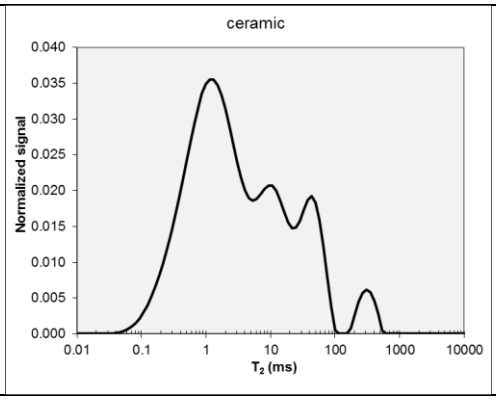	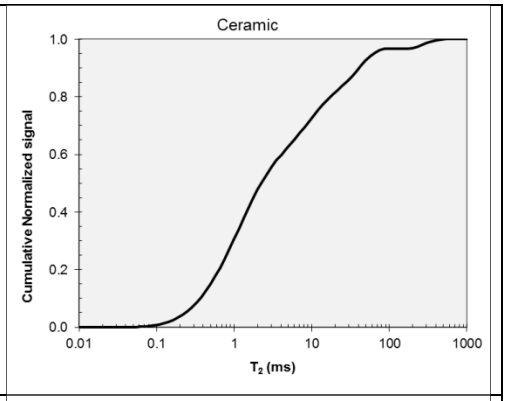
Plug After steady-state experiment	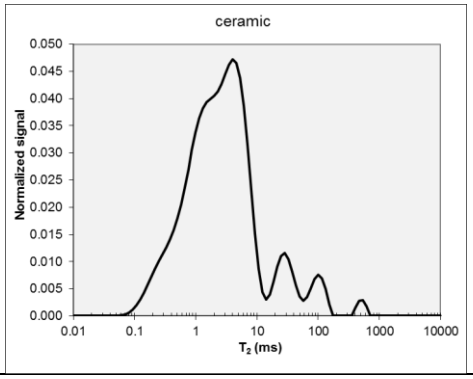	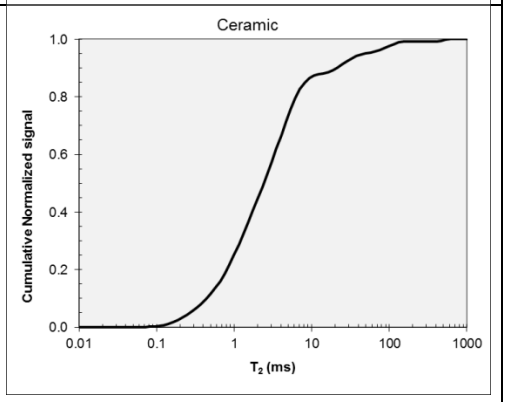

Name	**EBN 22**
Well name	**BRK – 2**
Depth	**3062.5 m**
Formation	**Jurassic**

Condition	Normalized Signal	Cumulative Normalized Signal
Chips "as-received"	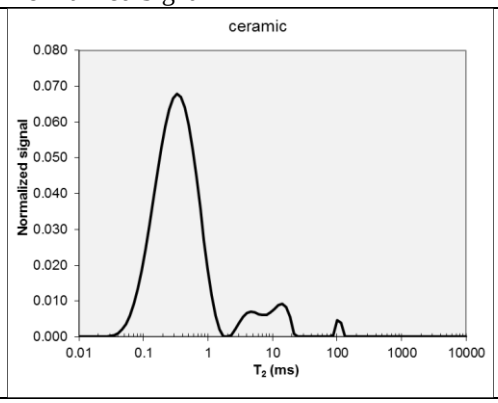	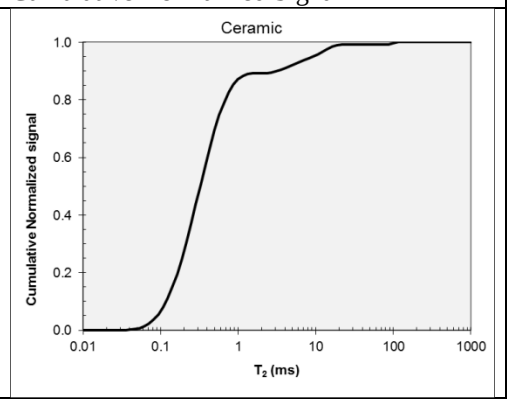

Name	**EBN 23**
Well name	**BRK – 02**
Depth	**3062.5 m**
Formation	**Jurassic**

Condition	Normalized Signal	Cumulative Normalized Signal
Chips "as-received"	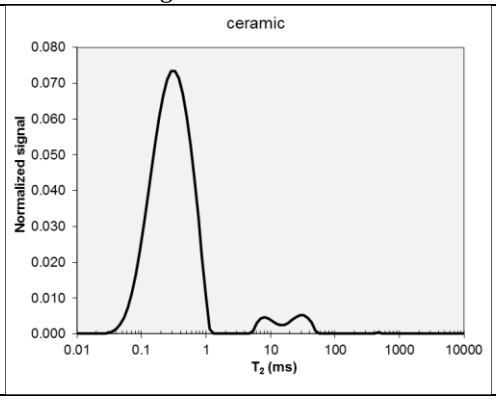	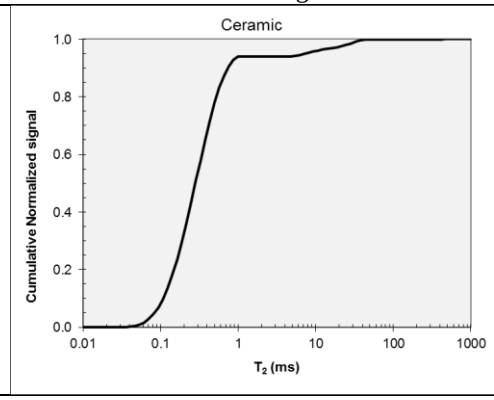

Name	**EBN 24**
Well name	**BRK – 02**
Depth	**3074.0 m**
Formation	**Jurassic**

Condition	Normalized Signal	Cumulative Normalized Signal
Chips "as-received"	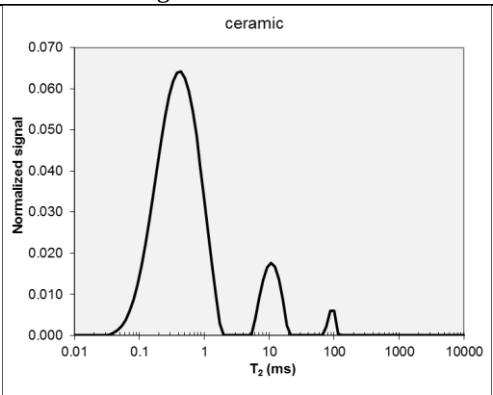	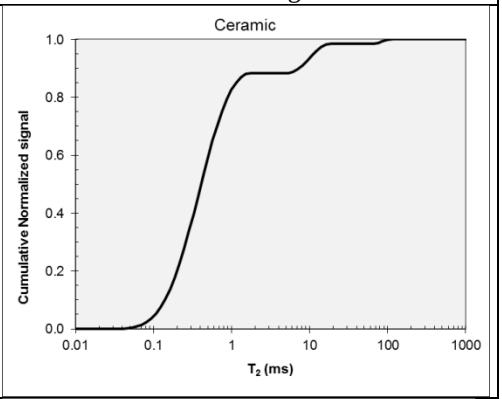
Chips Wet	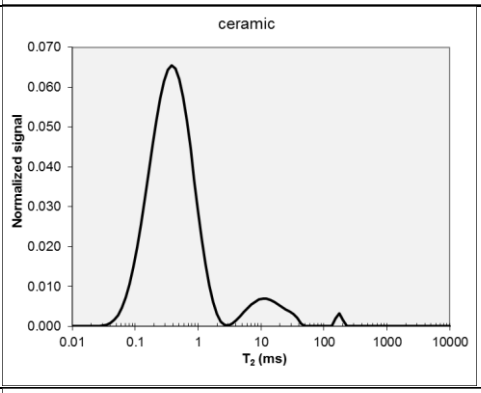	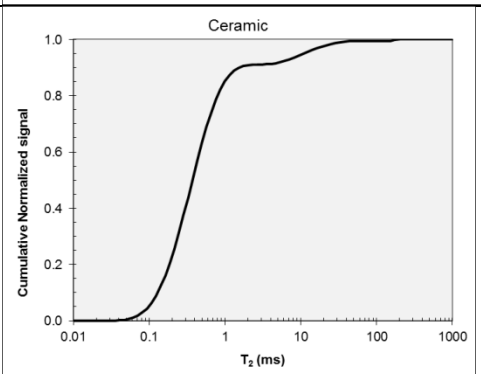
Chips Dry	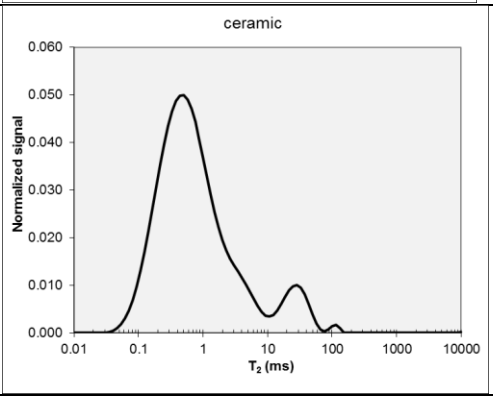	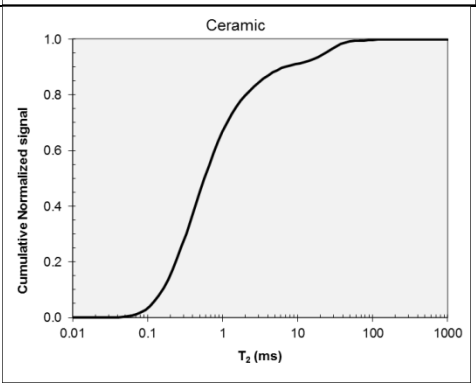

Name	**EBN 25**
Well name	**LOZ – 1**
Depth	**2509.5 m**
Formation	**Jurassic**

Condition	Normalized Signal	Cumulative Normalized Signal
Chips "as-received"	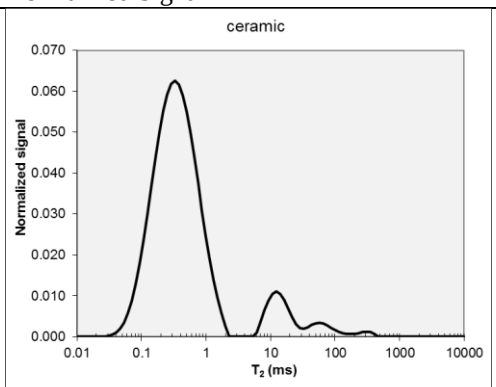	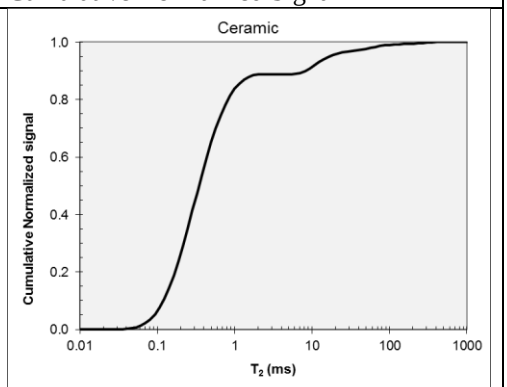
Chips Wet	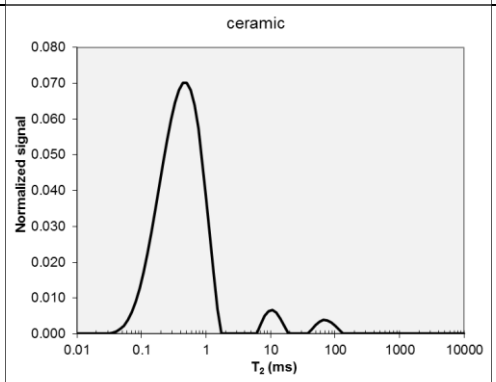	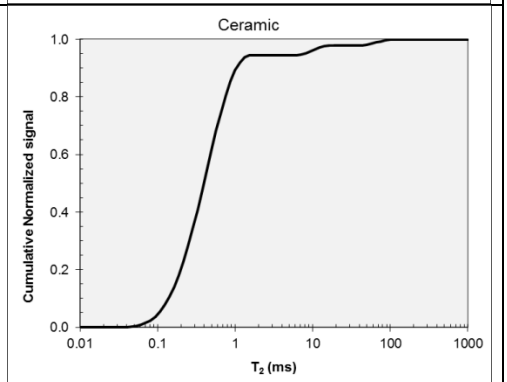
Chips Dry	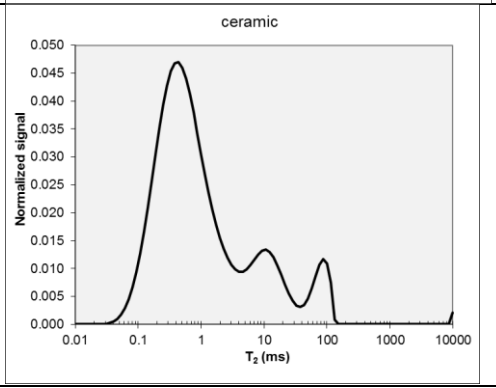	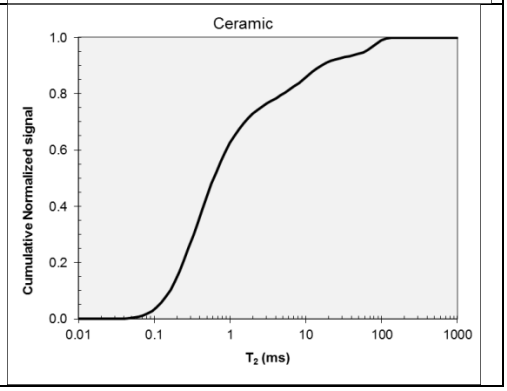

Plug ambient	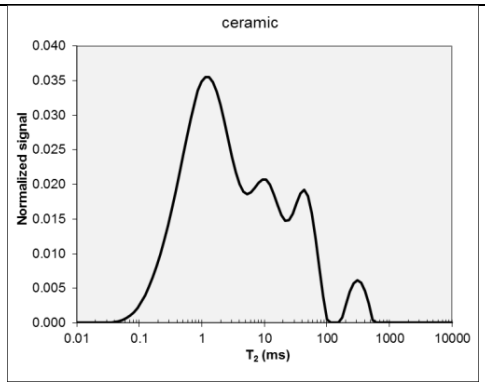	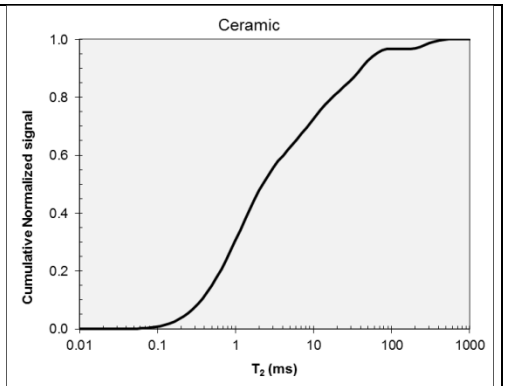
Plug After steady-state experiment	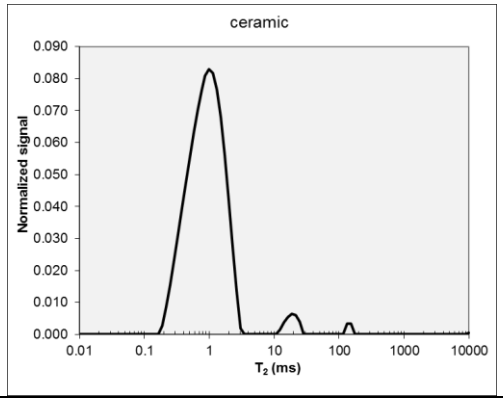	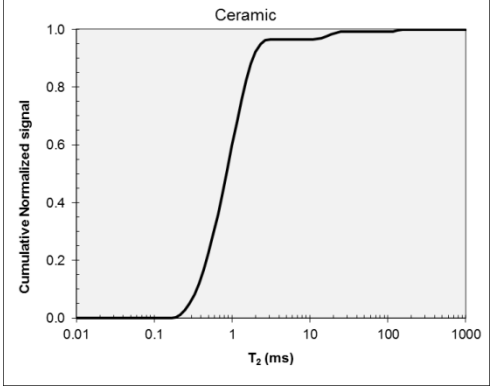

Name	**EBN 26**
Well name	**LOZ – 01**
Depth	**2510.0 m**
Formation	**Jurassic**

Condition	Normalized Signal	Cumulative Normalized Signal
Chips "as-received"	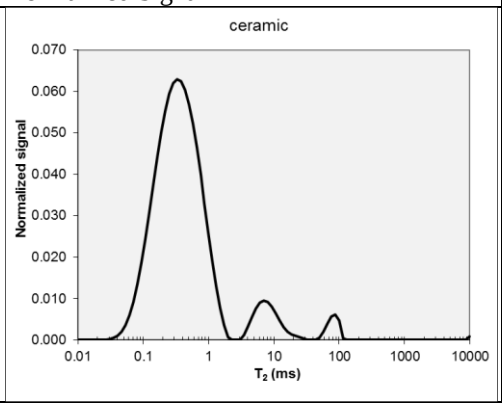	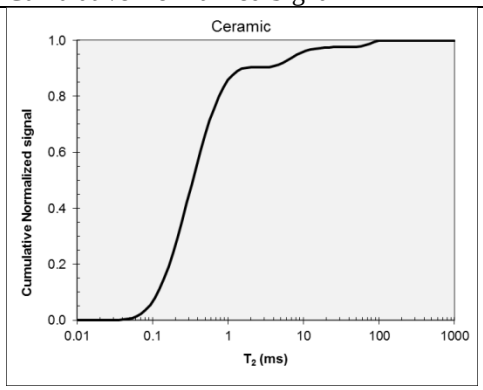

Name	**EBN 27**
Well name	**VLM – 1**
Depth	**1429.0 m**
Formation	**Jurassic**

Condition	Normalized Signal	Cumulative Normalized Signal
Chips "as-received"	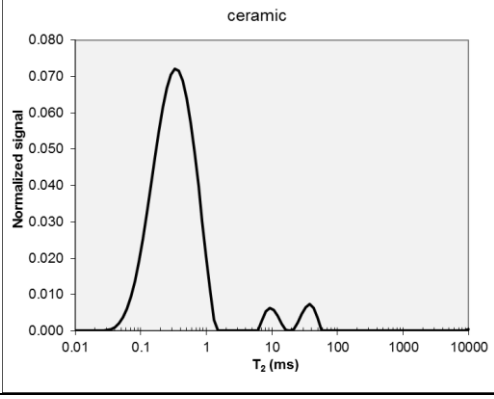	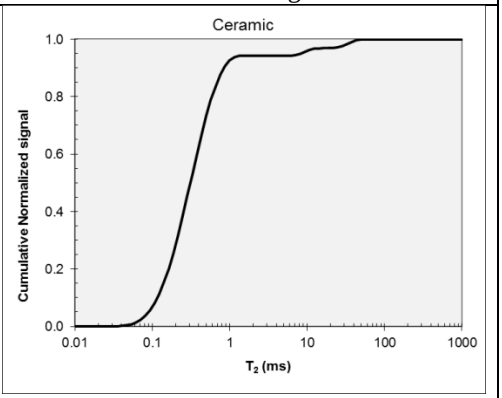

Name	**EBN 28**
Well name	**ZOM – 2**
Depth	**1675.0 m**
Formation	**Jurassic**

Condition	Normalized Signal	Cumulative Normalized Signal
Chips "as-received"	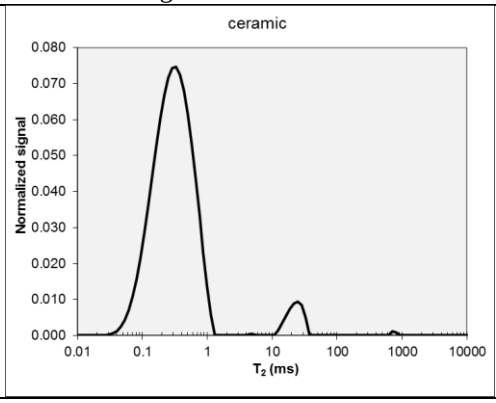	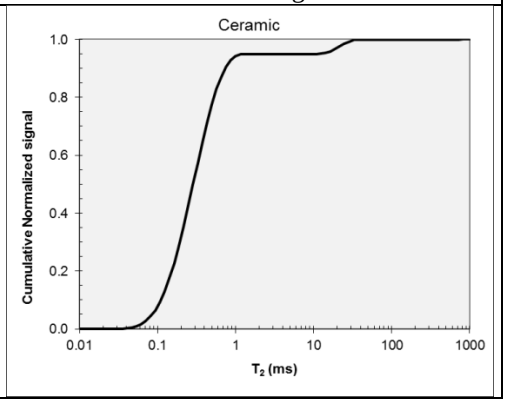

Name	**EBN 29**
Well name	**ZOM – 2**
Depth	**1678.0 m**
Formation	**Jurassic**

Condition	Normalized Signal	Cumulative Normalized Signal
Chips "as-received"	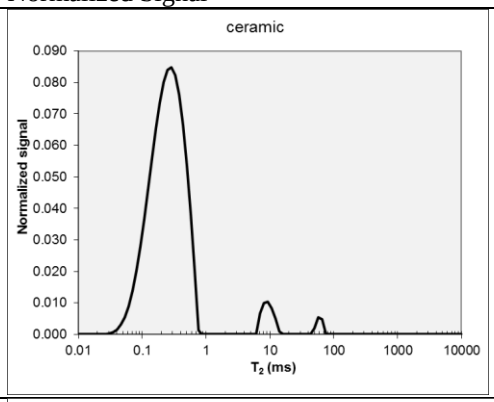	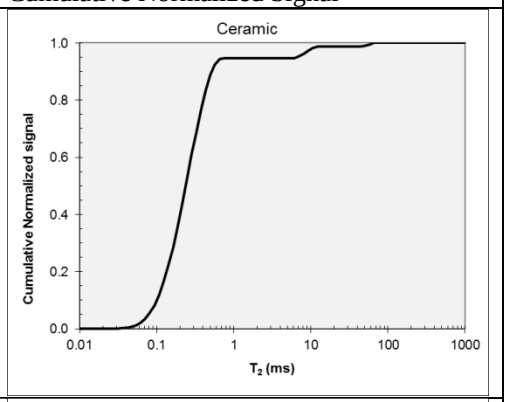
Chips Wet	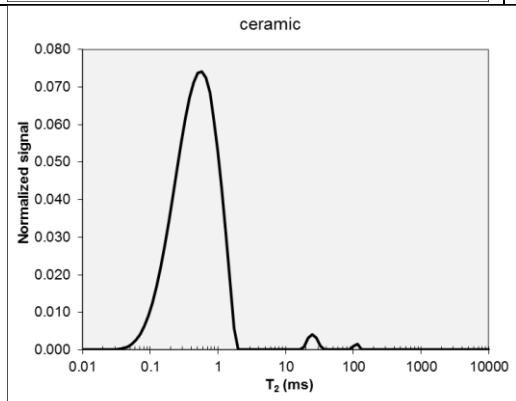	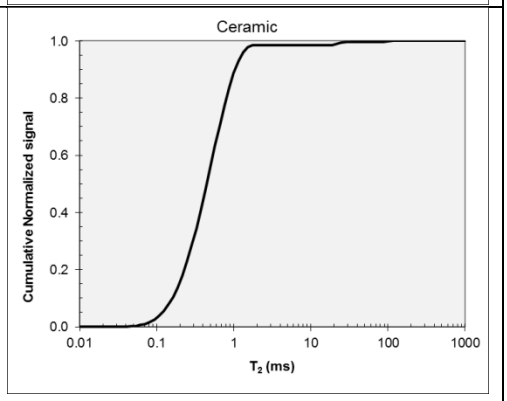
Chips Dry	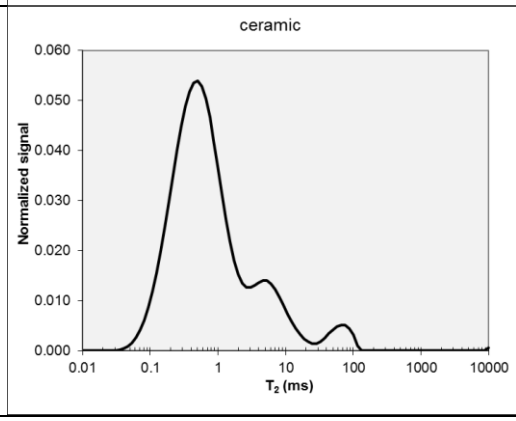	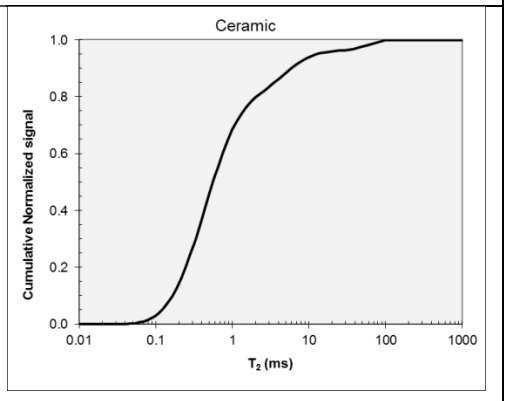

Plug ambient	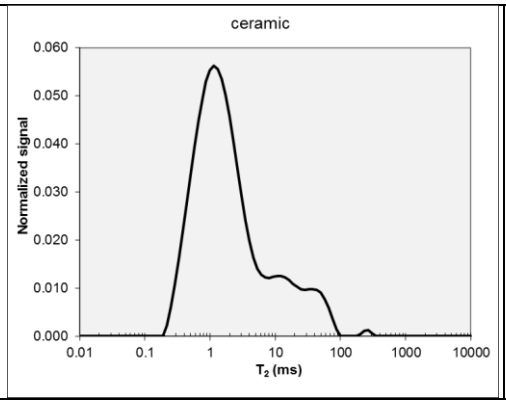	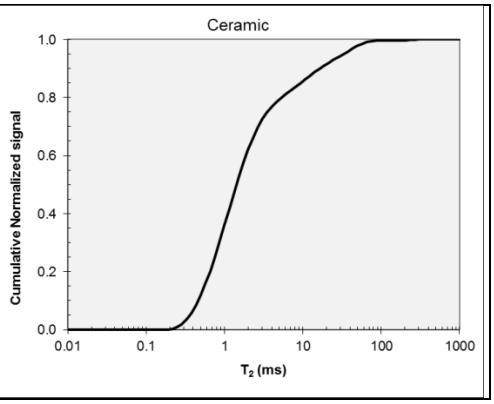

Name	**EBN 30**
Well name	**ZOM – 02**
Depth	**1678.0 m**
Formation	**Jurassic**

Condition	Normalized Signal	Cumulative Normalized Signal
Chips "as-received"	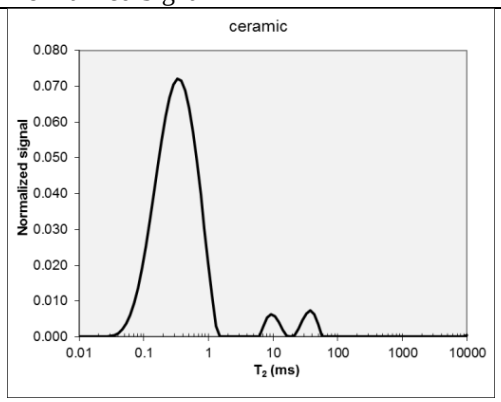	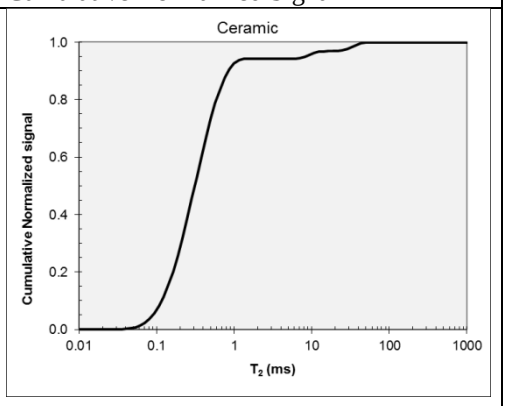
Chips Wet	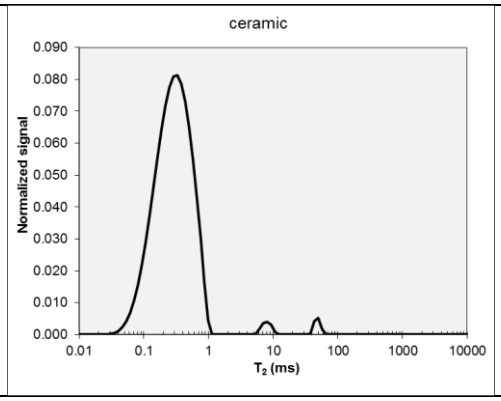	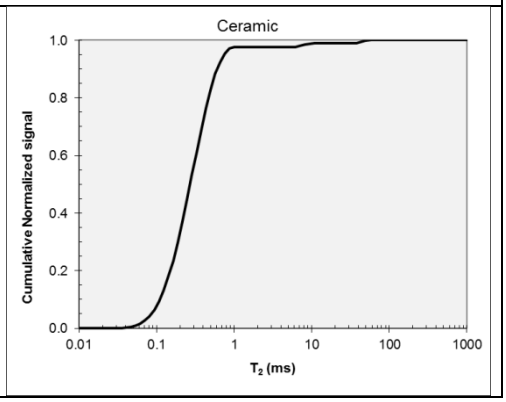

Name	**EBN 32**
Well name	**ZWE – 1**
Depth	**1233.0 m**
Formation	**Jurassic**

Condition	Normalized Signal	Cumulative Normalized Signal
Chips "as-received"	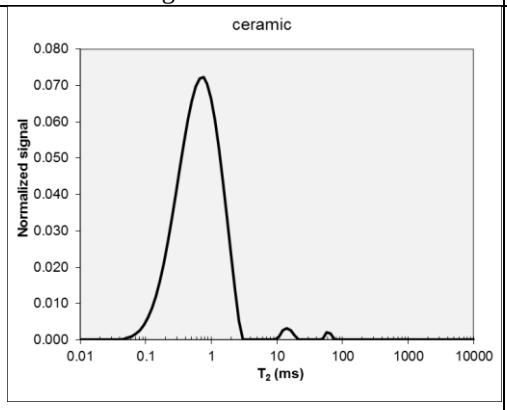	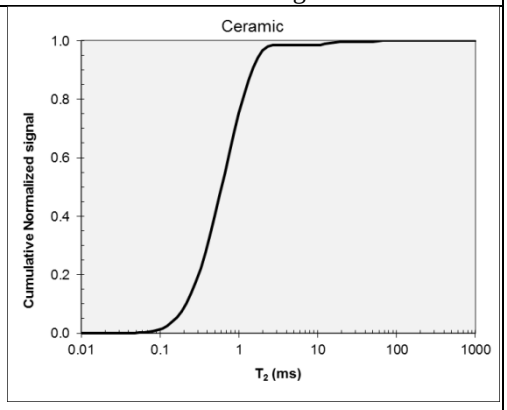

Name	**EBN 35**
Well name	**ZWE – 1**
Depth	**1242.5**
Formation	**Jurassic**

Condition	Normalized Signal	Cumulative Normalized Signal
Chips "as-received"	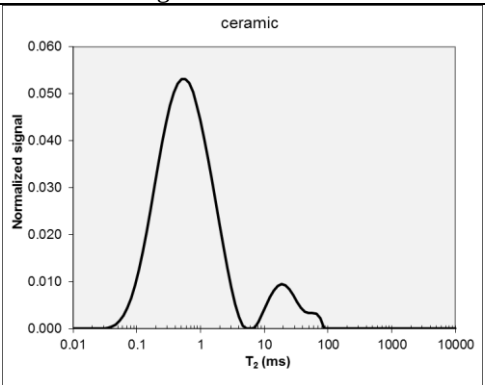	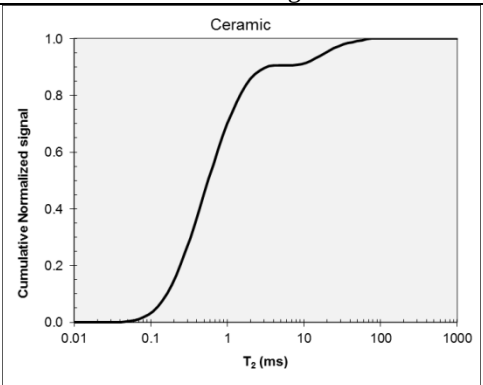
Chips Wet	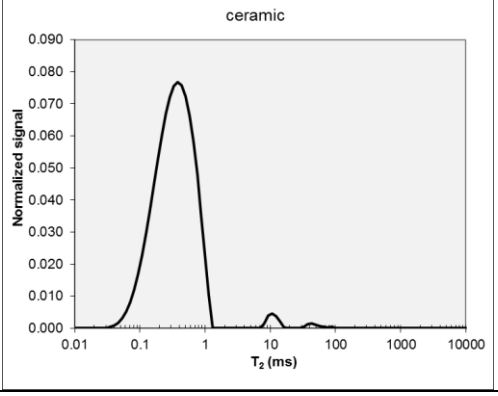	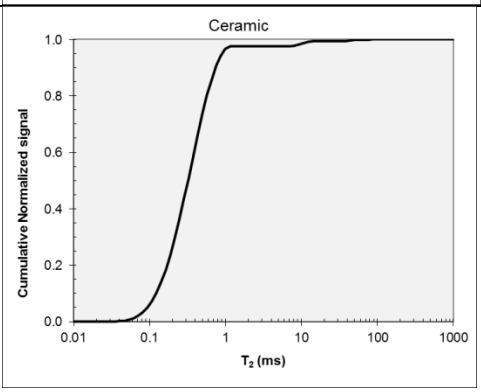

Appendix F.2

Sample	Bound Fluid < 5.5 ms	Capilary fluid 5.5< ms<100	Free Fluid >100ms
EBN 20	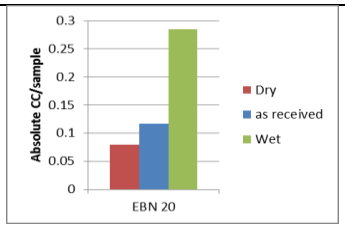	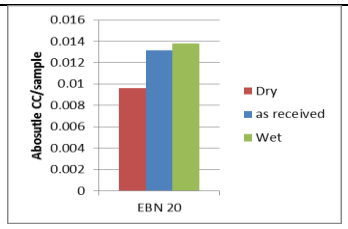	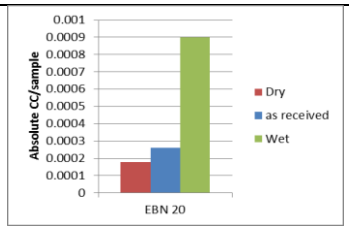
EBN 21	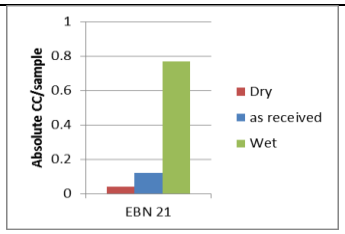	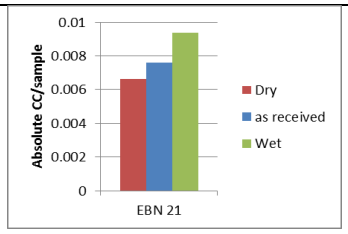	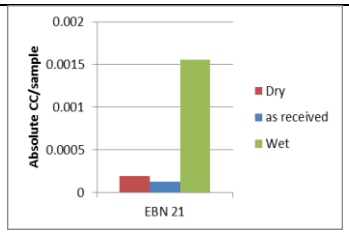
EBN 24	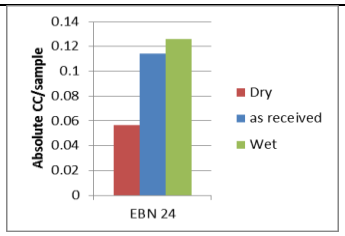	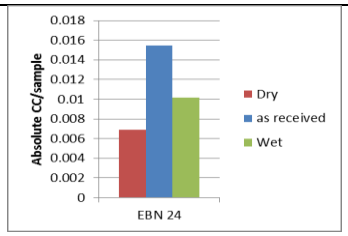	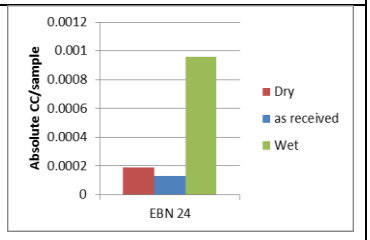
EBN 25	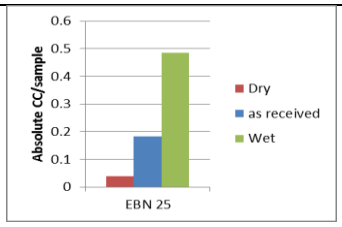	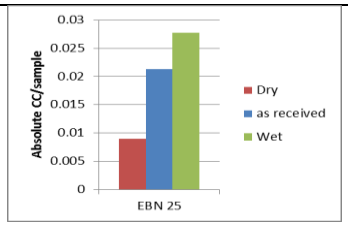	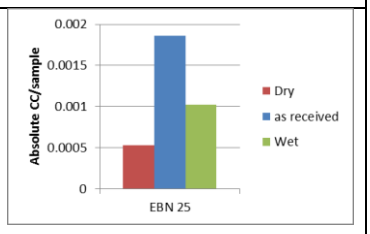
EBN 29	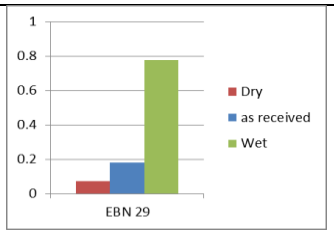	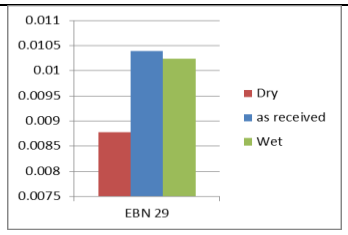	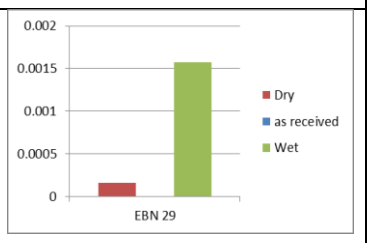

Absolute CC per sample on the Y-axis for different conditions of sample

APPENDIX G: Property Ranking and Distribution

Appendix G.1

Evaluation table to select the most promising samples

Sample	Porosity	NMR	T2 mean	SEM Open	non min	TOC	S1/TOC	PI	Average
EBN 20	**11**	**8**	**7**	**1**	**2**	**11**	**1**	**4**	**5.63**
EBN 24	**16**	**7**	**5**	**13**	**1**	**6**	**5**	**5**	**7.25**
EBN 25	**8**	**2**	**6**	**10**	**13**	**18**	**2**	**1**	**7.50**
EBN 29	**9**	**1**	**18**	**2**	**10**	**10**	**7**	**6**	**7.87**
EBN 35	**6**	**14**	**2**	**5**	**4**	**1**	**17**	**18**	**8.37**
EBN 21	**2**	**3**	**16**	**9**	**5**	**3**	**15**	**16**	**8.62**
EBN 30	13	5	14	3	3	16	8	7	8.62
EBN 23	15	6	17	11	6	12	3	3	9.12
EBN 28	12	4	15	6	8	7	12	10	7.87
EBN 22	14	11	10	8	7	8	10	8	8.37
EBN 26	10	10	8	12	14	17	4	2	8.62
EBN 32	18	18	4	4	9	9	6	11	8.62
EBN 33	3	16	3	16	16	4	9	12	9.12
EBN 34	4	12	9	17	17	2	11	13	9.25
EBN 19	1	9	11	14	11	13	14	15	9.50
EBN 31	7	17	1	15	15	5	16	17	9.62
EBN 27	17	15	13	7	12	15	18	9	9.87
EBN 36	5	13	12	18	18	14	13	14	9.87

Appendix G.2

Maps of showing the heterogeneity of the samples

Non-mineralogic content in percentage

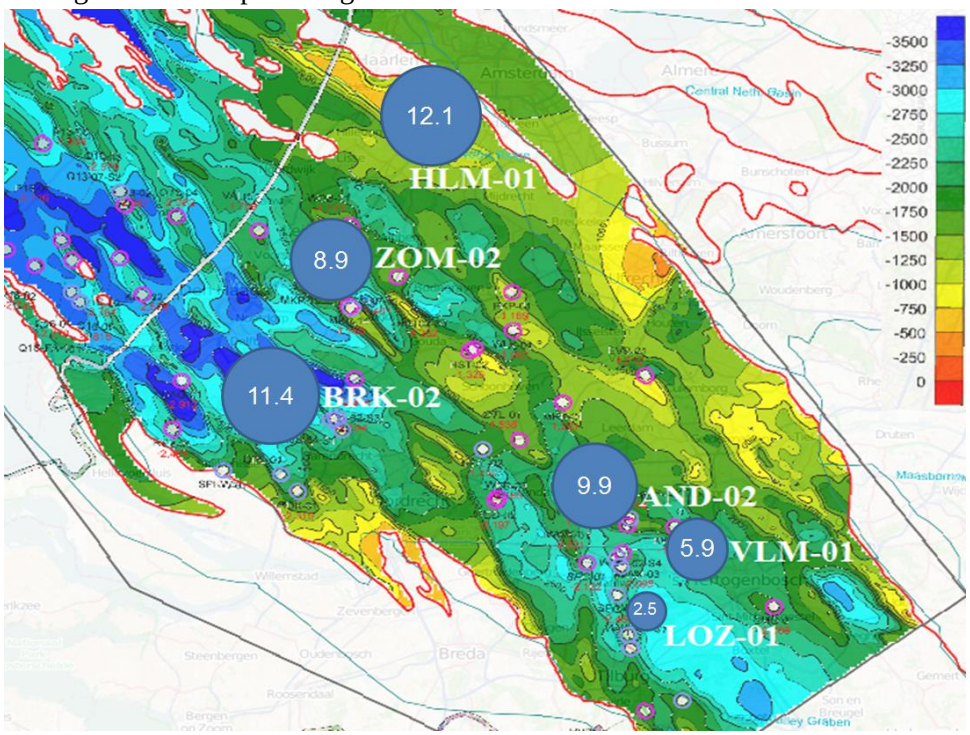

Open pore space in percentage

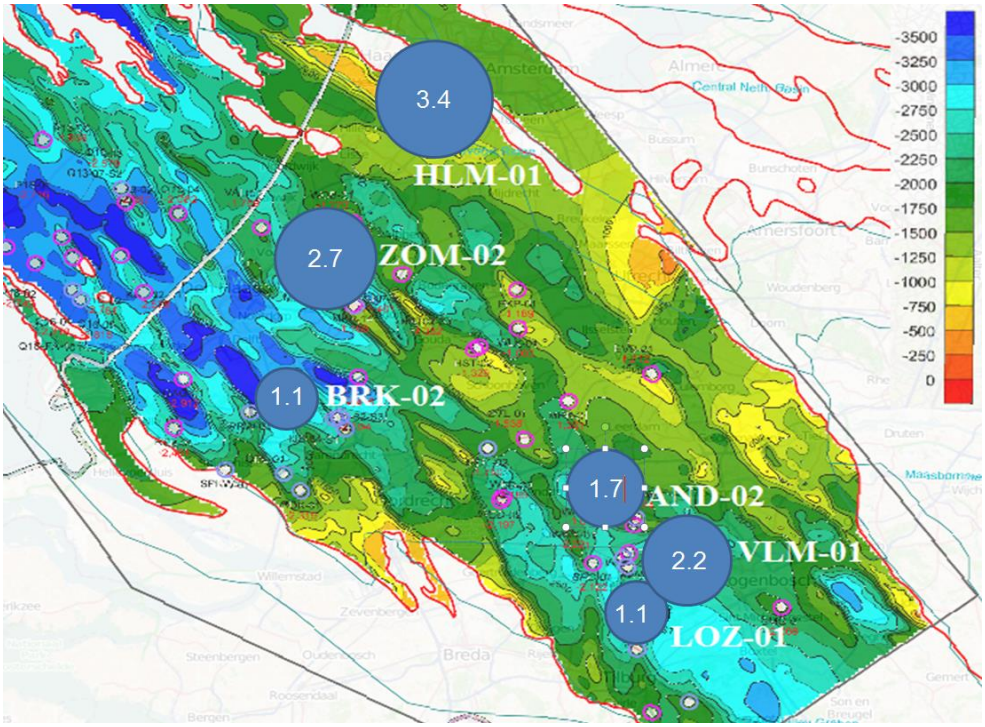

GRI porosity in percentage